



HAL
open science

Synthesis and investigation of oligomers based on phenylalanine as interfacial agents in fibre-reinforced thermoplastic composite materials

Jeroen Louwsma

► **To cite this version:**

Jeroen Louwsma. Synthesis and investigation of oligomers based on phenylalanine as interfacial agents in fibre-reinforced thermoplastic composite materials. Polymères. Université de Strasbourg, 2018. Français. NNT: 2018STRAF047. tel-03081184

HAL Id: tel-03081184

<https://theses.hal.science/tel-03081184>

Submitted on 18 Dec 2020

HAL is a multi-disciplinary open access archive for the deposit and dissemination of scientific research documents, whether they are published or not. The documents may come from teaching and research institutions in France or abroad, or from public or private research centers.

L'archive ouverte pluridisciplinaire **HAL**, est destinée au dépôt et à la diffusion de documents scientifiques de niveau recherche, publiés ou non, émanant des établissements d'enseignement et de recherche français ou étrangers, des laboratoires publics ou privés.

ÉCOLE DOCTORALE DES SCIENCES CHIMIQUES

Institut Charles Sadron

PSA Groupe

THÈSE

présentée par :

Jeroen LOUWSMA

soutenue le : 6 décembre 2018

pour obtenir le grade de : **Docteur de l'université de Strasbourg**

Discipline/ Spécialité : Chimie des polymères

Synthesis and investigation of oligomers based on phenylalanine as interfacial agents in fibre-reinforced thermoplastic composite materials

THÈSE dirigée par :

M. Jean-François LUTZ

Directeur de recherche au CNRS, ICS, Strasbourg

RAPPORTEURS :

M. Daniel GRANDE

Directeur de recherche au CNRS, ICMPE, Paris

Mme Jannick DUCHET-RUMEAU

Professeur, IMP, Lyon

AUTRES MEMBRES DU JURY :

M. Stéphane JOLY

Responsable innovation matériaux composites,
Groupe PSA, Vélizy-Villacoublay

Mme Delphine CHAN-SENG

Chargée de recherche au CNRS, ICS, Strasbourg

M. Thibault PARPAITE

Maître de conférences, ICS, Strasbourg

To my parents

ACKNOWLEDGEMENTS

The described work here was carried out both at PSA groupe (Vélizy-Villacoublay) and Institut Charles Sadron (Strasbourg). I would thusly like give my gratitude to this collaboration between Prof. Jean-François Lutz (ICS) and the industrial counterpart for allowing me to work in two very different environments. Additionally, I would like to thank the European Union's Horizon 2020 research and innovation programme under the Marie Skłodowska-Curie grant agreement No 642083 for generously funding this position.

I would then, first and foremost, like to thank my personal supervisors who have been with me in frequent meetings and with a high quality guidance: Delphine Chan-Seng and Stéphane Joly.

Delphine: after the three years I have no doubt that you are one of the most reliable and thorough scientists I have met and it really has shown in our discussions and corrections. I thank you for leading me through an admitted still hectic and sloppy beginning towards being a better scientist too.

Stéphane: the same goes for you, but I want to specifically stress our many fruitful discussions even outside of work hours that no doubt improved the whole quality of the thesis and your overall dedication and helpfulness.

On the side of ICS, I want to thank my great coworkers that made being in the lab and offices an absolute joy: Alireza, Aziz, Benoit, Chloé, Denise, Gianni, Lionel, Niklas, Guillaume, Romain, Roza, Sofia, Swann and Tathagata. I also want to thank Laurence Oswald for being a thorough on lab safety, Mélanie Legros and Catherine Saettel for their assistance with thermogravimetric analysis and differential scanning calorimetry experiments, Nicolas Genevaz for the brief use of the polarized optical microscope and Jean-Michel Guenet for our useful discussion on crystallinity.

On the side of PSA, I want to thank fellow (PhD) students and other employees for friendly lunch meetings: Adrien, Elise, Florian, Marie, Mohamed, the two Philippes. I want to thank Marjolaine Legouge and Samia Benchabane for allowing to work in the laboratories and their continued assistances with thermogravimetric analysis and differential scanning calorimetry experiments. I want to thank Guillaume Rebours, Sandrine Martinez and Tristan Thome for their continued assistance with scanning electron microscopy and X-Ray spectroscopy experiments and useful discussions. I want to thank Gwenaële Dauvillier and Cyril Conesa for their assistances with UV-Vis experiments. Lastly, I want to thank Mihai Socoliuc for continued support of PhD students in PSA, Anne Catherine Maisonneuve for her assistance with the European Union Audit at PSA and carpooling during the months of train strikes and finally Jamila Leite Costa for the administrative necessities through the years

From Institut Huber Curien (Strasbourg), I thank Dr. Jean-Marc Strub for measuring matrix assisted laser desorption ionisation time of flight mass spectra. From the institute of radical chemistry (Marseille) I thank Laurence Charles and from the mass spectrometry service of Institut de Chimie (Strasbourg) I thank Stéphanie Kouaho and Hélène Nierengarten for measuring electron spray ionisation mass spectra.

From the Altergen laboratory (Strasbourg) I want to thank Farokh Mazet for his continued assistance and discussions about purification and synthesis of oligomers.

From Institut de chimie et des matériaux Paris-Est (Paris), I want to thank Isabelle Lachaise for our discussion on centrifugal partition chromatography.

The project has been exciting and engaging due to the continued efforts from all people listed here and any persons I may have been in contact with which are not listed.

Best Regards,

Jeroen Louwsma

RESUME DE LA THESE

Introduction

L'industrie automobile est actuellement sous une forte pression visant à accroître la qualité environnementale de ses produits, en particulier par la réduction des émissions de CO₂ (**Figure 1**). Les émissions des véhicules automobiles sont réglementairement définies à l'échelle européenne. Le règlement en cours (EC 443/2009) voté par le parlement européen lors du conseil du 23 avril 2009 établit les « normes de performance en matière d'émissions pour les voitures particulières neuves dans le cadre de l'approche intégrée de la Communauté visant à réduire les émissions de CO₂ des véhicules légers » [1]. Le risque pour les constructeurs automobiles en cas de non-respect des obligations réglementaires est de s'exposer à une amende assise sur le nombre de véhicules neufs vendus dans l'année, à raison de 95 €/g CO₂ par véhicule. Les sommes en jeu sont considérables puisqu'un dépassement de 10 g de CO₂/km conduirait un constructeur généraliste à payer une amende proche du milliard d'euros par millions de véhicules vendus. Les considérations environnementales certes, mais également les considérations économiques font qu'une pleine et entière adhésion à ces règles est un incontournable.

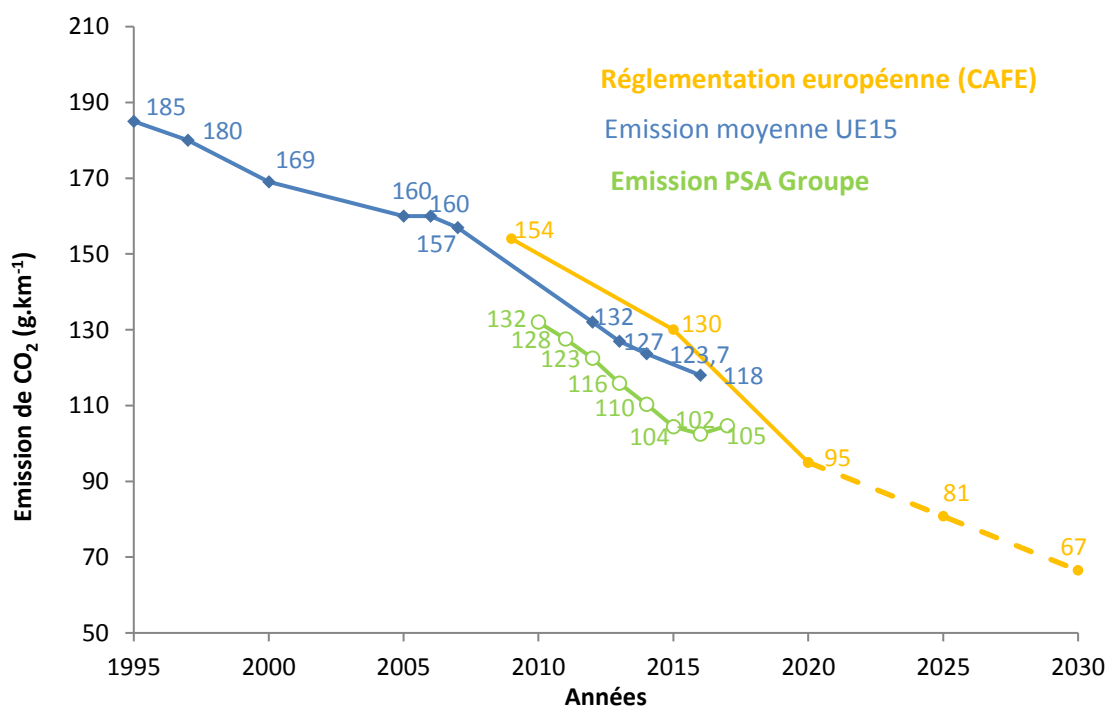


Figure 1 : Evolution de la réglementation sur le niveau maximal d'émission de CO₂ en g km⁻¹ admis au sein de l'Europe des 29 pour les véhicules de tourisme neufs.

La limitation des effets anthropiques sur le climat par l'industrie des transports nécessite un changement de modèle : le recours à des sources alternatives d'énergie. Les plus courantes sont celles découlant de la production d'électricité par des batteries au lithium d'une part, des piles à combustible d'autre part, couplée ou pas à un moteur thermique. L'avenir de l'automobile repose assurément sur un scénario multi-énergie : les énergies fossiles ne pouvant être raisonnablement rayées du paysage mondial d'un trait de plume. Dans tous les cas de figure, il sera vertueux d'être économe en énergie pour assurer d'une part de faibles émissions de gaz à effets de serre par les véhicules utilisant un carburant issu du pétrole, et d'autre part pour contribuer à l'accroissement de l'autonomie des véhicules. Dans ce contexte, la recherche de l'allègement des automobiles est une constante chez les constructeurs. L'intérêt pour les matériaux composites à matrice organique découle de leur faible densité ($d \sim 1,5$ à $\sim 1,8$) en comparaison à l'acier ($d \sim 7,8$), alors que leurs propriétés mécaniques fondamentales peuvent être similaires (module d'Young par exemple). Leur application sur pièces structurales, aujourd'hui très majoritairement réalisées en acier, confèrerait donc un potentiel d'allègement considérable des véhicules. Cependant, l'une des nombreuses difficultés retardant l'introduction de tels composites dans cette industrie, outre les coûts actuellement prohibitifs des matériaux, est leur faible capacité d'absorption d'énergie lors d'un crash véhicule.

Pour exemple, les fibres de carbone à haute résistance élastique (CF) sont certes rigides avec un module d'Young (E_{CF}) de 240 GPa (pour l'acier $E_{acier} = 210$ GPa) [2] et présentent une contrainte à rupture en traction satisfaisante, σ_{CF} , de 4 GPa ($\sigma_{acier} = 2$ GPa, acier à Ultra Haute Limite Elastique ou acier UHLE), mais elles sont fragiles : leur déformation à rupture de l'ordre du pourcent, $\varepsilon_{FC} < 1\%$, est cinq fois plus faible que ce même acier UHLE ($\varepsilon_{acier} < 5\%$) déjà peu ductile. La ductilité recherchée pour la dissipation d'énergie lors d'un choc pourrait être en partie obtenue par l'utilisation de fibres de renfort aramide pour lesquelles la déformation à rupture, bien qu'inférieure à celle d'un acier UHLE, culmine cependant à 3,6% [3]. Mais, le mélange de fibres macromoléculaires dans une matrice polymère peut représenter un défi en raison de leurs différences chimiques les rendant incompatibles. Or le transfert de la charge, de l'effort, de la matrice vers les fibres de renfort du matériau composite est primordial pour garantir de hautes performances mécaniques. C'est le rôle essentiel de l'interface entre la fibre et la matrice. Plusieurs approches ont été développées afin d'améliorer cette interface entre la matrice et la fibre. Parmi ces approches, la modification de la surface de la fibre ou de la matrice ainsi que l'ajout d'un agent interfacial sont les principales utilisées. Cette dernière est l'objet de la présente étude.

Le design et l'évaluation de nouveaux agents interfaciaux est le cœur de ce projet doctoral (**Figure 2**). En raison des avancées dans le domaine de la chimie des polymères en particulier des polymères à

séquences contrôlées [4], le projet s'est concentré sur la synthèse d'oligomères ayant une microstructure contrôlée afin d'identifier les paramètres structuraux conduisant à l'agent interfacial le plus performant. L'approche de synthèse choisie est une synthèse itérative proche de la synthèse peptidique en phase solide développée précédemment dans l'équipe [5]. Cette approche considère la synthèse de macromolécules en utilisant des acides aminés et des synthons aliphatiques ayant une séquence contrôlée et prédéfinie. L'étude concernant le système polyoléfine renforcé par des fibres de Kevlar, le choix de l'acide aminé s'est porté sur la phénylalanine pour interagir avec les fibres de Kevlar non seulement par liaisons hydrogène, mais aussi par interactions aromatiques. Les synthons aliphatiques sont des chaînes aliphatiques permettant la compatibilisation avec la matrice de polypropylène-co-polyéthylène. L'évaluation de ces oligomères en tant qu'agent interfacial pour le système polyoléfine renforcé de fibres de Kevlar a été envisagé dans un premier temps par l'étude de l'adsorption de ces oligomères sur des fibres de Kevlar de façon qualitative et quantitative. Des études préliminaires de ces fibres recouvertes d'oligomères dans une matrice de polypropylène-co-polyéthylène ont été amorcées en fin de doctorat.

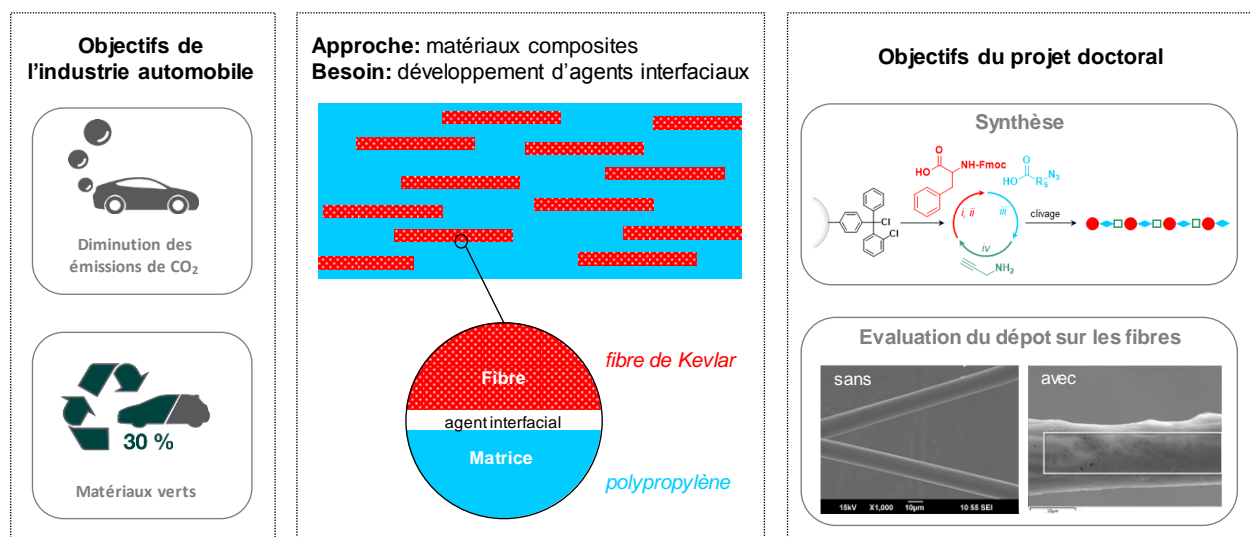


Figure 2 : Contexte et objectifs du projet doctoral.

Le manuscrit de cette thèse de doctorat se compose de trois chapitres. Le premier chapitre présente l'état de l'art sur les matériaux composites renforcés de fibres ainsi que les approches de synthèses permettant de préparer des polymères à séquences contrôlées. La première partie de ce chapitre permet de situer le contexte de ce travail en mettant en avant les approches précédemment employées pour améliorer la compatibilisation de fibres de type aramide dans une matrice polymère. La deuxième partie de ce chapitre décrit les différentes stratégies de synthèse pour contrôler finement la microstructure des polymères. Le deuxième chapitre expose la stratégie de synthèse utilisée pour préparer une librairie d'oligomères à base de phénylalanines et de synthons aliphatiques ayant une séquence spécifique ainsi que les difficultés et modifications apportées à la synthèse afin d'obtenir les

oligomères désirés. Le troisième chapitre se concentre sur l'évaluation de ces oligomères en présence de fibres de Kevlar pour estimer leur capacité à s'adsorber sur ces fibres en les comparant à des molécules commerciales. Cette étude a été réalisée qualitativement (microscopie) et quantitativement (gravimétrie). La fin de ce chapitre présente les résultats préliminaires de ces fibres de Kevlar avec un des oligomères synthétisés dans une matrice de polypropylène-co-polyéthylène pour des tests de fracture.

1. Etat de l'art sur les matériaux composites renforcés de fibres

Les matériaux composites renforcés de fibres sont utilisés dans de nombreux secteurs d'activités allant des transports [6] (automobile, aéronautique) au génie civil [7] (bâtiment, réservoirs industriels) en passant par le domaine médical [8] (bouteilles d'oxygène, tables de scanner), l'électronique [9] (boîtiers électriques, radôme), les loisirs (matériel de sport) et la balistique [10] (casque, vestes) en raison de leurs meilleures performances par rapport à chaque élément composant ces matériaux composites individuellement ou à des matériaux plus traditionnels. Cependant, en raison de la différence de composition chimique entre la matrice polymère et le renfort (ici une fibre), les propriétés de ces matériaux composites ne sont pas toujours optimales. En plus de la composition de la matrice polymère et de la fibre, la capacité de diffusion de chaque matériau et leurs propriétés morphologiques ont une influence sur l'interface entre ces deux matériaux. Ainsi, l'interface entre la matrice polymère et la fibre (**Figure 3**) joue un rôle crucial sur les performances de ces matériaux composites [11]. Un système peu optimal peut conduire à une mauvaise adhésion entre la matrice polymère et la fibre, et par conséquent, à des propriétés mécaniques modestes. En effet, cette interface permettant la transmission des efforts entre ces deux matériaux lors d'une sollicitation, l'endommagement d'un matériau composite peut être favorisé par la rupture à cette interface.

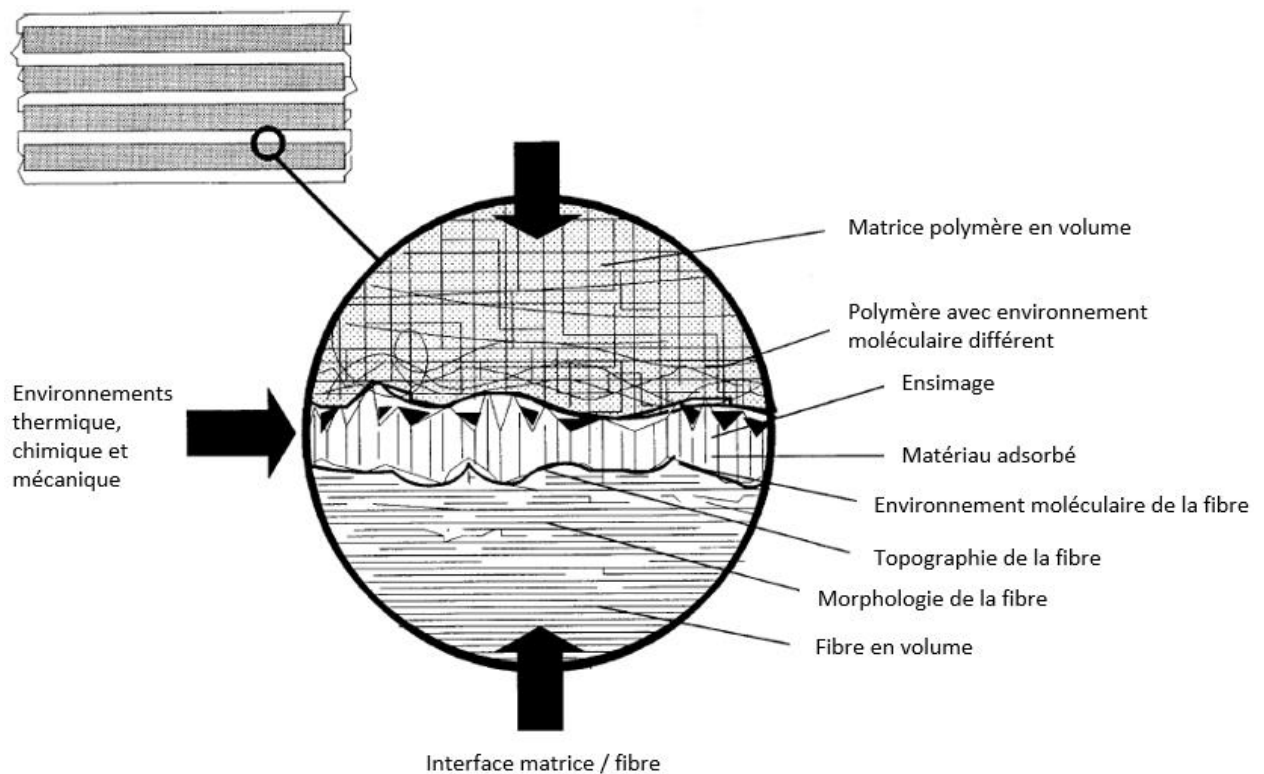


Figure 3 : Interface entre la matrice et la fibre pour des matériaux composites renforcés de fibres. Adaptée de la référence [12] avec la permission de Elsevier.

Afin d'améliorer les performances de ces matériaux composites renforcés de fibres, différentes stratégies ont été développées et décrites dans la littérature. Les principales consistent à 1) altérer la morphologie de la surface de la fibre et y introduire des groupes fonctionnels (par exemple, par traitement acide ou basique pour introduire des fonctions carbonyles ou hydroxyles [13] ou par l'utilisation de silanes [14]), 2) modifier chimiquement la structure de la matrice [15], et 3) utiliser un additif jouant le rôle d'agent interfacial (par exemple, en ajoutant le poly(propylène-*g*-anhydride maléique) [16]). Ces stratégies ont été développées pour un grand nombre de fibres naturelles et synthétiques, notamment pour les fibres de Kevlar.

Le Kevlar est un polyamide aromatique (aramide) utilisé pour un grand nombre d'applications en raison de ses propriétés. Les fibres de Kevlar ont des propriétés uniques en termes de résistance à la rupture et de stabilité thermique tout en ayant une faible densité [17] (**Tableau 1**). De nombreux matériaux composites renforcés de fibres de Kevlar ont été développés permettant de remplacer les métaux et d'obtenir une réduction de masse à iso-performance mécanique.

Tableau 1 : Comparaison des propriétés des fibres de Kevlar avec d'autres fibres [3].

	Densité (g.cm ⁻³)	Contrainte à rupture (GPa)	Module (traction) (GPa)	Allongement à la rupture (%)	Résistance spécifique à la traction* (GPa·cm ³ .g ⁻¹)	Coefficient longitudinal de dilatation thermique (10 ⁻⁶ . °C ⁻¹)	Température de décomposition (°C)
Kevlar® 29	1,44	2,92	69	3,6	2,03	-2,2	427-482
Kevlar® 49	1,44	3,00	110	2,4	2,08	-2,7	427-482
Verre (S)	2,49	4,59	83	5,4	1,84	1,7	850**
Verre (E)	2,55	3,45	69	4,8	1,35	1,6	730**
Fil d'acier	7,75	1,97	200	2	0,25	3,7	1500**
Nylon 6,6	1,16	0,99	6	18,3	0,85	-	254**
Polyester	1,38	1,16	14	14,5	0,84	-	256**
Polyéthylène haute résistance	0,97	2,59	117	3,5	2,67	-	149
Carbone haute ténacité	1,80	3,10	221	1,4	1,72	-0,1	3500

*La résistance spécifique à la traction est obtenue en divisant la ténacité par la densité ; **Température de fusion

2. Etat de l'art sur les polymères à séquences contrôlées

La chimie des polymères a fait de grands progrès pour développer des polymères de compositions, topologies et fonctionnalités variées. Récemment, des efforts se sont intensifiés concernant le contrôle de la microstructure des polymères afin de maîtriser plus finement la séquence des unités constituant les polymères. Un grand nombre des stratégies mises en place vise à utiliser les techniques de polymérisations "traditionnelles" (polymérisations par étapes et en chaîne) et d'ajuster les conditions de synthèse en vue de mieux contrôler la séquence des polymères. Parmi ces stratégies, l'utilisation d'acide de Lewis, le rôle des rapports de réactivités des comonomères utilisés, l'ajout de monomères de façon séquentielle, l'utilisation de monomères favorisant l'insertion unique d'un monomère et la préparation de macromonomères incluant une séquence prédéfinie ont été décrites dans la littérature [18] (**Figure 4**). D'autres stratégies sont issues de la biochimie en s'inspirant par exemple de l'hybridation sélective de l'ADN pour contrôler des réactions et donc induire la polymérisation de monomères dans une séquence induite par un gabarit. Des grandes avancées ont été également réalisées suite aux développements en synthèse en phase solide pour la préparation de peptides et d'acides nucléiques. En effet, ces techniques procèdent par l'ajout des unités une par une sur un support solide permettant de parfaitement contrôler la séquence de la molécule visée. La synthèse itérative s'est également développée en utilisant des monomères autres que les acides aminés et les acides nucléiques, mais aussi en exploitant l'utilisation de supports solubles, ainsi que d'autres stratégies de synthèse telles que les réactions multi-composants ou la croissance exponentielle itérative. Il est important de noter que le contrôle de la microstructure des polymères a un impact sur leurs propriétés. Le groupe de Simmons a, par exemple, montré par simulation moléculaire dynamique pour des mélanges de polymères que la molécule conduisant à la meilleure compatibilisation de ce

mélange de polymères n'est pas forcément un copolymère à blocs constitué d'un bloc de même nature que le premier polymère à compatibiliser et le deuxième bloc celui de même nature que le deuxième polymère à compatibiliser, mais un copolymère comportant des unités de même nature que les polymères à compatibiliser dans une séquence spécifique. Dans le domaine des matériaux composites, le groupe de Börner a publié des travaux sur des peptides dont la séquence influence leur degré d'absorption sur des nanoparticules inorganiques de MgF_2 [19]. Ces peptides conjugués à un poly(éthylène glycol) ont été par la suite utilisés en tant qu'agent interfacial entre des nanoparticules de MgF_2 et une matrice de poly(ϵ -caprolactone). Les auteurs montrent que ces peptides conjugués permettent d'améliorer non seulement le module d'élasticité, mais aussi la ténacité de ces matériaux composites [20].

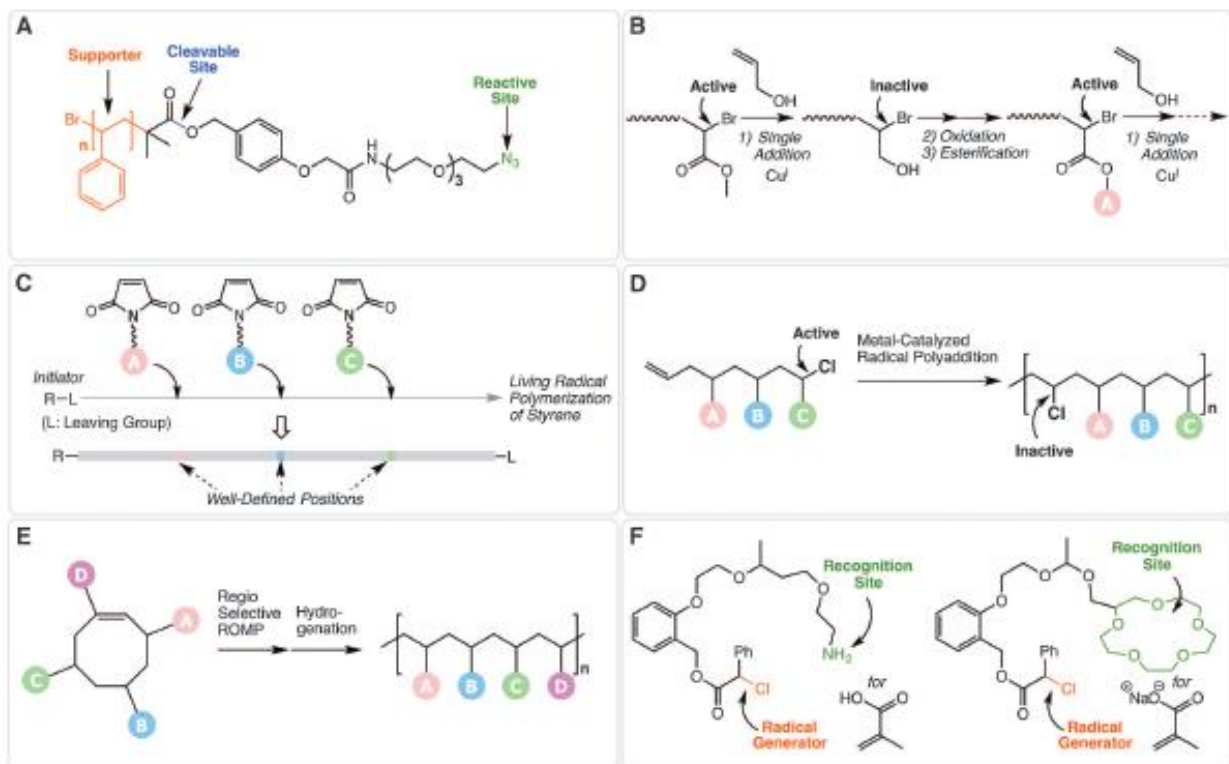


Figure 4 : Exemples de stratégies de synthèse pour préparer des polymères à séquences contrôlées [21].

3. Synthèse d'oligomères à base de phénylalanines et de synthons aliphatiques

Le premier objectif de ce travail doctoral a été de synthétiser une librairie d'oligomères de compositions et séquences prédéfinies en vue d'être utilisés en tant qu'agent interfacial entre des fibres de Kevlar et une matrice polyoléfine. L'approche de synthèse choisie est une synthèse itérative sur support solide composée de cycles de réaction comportant quatre étapes différentes (**Figure 5**) :

- 1) étape i : addition d'un acide aminé protégé par réaction d'amidification,
- 2) étape ii : retrait du

groupe protecteur fluorénylméthoxycarbonyle (Fmoc), 3) étape iii : addition d'un acide ω -azidoalcanoïque par réaction d'amidification, et 4) étape iv : ajout de l'amine propargylique par réaction de cycloaddition entre un azoture et une alcyne assistée par le cuivre [5]. Dans le cadre de cette étude, la phénylalanine a été sélectionné comme acide aminé afin de favoriser les interactions avec la fibre de Kevlar par des interactions de type liaisons hydrogène ainsi que des interactions aromatiques, alors les espaceurs issus des acides ω -azidoalcanoïques doivent permettre la compatibilisation avec la matrice de poly(propylène-*co*-éthylène). Cette stratégie de synthèse permet de moduler la composition et la séquence des unités constituant l'oligomère et donc de créer une librairie d'oligomères ayant des espaceurs de longueurs variées, mais aussi de jouer sur le nombre de phénylalanines consécutives par cycle de réaction et l'agence de ces unités le long de la chaîne de l'oligomère. Pour des raisons de simplifications, les oligomères seront notés de la façon suivante : F pour les résidus de phénylalanine, une lettre en minuscule pour l'espaceur (b pour un espaceur butyrique soit trois méthylènes, v pour un espaceur valérique soit quatre méthylènes, h pour un espaceur héxyle soit cinq méthylènes, et u pour un espaceur undécyle soit dix méthylènes sur l'espaceur) et • pour l'addition de l'amine propargylique conduisant à la formation d'une fonction triazole. A titre d'exemple, un oligomère obtenu en réalisant quatre cycles de réaction en insérant pour chaque cycle de réaction quatre phénylalanines, l'acide 6-azidohexanoïque et l'amine propargylique sera mentionné comme FFFFh•FFFFh•FFFFh•FFFFh.

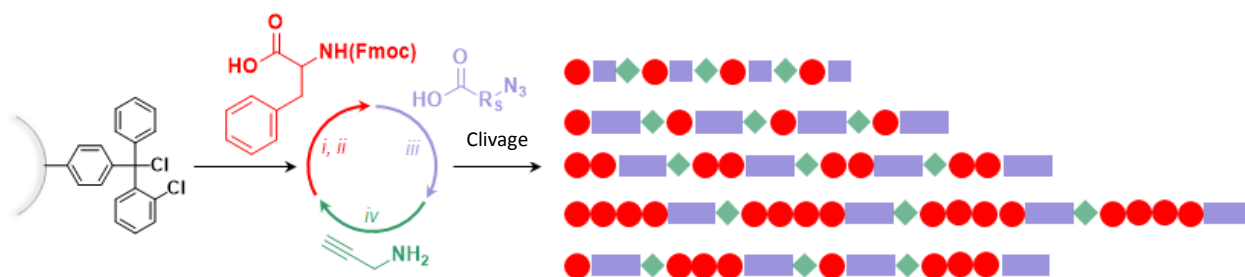


Figure 5 : Synthèse d'oligomères à base de phénylalanines et d'espaceurs aliphatiques en phase solide : i) Fmoc -Phe-OH, HBTU, HOBt, DIPEA, DMF, ii) pipéridine, DMF, iii) acide ω -azidoalcanoïque, HBTU, HOBt, DIPEA, DMF, et iv) propargylamine, CuBr, PMDETA, CH₂Cl₂.

Les premières synthèses ont été réalisées en utilisant les mêmes conditions expérimentales que celles précédemment utilisées dans l'équipe [5], c'est-à-dire en utilisant une résine de polystyrène faiblement réticulée comportant des points d'ancrage de type chlorure de 2-chlorotriptyle (résine CTC) comme support de synthèse. Pour les étapes d'amidification (étapes i et iii avec Fmoc-L-Phe-OH et l'acide ω -azidoalcanoïque respectivement), l'hexafluorophosphate de (2-(1*H*-benzotriazol-1-yl)-1,1,3,3-tetraméthyluronium (HBTU) est utilisé comme agent de couplage en présence de l'hydroxybenzotriazole (HOBt) comme agent permettant de supprimer la racémisation des molécules chirales et la *N,N*-diisopropyléthylamine (DIPEA) comme base dans le *N,N*-diméthylformamide (DMF).

La réaction est laissée sous agitation pendant une heure avant d'enlever le milieu réactionnel et de rincer la résine avec du DMF. Pour retirer les groupes Fmoc (étape ii), une solution de 25% de pipéridine dans le DMF est employée dans un premier temps pendant 3 min, puis après avoir enlevé le milieu réactionnel une solution fraîche est ajoutée et agitée pendant 20 min. Après rinçage de la résine avec du DMF, l'étape suivante peut être réalisée. L'étape iv de cycloaddition entre un azoture et un alcyne assistée par le cuivre est conduite avec le bromure de cuivre(I) en présence de la *N,N,N',N'',N''*-pentaméthyl-diéthylène-triamine (PMDETA) dans le dichlorométhane pendant 1 h sous argon. Lorsque la séquence visée est terminée, l'oligomère est clivé de la résine en utilisant une solution de trifluoroéthanol dans le dichlorométhane. Il est à noter que le clivage était difficile pour les séquences contenant un grand nombre de résidus de phénylalanine. De ce fait, la solution de clivage a été remplacée par une solution d'acide trifluoroacétique dans le dichlorométhane. Le produit est isolé par précipitation dans l'éther diéthylique. La caractérisation par spectroscopie par résonance magnétique nucléaire (RMN) et spectrométrie de masse (MS) de ces oligomères a révélée l'obtention du produit visé, mais aussi d'oligomères de séquences tronquées (**Figure 6**). Le rapport entre l'intégration correspondant aux cycles aromatiques de la phénylalanine (6,9-7,5 ppm) et celle au méthylène à côté de l'azoture terminal (3,2 ppm) sur spectre de RMN ¹H ne coïncide pas avec ce qui est attendu (**Figure 6a**). En effet, pour l'oligomère FFFFh•FFFh•FFFh•FFFh, si les cycles aromatiques des résidus de phénylalanine sont intégrés pour 80 protons, le pic correspondant au méthylène à côté de l'azoture terminal devrait intégrer pour deux protons. Cependant, une valeur de 0,8 est obtenue (1,39 pour Fh•Fh•Fh•Fh). De plus, le spectre de MS par ionisation laser assistée par une matrice (MALDI) montre bien la présence du pic correspondant à la molécule visée ($m/z = 3093$ pour $[M+H]^+$), mais également la présence d'oligomères de séquences tronquées et des espèces non identifiées (**Figure 6b**).

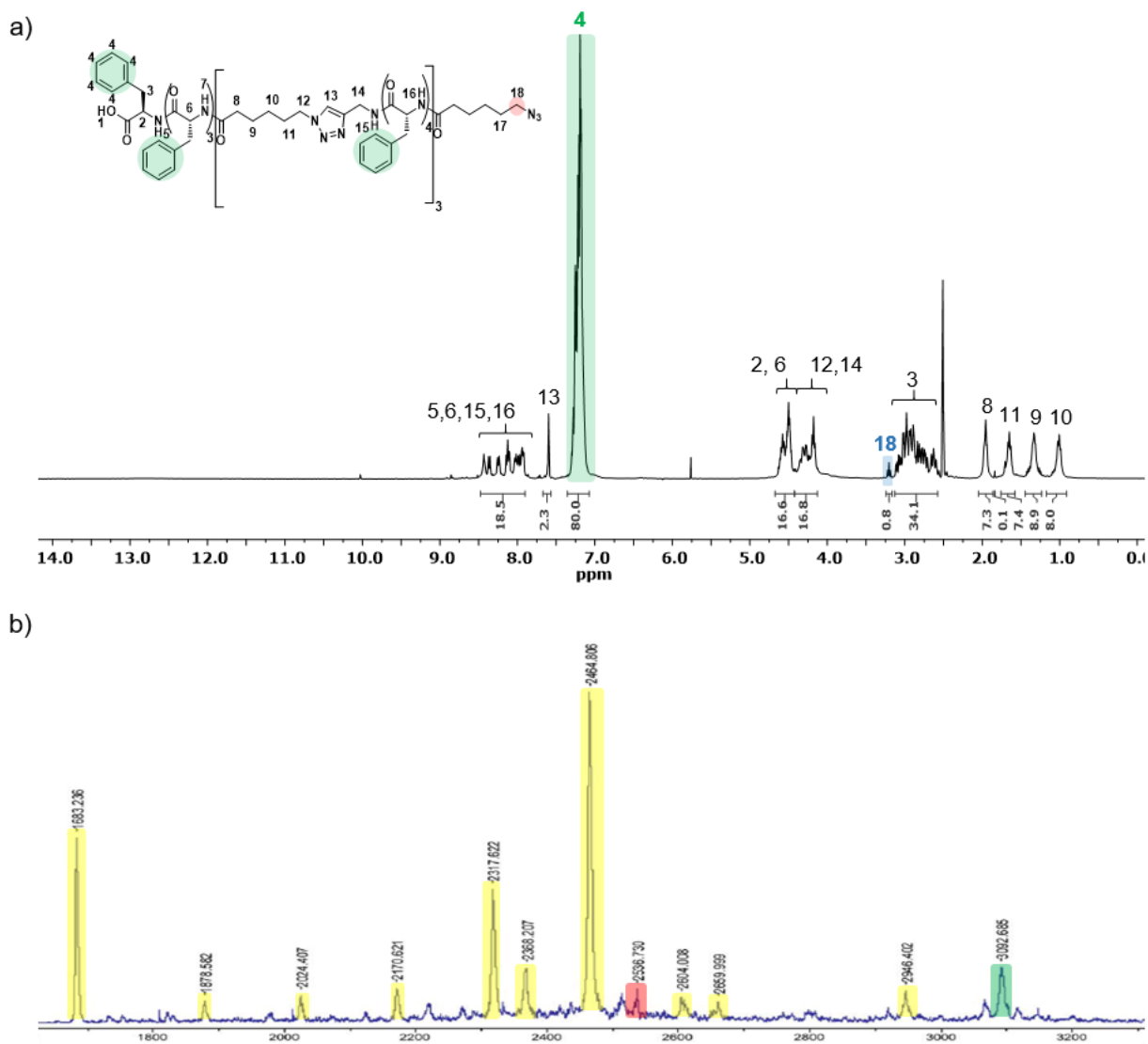


Figure 6: Caractérisation de l'oligomère FFFh•FFFh•FFFh•FFFh en utilisant les conditions de synthèses initiales par a) spectroscopie RMN ^1H dans le DMSO- d_6 (en vert le pic correspondant aux cycles aromatiques des résidus de phénylalanines et en bleu le méthylène à côté de l'azoture terminal) et b) spectrométrie de masse MALDI (en vert le pic de la molécule visée, en jaune des oligomères à séquences tronquées et en rouge des espèces non identifiées).

Afin d'optimiser la préparation de ces oligomères, un suivi de chaque étape de synthèse est réalisé en 1) utilisant le test colorimétrique de Kaiser qui permet de détecter qualitativement la présence d'amines primaires [22] et 2) identifiant la présence ou absence de la fonction azoture après l'addition de l'acide ω -azidoalcanoïque ou de l'amine propargylique respectivement. Ces tests de suivi ont mis en évidence que généralement la réaction de cycloaddition entre un azoture et une alcyne assistée par le cuivre ne rencontre pas de difficulté contrairement aux réactions d'amidification en particulier lors de l'addition de la phénylalanine protégée. Afin que les étapes i et iii soient complètes, ces réactions ont été répétées jusqu'à ce que le test de Kaiser indique l'absence d'amines primaires. Plusieurs hypothèses ont alors été émises concernant ces étapes de synthèse : 1) l'activation de l'acide

carboxylique n'est pas efficace, 2) le taux de greffage est trop élevé conduisant à une gêne stérique lors de la réaction, 3) l'utilisation de la phénylalanine induit la formation d'agrégats par formation de liaisons hydrogène et d'empilement des cycles aromatiques et 4) l'accessibilité des sites sur la résine est réduite. Ces hypothèses ont été testées en utilisant Fh•Fh•Fh•Fh comme oligomère modèle.

La première hypothèse a été étudiée en pré-activant l'acide carboxylique pour les étapes d'addition de Fmoc-Phe-OH (étape i) et d'acide 6-azidohexanoïque (étape iii). A cet effet, tous les réactifs sont préalablement mélangés ensemble avant de les ajouter à la résine. Malheureusement, la caractérisation par spectroscopie RMN ¹H ne montre aucune amélioration en ce qui concerne le rapport entre l'intégration correspondant aux cycles aromatiques de la phénylalanine et celle au méthylène à côté de l'azoture terminal.

Dans un deuxième temps, le taux de greffage a été diminué lors de la fonctionnalisation de la résine (ici 0,54 mmol par gramme de résine par rapport à 0,94 mmol par gramme de résine utilisé précédemment). Le spectre de RMN ¹H indique une amélioration du rapport entre l'intégration correspondant aux cycles aromatiques de la phénylalanine et celle au méthylène à côté de l'azoture terminal (1,89 par rapport à 1,39 précédemment).

La troisième hypothèse concerne la possibilité que l'oligomère en croissance sur la résine s'agrège en raison des liaisons hydrogène et l'empilement des cycles aromatiques induits par l'utilisation de la phénylalanine. A cet effet, les conditions de synthèse ont été modifiées afin de diminuer la formation d'agrégats en jouant sur plusieurs paramètres : 1) l'ajout de sels chaotropiques [23] et 2) la nature du solvant [24]. Les chaotropes sont notamment utilisés pour précipiter les protéines en interférant notamment dans les interactions entre la protéine et les molécules d'eau ou en dénaturant la protéine. Ces sels, tels que le chlorure de sodium et le thiocyanate de guanidine, perturbent les liaisons intra- et intermoléculaires faibles telles que les liaisons hydrogène, les forces de Van der Waals et les interactions hydrophobes. Le bromure de tétrabutylammonium a été utilisé ici comme sel chaotrope pour provoquer la rupture des liaisons hydrogène de ces agrégats. Les améliorations par analyse de spectroscopie RMN ¹H sont minimes : l'intégration du méthylène à côté de l'azoture terminal est de 1,41 par rapport à la réaction sans modification. La seconde approche pour rompre les agrégats est d'utiliser d'autres solvants comme le diméthylsulfoxyde ou un mélange de solvants. L'emploi d'un mélange de solvants (dichlorométhane, DMF et *N*-méthyl-2-pyrrolidone dans des proportions équimoléculaires) comme solvant de synthèse pour les étapes i et iii a permis d'améliorer le rapport entre l'intégration correspondant aux cycles aromatiques de la phénylalanine et celle au méthylène à côté de l'azoture terminal (1,80 par rapport à 1,39 pour la synthèse sans modification).

Finalement, la résine CTC a été remplacée par une résine Tentagel®. Cette dernière est une résine dont le point d'ancrage se trouve à l'extrémité libre d'une chaîne poly(éthylène glycol) (PEG) greffée sur la résine de polystyrène faiblement réticulée. Cette résine permet de faire des synthèses supportées tout en ayant une réactivité aussi élevée qu'en solution. La résine utilisée comporte des chaînes de PEG ayant une masse molaire de 3000 g·mol⁻¹, le point d'ancrage est une fonction alcool 4-hydroxybenzylique et le taux de fonctionnalisation est de 0,24 mmol par gramme de résine. La première différence avec toutes les conditions de synthèse décrites jusqu'à présent a été que le test de Kaiser indiquait l'absence d'amines primaires dès la première addition et donc aucune répétition d'une étape n'a été nécessaire. La caractérisation de l'oligomère obtenue par RMN ¹H (**Figure 7**) indiquait une nette amélioration par rapport aux conditions initiales : l'intégration du méthylène à côté de l'azoture terminal est proche de la valeur attendue (la valeur exacte était difficile à obtenir en raison de la superposition du pic avec celui de l'eau). Cependant, il est à noter que l'utilisation de la résine Tentagel® conduit à la présence de PEG dans le produit [25] ce qui est observé dans le cas de la synthèse de Fh•Fh•Fh•Fh (pic à 3,5 ppm sur le spectre de RMN ¹H).

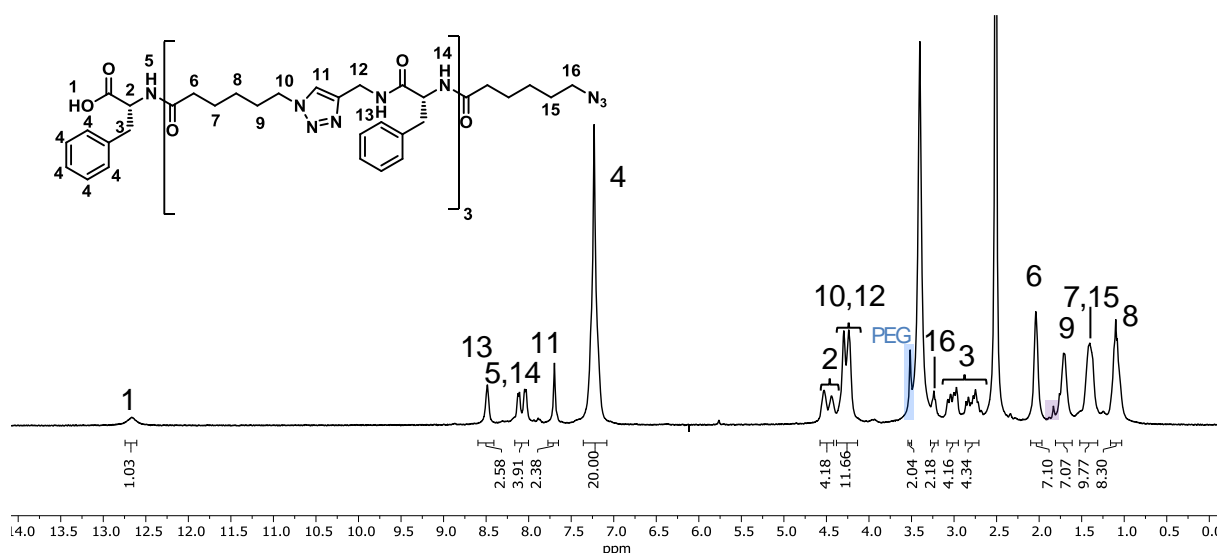


Figure 7 : Spectre RMN ¹H dans le DMSO-d₆ de l'oligomère Fh•Fh•Fh•Fh obtenu en remplaçant la résine CTC par une résine Tentagel® ayant un point d'ancrage de type alcool 4 hydroxybenzylique.

Même si ces dernières conditions de synthèse comportent quelques défauts (présence de PEG en bleu et d'impuretés non identifiées en violet sur le spectre RMN ¹H, **Figure 7**) pour préparer l'oligomère modèle Fh•Fh•Fh•Fh, celles-ci ont été identifiées comme les plus optimales pour la préparation des oligomères visés et ont été utilisées pour préparer une librairie d'oligomères en faisant varier notamment le nombre de phénylalanines additionnées par cycle de réaction et la longueur de chaîne des espaceurs. Il est à noter que pour la synthèse de certains oligomères comportant un plus grand nombre de résidus de phénylalanine, certaines étapes i et iii étaient incomplètes. Afin de remédier à ce problème, les étapes i et iii ont été réalisées avec un mélange de solvants (dichlorométhane, DMF et

N-méthyl-2-pyrrolidone dans des proportions équivolumentiques) et en répétant les étapes pour lesquelles le test de Kaiser indiquait encore la présence d'amines primaires. Ces oligomères ont été étudiés de façon exhaustive par spectroscopie RMN (¹H, ¹³C, DEPT, HSQC et HMBC) et par spectrométrie de masse (ESI et MALDI) afin d'identifier les défauts de synthèse incluant les séquences tronquées et les espèces présentes issues des conditions de synthèse utilisées (par exemple PEG par l'utilisation de la résine Tentagel®).

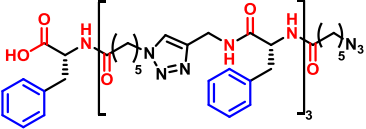
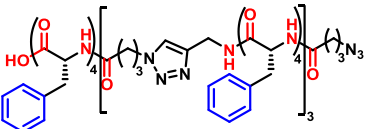
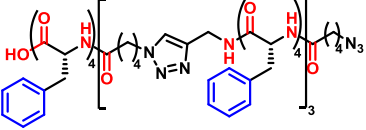
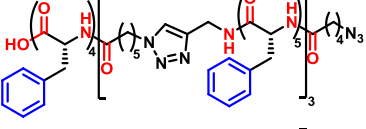
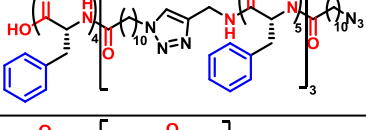
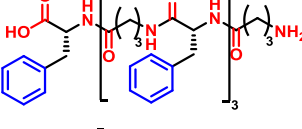
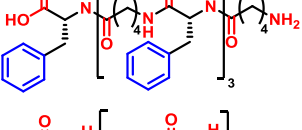
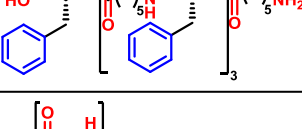
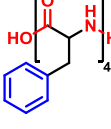
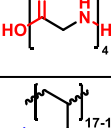
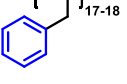
Plusieurs pistes de purifications pour ces oligomères ont alors été envisagées comme la chromatographie préparative en phase liquide à haute performance et la chromatographie de partage centrifuge. Afin de déterminer la faisabilité de la purification de ces oligomères en utilisant ces techniques, il a été nécessaire de faire une étude de solubilité de ces molécules. Ces oligomères à base de phénylalanine ont une forte tendance à s'agréger en raison des interactions existantes entre les résidus de phénylalanine et ont donc une solubilité réduite. Il est en effet bien connu de la littérature que des peptides de petites séquences de phénylalanine telles que la diphenylalanine et la triphenylalanine ont une forte tendance à l'auto-assemblage formant des agrégats de type fibrilles, nanotubes et rubans hélicoïdaux [26]. Cette étude de solubilité montre que le 4-méthyl-2-pentanone est le seul solvant permettant la dissolution des oligomères sans avoir recours au chauffage. Des alternatives sont l'utilisation du tétrahydrofurane et l'acétonitrile (ACN) en présence soit d'un à deux équivalents de bromure de tétrabutylammonium, soit de 10% d'acide chlorhydrique ou de 5% d'acide trifluoroacétique (TFA).

4. Evaluation de ces oligomères en tant qu'agents interfaciaux pour des matériaux composites à matrice polyoléfine renforcée de fibres de Kevlar

Pour rappel, l'étude est conduite sur une sélection des oligomères synthétisés, à savoir ceux obtenus en utilisant la résine Tentagel®. Deux paramètres ont été retenus pour cette sélection (**Tableau 2**): 1) le nombre de résidus de phénylalanine par cycle réactionnel et 2) la présence et la longueur des espaceurs. Le premier paramètre vise à mettre en évidence l'influence de la présence de plusieurs résidus phénylalanine quant à l'adsorption de ces oligomères sur les fibres de Kevlar. Le second a pour but d'accroître les degrés de liberté de conformation des molécules, de libérer les contraintes d'encombrement stérique lors de l'adsorption à la surface des fibres. Les espaceurs pourraient également permettre, dans un second temps, une compatibilisation de fibres avec la matrice polyoléfine. Les unités d'espacement entre groupes interactifs prennent la forme de chaînes aliphatiques, connues pour avoir un grand nombre de degrés de liberté de conformation. Pour compléter l'étude, plusieurs molécules modèles ont été synthétisées par le laboratoire ALTERGEN notamment. Elles visent à mettre en évidence la nature des interactions entre des oligomères sans

espaceur et la surface des fibres de Kevlar. La phénylalanine, en mesure d'interagir avec la surface des fibres de Kevlar par interactions de type liaison hydrogène, par interactions π - π voire par ces deux types d'interaction, il a été nécessaire de considérer trois molécules modèles : respectivement une oligoglycine, un polystyrène et une oligophénylalanine. De même, le rôle de la fonction triazole est étudié en comparant avec le cas de molécules ne portant pas ce groupe fonctionnel. En résumé, les molécules considérées dans cette étude se répartissent en quatre catégories: 1) les oligomères commerciaux dits « modèles » : tétraglycine (GGGG), polystyrène (PS), tétraphénylalanine (FFFF), ayant un nombre réduit de degrés de liberté de conformation entre les sous-unités interactives ; 2) les oligomères contenant un seul résidu phénylalanine par cycle réactionnel et une unité d'espacement entre chaque résidu, assurant un nombre supérieur de degrés de liberté ; 3) les mêmes oligomères contenant un seul résidu de phénylalanine par cycle et une unité d'espacement entre chaque résidu, ainsi qu'une fonction triazole ; enfin 4) le cas identique au précédent à l'exception du fait que les oligomères contiennent quatre résidus de phénylalanine par bloc (**Tableau 2**).

Tableau 2 : Oligomères utilisés dans la phase de traitement de surface des fibres de Kevlar.

Paramètres considérés	Molécule	Masse molaire (g·mol ⁻¹)
Oligomères synthétisés	Fh•Fh•Fh•Fh	 1327,71
	FFFFb•FFFFb•FFFFb•FFFFb	 2980,40
	FFFFv•FFFFv•FFFFv•FFFFv	 3036,47
	FFFFh•FFFFh•FFFFh•FFFFh	 3092,53
	FFFFu•FFFFu•FFFFu•FFFFu	 3372,84
Oligomères sans groupe triazole	FbFbFbFb	 946,46
	FvFvFvFv	 1002,50
	FhFhFhFh	 1058,53
Oligophénylalanine (interactions π et liaison hydrogène)	Tétraphénylalanine (FFFF)	 606,28
Oligoglycine (liaison hydrogène uniquement)	Tétraglycine (GGGG)	 246,46
Polystyrène (interactions π uniquement)	Polystyrène (PS)	 2100

L'objectif de ce projet étant de disposer de matériaux composites à matrice polyoléfine renforcée de fibres de Kevlar, les oligomères synthétisés comme agents interfaciaux doivent présenter une absence

de dégradation à la température du polymère fondu permettant sa transformation (moulage, injection, ...). En fait, la préparation des matériaux composites est réalisée typiquement 30 °C au-dessus de la température de fusion, T_f , du polymère utilisé comme matrice soit une stabilité à une température supérieure à 167 °C (Aceso®Lumicene® MR10MM0 de TOTAL, $T_f = 137$ °C). Les oligomères contenant un unique résidu phénylalanine par cycle réactionnel présentent une température de dégradation ne leur permettant pas de prétendre à être utilisés finalement dans une telle matrice (copolymère de propylène et d'éthylène). Pour les oligomères à quatre résidus de phénylalanine par cycle réactionnel, un début de dégradation thermique est observé au-delà de 214 °C. Le schéma de dégradation est analysé par chromatographie en phase gazeuse couplée à un spectromètre de masse. L'affinité comparée des oligomères sur le substrat Kevlar, a nécessité la mise au point de protocoles d'enduction des fibres aramide. D'une part, par trempage des fibres dans une solution de TFA/ACN 5/95 par volume contenant l'oligomère, d'autre part, par pulvérisation d'une solution contenant l'oligomère. Dans ces deux cas, la manipulation d'une fibre individuelle de 12 μm de diamètre moyen et d'une longueur proche de 5 cm s'est révélée être une difficulté expérimentale majeure. Les fibres après traitement de surface sont caractérisées qualitativement par microscopie électronique à balayage. Couplée à la spectrométrie de dispersion en énergie (EDS) des photons X, le revêtement de surface comme le substrat sont identifiés de façon univoque. L'influence de la concentration de la solution d'oligomères initie l'étude quantitative de l'adsorption des oligomères afin de déterminer les paramètres conduisant à l'obtention d'un traitement de surface sans effet parasite. En effet, le caractère filmogène des solutions d'oligomères peut conduire à la formation de films continus entre les fibres, phénomène sans lien direct avec les interactions entre les oligomères et la fibre de Kevlar donc à proscrire. Une première conclusion est issue de ces analyses qualitatives : Les dépôts de l'oligomère tétracyclic et de l'oligomère tétraphénylalanine diffèrent significativement, à iso-protocole d'enduction. Les interactions entre la tétracyclic et la fibre de Kevlar ne sont pas de nature à créer un dépôt à la surface des fibres (observation d'un démouillage) (**Figure 8**), au contraire des interactions entre la tétraphénylalanine et la fibre de Kevlar (**Figure 9**).

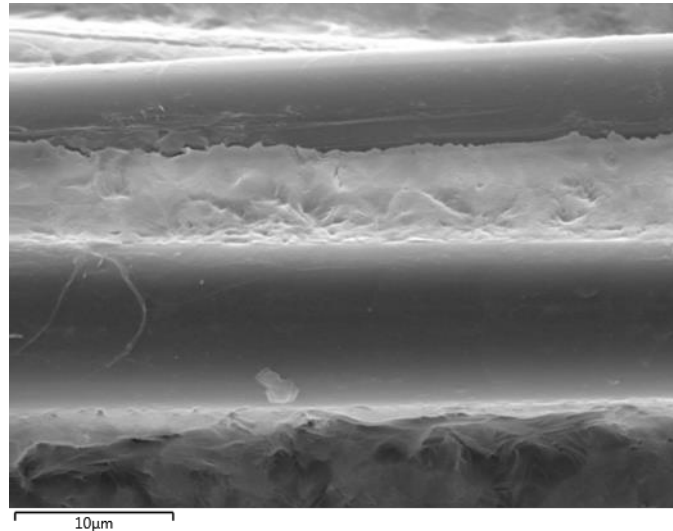


Figure 8 : Fibres de Kevlar et film de tétraglycine résultant du démouillage des fibres

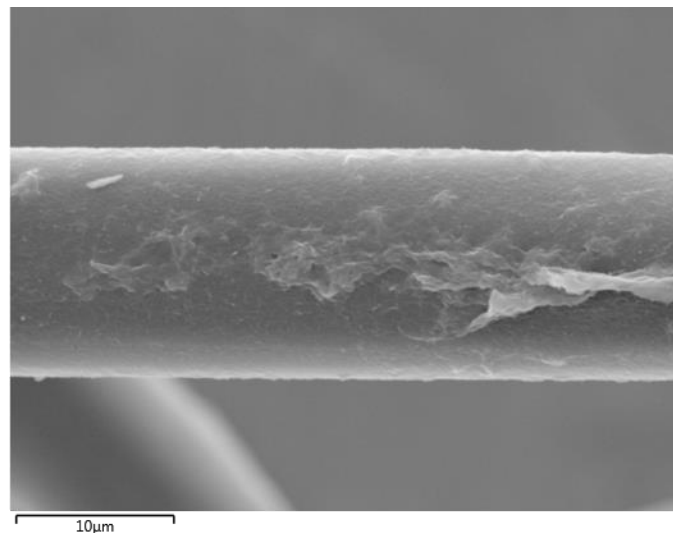


Figure 9 : Fibre de Kevlar enduite d'un film mince de tétraphénylalanine

Dans les différents cas de traitement de surface, l'observation qualitative du revêtement des fibres enduites suivant les deux protocoles, révèle la présence d'un film de morphologies variées. Cependant, afin d'établir l'influence de la structure moléculaire de l'oligomère sur les interactions avec la fibre de Kevlar, une quantification du dépôt est un incontournable.

La spectrométrie de dispersion en énergie des photons X (EDS) s'est finalement avérée insuffisamment précise pour aboutir à une quantification conduisant à des conclusions intéressantes. De même, la spectroscopie d'absorption UV/visible n'a pas conduit à des quantifications satisfaisantes. Finalement, une mesure par gravimétrie est utilisée. Dans ce cas, la différence de masse entre les fibres de Kevlar initialement nues et les mêmes fibres après traitement de surface est mesurée. Bien que la fourniture des fibres de Kevlar ait été de grande qualité, l'échantillon industriel est porteur d'une dispersion sur la valeur du diamètre des fibres, sur la longueur de celles-ci de telle sorte que l'obtention de valeurs

moyennes soit rendue nécessaire. De plus, avec une masse moyenne de (m_{fibre}) de $9 \mu\text{g} \pm 1 \mu\text{g}$, le travail sur fibre individuelle nécessitait une instrumentation indisponible au laboratoire. Des pastilles de Kevlar ont donc été élaborées (**Figure 10**), formant l'équivalent d'un mat de fibres, de volume (diamètre $d = 13\text{mm}$, épaisseur $w = 1\text{mm}$) et de masse ($m = 74,5 \text{ mg} \pm 0,3 \text{ mg}$) contrôlés (**Figure 11**).

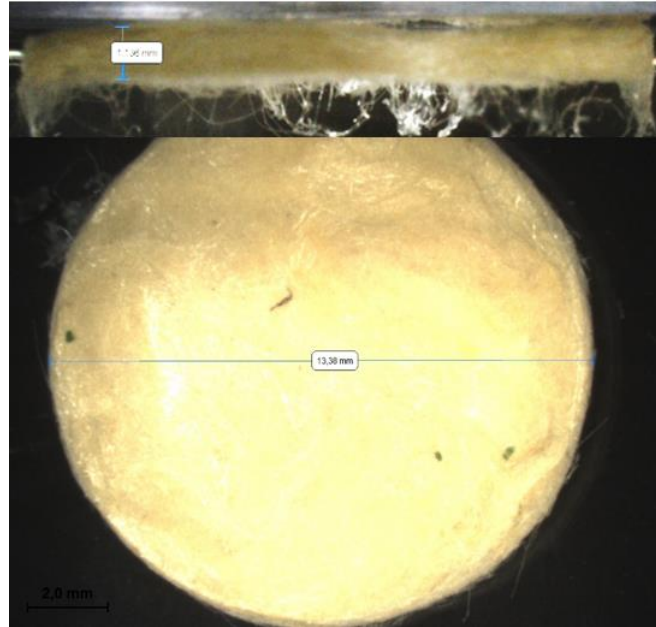


Figure 10: Pastille de Kevlar a) vue de profil ; b) vue de face

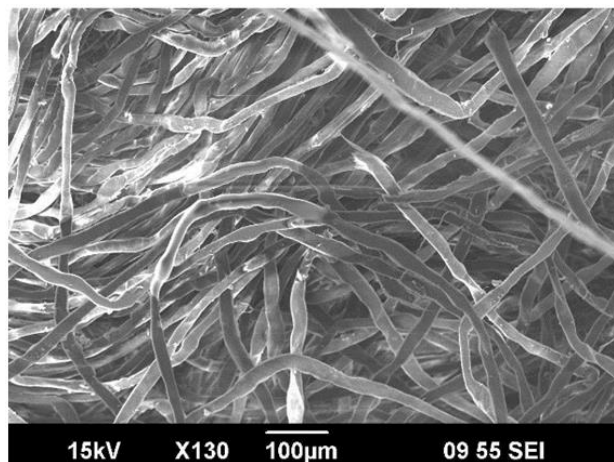


Figure 11: Enchevêtrement des fibres de Kevlar constitutives d'une pastille observée par microscopie électronique à balayage.

La mesure quantitative du dépôt sur des fibres à l'équilibre hygroscopique avec l'atmosphère ambiante, nécessite également de prendre en compte une masse résiduelle de solvant présente après la phase d'enduction. Enfin l'établissement d'une échelle relative d'affinité des différents oligomères énumérés ci-dessus (**Tableau 2**) est faite en fixant les paramètres du procédé de trempage: durée (5 min), concentration de la solution ($1 \mu\text{mol.mL}^{-1}$), répétabilité sur au minimum une série de trois pastilles. La grandeur comparée est proportionnelle à la fraction molaire d'oligomères adsorbés. Considérant l'oligomère de tétraphénylalanine comme une référence, la fraction molaire adsorbée est

fortement accrue (de l'ordre et au-delà d'un facteur trois par rapport à cette référence) dès lors que l'oligomère comporte une chaîne alkyle, l'espaceur, entre chaque résidu de phénylalanine. Or, dans les deux cas, le nombre de groupes aromatiques pour l'établissement d'interactions $\pi-\pi$ est identique. En revanche, le nombre d'interactions de type liaisons hydrogène pouvant potentiellement s'établir avec la surface du Kevlar est supérieur dès lors que l'oligomère contient un espaceur (implication des acides ω -azidoalcanoïques). En revanche, aucune différence significative d'adsorption n'est mesurée que l'oligomère soit doté d'un espaceur butyrique ou d'un espaceur hexyle. En revanche, le cas de l'espaceur valérique, présente une adsorption plus importante en surface des fibres de Kevlar (accroissement d'un facteur six par rapport à la référence). Or, ces trois oligomères présentent un nombre identique de fonctions à impliquer dans une interaction de type liaison hydrogène. En revanche, la conformation des oligomères diffère : soit ceux-ci comportent un espaceur alkyle constitué d'un nombre pair de groupes méthylène (cas de l'espaceur valérique), soit ils comportent un nombre impair de méthylènes (cas de l'espaceur butyrique ou hexyle). Il en résulte que la conformation pourrait être le paramètre d'influence. Concernant l'ajout de l'amine propargylique, elle est sans effet sur l'adsorption de l'oligomère testé.

Dans le cas des oligomères constitués de quatre résidus de phénylalanine par cycle réactionnel, la fraction molaire adsorbée est supérieure à celle mesurée pour une tétraphénylalanine (d'un facteur compris entre 1,5 et 2) et inférieure à celle décrite pour les oligomères constitués d'un résidu phénylalanine par cycle réactionnel. La nature de l'espaceur ne montre dans ce cas pas d'influence significative sur cette adsorption sur la fibre d'aramide.

Conclusion

Les objectifs de ce travail doctoral ont été d'une part de synthétiser une librairie d'oligomères de compositions et séquences prédéfinies, d'autre part de les utiliser en tant qu'agent interfacial entre des fibres de Kevlar et une matrice aliphatique. La comparaison avec des oligomères modèles commerciaux, permet d'établir que l'ajout d'un espaceur alkyle entre les résidus phénylalanine conduit à une adsorption supérieure au cas sans espaceur. Il est donc fort probable que le processus d'adsorption soit dicté par des interactions supramoléculaires et soit fortement dépendant non seulement de la quantité des interactions mais également des degrés de liberté de la molécule adsorbée. L'agent interfacial dont le dépôt à la surface des fibres d'aramide est le plus important est FvFvFvFv. Des tests préliminaires de fractographie basse température d'une matrice polyoléfine renforcée de fibres de Kevlar traitées en surface par un oligomère FFFFv●FFFFv●FFFFv●FFFFv ont montré que malgré le caractère non covalent de l'interaction entre l'oligomère et la fibre, le revêtement restait présent sur le matériau fibreux. En revanche, les premiers essais de déchaussement d'une fibre unique ne montrent pas d'amélioration de la contrainte de cisaillement entre une fibre de

Kevlar portant le traitement de surface précédemment mentionné comparée à une fibre de Kevlar nue.

Références

- [1] Règlement (CE) n °443/2009, JO L140 du 05.6.2009, p. 1-15
- [2] J.-M. Berthelot, Composite Materials, Mechanical behavior and structural analysis, Springer, New-York **1999**
- [3] Dupont de Nemours, Kevlar aramid fiber technical guide, H77848 4/00 USA
- [4] a) J.-F. Lutz *Macromol. Rapid Commun.* **2017**, *38*, 1700582; b) S. C. Solleder, R. V. Schneider, K. S. Wetzal, A. C. Boukis, M. A. R. Meier *Macromol. Rapid Commun.* **2017**, *38*, 1600711
- [5] D. Chan-Seng, J.-F. Lutz *ACS Macro Lett.* **2014**, *3*, 291
- [6] a) J. Holbery, D. Houston *JOM* **2006**, *58*, 80; b) C. Soutis *Prog. Aerosp. Sci.* **2005**, *41*, 143
- [7] C. E. Bakis, L. C. Bank, V. L. Brown, E. Cosenza, J. F. Davalos, J. J. Lesko, A. Machida, S. H. Rizkalla, T. C. Triantafillou *J. Compos. Constr.* **2002**, *6*, 73
- [8] a) H.-Y. Cheung, M.-P. Ho, K.-T. Lau, F. Cardona, D. Hui *Composites, Part B* **2009**, *40*, 655; b) M.-S. Scholz, J. P. Blanchfield, L. D. Bloom, B. H. Coburn, M. Elkington, J. D. Fuller, M. E. Gilbert, S. A. Muflahi, M. F. Pernice, S. I. Rae, J. A. Trevarthen, S.C. White, P. M. Weaver, I. P. Bond *Compos. Sci. Technol.* **2011**, *71*, 1791
- [9] C. Zweben *JOM*, **1998**, *50*, 47
- [10] M. J. N. Jacobs, J. L. J. Van Dingenen *J. Mater. Sci.* **2001**, *36*, 3137
- [11] J.-K. Kim, Y.-W. Mai, Y.-W. Mai *Engineered interfaces in fiber reinforced composites*, Elsevier, **1998**
- [12] P. J. Herrera-Franco, L. T. Drzal *Composites* **1992**, *23*, 2
- [13] R. Li, L. Ye, Y.-W. Mai *Composites, Part A* **1997**, *28*, 73
- [14] a) S. Shokoohi, A. Arefazar, R. Khosrokhavar *J. Reinf. Plast. Compos.* **2008**, *27*, 473; b) H. F. Wu, D. W. Dwight, N. T. Huff *Compos. Sci. Technol.* **1997**, *57*, 975
- [15] Z. Wu, J. Li, C. Huang, L. Li *Phys. Procedia* **2015**, *67*, 1068
- [16] J. S. Kim, D. H. Kim *J. Thermoplast. Compos. Mater.* **2015**, *28*, 1599
- [17] Z. Denchev, N. Dencheva in *Synthetic polymer-polymer composites*, Eds D. Bhattacharyya, S. Fakirov, Hanser, **2012**, 251
- [18] J.-F. Lutz, *Sequence-controlled polymers*, Wiley, **2018**
- [19] F. Hanßke, E. Kemnitz, H. G. Börner *Small* **2015**, *11*, 4303
- [20] a) F. Hanßke, O. Bas, C. Vaquette, G. Hochleitner, J. Groll, E. Kemnitz, D. W. Hutmacher, H. G. Börner *J. Mater. B* **2017**, *5*, 5037; b) V. Samsoninkova, B. Seidt, F. Hanßke, W. Wagermaier, H. Börner *Adv. Mater. Interfaces* **2017**, *4*, 1600501
- [21] J.-F. Lutz, M. Ouchi, D. R. Liu, M. Sawamoto *Science* **2013**, *341*, 1238149
- [22] E. Kaiser, R.L. Colescott, C.D. Bossinger, P. I. Cook *Anal. Biochem.* **1970**, *34*, 595

- [23] a) M. W. Pennington, I. Zaydenberg, M. E. Byrnes, R. S. Norton, W. R. Kern *Int. J. Pept. Protein Res.* **1994**, *43*, 463; b) A. Thaler, D. Seebach *Helv. Chim. Acta* **1991**, *74*, 617
- [24] R. C. L. Milton, S. C. F. Milton, P. A. Adams *J. Am. Chem. Soc.* **1990**, *112*, 6039
- [25] P. Seneci *Solid-phase synthesis and combinatorial technologies*, Wiley, **2000**
- [26] a) M. Reches, Y. Porat, E. Gazit *J. Biol. Chem.* **2002**, *277*, 35475; b) M. Pellach, S. Mondal, L. J. W. Shimon, L. Adler-Abramovich, L. Buzhansky, E. Gazit *Chem. Mater.* **2016**, *28*, 4341; c) E. Mayans, J. Casanovas, A. M. Gil, A. I. Jimenez, C. Cativiela, J. Puiggali, C. Aleman *Langmuir* **2017**, *33*, 4036

Table of contents

List of abbreviations	1
General introduction	5
Chapter I: Fibre-reinforced composite materials and sequence-controlled polymers	13
1. Fibre-reinforced composite materials.....	13
1.1. Towards Kevlar fibre-reinforced composite materials	13
1.1.1. Polymer matrices	13
1.1.2. Reinforcement fibres	14
1.1.3. Commercial applications for aramid fibre-based products	17
1.1.4. Fibre structure in matrix material.....	17
1.1.5. Aramid fibre-reinforced materials: Examples of different matrices.....	19
1.1.6. Conclusion.....	21
1.2. Parameters influencing the composite material performance	21
1.2.1. Rule of averages.....	21
1.2.2. Slab theory	22
1.2.3. The two body interface region of fibre-reinforced composite material	22
1.2.4. Conclusion.....	24
1.3. Optimisation of the interface region in aramid fibre-reinforced composite materials	24
1.3.1. Introduction	24
1.3.2. Modification of aramid fibre.....	25
1.3.3. Chemical treatments of polymer matrices	30
1.3.4. Usage of compatibilizer molecules (three-body interface)	35
1.3.5. Conclusion.....	38
2. Sequence-controlled polymers	39
2.1. Catalyst-induced control of the sequence	39
2.2. Kinetically regulated monomer insertion.....	41
2.3. Sequential chain copolymerisation	43

2.4. Single monomer insertion in chain growth polymerisation.....	44
2.5. Template chemistry.....	47
2.6. Sequence control via monomer design.....	51
2.7. Solid-supported iterative synthesis.....	54
2.8. Beyond solid phase iterative synthesis	55
2.9. Impact of sequence control on polymer properties	58
Chapter II: Preparation and characterisation of oligomers based on phenylalanine and aliphatic building blocks by solid-phase synthesis	74
1 Introduction.....	63
2. Synthesis of phenylalanine-based oligomers	65
2.1. Description of the synthetic strategy used	65
2.2. Synthesis of ω -azidoalkanoic acids.....	66
2.3. Preliminary synthesis of a library of phenylalanine-based oligomers	68
3. Attempts to optimize the synthesis of phenylalanine-based oligomers.....	74
3.1. Tools to monitor the reaction steps.....	74
3.1.1. Kaiser test.....	74
3.1.2. FT-IR spectroscopy	74
3.2. Approaches to improve reaction efficiency	75
3.2.1. Identification of the approaches of interest	75
3.2.2. Results	77
3.2.3. Oligomers synthesised using the optimised conditions.....	82
4. Characterisation of the synthesised phenylalanine-based oligomers	83
4.1. Example of FFFFv•FFFFv•FFFFv•FFFFv	83
4.1.1. Results of ^1H NMR spectroscopy.....	83
4.1.2. Results of ^{13}C NMR spectroscopy.....	84
4.1.3. Results of 2D NMR spectroscopy	85
4.1.4. Results of mass spectrometry	87
4.2. Evaluation of impurities potentially attributed to the use of a Tentagel [®] resin by ^1H NMR spectroscopy	90

4.3. Summary on all the phenylalanine-based oligomers synthesised from a Tentagel® resin....	91
5. Attempts at purifying the synthesised oligomers	93
5.1. Identification of the potential techniques for the purification of the oligomers	93
5.2. Evaluation of the solvent miscibility of synthesised oligomers	93
5.3. Analysis of some oligomers by HPLC.....	96
6. Summary and future outlooks.....	97
6.1. Prospects of optimizing synthesis	97
6.2. Prospects of purification	99
Chapter III: Evaluation of the synthesised oligomers as potential interfacial agents for Kevlar fibre-reinforced polypropylene materials	114
1. Introduction.....	103
2. Thermal stability.....	105
2.1. Thermogravimetric analysis of the molecules considered.....	106
2.2. Pyrolysis GC-MS results of the synthesised oligomers.....	107
2.3. Differential scanning calorimetry analysis	109
2.4. Concluding remarks.....	109
3. Coating procedures	110
3.1. Dip coating.....	110
3.2. Spray coating.....	111
4. Preliminary SEM/EDS studies	112
4.1 SEM/EDS studies: introduction	112
4.2. Preparation of substrate	113
4.3. Angle and morphologies effect	113
4.4. Determination of coating solution concentration and influence of spray coating.....	115
5. SEM/EDS qualitative analysis of dip and spray coating.....	116
5.1. Dip coating results.....	116
5.1.1. Dip coating of commercial molecules affording the distinction between hydrogen bonding and π interactions	116
5.1.2. Dip coating of oligomers with single phenylalanine unit per block.....	120

5.1.3. Dip coating of oligomers with four phenylalanine units per block	123
5.2. Spray coating	124
5.2.1. Spray coating of commercial molecules	125
5.2.2. Spray coating of oligomers with a single phenylalanine unit per block.....	127
5.2.3. Spray coating of oligomers with four phenylalanine units per block	128
5.3. EDS analysis of fibre surface.....	129
5.3.1. Untreated aramid fibre	130
5.3.2. Coating molecule compounds.....	130
5.3.3. Treated fibres.....	131
5.4. Conclusion	132
6. Preliminary quantification of coatings	132
6.1. Quantification by EDS.....	133
6.2. Quantification by gravimetry using fibre bundles.....	133
6.3. Quantification by UV-visible spectroscopy	135
6.3. Discussion and conclusion.....	136
7. Quantification by gravimetry using fibre pellets.....	136
7.1. Dip coating procedure using fibre pellets	137
7.2. Dimensional considerations	137
7.3. Drying process evaluation	139
7.4. Preliminary quantification tests	140
7.5. Quantitative analysis of coating behaviour of GGGG	142
7.5.1. Concentration effect	142
7.5.2. Time effect	143
7.6. Results of quantification of coating performed on fibre pellets.....	144
7.6.1. Quantification of coating behaviour commercial molecules affording the distinction between hydrogen bonding and π interactions	145
7.6.2. Quantification of coating behaviour for oligomers with a single phenylalanine unit per block.....	145

7.6.3. Quantification of coating behaviour for oligomers with four phenylalanine units per block.....	146
7.6.4. Relative comparison of coating behaviour	146
8. Preliminary results composites	147
8.1. Fracture test results	147
8.1.1. Protocol	149
8.1.2. Blank aramid fibre in matrix.....	148
8.1.3. FFFFv•FFFFv•FFFFv•FFFFv coated SFA A fibre in PP	148
8.2. Pullout test results	151
8.2.1. Protocol	151
8.2.2. Comparison pullout test FFFFv•FFFFv•FFFFv•FFFFv treated vs untreated aramid fibre in matrix.....	151
9. Interpretation of the results.....	150
9.1. Description of coating processes	150
9.1.1. Dip coating	150
9.1.2. Spray coating.....	151
9.1.3. Discussion.....	153
9.2. Physical models for diffusion of particles into fibrous media	154
9.2.1. Discussion.....	156
10. Summary	156
Conclusion	170
Experimental section	176
1. Materials.....	165
2. Characterisation	166
3. Synthesis of azidoalkanoic acids.....	169
4. Synthesis of macromolecules based on phenylalanine and aliphatic building blocks using a CTC resin.....	169
i) General procedure for functionalizing CTC resin	169
ii) Addition of 6-azidohexanoic acid.....	170

iii) Copper-assisted alkyne-azide cycloaddition with propargylamine	170
iv) Addition of Fmoc-L-Phe-OH	170
v) Cleavage from the resin and recovery of the phenylalanine-based oligomer.....	170
5. Cleavage of Fmoc-protected phenylalanine from Tentagel® resin.....	174
6. Synthesis of macromolecules based on phenylalanine and aliphatic building blocks using a Tentagel® resin.....	174
i) Deprotection of functionalised Tentagel® resin.....	174
ii) Addition of 6-azidohexanoic acid.....	175
iii) Copper-assisted alkyne-azide cycloaddition with propargylamine	175
iv) Addition of Fmoc-L-Phe-OH	175
v) Cleavage from the resin and recovery of the phenylalanine-based oligomer.....	175
7. Preparation of aramid fibre pellet	178
8. Procedures for the coating process of aramid fibre bundles.....	178
i) Spray coating procedure	178
ii) Dip coating procedure.....	178
9. Procedure for the coating process of aramid fibre pellets	179
10. Preparation and analysis of samples with SEM/EDS.....	179
i) Preparation of compounded samples from powder material	179
ii) Preparation of treated fibre samples.....	179
iii) Preparation of fibre/PP composite	179
11. Preparation of samples for analysis by UV-Vis.....	180
i) Determination of the baseline formula	180
ii) Procedure for measuring deposited coatings.....	180
Appendix A: Thermal analysis	182
A.1. Overview of thermogravimetric results.....	182
A.2. Overview of differential scanning calorimetry results.....	185
Appendix B: EDS analysis	188
B.1. Short aramid fibre	188

B.2. Coating compounds	189
B.3. Dip coated fibres using a solution at $1 \mu\text{mol}\cdot\text{mol}^{-1}$	194
B.4. Spray coated fibres using a solution at $0.01 \text{ mmol}\cdot\text{mL}^{-1}$	200
Appendix C: Adsorption data of concentrations of coating molecules onto the Kevlar fibre pellet surface	205
C.1. Adsorption behaviour of GGGG with variable concentration	206
C.2. Adsorption behaviour of GGGG with variable time	207
C.3. Quantification of coating behaviour commercial molecules	207
C.4. Quantification of coating behaviour oligomers with single phenylalanine unit	208
C.5. Quantification of coating behaviour oligomers with four phenylalanine units	209
References	210
Scientific production	226

List of abbreviations

ACN	acetonitrile
AFM	atomic force microscopy
ATRP	atom transfer radical polymerisation
b	4-azidobutyric acid spacing unit
BHT	butylhydroxytoluene
d	doublet
dd	doublet of doublets
CTC	2-chlorotriylchloride
CuAAC	copper-catalysed alkyne-azide cycloaddition
DCM	dichloromethane
DIPEA	<i>N</i> -ethyl-diisopropylamine
DMA	dynamic mechanical analysis
DMF	<i>N,N</i> -dimethylformamide
DSC	differential scanning calorimetry
EDS	energy dispersive X-ray spectroscopy
ESI	electrospray ionisation
e	7-azidoheptanoic acid spacing unit
eq	equivalent
F	phenylalanine
FFFF	tetraphenylalanine
G	glycine
GGGG	tetraglycine
Fmoc	fluorenylmethyloxycarbonyl
For	Forward similarity
FRCM	fibre-reinforced composite material
FT-IR	Fourier transform infrared
g	gram
GC-MS	gas chromatography-mass spectrometry
h	6-azidohexanoic acid spacing unit
HBTU	3-[bis(dimethylamino)methyl]imidazolium-3- <i>H</i> -benzotriazol-1-oxide hexafluorophosphate
HDPE	high-density polyethylene
HOBt	1-hydroxybenzotriazole
HPLC	high performance liquid chromatography
Hz	hertz
J	coupling constant
IR	infrared
m	multiplet or mass
MALDI	matrix-assisted laser desorption/ionisation
Me	methyl
MHz	megahertz
MS	mass spectrometry
MTDSC	modulated temperature differential scanning calorimetry

M	molecular mass
m/z	mass-to-charge ratio
NIST	National Institute of Standards and Technology
NMP	<i>N</i> -methyl-2-pyrrolidone
NMR	nuclear magnetic resonance
Ph	phenyl
F	phenylalanine
PEG	poly(ethylene glycol)
PMDETA	<i>N,N,N',N',N''</i> -pentamethyldiethylenetriamine
PP	polypropylene
ppm	parts per million
PS	polystyrene
PSA	<i>Peugeot Société Anonyme</i>
PTFE	poly(tetrafluoroethylene)
Rev	Reverse similarity
RAFT	reversible addition-fragmentation chain transfer
ROMP	ring-opening metathesis polymerisation
RT	room temperature
s	singlet
SEM	scanning electron microscopy
SPE	solid phase extraction
SPS	solid phase synthesis
SPPS	solid-phase peptide synthesis
t	triplet
TBAB	tetrabutylammonium bromide
TFA	trifluoroacetic acid
T _g	glass transition temperature
TGA	thermogravimetric analysis
TOF	time-of-flight
u	11-azidoundecanoic acid spacing unit
v	5-azidovaleric acid spacing unit
z	amount of charges present in mass spectrometry ion
XPS	X-ray photoelectron spectroscopy
●	triazole unit
δ	chemical shift
®	registered trademark
™	trademark

GENERAL INTRODUCTION

The automobile industry is under continuous pressure to improve not only the environment friendly quality of their products, but to help reduce emissions (particularly CO₂) as well. Emissions of automotive vehicles are strictly regulated by laws imposed by the European Union and the current regulation is Regulation (EC) No 443/2009 of the European Parliament and of the Council of 23 April 2009 “Setting emission performance standards for new passenger cars as part of the Community's integrated approach to reduce CO₂ emissions from light-duty vehicles” [G.1]. Several automobile manufacturers, excluding PSA Groupe, exceed the legally imposed limit and are obliged to pay UNECE a hefty fine. This is why, not only for environmental concern, but also economic concerns, it is very important for the enterprise and others like it to (continue to) adhere to these regulations.

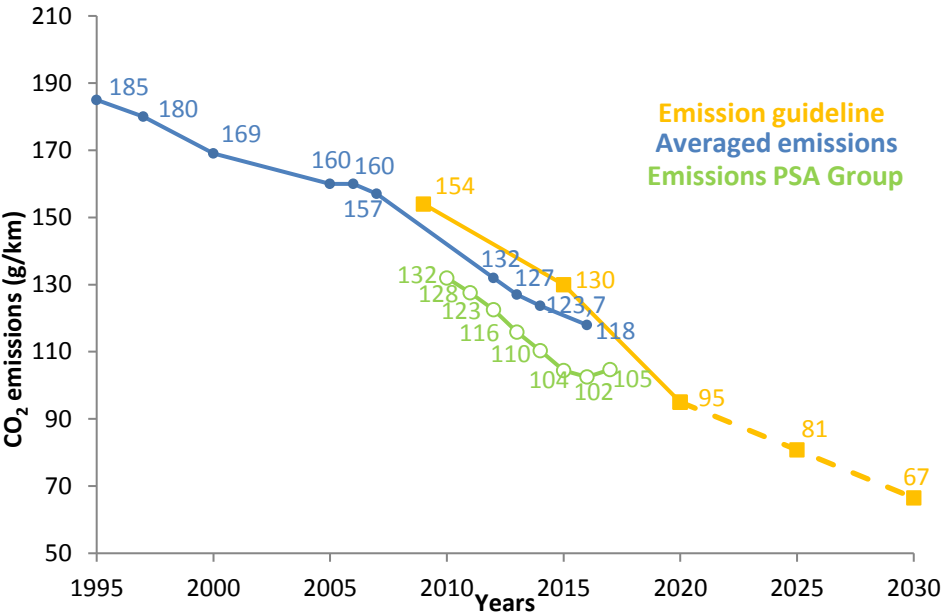


Figure G.12: Maximum CO₂ emission values for light vehicles imposed (yellow squares) average emissions recorded (blue circles) and emissions recorded for PSA groupe (green open circles). The imposed guideline values for 2025 and 2030 have not yet been explicitly communicated by the EU [G1-G3].

While progresses have been rapidly made owing alternative energy sources, such as hydrogen fuel cells and novel batteries based on lithium technologies, [G.4-G.5] low emissions should be assured regardless of the energy transport. For this content the mass decrease of the vehicle is an essential factor. According to a report of John Heywood more than 50% of the weight of light vehicles in 2006 consists of metals [G.6]. As can be seen in **Figure G.2**, the metals in a car are mostly steel, but also lighter metals like aluminium. These metals make up a large part of the essential car framework, the chassis. The metals function as load bearing components, showing needed mechanical properties like tensile strength, have a long lifetime owing to its low creep and additionally maintain the Faraday cage of the vehicle. However, owing to the large density of steel (ca. 7.8 kg·m⁻³) [G.7], metallic parts in the vehicle are attractive to be replaced by composite materials showing similar properties, yet decreased density.

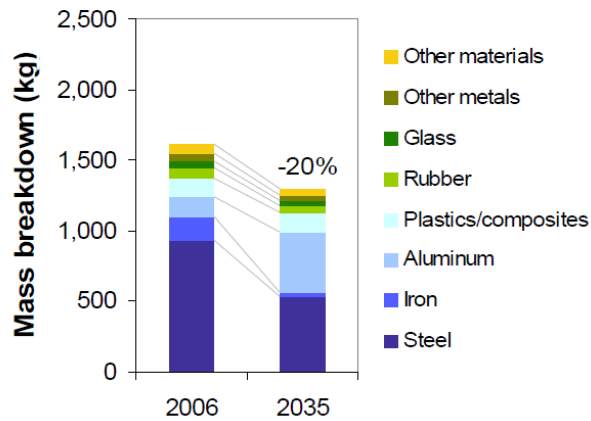


Figure G.2: Materials used in average light vehicles in 2006 and the projected expected use in 2035 [G.6].

Nowadays, polymer composite materials are widely applied in industry. By mixing in two compounds with different characteristics via for example compounding or moulding a material can be made with tailored mechanical, thermal and chemical properties, forming a composite material. One class of such composite materials is fibre-reinforced polymers of which carbon fibre-reinforced polymers are an example. This composite material consists of rigid fibres and a flexible polymer matrix such as polyester or polyamide, and can find itself applied structurally for various industries. Composite material can also be found in nature as, for example, wood and bone, with wood making use of cellulose fibres in a matrix of lignin [G.8]. Commonly applied in construction in the past, asbestos also belongs in this category [G.9].

PSA Groupe employs a specific strategy for weight reduction. The body in white (BiW) structure consists of multiple small parts (**Figure G.3**), each of them providing a specified need in mechanical properties. When researching the degree of utility of a new composite material, their properties can be compared with existing parts in a BiW and depending on similarity, replace them. At the moment, the only limit is the group’s own policy to not use composite material in parts that would absorb energy by ruin, as this would require additional predictive simulations.



Figure G.3: 3008 series Peugeot automobile: a) finished car, b) its BiW, partially incorporating fibre-reinforced material in the metal framework, and c) coloured image of the same BiW to represent different structural parts (red: steel, green: aluminium)[G.10-G.11].

PSA Group has already attempted this strategy by replacing the A51 side impact beam, part of the door structure (**Figure G.4**). The composite material used in this case is a commercial product called Vizilon SB63G1, which is a composite material produced by DuPont made of continuous glass fibres in polyamide 6,6 [G.12].



Figure G.4: The A51 side impact beam, as seen in the door structure of a Citroën C3 [G.13].

The application of composite materials is in theory limited by three factors: 1) the mechanical properties of a fibre, 2) the efficiency at which the resin can transfer load to a fibre and 3) the manufacturing costs. Therefore, in order to research the application of new composite material, all three of these factors must be taken into consideration. The first and latter point may be optimised by careful selection of material and production methods of the material itself. In particular, carbon fibres provide a high elastic resistance, with a Young elastic modulus (E_{CF}) of 240 GPa, trumping steel's modulus of 210 GPa and additionally provide a satisfactory tensile breaking stress (σ_{CF}) of 5 GPa versus ultra high strength steel's 2 GPa. However, carbon fibres are fragile and owing to the breaking strain ($\epsilon_{CF} < 1\%$) allow five times less deformation at break than ultra high strength steel ($\epsilon_S < 5\%$). Due to this final property, energy dissipation during an impact cannot be properly managed with carbon fibres. In comparison, aramid fibres provide an increased breaking strain (ϵ_{KF} ca. 3%) [G.7, G.14-G.15]. However, the second point in particular is dependent on not only the composite engineering process but also the physical and chemical properties of the two components. Therefore, in order to further increase the application possibilities of composite materials, steps have to be taken to optimise these properties via different physiochemical toolboxes. In particular, the key for obtaining ideal force transfer of fibre into polymer matrix material may be found in homogenising the surface tension at the interface. Unfortunately, current composite optimisation techniques are limited in scope, modifying these surface tension values in a crude fashion, via uncontrolled grafting and etching techniques.

An alternative approach is found in the application of interfacial agents, which function as a load transferring bridge between the reinforcement fibres and the ductile matrix, where molecular similarity with both parts allows an efficient gradient. These molecules are typically designed to bind covalently, being grafted on the fibre surface. While promising, this approach is one of trial and error, where the grafting procedure provides little information about the interactive properties between

interfacial agent and composite material parts as typically only the end result of composite mechanical properties is measured.

In this thesis a novel approach is proposed where these interfacial agents are designed from the ground up to function in a supramolecular fashion. In this way, specific interactive properties can be designed for full optimisation of the composite interface. As a proof of concept, particular highlight is given to a fibre-matrix system traditionally complicated to manufacture owing to a lack of supramolecular interactions: Kevlar® (aramid) fibre in polypropylene, a commonly used inexpensive polymer matrix in the automotive industry.

In **Chapter I**, the bibliographic background is given on the usage of fibre-reinforced composite materials (FRCM). Discussed are types of matrix materials, reinforcing fibres along with their effects on mechanical properties and at last real world examples of FRCM. Specific focus is given on aramid FRCM. Then, an overview is shown regarding the mechanical parameters of FRCM and the main area of interest: the interface region. Subsequently, optimisation techniques are given, including common etching and covalent grafting techniques on either the fibre or matrix material as well as commonly used analytical techniques. Finally, the three-body system is introduced, where the interface region is controlled with interfacial agents, in particular compatibilizer molecules. Owing to the need of control over the molecular structure when designing novel compatibilizers, a brief overview is given on the efforts on sequence control in polymer and oligomer molecules, including sequence control via catalyst properties, kinetic effects, single monomer insertion techniques, template based techniques, specific monomer design and finally iterative synthesis, including solid phase iterative syntheses and multicomponent reactions. Briefly, the effects of sequence control over oligomer and polymer properties are given.

In **Chapter II**, the synthetic procedure of sequence-controlled oligomers as compatibilizer molecules is described. For this, a solid-phase iterative synthesis similar to classic solid-phase peptide synthesis is chosen, which permits efficient workup between reaction steps and highly selective construction of oligomers. Reactants were specifically chosen to interact with the aramid fibre surface, *i.e.* phenylalanine and allow for compatibilization with the matrix of choice, *i.e.* aliphatic chains for a polypropylene matrix. Preliminary syntheses were not sufficient to obtain the oligomers in high purity, with notable deletion steps as indicated by nuclear magnetic resonance (NMR) spectroscopy and mass spectrometry (MS) analyses. For this reason, the adapted procedure had to be modified, of which several approaches were given in combination with monitoring of coupling reactions using the Kaiser test [G.16] to visualise coupling efficiency. Explored are the use of aggregate disruptors, preactivation of the reagents and changes in reaction conditions including concentration and solvent usage. Finally, the modification of the used solid phase resin led to an improvement in reaching lower dispersities, as

identified by NMR, MS and HPLC techniques. Despite this, the presence of unknown purities was still found, which were catalogued and may be a result of the used conditions. Additionally, owing to the limited solubility of the synthesised oligomers, an overview is given of workable solvents. Finally, several techniques are proposed to further increase the purity and efficiency of the used synthetic techniques.

In **Chapter III**, the application of the synthesised sequence-controlled oligomers as coatings for aramid fibres using adapted common industrial coating techniques (dip and spray coating) was described and compared to commercial products. Discussed are qualitative morphology differences which were analysed using scanning electron microscopy/energy dispersive X-ray spectroscopy (SEM/EDS), with noticeable differences in quantity, surface roughness, wettability of the fibre surface, and presence of (cracked) film and droplet shapes depending on the molecule chosen for coating as well as the coating method. For quantitative analysis, various methods were explored to determine the influence of the molecular structure of the oligomer on adsorption, including EDS, ultraviolet-visible light (UV-Vis) spectroscopy and quantification of mass differences. The latter technique proved successful as an analytical technique provided specific precautions were taken regarding the aramid sample preparation. Dimensional parameters such as the influence of the drying process, concentration and time were discussed. Finally, a relative comparison was given of adsorption of chosen molecules.

Lastly, the molecules were subjected to thermal analysis and preliminary measurements on treated fibres in polypropylene matrix are given as a perspective.

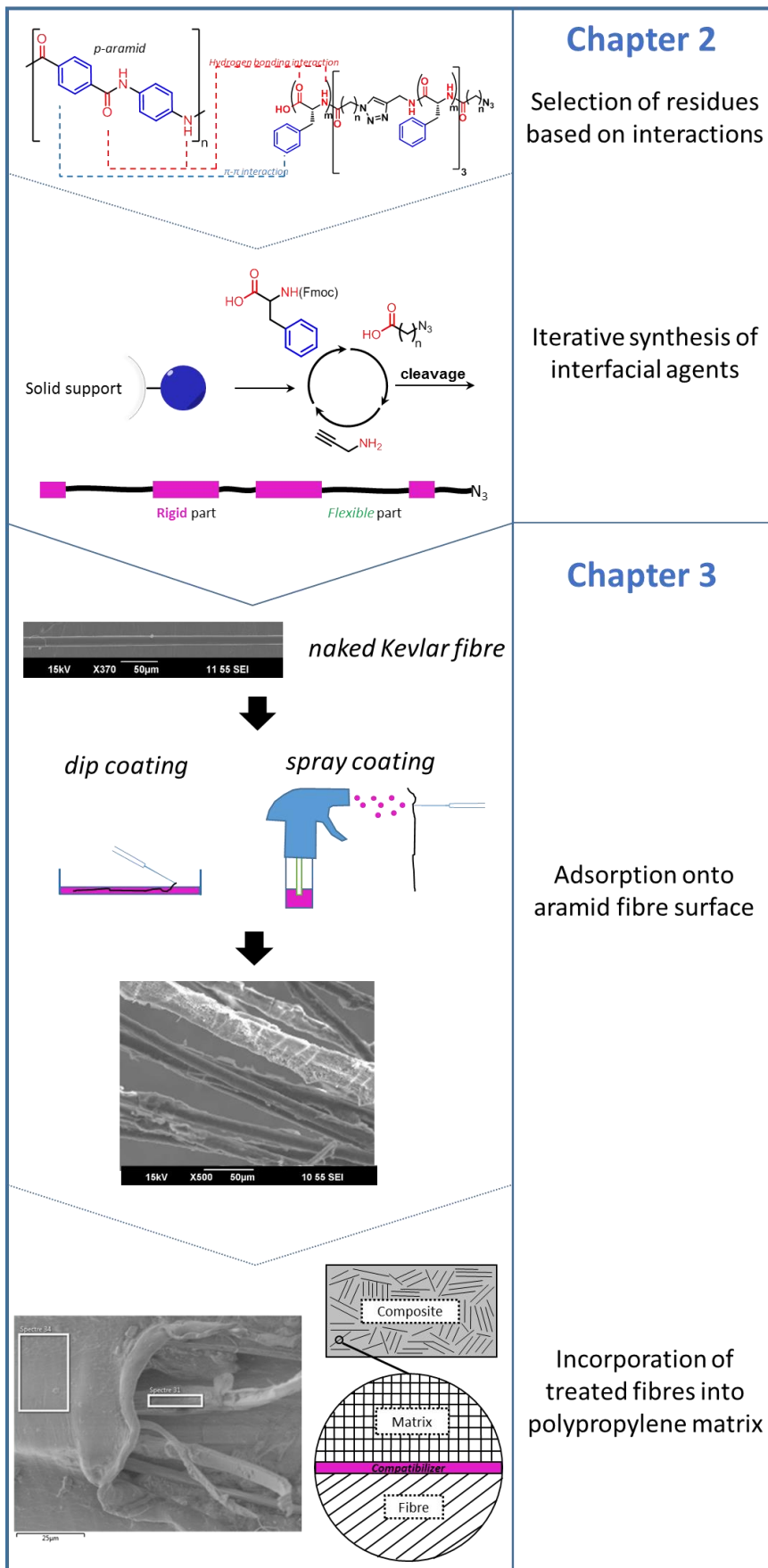


Figure G.5: An overview of the different aspects of the thesis

CHAPTER I

Fibre-reinforced composite materials and
sequence-controlled polymers

1. Fibre-reinforced composite materials

1.1. Towards Kevlar fibre-reinforced composite materials

A composite material is a mixture of at least two materials which leads to improvement in properties (e.g. mechanical, thermal, electrical) as compared to those materials used alone. With the exception of blends, composites consist of two indicative parts: embedding matrix and reinforcement. The reinforcing material such as particles and fibres provides strength and stiffness that the matrix by itself does not possess. While reinforcement fibres (glass, carbon and aramid) of known parameters (length and diameter depending on the manufacturing qualities) is the main load bearing component, the continuous matrix phase (usually polymers due to their low manufacturing cost, density and properties [1.1]) performs several critical functions, including keeping the location of the fibres intact as well as protecting them against environmental factors (heat, abrasion, light, etc.). Fibre-reinforced composite materials (FRCMs) are widely used in civil engineering, spacecraft, aircraft, and automotive industry to name a few. The sections below will describe the different elements of FRCMs, focusing especially on aramid fibres.

1.1.1. Polymer matrices

Two forces which largely influence load transfer and morphology of the interfacial structure of a FRCM are shear forces and other mechanical forces transversal to the fibre direction. In order to choose suitable matrix material for a certain application, several factors have to be considered including 1) mechanical properties, 2) thermal, chemical and wear resistant properties, 3) raw material and production costs, and 4) whether thermoplastics or thermosets are preferred. **Table I.1** summarises the most common polymer matrices used for FRCMs along with some of their characteristics and price range.

Table I.1: Characteristics of common polymer matrices used in FRCM [1.2-1.4].

Polymer matrix	Type	Young's modulus (GPa)	Tensile strength (GPa)	Density (g·cm ⁻³)	Price range estimate (€·kg ⁻¹)
Poly(acrylonitrile-butadiene-styrene)	Thermoplastic	1.10-2.90	0.03	1.10	1.50-4.50
Polyamide 6	Thermoplastic	2.60-3.20	0.04	1.13	4.50
Polyamide 6,6	Thermoplastic	2.60-3.20	0.06	1.13	4.50
Polycarbonate	Thermoplastic	2.00-2.44	0.05	1.18	6.00
Polypropylene	Thermoplastic	0.90-1.55	0.03	0.90	1.20-1.40
Epoxy	Thermoset	2.35-3.10	0.60	1.30	4.50-6.00
Unsaturated polyester	Thermoset	2.10-4.41	0.28	1.20	1.50

The main difference between thermoplastics and thermosets is whether the ability to melt the polymer into a viscous matrix for the formation of shapes is possible (thermoplastics) or the material is set into a certain shape by curing beforehand and will no longer be able to be liquefied (thermoset). A notable exception to this are vitrimers in which covalently bound crosslinks in a polymer network are

temperature controlled, leading to malleability despite initial thermoset like behaviour [I.5]. One example of both a thermoplastic and a thermoset will be used to discuss their advantages and drawbacks.

One example of thermoset is epoxy resins. Often applied in aerospace and military industries, epoxy resins are a popular choice for the ability to reach relatively high mechanical properties such as tensile modulus (**Table I.1**). Depending on the molecular structure of the precursor and hardener, the properties can start to resemble those of more common thermoplastics or can be completely tuned for varying degrees of functionalisation post-polymerisation or thermal and solvent resistibility. Furthermore, the manufacturing process of epoxy resins and similar thermosets allows to avoid the use of heating steps [I.6]. Despite the large amount of customisation possible with epoxy resin, the pricing is increased [I.4]. For this reason, polymers like unsaturated polyesters, more attractive in performance to cost ratio, are typically used in the automotive industry, with expected average annual compound rate of 5.3% between 2016 and 2021 [I.7].

Depending on the application, a higher degree of ductility may be desired, which may be difficult to achieve with thermosets and requires using thermoplastics. Polypropylene (PP) lends itself particularly convenient as matrix material for several reasons. The pricing is attractive for industry [I.4]. The ductility of the material is ideal for introducing shock absorbance into the composite, as is evident from its elongation to break (100-600%) [I.2]. As it is an aliphatic chain, the hydrophobicity is particularly high and the density can be as low as $0.9 \text{ g}\cdot\text{cm}^{-3}$ [I.2]. Additionally, the melting point is between 160 and 190 °C depending on the quality and crystallinity, making it easy to melt for injection moulding purposes and well within the standard range of operating temperatures of vehicles (-40 to 110 °C) [I.2]. The ductility of PP is partially derived from its semi-crystalline properties that become vitally important in the process of manufacturing composite material [I.8].

1.1.2. Reinforcement fibres

The reinforcement fibre is the main load-bearing component of a continuous fibre-reinforced composite. In order to choose suitable fibre material for a certain application, several factors have to be considered: 1) mechanical properties, of which high tensile strength is an important factor, 2) lifetime of the fibre (creep), 3) thermal, chemical and wear resistant properties, including brittleness, 4) raw material and production costs, and 5) density. **Table I.2** describes high mechanical performance reinforcement fibres and their properties.

Table I.2: Selected reinforcement fibres with given mechanical properties [I.9-I.19].

Reinforcement fibre	Young's modulus (GPa)	Tensile strength (GPa)	Density (g·cm ⁻³)
Basalt	89	4.50	2.60-2.80
Boron	365-440	3.60-4.00	2.48-2.82
Carbon (HS)	230	3.30	1.79
Glass (E)	69-72	3.10	2.54
<i>p</i> -aramid (Kevlar® 49)	135	3.60	1.44
<i>m</i> -aramid (Nomex®)	3.13*	0.31	0.72-1.13
Oriented HDPE	109-132 ²	1.96 ¹	0.97 ¹

¹Honeywell Spectra® 1000, ²Dyneema SK76, * Nomex® paper

The most commonly used reinforcement fibre for composites is glass. Among them, E-glass has become the industrial standard, accounting for more than 90% of all glass fibre reinforcements in commercial composites. Its composition is mostly of alumina-borosilicate glass with minute amounts of alkali oxides. Furthermore, glass surface is relatively easy to treat chemically for varying functionalisation. Although glass fibres show good resistance to several organic solvents, it will erode through exposure to water. For this reason, glass fibres are coated by a protective layer during production [I.20].

Other inorganic fibres are boron and basalt fibres. Boron fibres are produced by chemical vapour deposition processes in which elemental boron is deposited onto carbon or tungsten filaments. These fibres can show increased tensile properties in comparison to glass or carbon fibres with varying density. Basalt fibres are mineral-based fibres with good chemical resistance and mechanical properties that are similar to glass fibres [I.20].

A second popular reinforcement fibre is carbon fibre, produced by a variety of precursors of which polyacrylonitrile is the most common. Providing strong resistance to outside factors, it shows the highest mechanical properties in the fibre direction. Carbon fibres are electrically conductive, which can be a desired property in some composite applications. It complicates its use as any metals in contact with the fibre may corrode over time [I.20]. Although carbon fibres are popular for their mechanical properties on markets for which the cost is not the key parameter, improvement in the fibres is hindered by their relative inertness and lack of flexibility.

Aramid fibres in particular are fibres with excellent mechanical properties relative to a low density. The name itself is a shortened version of aromatic polyamide which are synthesised using a condensation reaction between an amine and a carboxylic acid halide. Commonly, this is realised using phenylenediamine and benzenedicarbonyl chloride and depending on the orientation of the reactive groups, para or meta aramids may be obtained. For para-aramids commercial fibre products include DuPont's Kevlar® and Teijin's Twaron® and Technora®. For meta aramids, DuPont's Nomex® is an example. The popularity of Kevlar® lead to multiple iterations of which the most commonly used forms

are named 29 and 49, with different mechanical properties, mainly owing to 49 having increased elastic moduli from the degree of annealing [I.21]. Aramid fibres deliver the highest relative tensile strength to its density (**Table I.2**). As these fibres have been mass-produced for over 50 years, finally the price range has become attractive for applications outside the military and aerospace industries and the market share is expected to increase past \$5 billion past 2024 [I.22]. The fibre consists of an aramid in the shape of multiple tightly woven filaments in a specific network. The reason why this is so easily and specifically spun into a filament lies within the liquid crystalline properties of the aramid solution. When spun out, the solution forms a highly ordered filament (**Figure I.1**) close to 100% crystalline. The aramid network can be viewed as having three different kinds of interactions, which constitute to their highly ordered behaviour. Along the y-axis is the strongest bond: the covalently bonded polymer chain. Along the x-axis the hydrogen bonding effect can be seen between amide groups and acts as a relatively strong supramolecular interaction. Lastly, along the z-axis π - π stacking interactions between the phenyl rings can be observed. In terms of strength, the hydrogen bonding effect dominates the π - π stacking effect. The x and y-axes make up a particular orientational order, but this is not the case for the z-axis. Because of this, there is no positional order and thusly this network can be considered to be a nematic liquid crystal [I.9].

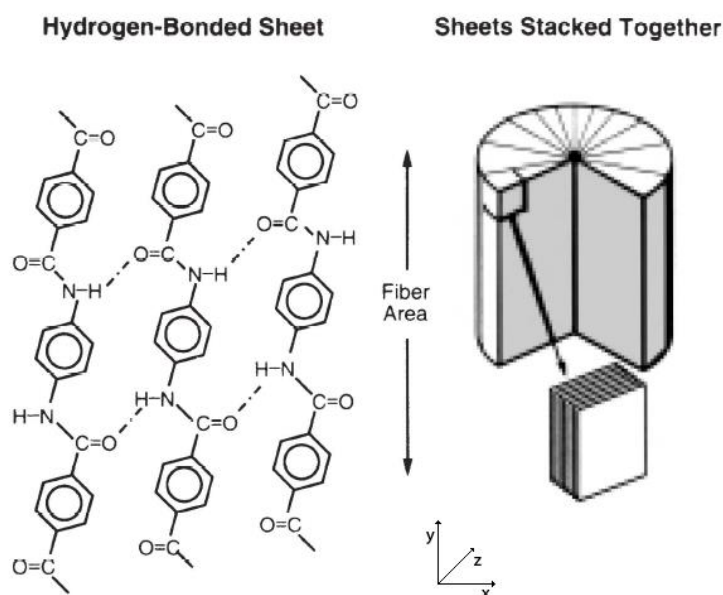


Figure I.1: Supramolecular interactions of para-aramid chains and its resulting structure [I.9].

Aramid fibre lends itself handy for many of the physical needs similarly given by metals: high tensile strength, stiffness, resistance to external parameters thermal degradation as well as degradation by water and several acids [I.9], but it still lacks some key properties, including ductility in the form of a high shear strength and compression abilities. Lastly, amongst the most important properties of Kevlar fibres is the low creep. For constant usage in mechanical applications, creep deformation has been proven insignificant in the span of decades [I.23], making this fibre particularly attractive for the

automotive industry due to the long lifetimes of vehicles.

1.1.3. Commercial applications for aramid fibre-based products

At the time of writing, aramids are widely used in several industries, both as composite materials in racing, military, maritime and aerospace engineering as well as sole fibre and pulp forms in belts, straps and hoses. Examples of applications are Kevlar-based body armour and helmets, which makes use of multiple layered Kevlar weaves. Specific body armours may incorporate Kevlar weaves in ceramic-based composite material [I.24]. Similar armours can also be used to protect vehicles. Inner plating typically consists of a laminate FRCM, which is called the spall liner [I.25]. For this purpose, aramid fibres can be compounded into a polymer matrix such as polyester, vinyl ester, epoxy or rubber [I.25-I.26]. One example of such an application is in the mine resistant ambush protected type vehicle, such as the BAE Land Systems South Africa RG33. The spall liner in this vehicle contains aramid fibres, which help protect against ballistic impact, shrapnel and heat [I.27].

Another use for aramid composite materials is in construction. The success of isotropic fibre-reinforced concrete (Kevlar FRCM using cement matrix) is not only thanks to the excellent properties of the fibre, but also because of a historical need to replace asbestos in construction [I.28]. Mechanical properties such as tensile strength, impact strength, Young's modulus and bending strength are explored and found 'sufficiently attractive to warrant further studies'.

Aramid FRCM in the automotive industry is found in helmet and head support (HANS) structures such as HANS devices [I.29] typically containing Kevlar or Zytel (Nylon) polyamide fibres as well as carbon fibres in a polyamide matrix. It is reported that in comparison to the previous non FRCM versions, this HANS-device shows improved mechanical properties and reduced weight. Additionally, in comparison to unreinforced polyamide, resistance to temperature and solvents is increased.

Sandwich structures of aramid are popular and often applied in the aerospace and racing industry, but the character of the fibres to be resistant against forces, temperature and solvents make aramids very applicable outside of composite material as well. Examples include hosing, brake pads and belts in the automotive industry [I.30]. Other common uses include Kevlar-based ropes [I.31], protective reinforcement in optical fibre cables [I.32], sports shoes [I.33] and bowstrings [I.34].

1.1.4. Fibre structure in matrix material

In material science and industry, the process of embedding the fibre into a matrix is called impregnation. This is why fibre types can be defined as unimpregnated or pre-impregnated, with the latter having the usable fibre already mixed in with the mouldable or liquid material. In the case of a thermoset matrix, a curing step takes place [I.35]. There are several ways to engineer FRCM. For this, we distinguish several sizes of fibres of which naming conventions are the following: continuous fibres (above dm range), chopped fibres (dm to cm range), long fibres (cm range), short fibres (mm range).

Typically, if the fibres used are above cm range the final product is referred to as a FRCM, while reinforced matrices using fibres of cm range and below can be referred to as a plastic reinforced material (PRM).

When relatively short fibres are embedded in the matrix the fibre orientation could be considered isotropic and the material comes closest to a homogenous mixture. The benefit of this is an easier manufacturing process, which can be achieved by injection moulding. PRM maximises the surface area of the fibre and the matrix. This means that the properties of the interfacial region will be stressed. With this type of composite material, the influence of the fibres might not be sufficient to achieve the desired mechanical properties. For this reason, slightly longer fibres may be preferred, in between sizes of 6 and 12 mm. However, when the size of the fibres increases to past cm range, the isotropicity may be disturbed and we can no longer speak in terms of PRM.

Although sub cm range fibres are more practical in terms of compounding, in principle an easier way of containing the mechanical properties of fibres and allow efficient load transfer is to orient them as continuous fibres in a particular direction. Two different types of structures are distinguished here: fibre mats and fibre weaves. The fibre mat is a non-woven collection of continuous fibres which are oriented randomly in multiple layers. These fibres may be held together through cross links induced by bonding agents [1.36]. In a fibre weave, however, the fibres are woven together in a certain orientation, which may induce additional strengthening effects through the anisotropy of the composite material, which can be transferred into a functional application [1.37]. One such example is the Kevlar military helmet, a composite material made typically with a Kevlar weave inside of a thermoset matrix such as phenolic resin, but combinations with other fibres, such as carbon fibre, and flexible matrices, such as poly(phenylene sulphide), also exist [1.38-1.39]. The main desired effect is the stopping force, which needs to be in the direction perpendicular to the incoming force. Therefore, the properties are much efficiently used in comparison to an isotropic fibre distribution.

An upcoming class of composite material is called hybrid composite material. This is a composite material in which two of the components are intertwined at the supramolecular level rather than a macromolecular level [1.40]. Subsequently, when in fibre-reinforced composites two different fibres are intertwined, the fibres themselves are referred to as hybrid fibres and the strength of which can be directly related to the supramolecular interactions between the different components [1.40]. Combinations of carbon fibre with glass or Kevlar fibre can be commonly seen, but other combinations include combinations of carbon fibre and carbon nanotubes or several combinations of natural fibre such as banana and hemp with synthetic fibres such as glass fibre [1.40-1.43]. Valenca *et al.* also illustrate the manufacture of a hybrid weave by intertwining Kevlar fibre with glass fibres in a 1:1 and

2:1 ratio, with the Kevlar fibre in the warp direction (0 °) and glass fibre in the weft direction (90 °) (**Figure I.2**) [I.44].

This Kevlar weave composite shows a relatively high tensile strength and elastic modulus in the warp direction, but it is decreased in the weft direction. This is expected considering the lower shear strength of Kevlar vs axial and propagates itself into differences in weave directions [I.45]. This is not the case for the hybrid composites, with the performance of the glass fibre in the weft direction dominating. This can be explained with the higher mechanical properties of glass fibre, particularly in the transversal direction [I.46]. Because of this, glass fibre will eclipse Kevlar fibre as the load-bearing component in when this load is applied mainly transversally, as is the case in the weft direction. Although the hybrid weave composites show relatively good performance, their weight rapidly increases with addition of glass fibre [I.44].

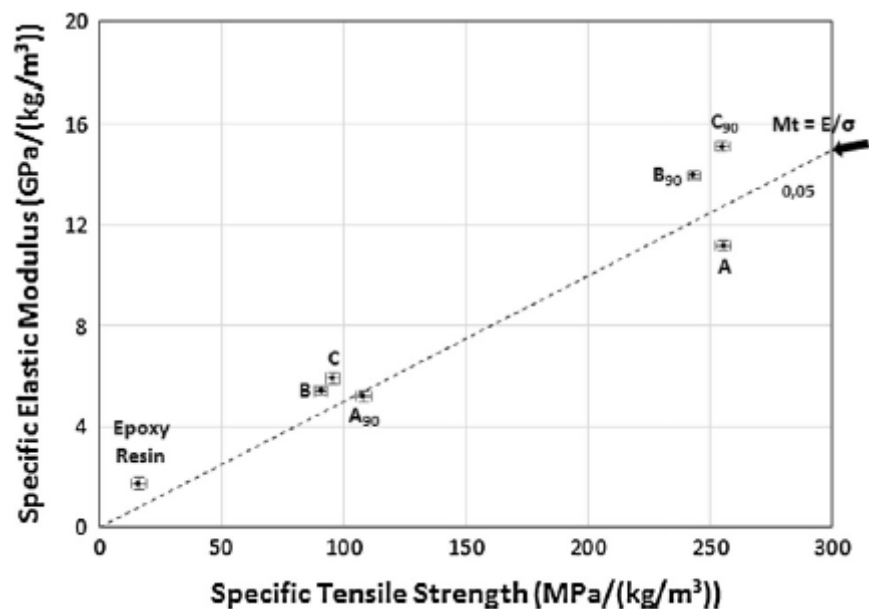


Figure I.2: Specific elastic moduli and strengths of three different FRCMs at 0 ° measurements with Kevlar (A), Kevlar:E-glass 1:1 (B) and Kevlar:E-glass 2:1 (C), where 90 denotes the perpendicular measurement using epoxy resin as a polymer matrix. Adapted from [I.44] with permission of Elsevier.

1.1.5. Aramid fibre-reinforced materials: Examples of different matrices

Several composite materials have been manufactured containing Kevlar fibres. Most popular resins are epoxy or formaldehyde (phenolic) based. However, both come with great disadvantages. Epoxy-based resins are typically expensive, ranging at maximally 4.5-6.0 € · kg⁻¹ [I.4] and require a precise mixing of the compounds to be able to cure it reasonably, making it more difficult to handle. Formaldehyde-based resins are cheaper, ranging at 1.60 € · kg⁻¹ [I.47], but show decreased mechanical properties and several safety hazards [I.48]. Since the high price of epoxy matrix, aramid-reinforced composite materials with this are most often found in military or aerospace industries. For example,

light aircraft like Y22 advanced tactical fighter plane or V22 Osprey helicopter are able to contain roughly 40% FRCM in its structural weight, partly aramid fibre-epoxy composites [I.49].

The usage of PP as an aramid fibre-reinforced composite matrix is interesting for industry, due to the low price as mentioned in Section 1.1. However, the usage of this matrix may be complicated due to the physical properties. For example, the tensile strength and strain of isotactic PP reinforced with 10 wt% Kevlar® 49 fibres can vary depending on the molecular weight of the isotactic PP [I.50]. Furthermore, the introduction of 30 vol% Kevlar® 29 fibres into isotactic PP induces crystallisation onto the fibre surface through transcrystalline effects [I.8]. Larin *et al.* have reported the crystalline behaviour of isotactic PP induced by chopped (ca. 3 mm) Kevlar® 49 fibres under flow, where the presence of aramid fibre increased crystallisation of the matrix [I.51] and shear stresses, where separate regions with different crystallinities may be formed within the matrix [I.52]. Interestingly, PP reinforced with various loadings of chopped (ca. 3 mm) Kevlar® 1414 fibres increases thermal resistance, including flame retardancy [I.53].

Brisson and coworkers have made some significant progress in developing Kevlar fibre-reinforced polyamide composites. They have studied the mechanical properties via rheology methods [I.54], interfaces via SEM/X-ray techniques [I.55] and performed the relevant mechanical modelling [I.56]. They have also compared several of these composites for variables related to the injection moulding process, including fibre orientation and crystallinity [I.57]. It is found that by selectively controlling moulding speed, the fibre orientation can be controlled to be above average parallel or perpendicular to the flow. Matrix orientation seems dependent on the unit cell matching between fibres and matrix. Furthermore, work done by Dorigato and Fambri involves the manufacturing of composite material of short Kevlar fibre in polyamide 12 [I.58]. Dynamic mechanical analysis (DMA) studies show that with weight percentages of Kevlar fibre ranging in between 10 and 30%, storage moduli are improved by 12-36% and coefficients of thermal expansion are greatly lowered by a factor of 1.3-2.2. This is also coupled with a sharp decrease in creep [I.58].

Other composites with Kevlar fibres seem scarcely applied in industry. In a paper from Yeung and Rao composites of Kevlar are explored in polyimide and polyester resins [I.59]. The two composites show similar tensional and flexural properties in a Kevlar FRCM but are outclassed by boron fibre composites. One reason for this could be the inefficient load transfer [I.60]. Kevlar® fibre-phenolic resin composites have been explored by Guo *et al.* to specifically test for friction properties [I.61] and hybrid polyether ether ketone composites with Kevlar® and carbon fibres were explored by Gupta, noting the improved mechanical behaviour of the hybrid fibre over individual fibre-reinforced composites [I.62].

1.1.6. Conclusion

Modern composite materials can be customized for different fibres and polymer matrix types, each influencing their mechanical properties. Owing to their properties and low density, Kevlar® fibres are increasingly attractive to use for industrial purposes. Polymer matrices likewise can offer lightweight and flexible solutions for composite materials using Kevlar® fibres. Compounding techniques provide various ways in which these composites can be engineered, most notably injection moulding, resin transfer moulding and rotational moulding, each with different applications, benefits and limitations. A number of examples of the use of aramid fibres in composite materials have been explored. It has been found that although aramid is widely used in composite materials of most notably body armours and aerospace structures, the usage in the automotive industry is limited. Interactions between aramid fibre and some matrix material may be poorly defined, owing to differences in crystallinity and subsequent insufficient mechanical adhesion. This results in an inefficient load transfer and high creep [I.63-I.67].

1.2. Parameters influencing the composite material performance

The performances of composite materials are largely influenced by the choice of reinforcement fibres, matrix and compounding technique. However, there are choice factors in play which directly influence the mechanical properties as well, indicating that the manufacture of the total product isn't always as straightforward as a simple sum of the two parts.

1.2.1. Rule of averages

When making use of a FRCM, the key factor is load transfer, or how efficiently outside forces are handled inside the composite material. Intuitively, when a composite is subjected to a certain force, the load is partially transferred to the matrix and partially to the fibre. The load carried by a matrix (and similarly for the fibres) across a surface is the product of average stress in the matrix over its sectional area. Therefore, the external load can be calculated by a sum of the two contributions, dividing by the total sectional area. This gives what is called the 'rule of averages' equation in composite theory and is in fact a simple summation of the average stresses of fibres and matrix [I.68-I.69]. In this equation (equation I.1) the stress of a surface A is defined with fractional coordinate f and stresses σ of the fibre and matrix respectively.

$$\sigma_A = f \sigma_M + (1 - f)\sigma_f \quad (I.1)$$

The fractional coordinate is a simple matter of how much space the fibres take in a composite material and can thusly be calculated by the volume fractions (equation I.2):

$$f = \frac{V_f}{V_f + V_M} \quad \text{with } v_f \text{ and } v_M \text{ the volume of the fibres and matrix respectively [I.68]} \quad (I.2)$$

The fractional coordinate is a function of the degree of reinforcement and the amount of fibre present in the matrix. If the composite material shows an elastic response, fractional coordinate f is independent of the applied load. The volume of the fibre will depend on the shape and orientation as well as any interactions with compatibilizers. A high fractional coordinate should naturally directly translate into a well reinforced matrix, meaning that most of the load is carried by the fibre. Generally, as the fibres have better mechanical properties, a higher fractional coordinate also increases the mechanical properties of the composite material itself. The rule of averages does not model an interfacial region and neither does it take into account differences in strain perceived by the fibre and the matrix, making this a rough approximation [1.68].

1.2.2. Slab theory

As mentioned above, the strain of both the fibres and the matrix is assumed to be equal under parallel force. In that case, the two components may be individually modelled as uniform 'slabs' (rule of mixtures) (**Figure I.3**) [1.68].

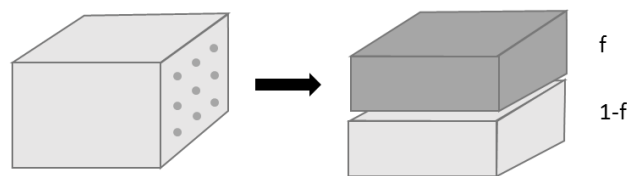


Figure I.3: 'Slab approximation' of composite material in the axial direction [1.69].

Here, the Young's modulus (E) can be split into parallel (E_1) and transversal (E_2) parts. Owing to the increased stiffness of the fibres compared to the matrix (and subsequent higher Young's modulus (E)) the fibres will dominate the load transfer in the parallel direction and the matrix term can be freely neglected [1.68]. Therefore, the Young's modulus in the parallel direction (E_1) is equal to the Young's modulus of the fibres (E_f). For the perpendicular direction, the same approximation cannot be made ($E_2 \neq E_f$). An often used solution is found in the empirical Halpin-Tsai equation, which may model transverse strength E_2 as a function of the matrix and fibre strengths as well as fibre orientations [1.70]. These equations are, however, only valid for sufficiently long fibre lengths. When the fibre length becomes smaller the rule of mixtures no longer holds true, since the stress of the fibres is not equally defined at the edges of the fibre and this term becomes more significant.

The combination of slab theory and empirical Halpin-Tsai equations still makes the assumption that the two components can act independently from one another and assume that perfect bonding is taking place in the composite, which is far from reality.

1.2.3. The two body interface region of fibre-reinforced composite material

As has become clear the FRCM is much more than just the sum of the two parts. The most critical area of a composite material which determines the mechanical properties is the interface region between fibre and matrix (**Figure I.4**).

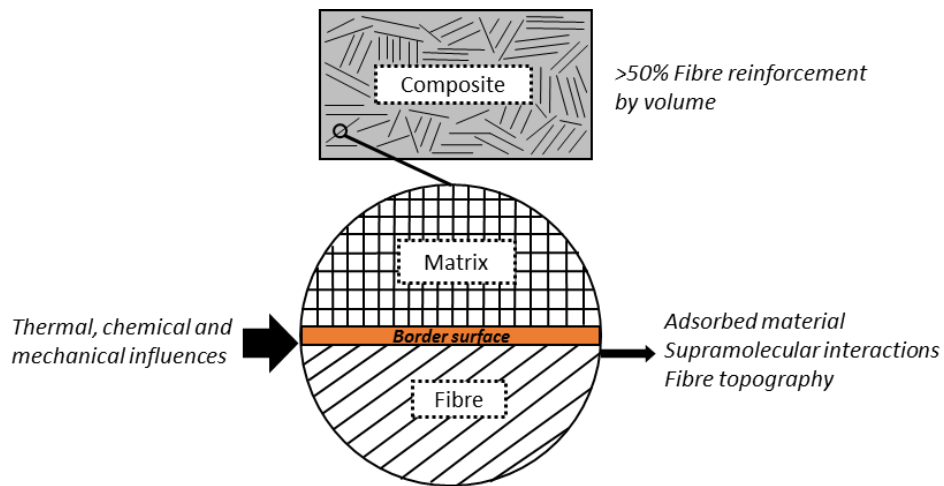


Figure I.4: Components of an interface region of FRCM. Adapted from [I.71] with permission of Taylor & Francis.

The morphology of the interface region will influence factors like surface area, crystallinity and strength of the interactions between the interface region and the fibre or matrix. This can have significant effects on the stiffness and creep of a composite material. The interactions of polymer systems with different fibres will depend partially on their crystallinity, affecting nucleation properties, including the formation of spherulites and the aforementioned transcrystallinity [I.8, I.72-I.73]. The interfacial region itself can be expressed in mathematical terms. Additionally, the surface area may be of effect. Higher surface area (or a less smoothly defined interface) leads to an increase in 'interlocking ability' of the matrix, improving load transfer. However, strength of the interactions may cause the material to be either too brittle or too flexible, resulting in an inefficient load transfer. Finding the right balance is the key to designing a proper composite material [I.37-I.74]. However, exactly what the role of a specific supramolecular effect is in the fibre-matrix interface is not a widely explored topic at the moment of writing.

In its simplest form, the interface between a matrix and fibre may be described as a generalised mathematical model, from which microscale forces acting on the fibre-matrix interface may be derived. Andrianov *et al.* propose a model of a two-dimensional interface region in a fibre-reinforced composite material which makes the following assumptions: 1) the fibre is considered as infinitely long and unidimensional without resistivity for bending (stiffness), 2) the matrix is considered an infinitely long two-dimensional plane, 3) all interactions in between matrix and fibre are supposed to be perfect and are modelled as ideal line-contact, and 4) loading is applied only to the fibre [I.75]. Although it may be possible to derive distinct forces acting on the fibres and contact forces between the fibre and matrix, the perfect bonding is still a large assumption. In this simple scenario, the stress/strain curve of the composite material will therefore depend independently on the properties of the two components and their contact, with as a result a logarithmic plot of the force between the fibre and matrix as a function of distance from the fibre [I.75]. These models do not take into account the

influence of a distinct layer between the fibre and the matrix which may propagate the forces in a different fashion and perform interlocking in a localized fashion.

1.2.4. Conclusion

Mechanical models have been reviewed for their application in describing composite materials. In popular forms, large assumptions have been made to simulate the load transfer between fibres and matrix materials, not properly taking into account the role of the interface region. While these models may assume a perfect load transfer, the reality is that owing to imperfect load transfers, performance of composites can be affected both in mechanical properties and creep. It is therefore essential to mitigate the imperfections in the interface region to assume the optimum load transfer is possible. In Section 1.3 several methods to optimise the interface region will be discussed.

1.3. Optimisation of the interface region in aramid fibre-reinforced composite materials

1.3.1. Introduction

The interface region of a composite material is largely indicative of how well load is transferred and thusly the quality of a composite material. It is therefore important to have the most optimal supramolecular or covalent interactions between fibre and matrix material. Additionally, for industrial applications, composite material typically needs to be strongly resistant against water or other factors, like temperature.

In the specific example of aramid fibres, although showing impressive mechanical properties with minor differences compared to other competitive fibres such as glass or carbon [1.76], they have one drawback that makes them not very widely applied in composite research.

The interactions which the fibre has with common matrices, like epoxy, PP or polyethylene are not strong enough to warrant convenient usage, which translates into an inefficient load transfer where properties are not optimally used and more load is carried by the matrix material as well as a high creep [1.77]. The reason for these poor interactions is twofold. Firstly, the structure of a matrix material is often either semi-crystalline or amorphous, while Kevlar fibre is highly crystalline. Intermediate structures at the surface of the aramid are therefore required to have a degree of crystallinity. This phenomenon has been observed in isotactic PP melt as transcrystallinity, where crystalline structures (spherulites) of the matrix nucleated at the interface with the aramid fibre [1.50]. Secondly, Kevlar fibres are produced by spinning, creating a smooth surface undesirable for load transfer. However, an advantage of aramids in composite materials hold over other market competitive is the presence of supramolecular interactions and functional groups at the surface. The aromaticity of the polymer makes π -interactions possible and the C=O and N-H groups can participate in hydrogen bonding interactions. In theory, this makes fibre treatment or compatibilization by modification of the structure

possible to realise and is commonly done to introduce supramolecular or covalent interactions directly to bind to the matrix or to increase the roughness of the surface. The principle cited behind the usefulness of the roughening lies in the potential dependence of the load transfer on the surface area in the interface region as well as interlocking mechanisms [1.78-1.79]. Several methods to directly modify the aramid fibre surface or the matrix will be explained in this section.

1.3.2. Modification of aramid fibre

1.3.2.1. Alteration of fibre surface roughness

A large surface area may be beneficial for micromechanical effects that govern adhesive properties. One effective way to increase the amount of surface area is to roughen the surface selectively. An example of this is found in using strong acids for a small period of time to selectively degrade the fibre, sacrificing a small part of the mechanical properties to hopefully gain a better load transfer. Treatment of Kevlar with phosphoric acid contributes to creating a more hydrophilic surface on the fibre in two different ways [1.59]. The major contribution is an electrophilic substitution on the phenyl ring, introducing hydroxyl groups and the minor contribution is hydrolysis. By varying concentration of phosphoric acid, the roughness of the surface can be controlled through partial degradation.

As expected, the mechanical properties greatly increased, with, for example, an increase of roughly 20% in flexural strength between untreated and treated fibres [1.63]. Similarly, it is possible to use high concentrations of sulphuric acid to swell Kevlar fibres and separate the microfibrils. Hydrolysis and bromination of Kevlar have been explored in an article of Looi and coworkers to alter the surface morphology of the fibres showing that hydrolysis is preferred over bromination as roughening of the fibres occur without fibrillation [1.64]. Introducing thermoset polymeric material onto a roughened surface replaces a loss in tensile strength by an increase in compressive strength [1.80].

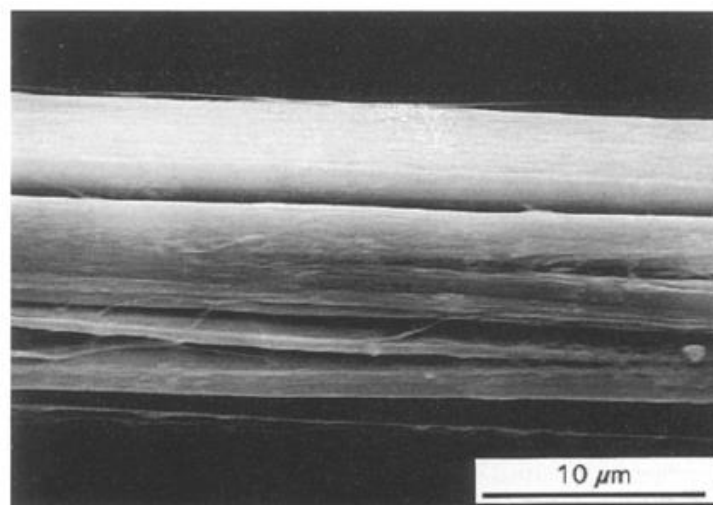


Figure 1.5: SEM image of a Kevlar fibre surface treated with sulphuric acid. Adapted from [1.80] with permission of Springer Nature.

1.3.2.2. Covalent insertion of functionalities onto aramid surface

After hydrolysis, further modification is possible, notably to embed metal catalysts on the surface of the fibre. In one particular example this is explored with Ziegler Natta catalysts to polymerise ethylene from the Kevlar fibre surface, potentially setting the way for efficient production techniques. This is why these types of techniques are aptly named polymerisation compounding [1.65].

Plasma-mediated modification techniques can be applied to aramid fibres, allowing for grafting of various functional groups, the easiest being halogens. By introducing fluorine or chlorine atoms into the aramid backbone, the electronegativity is changed at the cost of the hydrogen atoms. This means that hydrogen bonding effect at the surface will be diminished, but the hydrophobic balance will be adjusted, which could be beneficial for improving the affinity with a compatibilizer.

An example of this is found in an article by Maity *et al.* that explored the possibility of using fluorine plasma to functionalise Twaron® aramid fibres as reinforcement fibre in PP matrix, leading to an increase in the crystallinity of the aramid surface, a subsequent increase in surface energy and improved stress/strain curve, allowing the composites to withstand roughly twice the stress before fracture occurs [1.81]. Fluorinated fibres can then be functionalised with surface agents to further improve adhesion with the PP matrix [1.82]. Similar treatment can be performed on other composite systems such as modified Kevlar fibre/4,4-bismaleimidodiphenylmethane+diallylbisphenol A that is used to construct a laminate composite material [1.83]. The interlaminar shear strength is measured for different plasma treatment times and intensity. Optimal treatment parameters lead to an increase of the fibre/thermoset polymer matrix interactions proven by electron microscopy observations of the fracture surface topography. This plasma treatment is not limited to halogens like fluorine or chloride. More complex groups can also be introduced. In a similar system as the one described above, meta-aramid fibres have been treated to introduce dopamine groups onto the fibre as compatibilization for aramid-rubber composites. The underlying mechanism relies on the oxidative self-polymerization of the dopamine groups to form a thin layer on any substrate. As a result of this, the adhesion strength is improved [1.84]. In particular, work by Wu *et al.* explore the possibilities to functionalise Kevlar® fibres using various plasmas (water, ammonia, oxygen), which is then followed up by covalent bonding of chlorosulfonic acid and subsequent covalent bonding of reagents, including glycine and butanol [1.85]. The surfaces are then analysed using X-ray photoelectron spectroscopy (XPS) to confirm the presence of the treatments, followed by mechanical analysis of treated fibre/epoxy composites. Notable differences are seen for the mechanical peeling tests of functionalised fibre composite layers delivering between 138 and 144% of the original strengths depending on the end functionalised group.

Another example of exploring the lability of the N-H bond in Kevlar is the use of a methylsulfinyl carbanion. In a solution of sodium hydride in DMSO, this carbanion is readily formed and can

deprotonate the N-H bond, making it susceptible for attack by a nucleophilic group. An article by Koga and coworkers explores the reaction of the Kevlar salt with hydrophilic groups to improve the affinity for Kevlar with epoxy resin [1.86]. The interfacial shear strength is greatly increased when the Kevlar fibre surface is treated, with an increase of more than 200% for Kevlar fibre functionalised with epoxy groups. This approach can in principle introduce other moieties as well, such as linear alkanes [1.87]. A downside to this technique is that, unlike untreated Kevlar fibre, the formed salt will be slowly dissolved in the DMSO, limiting the reaction conditions and thus the moieties that can be introduced. Another two-step strategy for functionalising aramid fibres involves selective hydrolysis using sodium hydroxide, after which free amide groups can be coupled with toluenediisocyanate and allow subsequent coupling to the remaining isocyanate group. Zhao *et al.* have used this strategy to functionalise short Kevlar® fibre with caprolactam moieties [1.88].

1.3.2.3. Analysis of modified aramid fibres

In order to evaluate the effects of fibre modifications it is important to distinguish different analytical methods: a) to analyse directly the mechanical and morphological effects on the fibre surface and how it propagates forces that will be discussed in this section and b) the impact of fibre and matrix modification on the mechanical properties of composite materials. It is not straightforward to set up an experiment that could directly measure the interactions between treatments and fibres on which they act. However, a multitude of techniques exists to evaluate the interfacial energies as a function of interfacial tension between two materials, which can be a consequence of any differences in intermolecular forces. In a two-component system a comparison can be made by using the ratio of change in interfacial tension over the intrinsic interfacial tension. Two different techniques to analyse and quantify treatments in respect to intramolecular forces will be described here: force response studies via droplet detachment **(a)** and contact angle studies **(b)**.

a) Droplet detachment. In droplet detachment studies, the forces required to remove a droplet of material from a solid are measured and will be dependent on the kinds of interactions the droplet has with the material. Typically, an atomic force microscopy (AFM) tip is embedded into the droplet and a force can be measured which is required to pull free the droplet from the fibre [1.89]. A difficulty of this setup is that in essence two different detachment events can take place: detachment of a droplet from the fibre or detachment of the AFM tip from the droplet. Depending on the interactions, one or the other will dominate and unfortunately complicates making a useful comparison of values. Kasper and coworkers note that while using different kinds of fibres (steel, glass, polyester and polypropylene), the same mineral oil gives rise to a difference in the kind of detachments [1.89]. For these reasons, Amrei *et al.* have used ferromagnetic particles embedded in a commercially available ferrofluid to measure detachment force from a single polyamide 6 fibre as a function of applied

electromagnetic effects (**Figure I.6**) [I.90]. This method does not involve the application of external forces which introduce additional parameters into the system. A differentiation is made between in and out of plane detachments. Out of plane detachments are measured on a single fibre placed perpendicular to the axis of gravity while in plane detachments are done with two intersecting fibres with a variable angle perpendicular to the axis of gravity.

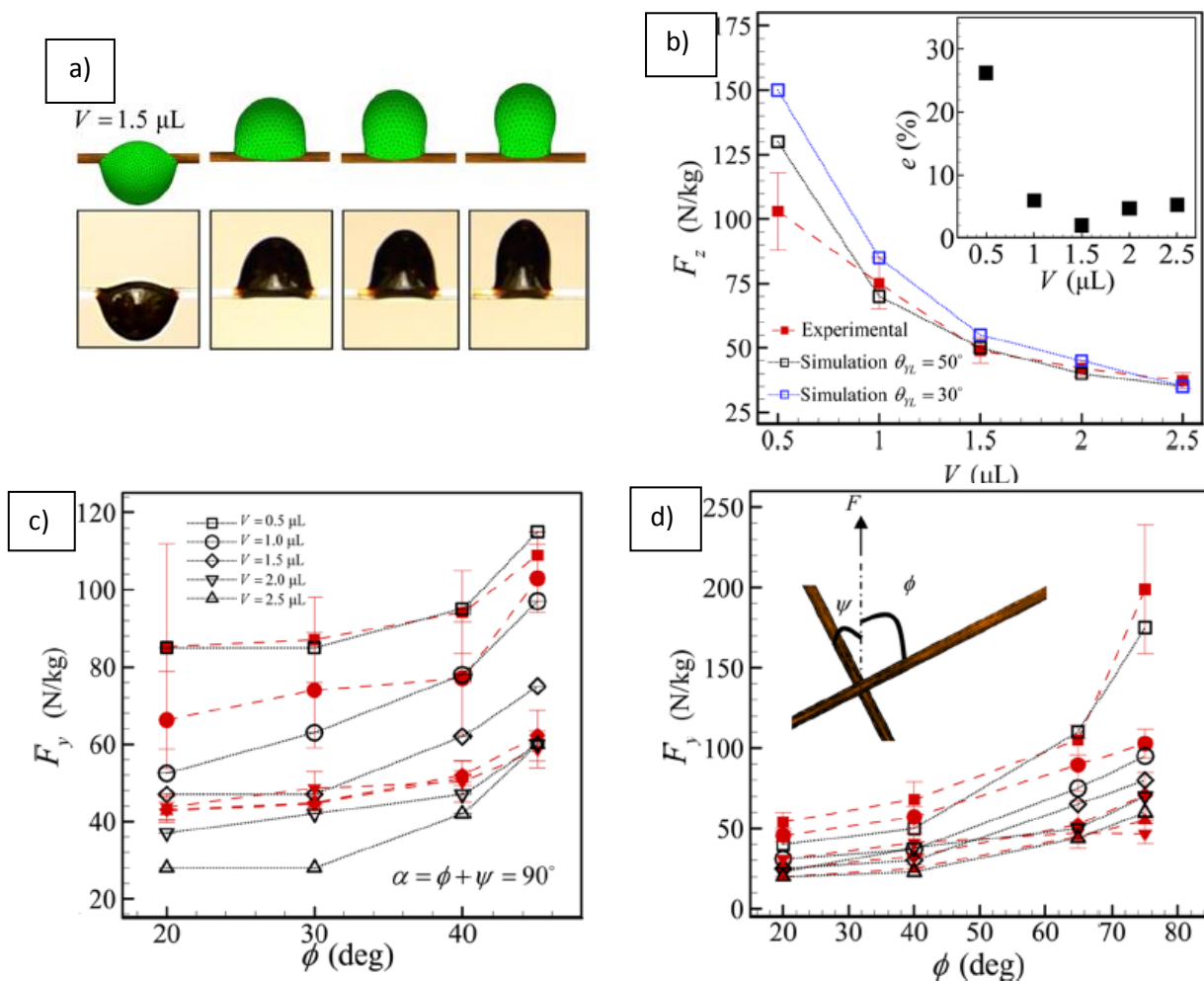


Figure I.6: Fe_3O_4 -based ferrofluid droplet detachment from a single fibre: a) simulated and experimental images of droplets subjected to forces of $g = -9.8, 30, 50$ and $55 \text{ N}\cdot\text{kg}^{-1}$ and b) simulated and experimental detachment force curve vs droplet size (simulations done with Young Laplace contact angle values of 30° and 50°), c) detachment forces vs angle ϕ from intersecting fibre experiments for droplets of different volumes (experimental results in red, simulated ones using a Young Laplace contact angle value of 50° in black), and d) extension of the experiments conducted in (c) for higher values of ϕ . Adapted from [I.90] with permission of American Chemical Society.

Although arguably harder to set up, a more accurate force measurement between two components can be found using AFM in solid phase. Li *et al.* describes the use of functionalised AFM tip with biomolecules to measure directly the supramolecular interactions they have with biological membranes [I.91]. One such example can be found in the work of Pan *et al.*, who functionalise the AFM tip with a SIRP α protein known to have specific interactions with the CD47 receptor on a red blood cell surface (**Figure I.7**) [I.92]. The results they obtain in pN scale allow to directly obtain

information regarding the attachment and detachment processes between two macromolecules. Subsequently, the energy barrier to perform such reactions can be determined and the effect of environmental factors, such as the age of the red blood cells.

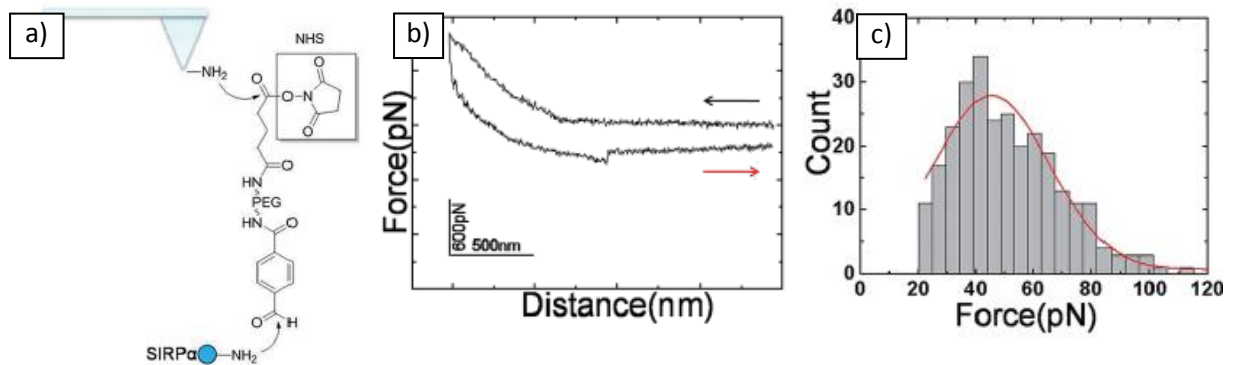


Figure 1.7 a) Functionalisation of the AFM tip with SIRP α protein. b) Typical force-distance curve of a SIRP α -CD47 single molecule force spectroscopy experiment. c) a histogram of the unbinding (detachment) forces required to remove the protein from the cell surface. Adapted from [1.92] with permission of RSC Pub.

b) Contact angle studies. Contact angle goniometry studies evaluate the wetting angle that a droplet of liquid or solution can make with a solid material. Contact angle measurements can give an indication of the difference in surface energies between two types of materials, which can be caused by supramolecular interactions. For fibre treatments in the composite industry, goniometry can be applied. Simonsen and coworkers describe an example of how commonly used techniques can be adapted for single fibres (**Figure 1.8**) [1.93]. In their system, uncoated and coated glass fibres are used. The fibres are submerged in water or uncured epoxy resin and subsequently a contact angle profile is measured by projecting the image onto known mathematical models. High contrast is obtained using white light emitting diode light and a telecentric lens is used for capturing images, allowing a spatial resolution of 4 μm . Different silane-based commercial coatings are compared when dipped in uncured epoxy solutions. The difference in results is significant, with a range of contact angles between roughly 28 and 65 degrees. Although it is unfortunate that the structures of the silane coatings are unknown, these results prove the sensitivity of such contact angle measurements for probing fibre coatings and the interactions they might have with polymer matrices.

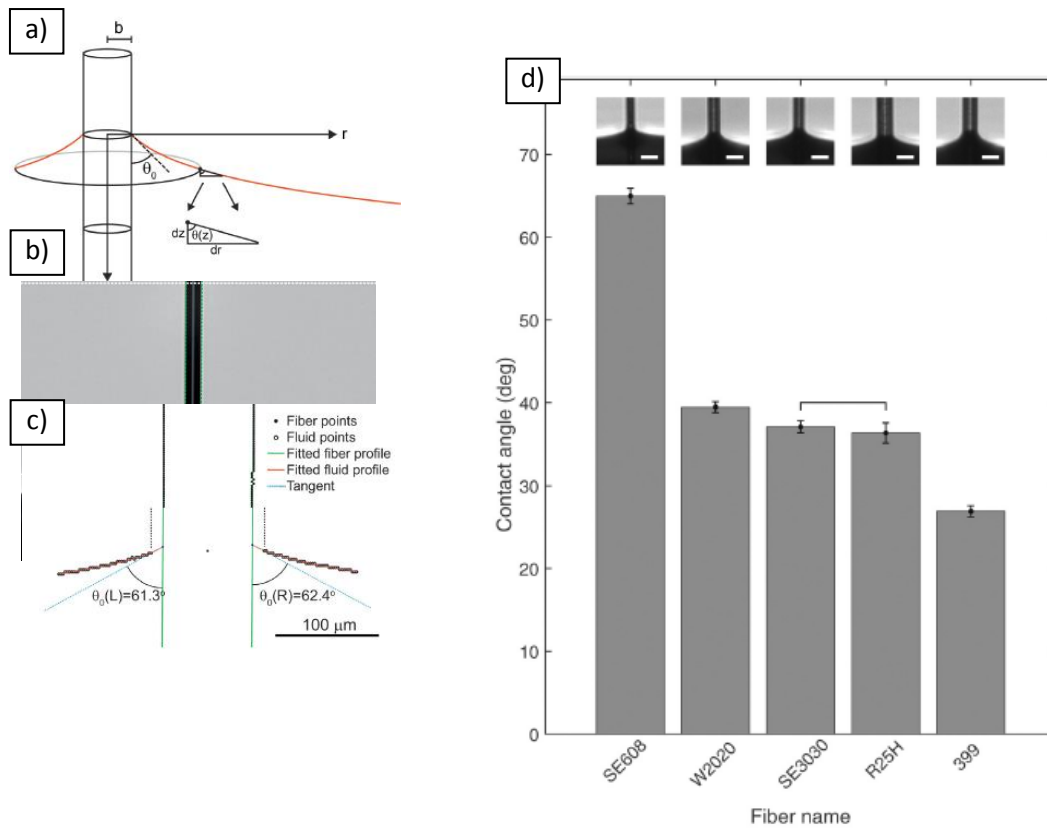


Figure 1.8: a) Mathematical model of a contact angle (θ_0) measurement of wetted fluid on a cylindrical fibre, b) real image of poly(methyl methacrylate)-coated glass fibre submerged in water, c) projection of image onto catenary curve and subsequent determination of contact angle (θ_0) and d) comparison between five different commercially available glass fibres, coated with different silane-based interfacial agents. Adapted from [I.93] with permission of Elsevier.

1.3.3. Chemical treatments of polymer matrices

In addition to fibre treatments, the matrix material can also be selectively modified to improve the interfacial region. Two different strategies will be discussed: the introduction of adducts into the matrix material and modification of the surface layer.

1.3.3.1. Matrix control using adducts

A popular technique for the modification of matrix mechanical properties is the introduction of a nanophase, which in practice means that nanoparticles are embedded into the matrix material. One example of this can be found in the work of Sprenger and coworkers, who have successfully manufactured flax fibre and cellulose fibre-reinforced epoxy matrices with adducts of rubber microparticles and silica nanoparticles (**Figure 1.9**) [I.94]. AFM elucidates that the previously homogenous nature of the nanophase is changed in FRCM forming aggregates.

The inclusion of micro- and nanoparticles into the matrix material not only affected morphology but additionally increased the interlaminar fracture energy by a factor of roughly two to eleven of the bulk epoxy matrix material and 1.17 to 1.74 of the composite material, which may be a result of improved interactions at the interfacial region [I.94].

1.3.3.2. Analyses of modified composite materials

Several analysis techniques enable to determine composite properties as well as the influence of a treatment. For industrial applications, measurements of mechanical properties are of interest. Tensile strength, tensile modulus, shear strength and shear modulus are amongst the values that are of particular interest for applying rigid composite material. To measure such properties, several techniques include direct tensile and shear tests like pulling **(a)** and indentation **(b)** studies or indirect tests like rheology and dynamic mechanical analysis. These tests usually involve applying a force and measuring the resulting strain while varying certain parameters. Spectroscopic techniques are preferred to investigate the interfacial region of composite materials **(c)**.

Pulling studies. Pulling studies record the amount of force needed to remove fibres from a solid material, including polymer resin. This test can be applied to bundles of fibres, but also on single fibres, using the single-fibre pull-out test. Depending on how well defined the interface area of the fibre and resin is, the amount of force required will be different and will be an indication of the shear strength between the fibre and matrix. Pulling studies provide direct insight towards forces in a composite material interface, as the debonding of the fibre from matrix and the resulting post-debond frictional sliding are energy dissipating mechanisms directly influenced by the fibre surface [1.95]. In work done by Sockalingam and Nilakantan a glass fibre is placed in an epoxy resin, after which the resin is cured **(Figure I.9)** [1.95]. The sample is then loaded onto a loading blade after which a machine starts pulling the sample. A graph of the displacement over force shows four characteristic areas (I-IV). The first area (I) is a linear response up until the force reaches F_d , the minimal force required for debonding. This represents an area in which the material does not deform irreversibly. After reaching F_d , cracks start to appear in the resin from which recovery is no longer possible. These cracks propagate in the second area (II), showing an increased response of the resin towards additional force. The third area (III) shows a sudden drop in the amount of force needed to move the fibre and is representative of the fibre breaking free from the resin. The last area (IV) shows a constant response to force and represents the fibre sliding along the resin freely.

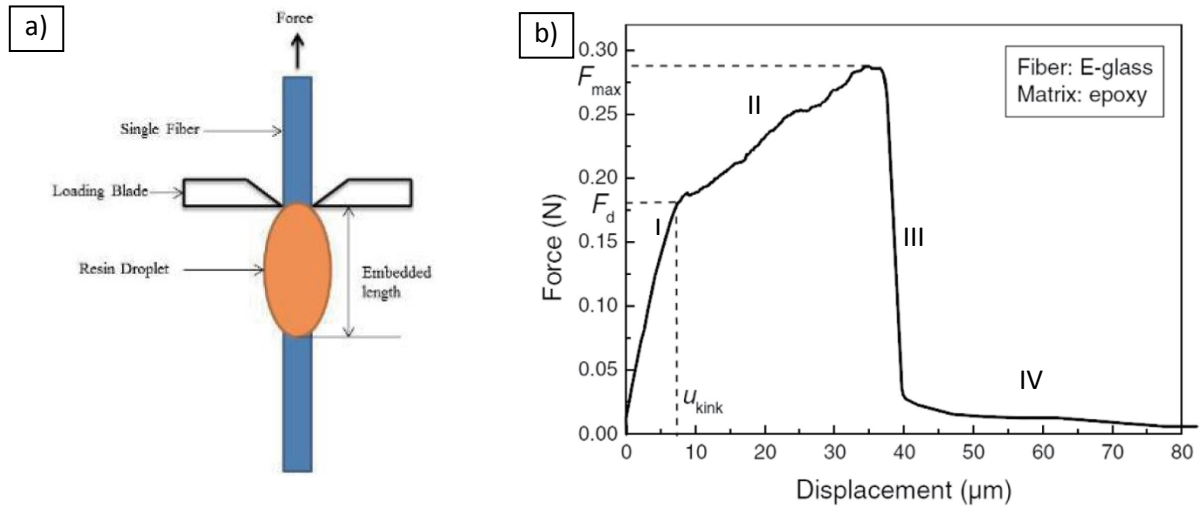


Figure 1.9: a): Pull-out test of a fibre/matrix droplet system, b): Force/displacement curve of a pull-out test performed on an E-glass-epoxy composite. Adapted from [1.95] with permission of Springer Nature.

The interface shear strength of the interface is now given with the following equation:

$$\tau = \frac{F_{max}}{2\pi r l_e} \quad (1.3)$$

with τ the interface shear strength, F_{max} the peak load at which complete debonding occurs, r the radius of the fibre and l_e the embedded length of the fibre.

After debonding occurs (**Figure 1.9**, region III), only friction will occur, describe by interfacial frictional stress:

$$\tau_f = \frac{F_b}{2\pi r l_e} \quad (1.4)$$

with τ_f the interfacial frictional stress and F_b the minimum force required to move the fibre.

A limiting factor to the single-fibre pull-out test is that the debonding of the fibre from the matrix has to occur without the fibre breaking. The parameters of the fibre influence how much of the fibre is allowed to be embedded:

$$l_e < \frac{\sigma_f D_f}{4\tau} \quad (1.5)$$

with σ_f and D_f the (ultimate) tensile strength and diameter of the fibre [1.95].

The notable drawback of the single-fibre pull-out test is the deviation of the experimental data. As only a single fibre is considered, changes in orientation, deviations of embedded length, loading blade separation distance and fibre diameter may quickly cause large differences in the measured shear strengths. Additionally, the viscous relaxation of the polymer matrix during processing, nature of the loading, shape of the droplet or differences in stress and plastic yielding of the matrix make the reproducibility of this method difficult, requiring a large amount of measurements for workable data [1.95]. Despite these limitations, the single-fibre pull-out test has been applied to a variety of fibre/matrix systems, including Kevlar® fibre-reinforced composite materials, such as Kevlar® 49 with an epoxy matrix [1.96], but also with polyethylene, polyamide, and poly(methyl methacrylate) matrices

[I.97]. The pull-out test has been used successfully to indicate differences caused by covalently bonding treatments on the Kevlar® fibre surface, such as with epichlorhydrin, carbocymethyl and epoxy functional groups [I.86].

Nanoindentation. In nanoindentation studies a direct stress-strain response of the materials to a mechanical local load is obtained. A tip of known mechanical properties and size (nm- μ m range) is pressed into a sample with unknown mechanical properties. The localised nature of nanoindentation could give an accurate image of the effect of sizings or compatibilizers [I.98]. An example applied to glass fibres is found in the work done by the group of Hurtado-Macias. Their research shows a significant difference in hardness curves of untreated glass fibres vs glass fibres coated with silver oxide nanoparticles, particularly in the 0-80 nm range [I.99]. However, nanoindentation can also be used to analyse composite materials. To understand how forces on a localised level are propagated into a matrix, the indentation experiments can be set up for embedded fibres and may act complimentary to pulling studies. Diss *et al.* provides an example of this kind of work done on carbon fibres in a graphite matrix [I.100]. In order to minimise dislocation effects, a cyclic loading technique is used, where the nanoindenter is repeatedly oscillated with increasing depth [I.101]. The FRCM is prepared by making use of chemical vapour infiltration to deposit the matrix onto the fibres preform. The composite material was then cut in several shapes, allowing for visualisation of different types of fibre orientation in the matrix with respect to the angle [I.100]. A difference in force response can be seen for all the four orientations (**Figure I.10**) indicating that force transfer in such a composite material is locally managed and sensitive to the angle of the fibre in respect to the applied force, with the largest variation found for fibres perpendicular to the indenter. When fibres are indented in parallel, the elastic modulus decreases more rapidly over distance, indicating significant degradation [I.100].

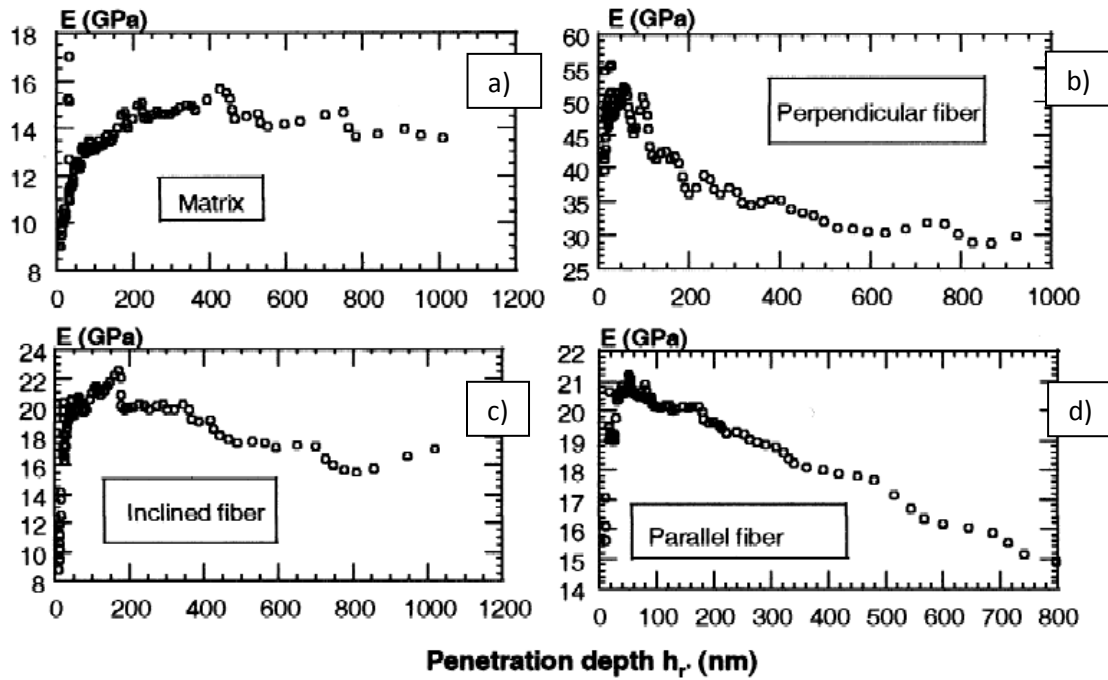


Figure I.10: Elastic moduli as a function of indentation distance on carbon fibre-reinforced graphite composite material for (a) pure matrix, localized (b) perpendicular, (c) angled and (d) parallel fibre in respect to the indenter. Cyclic loading frequency was 32 Hz and forces used did not exceed 50 mN. Adapted from [I.100] with permission of Cambridge University Press.

Spectroscopic techniques. There are several ways to characterise the interfacial region of a composite material spectroscopically, among which microscopy and X-ray techniques are popular [I.83, I.102]. For microscopy in particular, electron microscopy is a convenient tool as it allows direct combination with X-ray techniques to directly measure atomic ratios of surfaces, particularly energy dispersive X-ray spectroscopy (EDS). Here, a sample surface in high vacuum is irradiated by an electron beam, which will excite the atoms. Through subsequent relaxation X-rays are generated which are then absorbed by a crystal detector inside the spectrophotometer, which generates electrons in a controlled matter, following the photoelectric effect with energy levels depending on the orbital shell via:

$$E_k = h\nu - E_B - \phi_s \tag{I.6}$$

with E_k the kinetic energy of an electron, $h\nu$ the energy of the irradiating X-ray, E_B the binding energy of the electron to its respective orbital and ϕ_s the work function of the spectrometer [I.103].

Here, X-rays can be generated anywhere from 100 nm to micrometer scale [I.104-I.105]. EDS has been used to characterise corrosion effects on glass fibres [I.106], as well as volumetric analysis of fibre reinforced composites [I.107-I.108].

However, the resolution of EDS provides limitations, which can be circumvented using X-ray photoelectron spectroscopy (XPS) which functions by irradiating the surface directly with monoenergetic X-rays (typically from a metallic source) under high vacuum to obtain the electrons. Owing to small path length of the generated electrons, XPS allows for layers in the orders of 2-10 nm

to be quantified and it allows for precise determination of surface composition [I.109]. It thusly has been used with some success to characterise treatments on fibres [I.109], including plasma treatments of Kevlar fibre [I.102].

Secondary ion mass spectrometry is another quantitative technique that makes use of secondary ions of substrates to determine composition and layer quantity. Although this technique can show high resolution (up to 10 nm), it is a destructive technique and requires significant effort to be used for quantification [I.110]

Although optical microscopy will give some indication to the extent of oligomer presence on a fibre, it will not typically give sufficient information on coverage and morphology. Scanning electron microscopy (SEM) allows for a more detailed characterisation. Resolution of images depends on the sample and electron beam but can range anywhere between 1 and 100 nm [I.111].

When making use of covalent crosslinking techniques between fibres, treatments and matrix material, infrared (IR) spectroscopy allows monitoring the formation of covalent bonds, for example by monitoring significant shifts in ester, ether and alcohol bands at the interface of covalently modified natural fibre and polystyrene [I.112]. However, for systems on which the difference in spectra of components at an interface are expected to be small, the sensitivity of IR spectroscopy may not be sufficient. Raman spectroscopy can act not only complimentary to IR spectroscopy but also offers an increase in resolution and can be particularly well used to distinguish crystallinity differences [I.113], which can be used to analyse not only carbon fibres but also aramid fibres to obtain interlaminar shear strength indirectly [I.113].

1.3.4. Usage of compatibilizer molecules (three-body interface)

1.3.4.1. Introduction

A particular problem that is common in composite development is that oftentimes fibre and matrix do not mix that well together, either because of a difference in polarity, size or otherwise. A lack of ideal mixing can be expressed in thermodynamic terms. To circumvent this problem of unoptimised mixing, the fibre or matrix is chemically treated or a third component is used to increase fibre/matrix compatibilization.

In the case of a single molecule, no matter which form, it is called a compatibilizer. These are typically oligomers or polymers that include affinity for both parts of a composite, effectively 'gluing' these parts together, forming an adsorbed layer in between [I.114]. In industry the component that improves fibre/matrix interactions is often a mixture of compatibilizers with several additives, like anti-static agents, surfactants, film forming agents and anti-foaming agents and is commonly referred to as sizing. It is applied as a coating to the fibre before making a compound. Aside from improving adhesion at the interface region, sizing may also protect fibres from abrasion and other damages from environmental

factors, improve wettability and may give additional stiffness to the fibres, as is common for glass fibre treatments [I.115]. Gorowara *et al.* has evaluated the composition of common glass fibre sizing and found that on average, the majority of the sizing consists of the film forming agent (ca. 79%), while only a small part (ca. 10%) will be the compatibilizer [I.116].

In essence, the matrix, the fibre and sizing may be referred to as the three-body interface, which can therefore be illustrated as fibre/matrix system with separate regions (**Figure I.11**) [I.117].

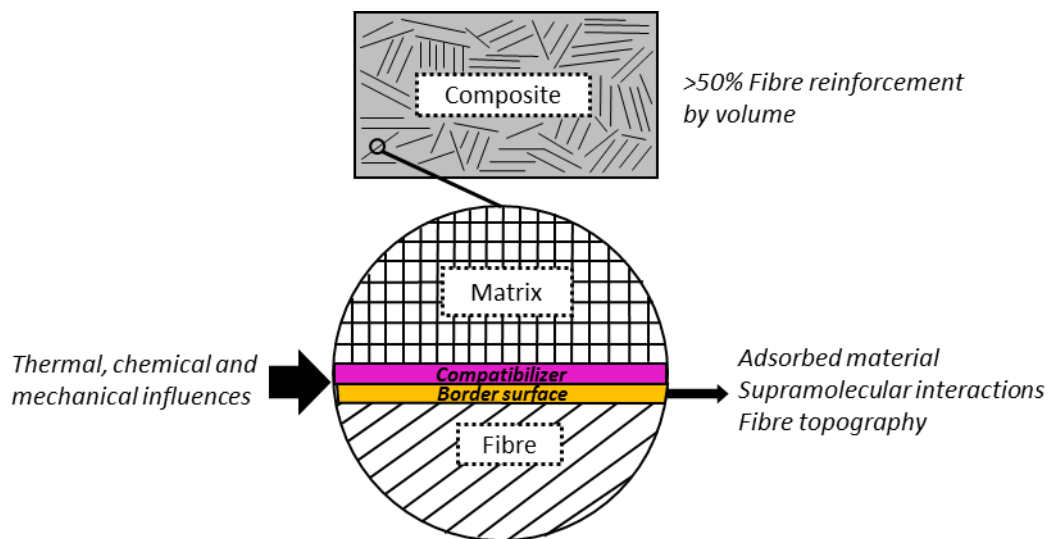


Figure I.11: Different components of a FRCM with an added compatibilizer layer [I.117]

The morphology of the interface may be affected in several ways. One of these are surface forces between the components which may be caused by covalent or non-covalent interactions. Additionally, mechanical effects, such as interlocking between the different layers may play a role. Another factor may be the ability of any component to perform diffusive movements inside the interface region, for which the molecules themselves require to be unbound and scarcely affected by crystallinity. To summarise, roughly three different factors are present to govern the interface: 1) chemical bonding (including strong supramolecular bonds) caused by thermodynamic potentials, 2) physical adhesion, related to surface crystallisation and tension and 3) mechanical adhesion, caused by interlocking, diffusion and other relevant mechanical effects [I.118].

1.3.4.2. Choice of compatibilizer

Commonly used compatibilizers for FRCM are polymers functionalised with maleic anhydride groups, such as polystyrene, styrene-based block copolymers and olefins [I.119]. A specific example is maleic anhydride-grafted polypropylene (MA-g-PP) (**Figure I.12**). This polymer has been successfully employed in various FRCM including with Kevlar fibres [I.120-I.122].

These polymers exhibit similar functionality, in being polymers that can be bound covalently to a fibre surface using the maleic anhydride group, after which the surface properties may be changed, including supramolecular interactions at the surface [I.123].

The versatility of the maleic anhydride group additionally allows for supramolecular interactions mediated by the electronegative and hydrophilic character of the carbonyl groups [I.124]. Thanks to the olefin backbone, a variety of hydrophobic matrices can be employed, making this a general purpose compatibilizer [I.125-I.127]. MA-*g*-PP forms a characteristic structure in which the maleic anhydride group is well ordered against the fibre and the aliphatic parts stick out perpendicular to the fibre. This increases the surface area and causes easier matrix entanglement. Varieties on the compatibilizer exist where the PP backbone is replaced by another olefin polymer like polybutadiene [I.128].

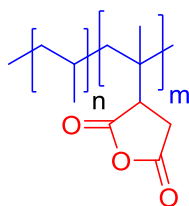


Figure I.12: Structure of MA-*g*-PP [I.119].

As mentioned earlier in Section 1.3.2.2., aramid fibres can be modified with plasma to introduce coupling groups for effective functionalisation. This can be used effectively to introduce the MA-*g*-PP compatibilizer onto the aramid surface as explored by Maity *et al.* [I.81]. A comparison is made between different Kevlar® fibre-reinforced PP composites with an increase of up to 60% in tensile strength and 110% in tensile modulus as well as a decrease of 60% in elongation at break, clearly indicating the improved stiffness of the composite [I.81]. Similarly, MA-*g*-PP has been applied for Kevlar® fibre-reinforced poly(ethylene-*co*-propylene) composites [I.66].

The usage of compatibilizers may be more efficient in more complex systems, such as hybrid blend composites of short Kevlar fibre/polyamide or isotactic PP [I.88] or Kevlar fibre-reinforced PP composites prepared as multi-layered hybrid fibres [I.131].

In the work of Li and coworkers, Kevlar fibre is treated with toluenediisocyanate to graft caprolactam functionality and compatibilizer is introduced onto the PP by grafting from maleic anhydride and PS [I.88]. Varying the amount of Kevlar fibre, polyamide fibre and compatibilizer allow for a precise control over tensile strength, flexural strength and impact strength. Additionally, there is a difference between the crystallisation curves of the composite material and PP matrix as the crystallisation of the composites is inhibited (**Figure I.13**).

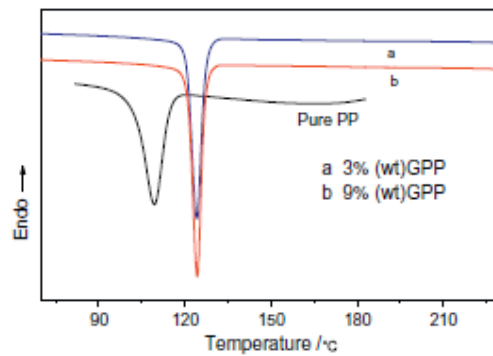


Figure I.13: DSC graph illustrating the crystallisation curves of pure PP and composite material with varying amounts of compatibilizer (GPP). Adapted from [I.88] with permission of Elsevier.

Due to the highly specific nature of a compatibilizer molecule depending on the composite material, many innovations in this area have been held by private companies with patented structures, such as DuPont's Fusabond, Polygroup's Propolder and Arkema's Lotader family of compatibilizers [I.130].

1.3.5. Conclusion

The interface region of a composite material is much more important than simply being a boundary region and critically affects the properties of a FRCM, with a smooth transition between the different phases preferred in terms of crystallinity and surface tension. Unfortunately, aramid fibres and several matrices show poor interactions, so treatments to modify the interface region are necessary to obtain market competitive FRCM. Different techniques are employed (and often combined) to realise this: abrasion of fibre and matrix to increase surface area and mechanical adhesion, chemical functionalisation of fibre or matrix to introduce additional functionality or changed parameters, like plasma grafting, hydrolysis and covalent bonding and the use of a compatibilizer, most notably maleic anhydride-grafted olefin polymers.

Techniques used to analyse the interactions between fibres and materials that come in contact with it (e.g. liquids) can be categorised as using force-based techniques like droplet detachment and nanoindentation.

Techniques used to analyse composite material range from mechanical tests, like pulling and indenting studies to microscopy techniques like SEM and X-ray based techniques for investigating surfaces and interfaces.

The techniques to improve composite material behaviour mentioned above, while providing improvements over the interface region properties, use increasingly exotic (acidic, high temperature, expensive) conditions, which makes them undesirable for industrial purposes. For this reason, an alternative 'bottom up' approach may be more desirable to improve the interface region, where by gaining control over the specific molecular structure of components used, properties may be more efficiently optimised. For this reason, several techniques to control precisely the structure of polymeric or oligomeric material will be discussed below.

2. Sequence-controlled polymers

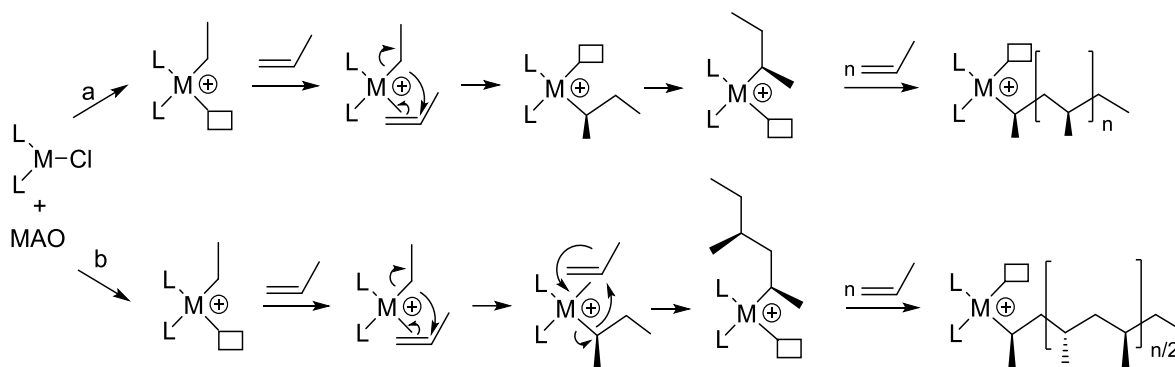
Thanks to their macromolecular structure, polymers hold distinct functional properties that are often exploited by both nature and chemists. Besides tuning their architecture and functionality, the control of microstructure of polymers is an important parameter in macromolecular engineering that has an influence on the properties of polymers. Monomer sequences have been studied regarding two aspects: (1) tacticity focusing on the stereochemical arrangement of the repeat units along the polymer chain [I.131-I.134] and (2) order of comonomers on the polymer backbone. Various approaches including catalyst-mediated copolymerisation, sequential copolymerisation, kinetically sequence-regulated copolymerisation, single monomer insertion in chain-growth polymerisation, template chemistry, monomer design and iterative synthesis have been proposed to control polymer microstructures. These strategies will be discussed in this section. This section does not aim at extensively covering the field, but at giving a brief overview of the different strategies developed and illustrating them with few selected examples.

2.1. Catalyst-induced control of the sequence

The nature of the catalyst used during the polymerisation can significantly influence the tacticity of polymers. Ziegler-Natta catalysts and metallocenes are industrially used to prepare stereospecific poly(α -olefin)s such as polypropylenes [I.135-I.136]. For example, isotactic (all substituents of the polymer backbone exhibit the same stereochemistry) polypropylenes have been prepared using TiCl_3 with diethylaluminium chloride as activator [I.136]. A commonly cited explanation for this result is the monometallic mechanism proposed by Cossee and Arlman (**Scheme I.1a**) [I.137].

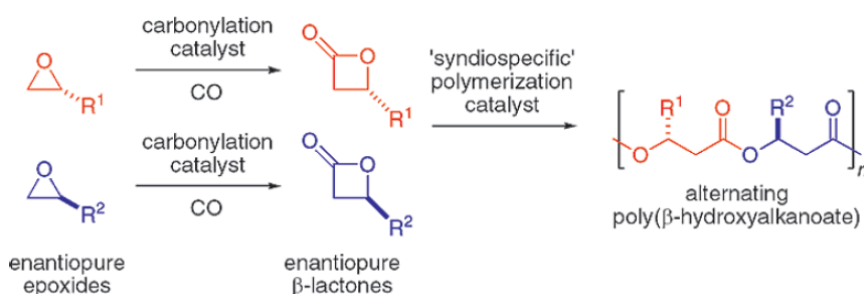
The aluminoxane undergoes a fast ligand exchange reaction with the transition metal chloride, leading to an alkylated transition metal and abstraction of one chloride from the transition metal catalyst by the aluminoxane. Then, a propylene monomer coordinates and subsequently inserts into the metal-alkyl bond. The more substituted carbon atom in this case will insert. Then, a migration takes place with which the growing chain is moved to the other vacant site on the metal centre. The process is repeated leading to isotactic polymers.

However, when a *ansa*-metallocene catalyst such as iso-propylidene(cyclopentadienyl)(fluorenyl) zirconium dichloride is used in conjunction with methylaluminoxane, syndiotactic (all substituents of the polymer backbone exhibit alternating stereochemistry) polypropylenes is obtained [I.138]. In this case, the migration step to move the growing polymer chain to a vacant site does not take place due to the steric arrangement of the ligands, causing an alternated insertion of the monomer (**Scheme I.1b**).



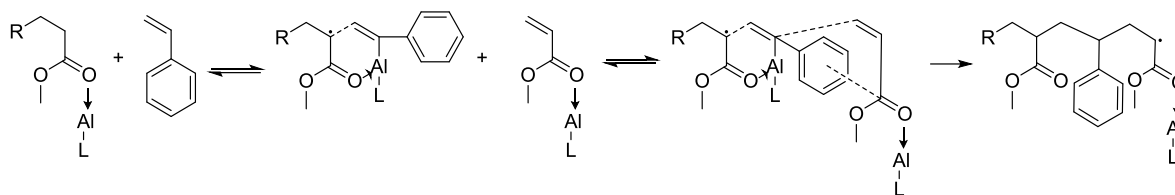
Scheme I.1: Coordination polymerisation leading to isotactic (M = Ti-based Ziegler-Natta catalyst, Cossee-Arlman mechanism) and b) syndiotactic (M = Zr-based *ansa*-metallocene) polypropylenes (L represents a ligand and □ a vacant site) [I.137].

More recently, Thomas and coworkers use syndiospecific bis(phenolate) yttrium polymerisation catalysts to synthesise alternating copolymers using a mixture of enantiopure lactones (**Scheme I.2**) [I.139]. As a first step, carbonylation is performed on epoxides to synthesise enantiopure lactone monomers followed by ring-opening polymerisation to form a poly(β -hydroxyalkanoate). Using these syndiospecific catalysts, copolymers with a high degree of alternation (91 to 94%) are obtained with possible sequences of AB and AAB.



Scheme I.2: Formation of alternating lactone-based copolymers. Adapted from [I.139] with permission of American Chemical Society.

Aside from metal catalysts, a classical method for obtaining alternating polymerisation lies in the use of coordination of Lewis acids. Early on, Imoto *et al.* have reported the coordinating effects of monomer pairs with zinc chloride [I.140-I.141], and Hirooka and coworkers followed up by reporting similar effects using ethylaluminium dichloride [I.142]. The Lewis acid acts as a catalyst, inducing a coordinating effect in the comonomer pair. The exact mechanism is unknown, but one model to explain this effect suggests that a charge transfer complex is formed via interaction between the monomer and Lewis acid which is unable to self-propagate and strongly enhances cross-propagation mechanism (**Scheme I.3**) [I.143-144].



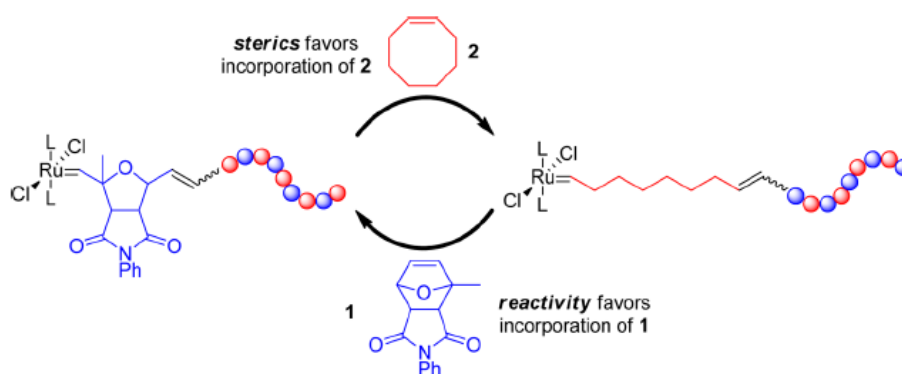
Scheme I.3: Proposed mechanism for the alternating copolymerisation of Lewis acid activated styrene and methyl acrylate [I.145].

A later example is found in using diethylaluminium chloride as Lewis acid to mediate alternating copolymerisations of styrene and methyl methacrylate by controlled radical polymerisation as described by Lutz, Kirci and Matyjaszewski [I.143]. The alternating polymerisation can alternatively occur with methacrylates or methyl methacrylates and alkenes using $\text{Sc}(\text{OTf})_3$ or activated acidic aluminium oxide as a Lewis acid [I.146-I.147].

In summary, catalyst-mediated polymerisations have been used to control the stereochemical arrangement of repeat units of same nature on the polymer backbone by choosing the proper stereospecific catalyst, but also to prepare alternating copolymers using Lewis acids.

2.2. Kinetically regulated monomer insertion

Besides using Lewis acid, the reactivity ratios of comonomers can be exploited to prepare alternating copolymers. In fact, alternating and periodic polymers are obtained in one-pot synthesis for specific monomer pairs and combinations respectively. The main reason for this alternating behaviour of the monomers is thanks to the formation of a comonomer pair complex in solution. In this comonomer pair, one monomer functions as an electron donor (e.g. styrene and vinyl ether) and the others as the acceptor (e.g. maleic anhydride and *N*-substituted maleimide). With this comonomer pair, cross-propagation is then favoured over homopropagation [I.148]. Typical examples of comonomer pairs are styrene with maleic anhydride for radical polymerisation [I.149], aromatic aldehyde with vinyl ether for cationic polymerisation [I.150] and ketene with aldehyde for anionic polymerisation [I.151]. The ability to form alternating copolymers has also been explored for ring-opening metathesis polymerisation (ROMP) [I.152-158]. The group of Sampson polymerises cyclobutene 1-esters and cyclohexenes due to kinetically favoured cross-polymerisation and inability of the monomers to perform homopolymerisation [I.152], while Deaffler *et al.* uses substituted oxanorbornene and cyclooctene (**Scheme I.4**) taking advantage of the low reactivity of the substituted oxanorbornene and steric hindrance effects and the proper choice of the ruthenium-based catalyst [I.153].



Scheme I.4: Alternated copolymer based on substituted oxanorbornene **1** and cyclooctene **2** prepared by ROMP. Adapted from [I.153] with permission of American Chemical Society.

Using the specificities of styrene and maleic anhydride copolymerisation, the group of Hawker demonstrates the nitroxide-mediated polymerisation of styrene in the presence of a small amount of maleic anhydride leading to the random insertion of maleic anhydride on the polystyrene chains at the early stage of the polymerisation followed by homopolymerisation of styrene once maleic anhydride is fully consumed [I.159]. Taking advantage of this feature, the group of Lutz locally inserts *N*-substituted maleimides at multiple positions along polystyrene chains under atom transfer radical polymerisation (ATRP) and nitroxide-mediated polymerisation conditions [I.148] as depicted on **Figure I.14**. A similar approach has been explored by the group of O'Reilly by ROMP based on the difference in reactivity of *exo* and *endo* norbornene isomers [I.160].

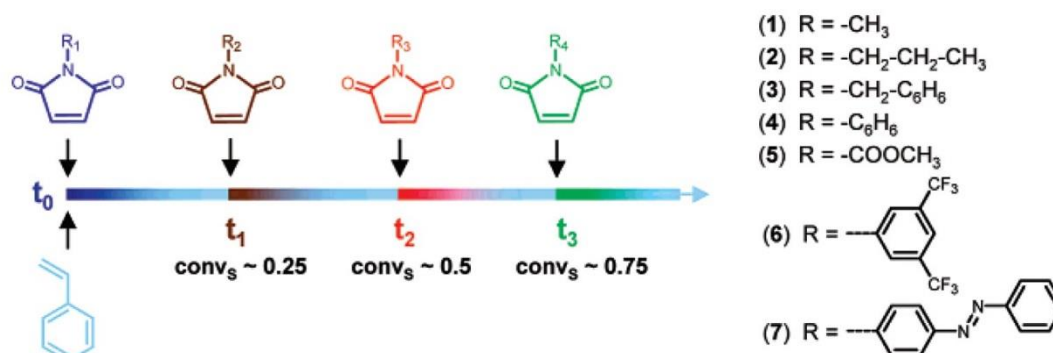
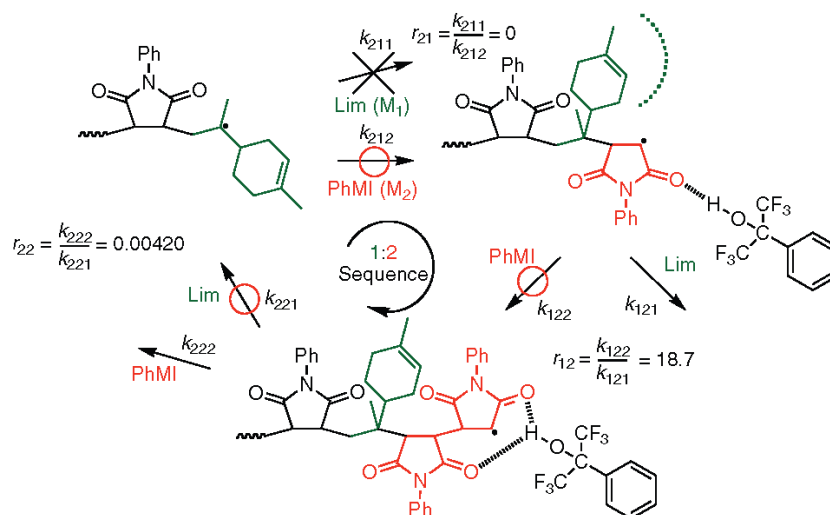


Figure I.14: Maleimide derivatives used for radical chain polymerisation reactions. Adapted from [I.148] with permission of American Chemical Society.

This behaviour shows versatility and can be used to synthesise not only alternating polymers with AB sequences, but also ABC and ABB periodic polymers depending on the monomers and conditions [I.161-I.164]. For example, AAB sequences is achieved using solvent interaction when making copolymers with *N*-phenyl maleimide (A) and limonene (B) monomers under ATRP conditions (**Scheme I.5**) [I.165]. In this reaction, the hydrogen bonding interactions caused by the solvent (fluorinated cumyl alcohol) are strengthened thanks to the solvent being fluorinated. This causes the solvent to have a preference to interact with two maleimide monomers and this strong interaction makes it possible for an AAB-sequence to be formed.

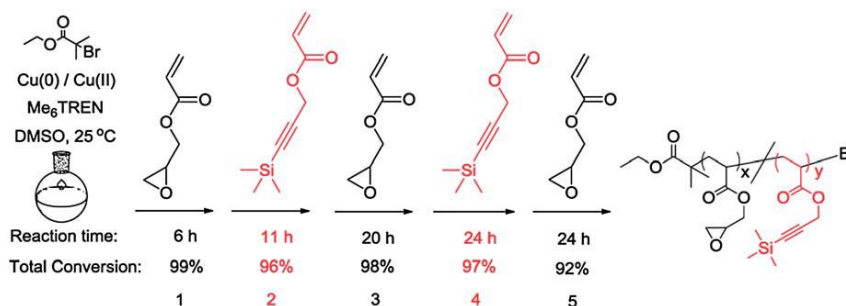


Scheme 1.5: Formation of the AAB periodic polymers via ATRP using hydrogen bonding interactions of fluorinated cumyl alcohol. Adapted from [I.165] with permission of American Chemical Society.

In summary, taking advantage of the reactivity of specific pairs of comonomers allows to prepare alternating and periodic polymers by controlled radical polymerisation and ROMP. Furthermore, the local positioning of a comonomer along a polymer has been demonstrated by timely adding a very small amount of rapidly consumed comonomer during the polymerisation of monomer mainly constituting the polymer backbone.

2.3. Sequential chain copolymerisation

Timely additions of comonomers after full conversion of the previous monomers have been studied since more than three decades to prepare block copolymers [I.166]. Recently, the investigation of multiblock copolymers synthesised by sequential chain copolymerisation has been pushed to the extreme to obtain copolymers with a large number of blocks [I.167-I.173]. In one recent example, pentablock copolymers are prepared by sequential addition at timed intervals of glycidyl acrylate and acrylic acid 3-trimethylsilylanyl-prop-2-ynyl ester under ATRP conditions (**Scheme 1.6**) [I.174]. By careful addition via cannula and correction for increased reaction time owing to the dilution when reactants are added, a balance is achieved between high conversion rate and low chain termination, leading to multiblock copolymers with dispersities of maximally 1.21.



Scheme 1.6: Synthesis of multiblock copolymers via timed addition. Adapted from [I.174] with permission of Royal Society of Chemistry.

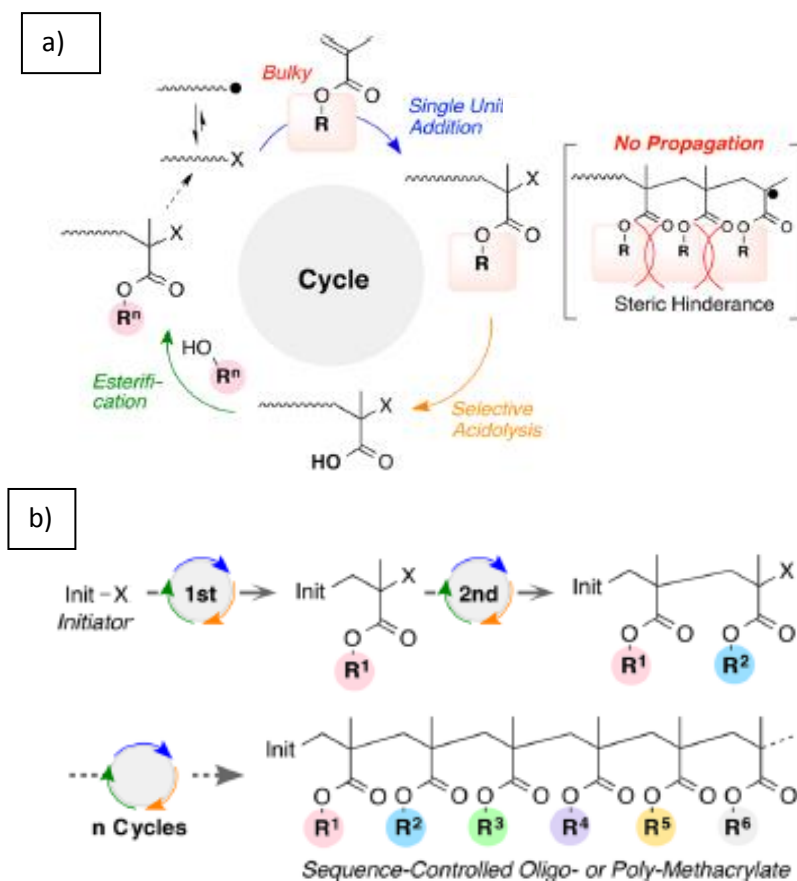
Polymerisation processes using external regulatory devices have the ability to be turned on and off

upon application of a stimulus, such as light, voltage and mechanical force, and have been applied to synthesise multiblock copolymers [I.175]. One example is the use of UV light to control the sequence of multiblock copolymers (up to 23 blocks) of acrylic monomers (methyl acrylate, ethyl acrylate, ethylene glycol methyl ether acrylate, and solketal acrylate) with variable block size (2 to 100 monomers per block) by ATRP [I.176-I.177]. UV light promotes photoinitiation by converting $\text{Cu(II)(Me}_6\text{-tris(2-aminoethyl)amine)Br}_2$ into $\text{Cu(I)(Me}_6\text{-tris(2-aminoethyl)amine)Br}$ with relatively high control over the rate owing to the ligand. The subsequent monomer is added to the reaction flask after polymerisation of the previous one without any purification and polymerised upon irradiation of the UV light, allowing for more rapid and convenient synthesis of high molecular weight polymers with relatively low dispersity, such as an undecablock copolymer with a molecular weight of $150 \text{ kg}\cdot\text{mol}^{-1}$ and a dispersity of 1.22.

In summary, various kinetic control techniques can be used to modify existing controlled radical polymerisation methods, allowing for sequence control over synthesised polymers, including functionalisation. Advances have been made in using timed additions, UV-light and temperature.

2.4. Single monomer insertion in chain growth polymerisation

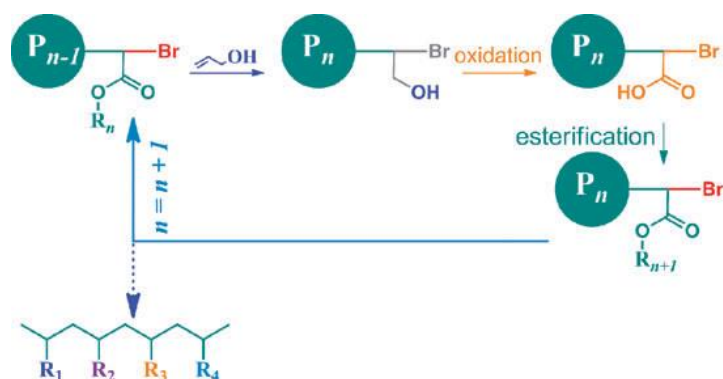
While sequential chain copolymerisation leads to block copolymers with some degree of control of the polymer microstructure, chain-growth polymerisation has also been used to perform iterative synthesis by means of single unit additions. Sawamoto and coworkers uses monomers with bulky side chains, such as adamantyl and isopropyl groups, to hinder propagation due to steric effects (**Scheme I.7**) [I.178]. After monoinsertion of the monomer, acidolysis is performed to remove the bulky group followed by esterification to introduce an arbitrary side group. After this, the next single unit addition takes place and the cycle is completed. This cycle can be repeated as many times as needed. As a proof of concept, various trimers including alkyl, alkene, alkyne and aromatic side groups have been synthesised using this method. The single unit addition iterative synthesis has also been extended to RAFT polymerisation using styrene, *N*-isopropylacrylamide, acrylates and acrylamide [I.179-I.184], but also conducted under photo-activation [I.185-I.187].



Scheme 1.7: a) Synthetic procedure of single unit addition using controlled radical polymerisation and b) formation of a sequence-defined polymer by the cycle described in a). Adapted from [I.178] with permission of American Chemical Society.

In a similar fashion, single addition has also been achieved for cationic polymerisation, making use of specifically functionalised vinyl ethers during polymerisation of isobutylene [I.188] or other vinyl ethers [I.189]. Owing to the bulky or strongly supramolecularly interacting nature, like Boc-vinyl ethers or diphenylethylene, mono-addition is favoured [I.189]. Steric hindrance effects also allow for single monomer addition in ROMP conditions using bulky cyclopropanes [I.190]

Another example of realising the single monomer insertion lies in selective reactivation of radical chain ends. As a proof of concept, Tong *et al.* has synthesised poly(methyl acrylate) using ATRP conditions which is subsequently modified for single monomer addition (**Scheme 1.8**) [I.191]. In the first step, the bromide-functionalised polymer is reacted with an excess of allyl alcohol. The hydroxymethyl group is then selectively oxidised into a carboxylic acid and finally esterified to obtain different side groups. Since the bromide remains active on the polymer, this technique can potentially be followed up with further controlled radical polymerisation or subsequent single monomer insertions.



Scheme I.8: Single monomer addition using allyl alcohol and its subsequent modification into acrylate unit. Adapted from [I.191] with permission of Royal Society of Chemistry.

Single monomer insertion has been also explored using metal-catalysed radical additions for the synthesis of vinyl polymers (**Figure I.15**) [I.192]. In this example, a specific initiator containing monomer is designed, containing two cleavable but renewable bonds (**Figure I.15a**), one of which being *N*-hydroxysuccinimide(NHS)-ester bond and the other ortho-pyridyl disulphide (Py-SS). The NHS-ester bond is cleaved upon attack of a primary amine, giving amide and NHS. The NHS-ester bond is then regenerated via esterification with an acid halide. The Py-SS bond is cleaved using alkyl thiol, giving disulphide and Py-SH. Then, using activated disulphide with electron withdrawing group adjacent to the S-S bond, the Py-SS bond is regenerated. The monomer-initiator is subsequently designed with the radical polymerisation mechanism in mind, owing to the bromide moiety on the initial NHS-ester side and methacrylate moiety on the Py-SS side. Dilute reaction conditions allow for monomer radical additions (**Figure I.15b**) driven by the proximity of the alkene group to the initiator moiety. Functionalisation can be realised through side chains of the introduced reagents on either the NHS-ester or Py-SS side (**Figure I.15a**). The reaction conditions allow thusly to use the specifically designed monomer-initiator as a tool for stepwise iterative insertions applied to RCP. As a proof of concept, a vinyl trimer has been synthesised with this procedure, recording coupling and cleavage yields >90%.

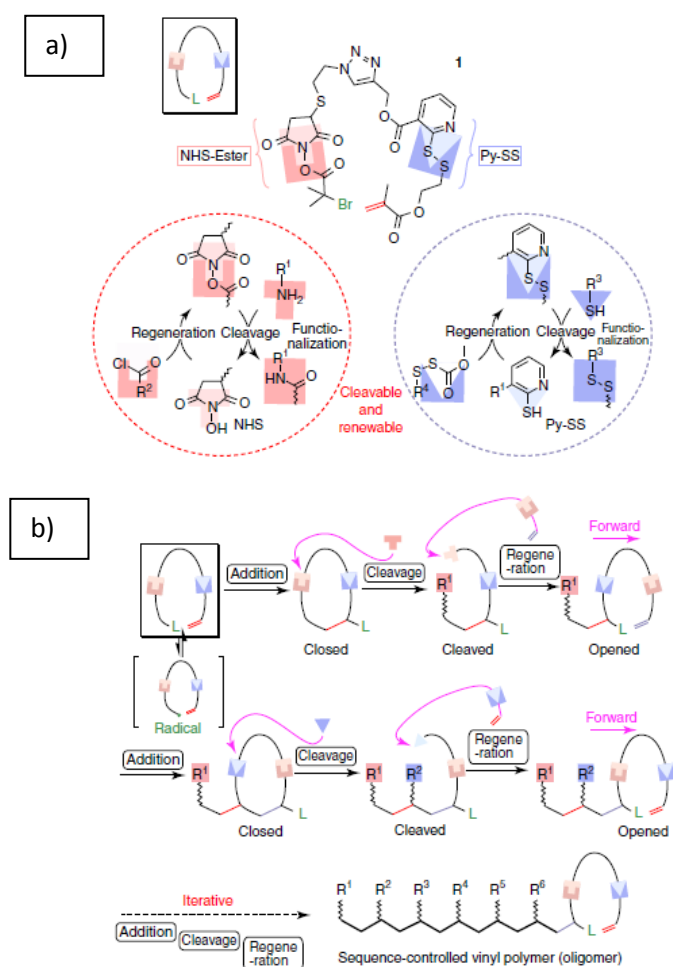


Figure 1.15: a) Design of the inimer bearing labile bonds that can be cleaved and regenerated and b) process involved for the synthesis of sequence-controlled vinyl polymers. Reproduced from open source [I.192].

In summary, single monomer insertion techniques have been used to modify controlled radical polymerisation to allow iterative synthesis, allowing for selective introduction of functional groups into polymers and increased sequence control.

2.5. Template chemistry

Inspired by Nature, supports (also called templates) can be used to non-covalently guide the synthesis of sequence-controlled polymers [I.193]. Monomers pre-organise on the template surface, before being polymerised (**Figure 1.16**). The mobility of the monomers and absorption/desorption processes play a role, with the possibility to gain control through non-covalent interactions.

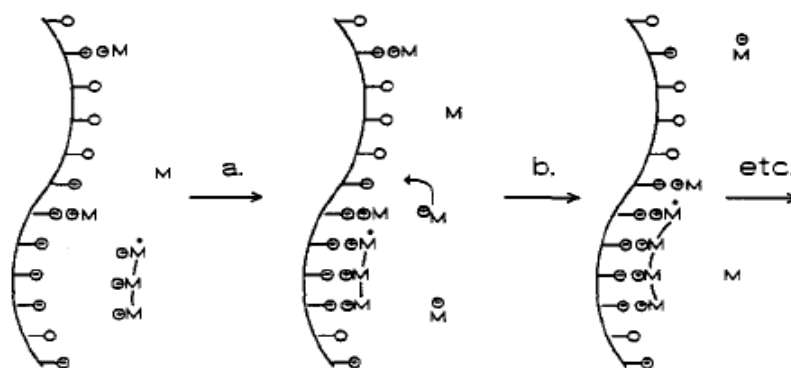


Figure I.16: Effect of using a supramolecular template for the polymerisation of *N*-vinyl imidazole. Adapted from [I.193] with permission of American Chemical Society.

Work has also been performed making use of DNA as a template in order to perform reactions [I.194]. This approach utilises the selectivity of DNA hybridisation to control reactions. Reactive groups are attached to oligonucleotide adaptors (using carbodiimide coupling chemistry and iodine based addition onto reactive triphenylphosphine) and reactions between the reactive groups are triggered by using hybridisation of the single strands to link reactants together, increasing their effective molarity and therefore reaction rate. The single strand oligonucleotides can then be abstracted selectively and stepwise coordination can take place with other functionalised oligonucleotides. (**Figure I.17**). The reaction is initiated with functionalised oligonucleotide A allowing functionalised oligonucleotide B to hybridise. Then, the oligomer is propagated a select amount of time with functionalised oligomers B and C sequentially using Wittig coupling reactions. Finally, monomer D is coupled to the chain and the chain is simultaneously cleaved in one step using another Wittig coupling reaction. All monomers contain specific side chains allowing for them to be identified using mass spectrometry techniques. This approach can be used to obtain decamers or even longer structures, with the possibility to incorporate different monomers and obtain more sequence control, but a limiting factor is the yield, with one step containing up to 37% impurities.

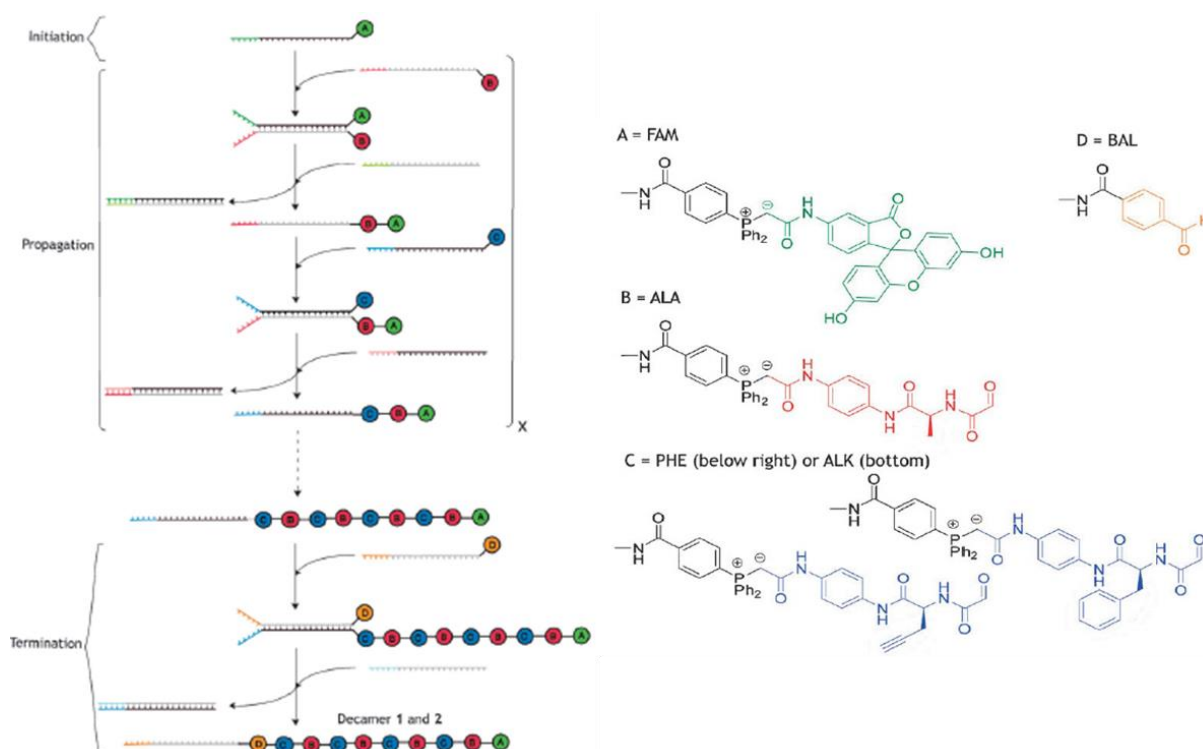


Figure I.17: Synthesis of a sequence-defined decamer using DNA as a template. Adapted from [I.194] with permission of Royal Society of Chemistry.

The group of Leigh has synthesised a synthetic ribosomal system and considered a covalent approach to prepare a peptide (**Figure I.18**) [I.195]. Firstly, the template is synthesised by copper-catalysed alkyne-azide cycloaddition (CuAAC) reaction to prepare a rotaxane comprising a macromolecule presenting amino acids at different positions. The template is capped at one of its extremity with a bulky ligand preventing the rotaxane from moving away from the starting position before performing the coupling reaction with the closest amino acid. Each coupling of the amino acids on the rotaxane takes place under basic conditions using native chemical ligation. After coupling reactions have taken place, the rotaxane is separated from the template and the protecting groups removed to obtain the final product.

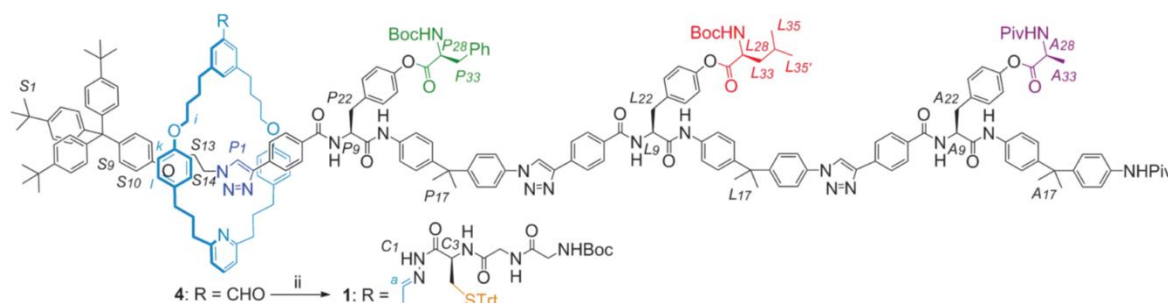


Figure I.18: Structure of the synthetic ribosomal system used to prepare FLA peptide. Adapted from [I.195] with permission of The American Association for the Advancement of Science.

This approach has been applied to chain-growth polymerisation. The group of Sawamoto has approached the template synthesis using molecules bearing an initiating site and a recognition site to specific monomers. Primary amines have been used to recognise specifically methacrylic acid when copolymerising methacrylic acid and methyl methacrylate that shows low reactivity as not recognised by the template [I.196], while crown ethers have been chosen to recognise cationic species of precise size [I.197]. More complex templates with multiple recognition sites have been developed through the use of a molecule with two initiating species, each initiating a specific polymerisation technique, i.e. cationic and radical polymerisations (**Figure I.19**) [I.198]. The cationic initiating site is first used to prepare the template, while the radical initiating site is then used to selectively polymerise methacrylic acid over methacrylates.

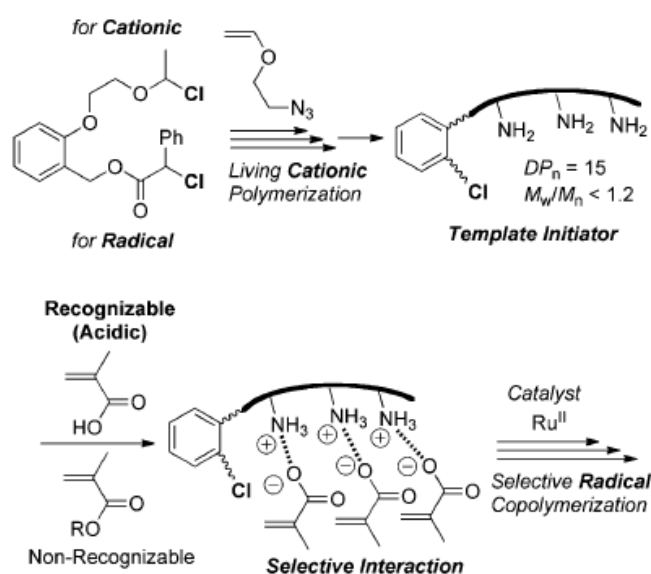


Figure I.19: Template-assisted sequence-regulated polymers through formation of a template by cationic polymerisation able to selectively polymerise methacrylic acid in the presence methacrylates. Adapted from [I.198] with permission of John Wiley and Sons.

Another approach consists of attaching the different comonomers on a template to induce the sequence upon polymerisation. For example, a methacrylate and an acrylate have been coupled to a naphthalene template resulting in an AB monomer (**Figure I.20a**). After performing ATRP, the template can be split off and an $(AB)_n$ -type polymer is formed. However, as proven by NMR analysis, the polymers only show 80% sequence specificity [I.199]. AAB periodic polymers have also been prepared using template polymerisation techniques using for example a palladium-based template for the polymerisation of styrene derivatives (**Figure I.20b**) [I.200]. The template functions by having two 4-vinylbenzylamines coupled to the template, while vinyl pyridine is coordinated to palladium in a square planar conformation, making certain that the monomers coordinate in an ABA sequence. Then, radical polymerisation takes place to synthesise the ABA sequence containing polymers. In order to prevent the styrene derivatives attached to the template from twisting into a less favourable conformation, 1,1,1,3,3,3-hexafluoro-2-phenyl-2-propanol is used as solvent which provides a strong

hydrogen bonding interaction to the carbonyl groups at the template. Thanks to the bulkiness of this group, the styrene derivatives stay in the conformation favourable for polymerisation, additionally showing π - π stacking behaviour. Using this method, the favourable conformation is achieved at a ratio of 95% at maximum.

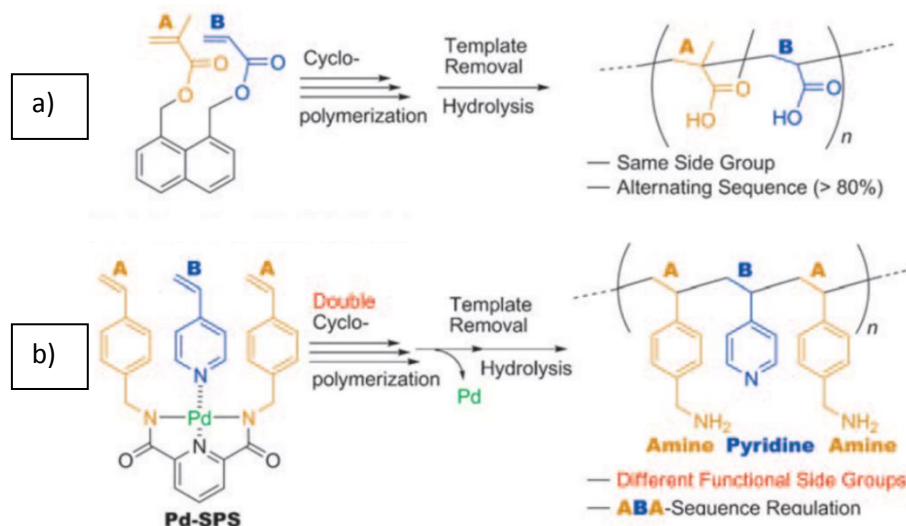


Figure 1.20: Synthesis of sequence-regulated copolymers using comonomers bearing template: a) naphthalene-[I.201] and b) palladium-based template. Adapted from [I.200] with permission of John Wiley and Sons.

In summary, several techniques to induce sequence control using a coordinating template have been described in literature, allowing for sequence control in existing synthetic techniques by pre-organisation of monomers. This allows for increased control over macromolecule sequence.

2.6. Sequence control via monomer design

As suggested in the last examples of the previous section, rather than using different monomers like A, B and C and tuning the reaction so that an ABC sequence is achieved, the design of ABC-constituting monomers that are then polymerised is an interesting strategy. The work of Hillmyer and coworkers on sequence-specific vinyl copolymers uses cyclooctenes bearing functional groups at well-defined positions (**Figure 1.21**). Regioselective ROMP is realised by using cyclooctenes functionalised on the 3 position and Grubbs' second or third generation catalysts [I.201]. After polymerisation, the polymer backbone is hydrogenated to obtain a polyethylene bearing substituents every two carbons in a specific sequence [I.202]. The R groups can be varied indifferently, however R_1 cannot be a proton as it would lead to a loss in regioselectivity. In order to overcome the limits related to the design of sequence-defined cyclic monomers for ROMP, the group of Meyer has designed sequence-defined oligomers terminated at both extremities with allyl groups [I.203]. This oligomer is then converted into a macrocycle by ring-closing metathesis in dilute conditions before performing ROMP.

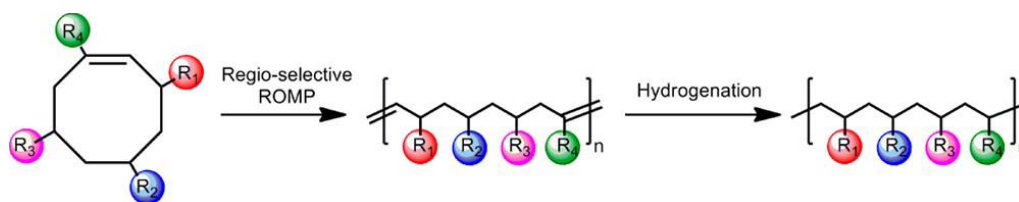


Figure 1.21: Synthesis of an ABCD polymer using a cyclooctene ABCD monomer. Adapted from [I.202] with permission of American Chemical Society.

An alternative approach to improve ROMP of sequence-controlled monomers lies in incorporating a designed enyne containing polymerisation trigger into an unstrained arbitrary macrocycle (**Figure 1.22**) [I.204]. After this, ROMP is performed to obtain sequence-controlled polymers containing different functionalities such as amide, ester, and sulphonamide.

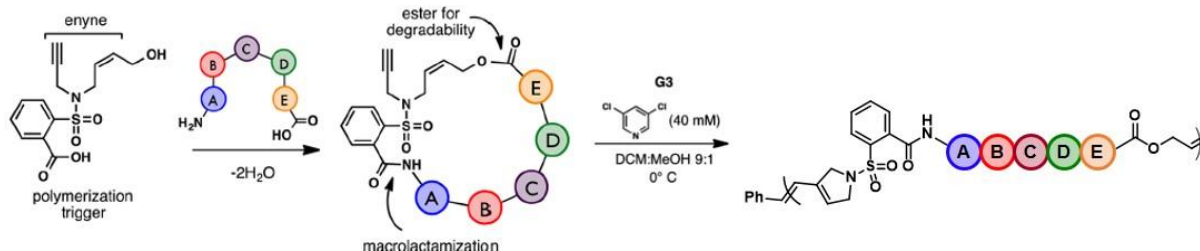


Figure 1.22: Incorporation of a polymerisation trigger molecule into an unstrained macrocycle and its ROMP. Reproduced from open source [I.204].

A similar technique is based on the synthesis of different types of monomers comprised of short monomer sequences which are then used in Kharash additions (**Figure 1.23**) [I.205]. The mechanism is an anti-Markovnikov type radical addition to alkenes, using a halogen containing initiator molecule. The ABC type monomer (A: chlorine, B: aromatic and C: ester functionalised vinyl monomer) is synthesised in two steps: firstly, using a ruthenium catalyst for a Kharash addition and then allylation using a titanium catalyst. The ABC-type monomer is then polymerised. Other ABC monomers along with ABCC monomers have been synthesised showing the wide versatility of this approach. One possible side reaction during the polymerisation is cyclisation. Depending on the ester substituents of the monomer (R^1) the amount of cyclisation can be anywhere in between 6 to 31% for the ABC monomers and down to 2% for the ABCC monomers [I.202, I.205].

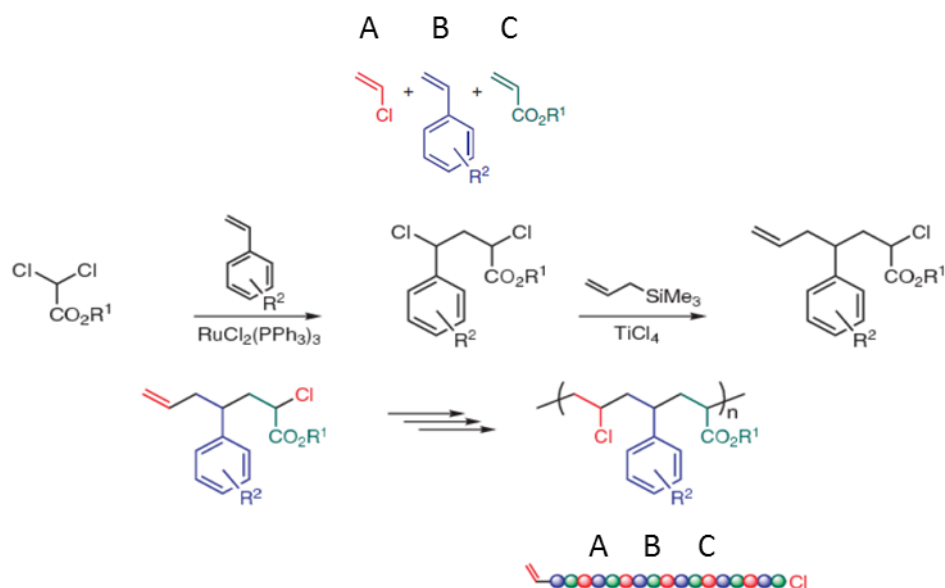


Figure 1.23: Synthesis of ABC-type sequence-controlled polymers using an ABC type of monomer. Adapted from [I.205] with permission of Springer Nature.

Segmer assembly polymerisation has been devised by the group of Meyer (**Figure 1.24**) [I.206]. This method consists of synthesising AB or ABA monomers by making use of protecting groups. After removing the protective groups, polymerisation occurs to form sequence-controlled polymers. This method has been applied to phenylene-vinylene-based polymers [I.206] and aliphatic polyesters [I.209]. However, if a sequence other than AB or AAB is desired, the group of Meyer predicts that catalysts properties would have to be exploited [I.206].

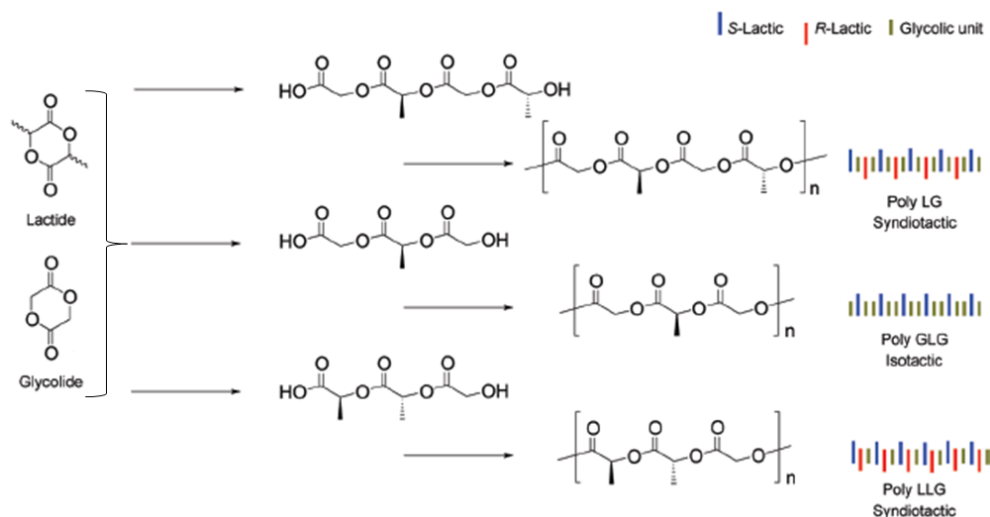


Figure 1.24: Segmer assembly approach using lactide and glycolide precursors. Adapted from [I.206] with permission of American Chemical Society.

In summary, sequence control has been introduced by selective design of monomers. While this method does not make use of sequence-controlled polymerisation reactions, the end result is a polymer with guaranteed targeted sequence which can rapidly be applied to existing polymerisation techniques.

2.7. Solid-supported iterative synthesis

Solid-phase peptide synthesis (SPPS) has been first described by Merrifield (**Figure I.25**) [I.208]. This synthesis utilises a resin bearing a linker as support which can be functionalised by any amino acid. For the addition of the subsequent amino acids, coupling reactions are achieved using a coupling reagent like *N,N*-dicyclohexylcarbodiimide. During any of the synthesis steps the growing peptide chain remains on the solid-phase support. SPPS has seen many innovations over the years, including those in automation for rapid synthesis [I.209].

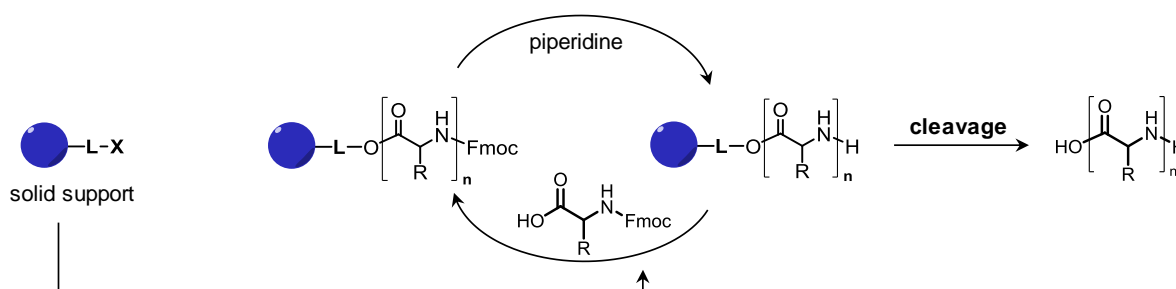


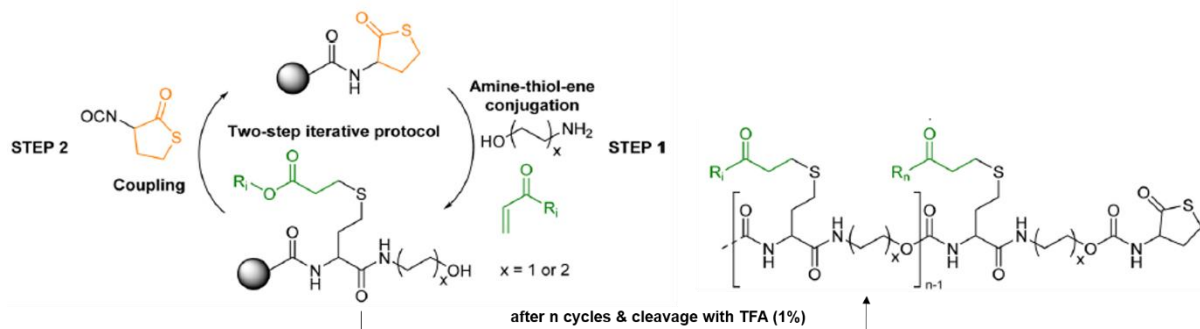
Figure I.25: Solid-phase peptide synthesis using Fmoc protecting groups. L = linker molecule, X = leaving group.

SPPS allows to make use of non-natural amino acids [I.210-I.211], but also to prepare sequence-defined polymers. One of the drawbacks of solid support-based synthesis for peptides is the yield. With each monomer addition to a growing oligomer chain, another deprotection step is required. However, some approaches have been developed applying reactions such as aromatic substitutions, condensations, Grignard reactions, Michael additions, oxidation/reduction and olefinations, which are commonly used in organic synthesis [I.212]. For example, Zuckermann and coworkers have prepared a broad spectrum of peptoids, i.e. poly(*N*-substituted glycine)s, with coupling efficiencies similar to those of peptides, but with eliminated needs of protection groups, allowing for convenient synthesis of various long peptoids [I.213-I.215], which can be extended to be used in a combinatorial fashion [I.216].

Lutz and coworkers have developed approaches that do not require deprotection steps by solid-supported synthesis using a binary system [I.217], known as an AB + CD process (here with the letters labelling functional groups: A = carboxylic acid, B = alkyne, C = amine, D = azide). The important properties of these AB and CD units is that A solely reacts with C and B solely with D. In practice, this means that there are no protecting groups required for this solid-supported synthesis and there remains a possibility of using different types of monomer in sequence. As a proof of concept, the synthesis is done using a Wang resin and two different AB type units, one containing a methyl group (1) and one without (0). Using this technique, eight different oligomers with sequences ranging from 000 to 111 have been synthesised with high unimolecularity and purity.

The AB+CD solid phase approach has been extended for the synthesis of different oligomers such as oligurethanes [I.218] and oligomers with a triazine backbone [I.219]. In particular, work done by Du Prez and coworkers uses thiolactone chemistry (**Scheme I.8**) to obtain thiol-functionalised oligomers

[I.220-I.221], which can be modified with PEG [I.222] or various aromatic and aliphatic groups [I.223]. In the first step of the synthetic cycle, thiolactone on solid support is selectively opened by reacting with the amine function of an amino alcohol (ethanolamine or 4-amino-1-butanol). As a result, a thiol is released, which reacts with any functionalised acrylate or acrylamide through thiol-ene chemistry, incorporating functionality. Finally, chain extension is performed via the reaction of the readily available and stable α -isocyano- γ -thiolactone with the remaining alcohol function [I.220].



Scheme 1.8: Iterative AB+CD approach using thiolactone chemistry. Adapted from [I.220] with permission of Royal Society of Chemistry.

The group of Lutz has extensively researched phosphoramidite chemistry on solid support as a tool for synthesising sequence-defined polymers with relative convenience to be analysed using mass spectrometry techniques [I.224-I.226]. This phosphoramidite chemistry has been also combined with nitroxide radical coupling reaction [I.227]. The first coupling step involves functionalisation of a solid support using the reaction of a phosphoramidite monomer functionalised with bromine reacting to a hydroxyl group. This is followed by oxidation of the phosphite linkage into a phosphate bond. Then, the nitroxide radical coupling reaction is utilised making use of a copper catalyst. The difference in monomer side chains is exploited to encode data. Nitroxide radical coupling reaction has been also combined with amine and acid anhydride chemistry [I.228].

In summary, solid supported iterative synthesis has been classically used alongside the development of polymerisation techniques to synthesise peptides and peptide derivatives. However, the application of solid supported iterative synthesis has been extended to other techniques, including orthogonal (AB+CD) and phosphoramidite chemistry.

2.8. Beyond solid phase iterative synthesis

Although the solid phase resin was initially developed as a convenient tool for intermediate purification and synthesis of growing macromolecules, there are a number of limitations, such as compatibility between the resin and the type of chemistry, necessity for loading and cleaving techniques, difficulties with scale up and potential external parameters such as temperature and pressure [I.229]. It is for these reasons that in recent years, some techniques have been proposed to move away from the solid phase constraints.

The first approach consists in using a liquid support that could be a polymer tag [I.230] or smaller molecules with specific abilities of separation [I.231]. For example, the group of Alabi combines photo-initiated thiol-ene click chemistry with phosphine-catalysed Michael addition between thiols and acrylamide groups in a AB+CD approach on a fluororous support. This support solubilises to perform chemistry similar to what is known for solution phase, but is used in purification similar to a solid phase support. The fluororous support approach has been extended to use dithiols and *N*-allylacrylamides [I.232], and also to include aromatic, amine and hydroxide moieties within the macromolecules [I.233]. Multicomponent reactions aim at conducting consecutive reactions in the presence of multicomponents in a single process. The main multicomponent reactions are Passerini and Ugi reactions. The Passerini three-component reaction uses an isocyanide, a carboxylic acid (stearic acid) and an aldehyde olefin (**Figure I.26**). The Passerini reaction is repeated up to a desired number of sequences and optionally thiol-ene addition is used to introduce functional groups [I.234]. Meier and coworkers have applied this multicomponent reaction to the synthesis of a decamer. Here, the sequence itself is controlled by stepwise addition of the isocyanide monomer with variable aldehydes [I.235]. Alternatively, additional functionality may be introduced by modifying the Passerini three-component reaction into the Ugi four-component reaction, which includes the addition of an amine as one of the reactants. A drawback for this method is the decreased total yield of the tetramer over similar amount of steps (15% vs 34% for the Passerini three-component reaction) [I.236]. The Ugi four-component reaction has been applied for the incorporation of various side groups, including sugars [I.237].

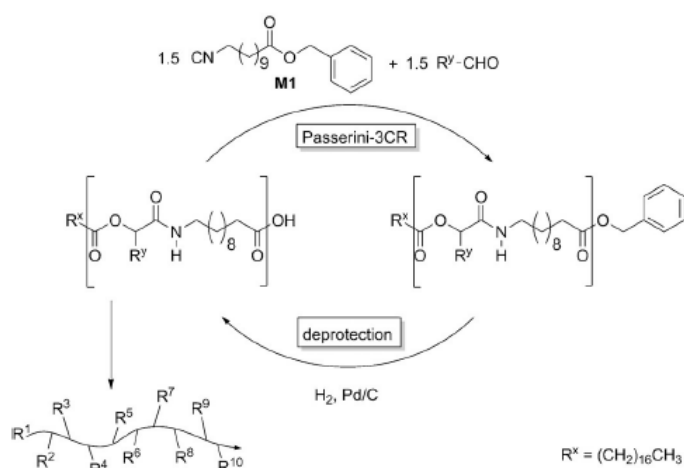
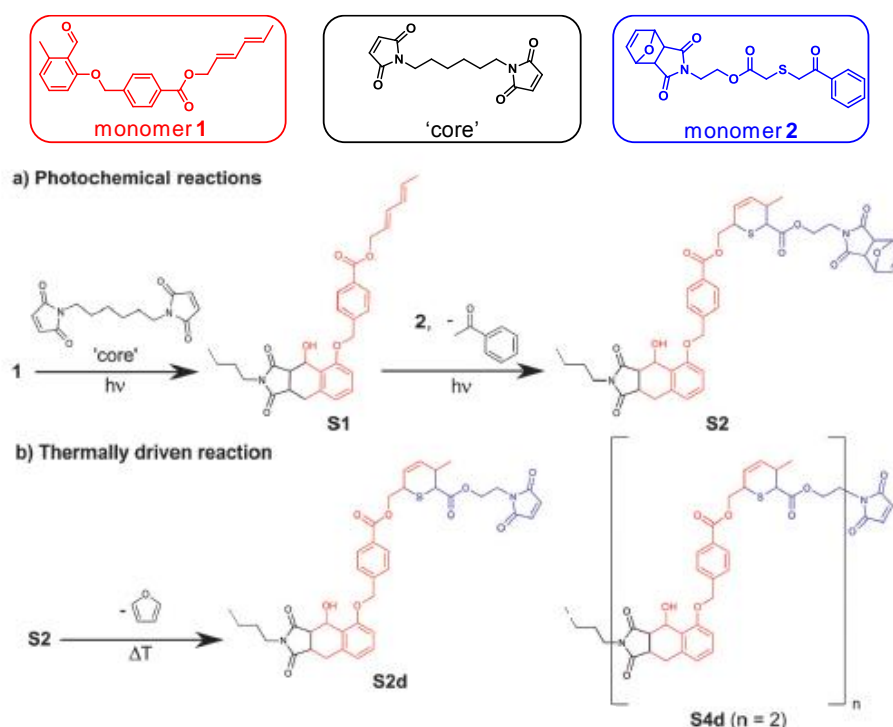


Figure I.26: Synthesis of a sequence-defined decamer using the Passerini three-component reaction. Adapted from [I.235] with permission of John Wiley and Sons.

Besides the Passerini and Ugi reactions, other synthetic routes using a multicomponent strategy have been explored. AB+CD chemistry can be performed in solution in one-pot making use of a photoinitiator [I.238]. Thiol-ene click chemistry can also be expanded by making use of consecutive alkyne-azide-amine and amine-thiol-ene conjugations to achieve multiple AB+CD reaction in one-pot,

achieving ABCBA and DABCBADE sequences [I.239]. More examples of AB+CD approaches include Diels-Alder cycloadditions, strain-promoted azide click reactions [I.240] and the use of elemental selenium [I.241].

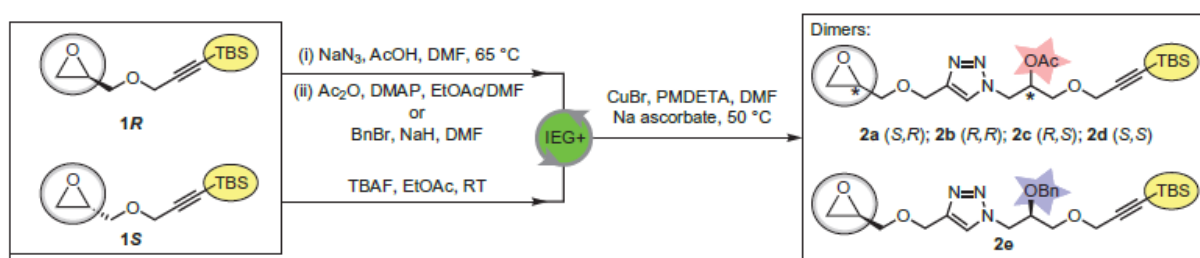
Exploiting the ability of maleimide groups to undergo Diels-Alder transformations and orthogonality with furan protective groups, Barner-Kowollik and coworkers have set up a proof of concept for the iterative synthesis of a unimolecular decamer in solution (**Scheme I.9**) [I.242]. A core bismaleimide undergoes a Diels-Alder ligation with a photoenol (monomer 1) under UV light. A phenacylsulfide (monomer 2) is then added to the growing chain via another photo-activated reaction, using highly reactive thioaldehyde. The furan protective group is then removed via a thermally activated retro Diels-Alder reaction, after which additional maleimide groups are available for further photochemical reactions. The orthogonality of the reactions and subsequent unimolecularity of the product have been proven using NMR and MS.



Scheme I.9: Synthetic procedure of a unimolecular oligomer using iterative photochemical and thermally driven reactions. Reproduced from [I.242] with permission of Royal Society of Chemistry.

To increase the size of sequence-defined oligomers, the iterative exponential growth (IEG) has been developed that can be combined with side chain functionalisation of the polymer (IEG+) achieving sizes up to $12\,000\text{ g}\cdot\text{mol}^{-1}$ at gram scale [I.243-I.244] or automated in flow [I.245]. Similar to the AB+CD approach, the IEG procedure makes use of two orthogonal reactive groups on a single monomer (**Scheme I.10**). The epoxy and TBS-protected alkyne groups are converted into a reactive alkyne and azide, suitable to use for CuAAC, which results in a dimer with once again epoxy and TBS protected alkyne ready for the next coupling steps. The exponential part lies in the ability to continue to couple triazole containing oligomers to each side of the growing chain, exponentially increasing the size of the

macromolecule. For example, two dimers will form a tetramer, two tetramers an octamer and so on. Sequence is now stored in the side chain difference. However, as can be expected, the control over this sequence diminishes with each exponential growth step, limiting this iterative technique. In a similar fashion, work done by Monteiro and coworkers allows for the synthesis of high molecular weight sequence-controlled polymers using alkynyl alcohol monomer [I.246]. After performing CuAAC between the terminal alkyne and an available azide moiety, the alcohol group on the monomer is converted into an azide using phosphorazidate, forming an oligomer with continuous azide and alkyne reactive groups.



Scheme I.10 IEG+ synthetic procedure leading to the formation of dimers with different side groups. Adapted from [I.243] with permission of Springer Nature.

In summary, iterative synthetic techniques popularised by solid phase methods have been extended beyond the solid phase constraints, including using soluble supports, orthogonality of reactive groups in solution phase and multicomponent one pot reactions.

2.9. Impact of sequence control on polymer properties

A multitude of techniques have been developed to gain control over monomer sequence for the preparation of sequence-controlled polymers. To control the microstructure at the repeat unit level, some of these approaches aims at tuning the conditions of chain-growth polymerisations, while others take advantage of the developments in biochemistry to extend well-established techniques using modern chemistry routes to prepare unnatural sequence-defined polymers.

The use of sequence-controlled polymers has already shown some impacts on the mechanical, thermal and crystalline performances of various polymer materials. For example, aromatic polyethers with sulfone and biphenyl subunits have shown drastic differences in crystallinity owing to the differences in crystalline behaviour of the monomers, with the highest amount of crystallinity for polymers having systematically triplets of biphenyl subunits and the lowest for alternating sulfone and biphenyl subunits [I.247]. A similar effect has been obtained for poly(ether ketones) synthesised using 4,4-dihydroxybenzophenon and 1,3-bis(4-fluorobenzoyl) benzene monomers, showing a decrease in crystallinity with increasingly randomly organised copolymers [I.248]. Furthermore, poly(lactic-co-glycolic acid)s with specifically incorporated AB, ABA or AAB type segmers have shown unique, but yet undetermined, conformational differences in solution, as indicated by both NMR and SEC. Additionally, differences in T_g have been observed depending on the sequence [I.206]. Moreover, studies on

oligomeric *p*-phenylene-vinylene and benzothiadiazole also shows differences in electrochemical behaviour. Notably, extremities in HOMO-LUMO gap sizes are found with more block like structures in oligomers such as ABBBB or AAABBB while more averaged gap sizes are found for more alternating oligomers (ABA or AAB). The monomer which is placed at the extremity of the oligomer has a large influence on the oxidation potential, melting point and extinction coefficient [1.249-1.250].

Control over tensile toughness was achieved using sequence-defined peptide-polymer hybrids as interfacial agents for nanoparticle reinforced composite materials. In the work of Börner and coworkers, peptide- poly(ethylene oxide) conjugates (MBC) are used to bind to magnesium fluoride nanoparticles embedded in poly(ϵ -caprolactone) (PCL) matrix [1.251-1.252]. In earlier work, peptides were identified by phage display biospanning to show material-specific adsorption onto inorganic or soft matter surfaces. In particular, the peptide sequence Thr-Gln-Tyr-Tyr-Ala-Tyr-Ser-Thr-Thr-Gln-Lys-Ser was found to specifically bind onto MgF [1.253]. This sequence was then further functionalized using a fluorescent dye on the N-terminus and PEG on the C-terminus [2.252].

An overview of the mechanical properties is given below (**Figure 1.27**) [1.251]. What is found is that the tensile, compressive and indentation moduli are increased for compatibilized composite materials in comparison to pure matrix, matrix/compatibilizer mixtures or matrix/untreated nanoparticle mixtures. Especially using low weight percentage of nanoparticles allowed for modulus increases of up to two times the uncompatibilised composites, indicating a strong effect of the compatibilizer [1.251].

The researchers found that the mechanical properties are likely correlated to the crystallinity of the poly(ethyleneoxide) and specifically cite the existence of β -sheet fibrils in the compatibilizer as driving factor [1.252].

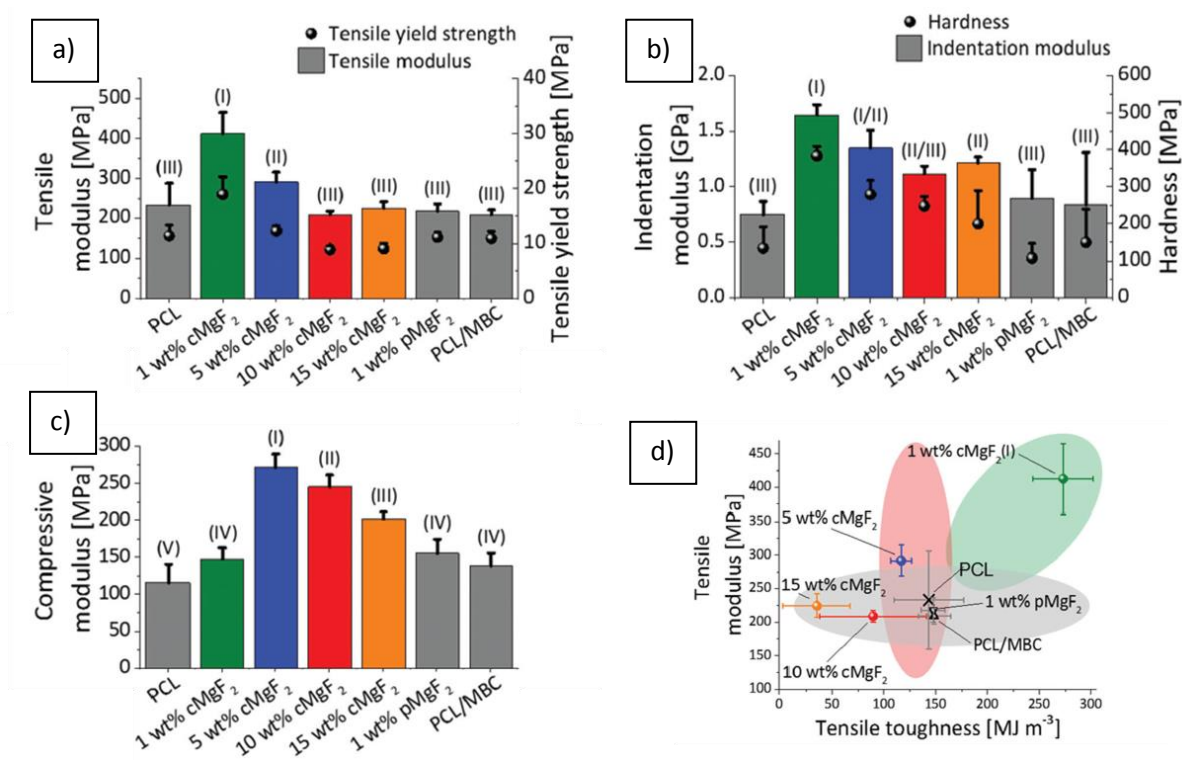


Figure 1.27: Mechanical tests for a) tensile modulus, b) indentation modulus, c) compressive modulus of pure matrix (PCL), matrix compatibilizer blend (PCL/MBC) and matrix reinforced by either untreated (pMgF₂) or treated (cMgF₂) nanoparticles. d) An overview of the tensile modulus vs tensile strength of the reviewed composite materials. Reproduced from [1.251] with permission from Royal Society of Chemistry.

More recently, the molecular dynamics simulation work of the group of Simmons demonstrates the potential enhancement of the compatibilization of polymer blends using sequence-defined polymers with specific sequences that are not block copolymers [1.254]. The sequence of differently sized blocks is varied and lead to different surface energy values as a result. The lower surface energy stabilises the existence of the compatibilizer at the interface region. The best compatibilization (or lowest surface energy) is achieved with compatibilizers showing a disperse block length distribution relative to the possible amount of molecules per area. As most processes related to supramolecular interactions, entropy and enthalpy tradeoffs are especially relevant. The authors conclude that sequence-specific compatibilizers have the potential to substantially outperform blocky and random sequence compatibilizers in the reduction of interfacial energy at interfaces with a large difference in surface energy.

Having considered the conclusions of the work of Börner and coworkers and Simmons and coworkers, the development of specific sequence seems to be a key parameter for the tuning of properties of interfacial agents. Furthermore, notable research has been done in iterative sequence control. With this in mind, Chapter II will highlight the application of sequence control in the synthesis of new compatibilizer molecules, specifically designed for the interface region of aramid fibres and polymeric matrix.

CHAPTER II

Preparation and characterisation of oligomers based on phenylalanine and aliphatic building blocks by solid-phase synthesis

Chapter II: *Preparation and characterisation of oligomers based on phenylalanine and aliphatic building blocks by solid-phase synthesis*

1 Introduction

As mentioned in Chapter I, the design of suitable compatibilizer molecules for fibre-reinforced composite materials mainly lies in the utilisation of covalent and non-covalent bonds to equalize surface tension differences between different parts of a composite material [II.1]. Most commonly described for commercial products are block copolymer or grafted polymer compatibilizers, such as polystyrene-*block*-polyethylene, or olefins with grafted maleic anhydride groups. In its most simple form, the block copolymer compatibilizer resembles the two parts of a composite material, with block copolymer compatibilizer $((A)_n-(B)_k)_m$ for any given composite of materials A and B. Interactions may then further be governed by the use of covalent bonding or morphology of the compatibilizer used. However, in the case of FRCM, the compatibilization process may quickly become more difficult to realise.

Similarly described in Chapter I, aramid fibres, despite having desirable mechanical properties for composite materials, are not widely applied as such due to poor interactions between it and common matrix materials [II.2-II.3]. While several techniques have been described to modify the fibre surface or matrix in Chapter I, they are not sufficient to encourage further use of aramid fibre in composite material. In order to achieve an improved interface between aramid fibres and various polymeric matrix material, specific design of compatibilizer can be considered. Molecular dynamic simulations on polymer blends have predicted that the copolymer structure is a determining factor in proper dispersion of the surface energy, with irregular structures favoured over regular structures like block copolymers [II.4]. It may very well be comparable for FRCMs. Various methods of achieving sequence control over oligomers or polymers have been discussed in Chapter I. As concluded, precise control is possible using iterative synthetic procedures and as such it has been chosen as a suitable method for the synthesis of specific compatibilizers.

For the application of compatibilizers the design should rely on specific building blocks to mitigate interactions with previously mentioned aramid fibres and a chosen polymer matrix material, here polypropylene. Phenylalanine units were considered here as the main contributor of interactions between the compatibilizer and the aramid fibre. Illustrated in **Figure II.1** is an overview of the overlap of interactions phenylalanine residues can have with aramid groups as compared to model molecules (oligoglycine and oligostyrene).

Chapter II: Preparation and characterisation of oligomers based on phenylalanine and aliphatic building blocks by solid-phase synthesis

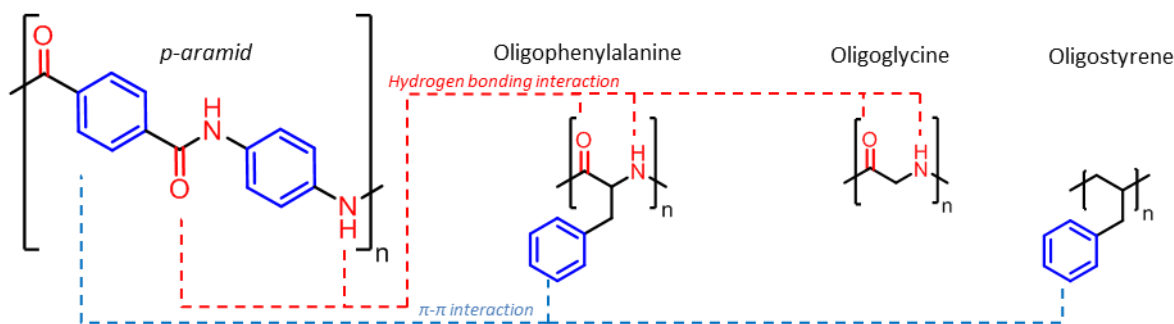


Figure II.1: Illustration of the potential interactions (π - π and hydrogen bonding) between p-aramid and model molecules such as oligophenylalanine, oligoglycine and oligostyrene.

The first type of visible interactions possible with aramid polymers are hydrogen bonding interactions. These are a strong type of interactions (typically $14\text{--}15\text{ kJ}\cdot\text{mol}^{-1}$) [II.5] and in nature are the main provider of various structures in macromolecules, aromatic polymers and biomolecules like DNA and proteins, such as turns, folds and more pronounced structures like beta-sheets, beta-barrels and alpha-helices [II.6-II.7]. Common to all peptides are the amide bonds (H-N-C=O) which allows them to perform those hydrogen bonding interactions and it is likely that they are able to perform those types of interactions with the aramid surface.

The second type of interactions visible in **Figure II.1** is π -type interactions, including sandwich (face-to-face π - π stacking), T-shaped (edge-to-face π - σ interactions), and parallel displaced (offset π - π stacking), resulting of the quadrupole of the aromatic group, which effectuates an enthalpic energy gain by associating with similar groups. The orientation and strength of this interaction is dependent on its molecular structure, any present solvents and availability in the 3D environment [II.6]. Examples of these kinds of aromatic interactions have been exploited for systems such as Bucky ball catchers [II.8] or foldamer structures [II.9], indicating the similar strength to hydrogen bonding the interaction has over the structure of macromolecules. In protein structures, phenylalanine serves as a main contributor to π - π stacking interactions [II.10]. With an energy gain of up to $3.3\text{ kJ}\cdot\text{mol}^{-1}$, the interaction is significant and provides reason for the complex type of orientations necessary for proteins to perform their desired function. Theoretical research has shown that the orientation of the phenyl groups in respect to each other is a large factor in their interaction, with structures with slight differences in orientation being favoured as well as T-shaped interactions [II.11-II.13]. Therefore, the π -interactions are not merely attractive; they also introduce constraints into the conformation of two molecules in respect to each other.

Considering these two types of interactions, phenylalanine is of particular interest as a suitable building block for compatibilizer molecules for aramid fibre-reinforced composites. One way to control this orientation and flexibility to orient the phenylalanine residues lies in the use of variable length flexible spacers. Considered was the simplest form of those spacing, namely aliphatic groups. These had been

Chapter II: Preparation and characterisation of oligomers based on phenylalanine and aliphatic building blocks by solid-phase synthesis

chosen in order to reduce any possible influence the spacing may have other than flexibility. To obtain control over the type of interactions with the aramid surface and the influence of the spacing length, iterative synthetic techniques were chosen to allow sufficient precision in structure design. We find our solution in solid-phase synthesis, which has been used in large amounts for a little over 50 years to obtain various peptide structures [II.14]. As a starting point for the synthesis, protocols already developed at the ICS [II.15] were adapted. This chapter will focus on improvements in the adapted protocols for the preparation of the targeted molecules, analysis and characteristics, such as their solubility and advances in purification.

2. Synthesis of phenylalanine-based oligomers

2.1. Description of the synthetic strategy used

The approach considered three types of building blocks (amino acid, spacers and linker) [II.15]. As discussed in the introduction, phenylalanine (F) was considered as the amino acid to promote the interaction with p-aramid fibres. ω -azidoalkanoic acids were applied as spacers in various lengths to gauge the effect of the aliphatic chain length. Lastly, the linker precursor was propargylamine (\bullet). The iterative synthetic procedure made use of a solid-phase resin possessing 2-chlorotritylchloride (CTC) functional groups (**Figure II.2**).

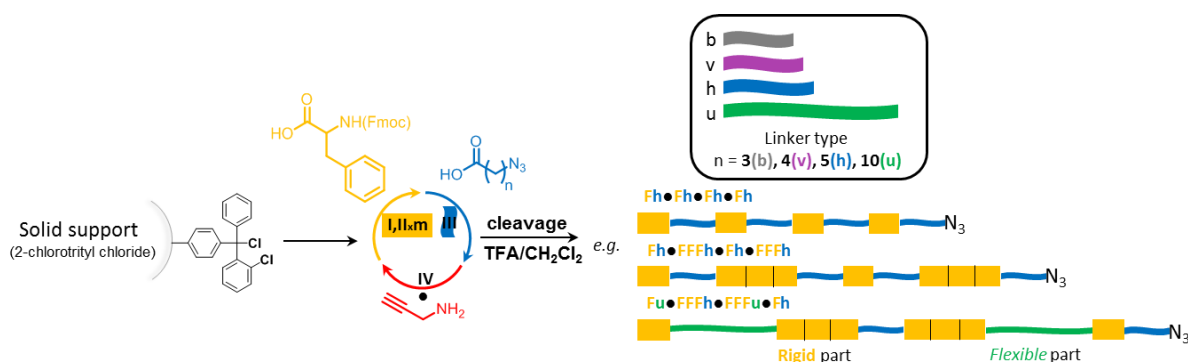


Figure II.2: Synthetic approach to prepare the targeted phenylalanine-based oligomers. The synthesis was performed on a CTC resin with four repetition cycles consisting in: **I**) addition of phenylalanine residue (Fmoc-Phe-OH, HBTU, HOBT, DIPEA, DMF), **II**) Fmoc removal (piperidine in DMF), **III**) addition of spacer (ω -azidoalkanoic acid, HBTU, HOBT, DIPEA, DMF) and **IV**) addition of linker precursor (propargylamine, CuBr, PMDETA, DCM).

In **step I**, phenylalanine was added using the protected amino acid, Fmoc-Phe-OH, indicated in orange on **Figure II.2**. The synthesis was performed using 2-(1H-benzotriazol-1-yl)-1,1,3,3-tetramethyluronium hexafluorophosphate (HBTU) as coupling agent in the presence of 1-hydroxybenzotriazole (HOBT) and diisopropylethylamine (DIPEA) in DMF. In **step II**, the Fmoc protecting group was removed under basic conditions using a solution of piperidine in DMF (25/75 by volume). In **step III**, the spacer was added using similar reaction conditions as in **step I** as depicted in blue on **Figure II.2**. In **step IV**, propargylamine was added by CuAAC using copper(I) bromide and N,N,N',N'',N''' -pentamethylenediethylenetriamine (PMDETA) in DCM as depicted in red on **Figure II.2**. These steps were repeated until the targeted sequence was obtained and the oligomers were

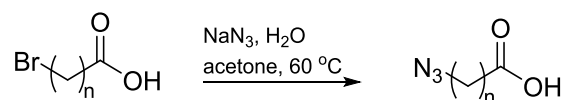
Chapter II: Preparation and characterisation of oligomers based on phenylalanine and aliphatic building blocks by solid-phase synthesis

recovered after cleavage from the resin under acidic conditions using either a solution of trifluoroethanol in DCM (25/75 by volume) for oligomers with less than eight phenylalanine residues or trifluoroacetic acid (TFA) in DCM (50/50 by volume) for any others.

Because the oligomer remained attached to the resin during every reaction step, purification was simplified between steps. Reactions could be performed successively and any impurities could be removed by filtration. The limits were the amount of time and steps as the yield will be lower with each additional step. To obtain quantitative coupling yields, excess of reagents was used.

2.2. Synthesis of ω -azidoalkanoic acids

In order to facilitate the synthesis of oligomers by varying the spacing between phenylalanine residues, aliphatic spacing units were synthesised. Targeted spacing units were unsubstituted ω -azidoalkanoic acids varying the number of methylene groups between three and ten, i.e. 4-azidobutyric acid (**b**), 5-azidovaleric acid (**v**), 6-azidohexanoic acid (**h**), 7-azidoheptanoic acid (also called 7-azidoenanthic acid, **e**) and 11-azidoundecanoic acid (**u**). Adapting an earlier known procedure [II.15], ω -bromoalkanoic acid were converted to ω -azidoalkanoic acid using sodium azide in a mixture of water and acetone (2/1 by volume) at 60 °C for 5 h (**Scheme II.1**). This strategy allowed the synthesis of 6-azidohexanoic acid (**h**), 7-azidoheptanoic acid (**e**) and 11-azidoundecanoic acid (**u**). The structural integrity of the synthesised ω -azidoalkanoic acid was verified by nuclear magnetic resonance (NMR) spectroscopy and the presence of the azide group was confirmed by FT-IR spectroscopy as illustrated in **Figure II.3** for the synthesis of 11-azidoundecanoic acid.



Scheme II.1: Synthesis of ω -azidoalkanoic acid from ω -bromoalkanoic acid.

Chapter II: Preparation and characterisation of oligomers based on phenylalanine and aliphatic building blocks by solid-phase synthesis

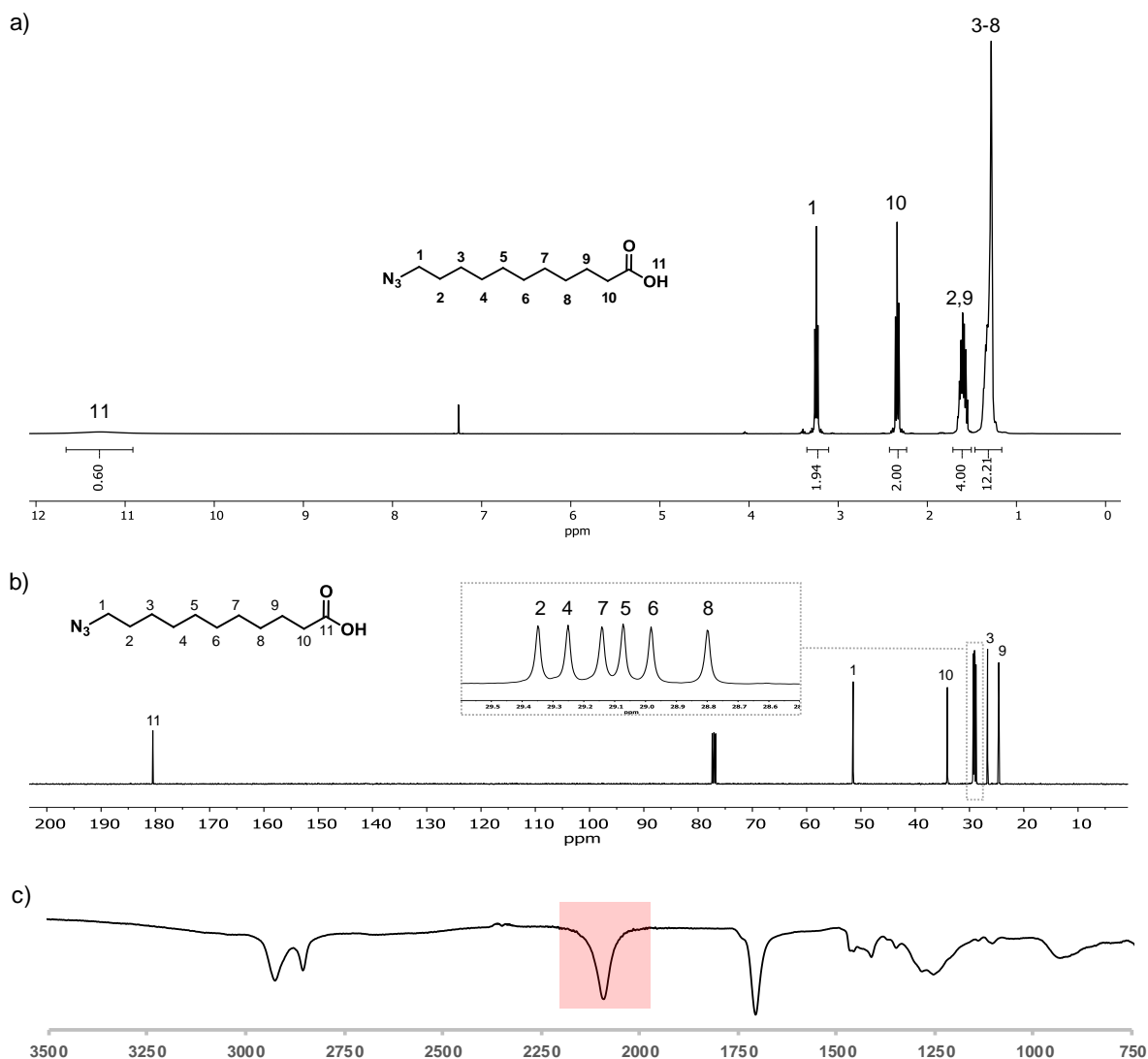
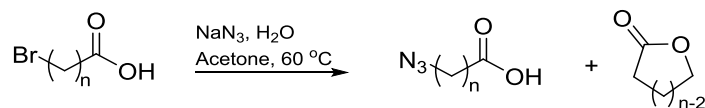


Figure II.3: Spectroscopic analysis of 11-azidoundecanoic acid: (a) ^1H and (b) ^{13}C NMR spectra in DMSO-d_6 and (c) FT-IR spectrum for which the characteristic azide absorption band at 2100 cm^{-1} is highlighted in red.

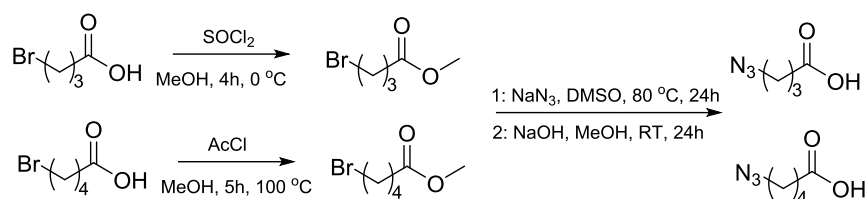
However, this approach could not be similarly applied for the synthesis of 4-azidobutyric acid and 5-azidovaleric acid due to ring closing side reactions leading to the formation of lactones (**Scheme II.2**).



Scheme II.2: Side reactions occurring during the synthesis of 4-azidobutyric acid ($n = 3$) and 5-azidovaleric acid ($n = 4$) when converting the corresponding ω -bromoalkanoic acid directly in the presence of sodium azide.

For this reason, other procedures were used for the synthesis of 4-azidobutyric acid and 5-azidovaleric acid through the formation of a methyl ester as intermediate to protect the terminal carboxylic acid (**Scheme II.3**). Sacchetti et al. [II.16] proposed the synthesis of 4-azidobutyric acid using methanol with thionyl chloride to form methyl 4-bromobutyrate that was then reacted with sodium azide followed by a deprotection of the carboxylic acid group under basic conditions (NaOH). Similarly, Voliani et al. [II.17] reported a similar procedure for the synthesis of 5-azidovaleric acid replacing thionyl chloride by acetyl chloride.

Chapter II: Preparation and characterisation of oligomers based on phenylalanine and aliphatic building blocks by solid-phase synthesis



Scheme II.3: Synthesis of 4-azidobutyric and 5-azidovaleric acids via protection of the carboxylic acid group.

All the ω -azidoalkanoic acids were synthesised in good yield. An overview of their synthesis can be found in **Table II.1**.

Table II.1: Overview of the synthesis of ω -azidoalkanoic acid spacing units by direct reaction^a of ω -bromoalkanoic acid with NaN_3 or through the protection of the carboxylic acid before addition of NaN_3 ^b.

Structure	Name	Abbreviation	Amount (g)	Yield (%)
	4-azidobutyric acid ^b	b	3.1	78
	5-azidovaleric acid ^b	v	2.6	65
	6-azidohexanoic acid ^a	h	7.4	92
	7-azidoheptanoic acid ^a	e	1.7	85
	11-azidoundecanoic acid ^a	u	23.0	96

2.3. Preliminary synthesis of a library of phenylalanine-based oligomers

Considering the strategy described in section 2.1, a library of oligomers based on four repetition cycles was synthesised (**Table II.2**). Three parameters were considered:

- 1) *number of phenylalanine residues per repeating cycles*. The biggest effect on the π - π interactions with aramid fibres is expected to be derived from the length of the phenylalanine blocks. It was explored by creating two libraries using hexyl and undecyl spacers respectively for which the number of phenylalanine residues per repeating cycles was varied between one and four. Increasing the block size would increase the amount of donated π interactions.
- 2) *spacing unit*. Here the chain length of the spacers was varied between three and ten methylene groups. The number of spacing units could not only affect the interaction of the oligomer with the fibre through different arrangements on its surface, increase the flexibility of the molecule to organize itself across the fibrous surface (degrees of freedom), it could also modify the interaction with the polymer matrix. A change in spacing length could also affect the amorphous versus crystalline character of the oligomer.
- 3) *sequence of the building blocks*. According to the simulation work of the group of Simmons on polymer blends [II.4], polymers with varying lengths of alternating interactive parts are expected to

Chapter II: Preparation and characterisation of oligomers based on phenylalanine and aliphatic building blocks by solid-phase synthesis

perform better than their uniform block length counterparts. In order to evaluate a similar effect, oligomers with scrambled sequences were prepared.

Table II.2: Library of oligomers synthesised using a CTC resin with four reaction cycles by adapting conditions reported in [II.15]. For convenience, the following abbreviations have been used: F for phenylalanine residues, b for the butyric spacer, v for the valeric spacer, h for the hexyl spacer, e for the heptanoic spacer, u for the undecyl spacer, and • for the linker corresponding to the addition of propargylamine.

Parameters investigated	Oligomer composition	Yield (%)
Effect of the number of phenylalanine residues per cycle using an hexyl spacer	Fh•Fh•Fh•Fh	83
	FFh•FFh•FFh•FFh	79
	FFFh•FFFh•FFFh•FFFh	86
	FFFFh•FFFFh•FFFFh•FFFFh	77
Effect of the number of phenylalanine residues per cycle using an undecyl spacer	Fu•Fu•Fu•Fu	85
	FFu•FFu•FFu•FFu	93
	FFFu•FFFu•FFFu•FFFu	95
	FFFFu•FFFFu•FFFFu•FFFFu	71
Effect of spacer length	FFFFb•FFFFb•FFFFb•FFFFb	85
	FFFFv•FFFFv•FFFFv•FFFFv	76
	FFFFe•FFFFe•FFFFe•FFFFe	77
Effect of the distribution of phenylalanine using an hexyl spacer	Fh•FFh•Fh•FFh	87
	Fh•FFFh•Fh•FFFh	87
	Fh•FFFh•FFFh•Fh	85
Effect of the distribution of phenylalanine using an undecyl spacer	Fu•FFu•Fu•FFu	92
	Fu•FFFu•Fu•FFFu	72
	Fu•FFFu•FFFu•Fu	97
Effect of the distribution of phenylalanine and the use of different spacers	Fh•FFFu•FFFh•Fh	81
	Fu•FFFh•FFFu•Fh	81

The oligomers were analysed by ¹H and ¹³C NMR spectroscopies to verify the structural integrity of the molecules synthesized. FFFFh•FFFFh•FFFFh•FFFFh was used here as an illustration. Analysis by ¹H NMR spectroscopy in DMSO-d₆ confirmed the presence of characteristic peaks corresponding to the desired oligomer. For the phenylalanine residues the protons of phenyl groups were observed at 7.25 ppm, while the protons of the methylene groups had a chemical shift between 2.50 and 3.20 ppm. The characteristic signals of the hexyl spacer were observed at 1.00 (methylene in γ position to the amide), 1.30 (methylene in β position to the amide), 1.70 (methylene in δ position to the amide), 2.00 (methylene in α position to the amide), 3.20 (methylene next to the terminal azide) and 4.20 ppm (methylene next to the triazole). The linker formed from the insertion of propargylamine showed a chemical shift at 4.20 (methylene) and 7.60 ppm (proton of the triazole). The integration of the oligomer signals was a good fit provided the normalisation is over the phenyl protons (7.25 ppm, five protons for each aromatic group). Although the aliphatic signals in the 2-0.9 ppm range (eight for each aliphatic linker) did not individually match up with their eight protons, the sum of these signals does (31.6).

Chapter II: Preparation and characterisation of oligomers based on phenylalanine and aliphatic building blocks by solid-phase synthesis

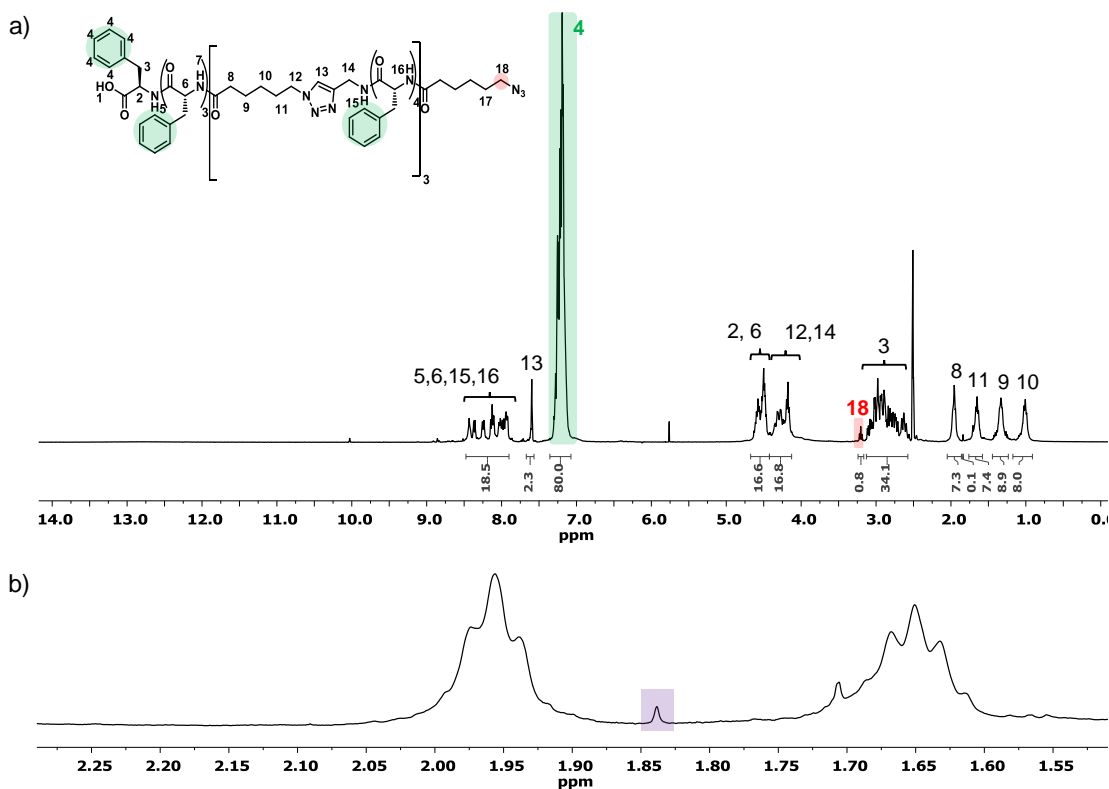


Figure II.4: ¹H NMR spectrum in DMSO-d₆ of FFFFh•FFFFh•FFFFh•FFFFh synthesised using a CTC resin. a) Full spectrum and b) zoom on the 2.3-1.5 ppm region. The phenyl groups of the phenylalanine residues are highlighted in green, the methylene next to the terminal azide group in red, and the unidentified peaks in purple.

In order to reliably assess the purity of the oligomer via ¹H NMR spectroscopy, there is one type of signal which is only caused by one group of protons in the molecule, namely the methylene next to the azide (two protons per oligomer). These protons at 3.20 ppm ($\text{CH}_2\text{-N}_3$, highlighted in red on **Figure II.4,a**) present on one of the extremity of the oligomers showed a deviation in integration values. More precisely, the integration for the $\text{CH}_2\text{-N}_3$ signal was 0.8 while it was expected to be 2 when normalizing against the eighty phenyl protons (highlighted in green **Figure II.4,a**). This suggested a partial absence of the terminal spacer or a mixture of oligomers of different composition. Additionally, an unknown impurity was visible (highlighted in purple on **Figure II.4,b**).

The impurities present in the oligomer crude mixtures synthesised by CTC resin were also indicated using mass spectrometry (MS). Electrospray ionisation mass spectrometry (ESI-MS) showed trouble to measure the $[\text{M}+\text{H}]^+$ ($m/z = 3093.54$) peak of the oligomers. Overall peaks were observed for molecules having a m/z below 2000. Indicated in **Figure II.5**, the major peaks for which an assignment could be done (highlighted in yellow) were identified as oligomers with deletion sequences, while some remained unidentified (in red).

Chapter II: Preparation and characterisation of oligomers based on phenylalanine and aliphatic building blocks by solid-phase synthesis

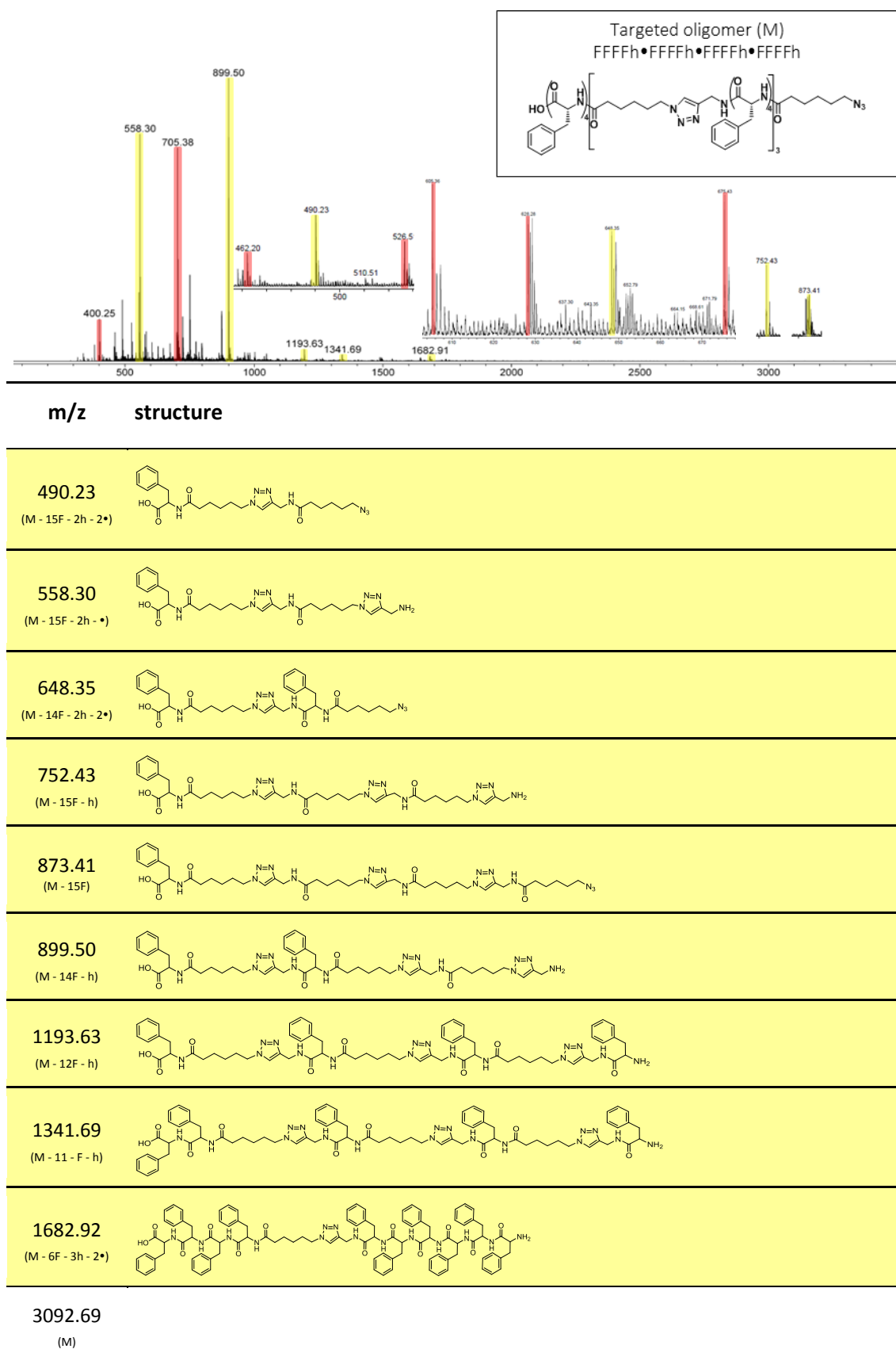


Figure II.5: ESI-MS spectrum of FFFFh•FFFFh•FFFFh•FFFFh along with a table summarising the assignment of the peaks. The expected molecular ion peak (m/z calculated for $[M+H]^+$ or $C_{177}H_{198}N_{31}O_{21} = 3093.54$) was not observed. Some of the peaks present on the spectrum were identified as oligomers with deletion sequences (in yellow), while others remained unidentified (in red).

Chapter II: Preparation and characterisation of oligomers based on phenylalanine and aliphatic building blocks by solid-phase synthesis

This oligomer was also characterised by matrix-assisted laser desorption/ionisation time of flight (MALDI-ToF) mass spectrometry, another soft ionisation mass spectrometry technique. While the peak corresponding to the molecular ion of the targeted oligomer indicated in green on **Figure II.6** was observed, the presence of additional peaks was noticeable. Some of these peaks were assigned to oligomers with deletion building blocks indicated in yellow on **Figure II.6**, while the unidentified peaks are indicated in red. This result confirmed what was suspected by ^1H NMR spectroscopy (**Figure II.4**) indicating that the samples were composed of a mixture of oligomers, i.e. the targeted oligomer along with oligomers with deletion sequences.

Chapter II: Preparation and characterisation of oligomers based on phenylalanine and aliphatic building blocks by solid-phase synthesis

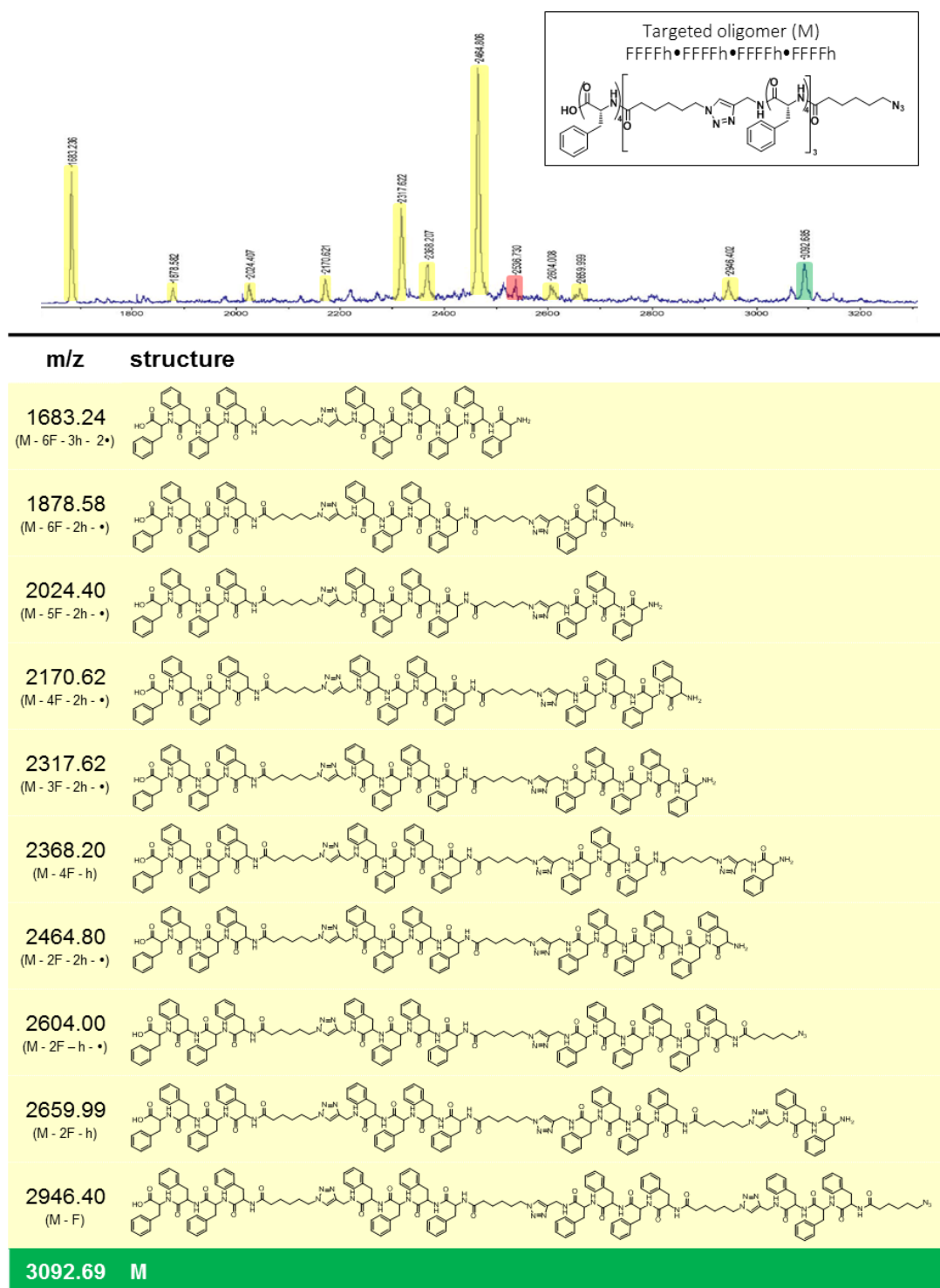


Figure II.6: MALDI-TOF spectrum of FFFFh•FFFFh•FFFFh•FFFFh. The expected molecular ion peak (m/z calculated for $[M+H]^+$ or $C_{177}H_{198}N_{31}O_{21} = 3093.54$) was present (in green). Some of the peaks present on the spectrum were identified as oligomers with deletion sequences (in yellow), while some remained unidentified (in red).

In summary, the oligomers obtained using the previously reported conditions were lacking regarding the precise control of the microstructure and leading to a mixture of oligomers containing the targeted oligomer, but also oligomers with deletion sequences. The following sections present the investigation of the optimisation of the synthesis of these oligomers (Section 3) along with the extensive characterisation of one selected sample (Section 4).

3. Attempts to optimise the synthesis of phenylalanine-based oligomers

3.1. Tools to monitor the reaction steps

To identify the potential steps that could be problematic the Kaiser test and Fourier transform infrared (FT-IR) spectroscopy were utilised.

3.1.1. Kaiser test

The initial results of oligomers synthesised using CTC resin led us to investigate the efficiency of the coupling reactions. For this, the Kaiser test [II.18] was employed to check for the depletion of free amine groups. In the reaction of this test, the formation of the dye Ruhemann's purple is induced via ninhydrin (**Figure II.7**). The formation of the chromophore is preceded by a condensation reaction between the amine and a ninhydrin molecule, leading to the formation of a Schiff-base. This intermediary can then perform a dehydration reaction, re-dissociating itself into the solution from the solid support as a primary amine. The condensation takes place a second time with another ninhydrin molecule after which the Ruhemann's purple dye is formed.

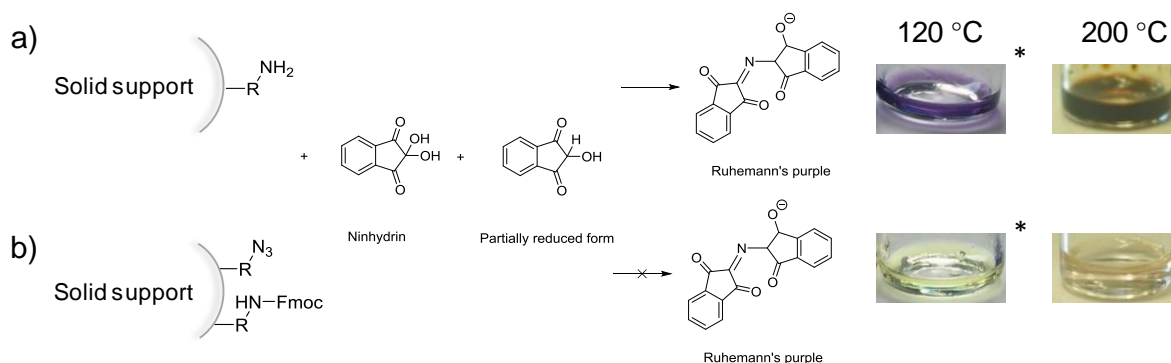


Figure II.7: Reaction involved in the a) formation of Ruhemann's purple in Kaiser test conditions in the presence of a primary amine and b) lack of formation of the dye if no amine is present under two different temperatures [II.16]. *Images taken by D. Chan-Seng.

It is important to mention that the Kaiser test conditions were modified from the conditions reported [II.18], splitting the heating in two steps: 1) at 120 °C and 2) if no change was observed at 200 °C. Additionally, this heating was done by a heat gun, with which the accuracy of the temperature cannot be guaranteed. Because of the uncontrolled heating at a higher temperature, although more likely to give an indication of colour, it is possible that the colour change was mediated through a degradation mechanism rather than staining of present amine groups.

3.1.2. FT-IR spectroscopy

Using FT-IR spectroscopy, the presence of azide groups during synthesis was monitored as the absorbance band characteristic of the asymmetric stretching vibration of azide groups observed around 2100 cm^{-1} . Thus, FT-IR spectroscopy was performed after each CuAAC reaction to verify the absence of this characteristic absorbance band confirming the completion of this reaction step. **Figure**

Chapter II: Preparation and characterisation of oligomers based on phenylalanine and aliphatic building blocks by solid-phase synthesis

II.8 depicts the characteristic absorbance band of azide groups as illustrated for 7-azidoheptanoic acid and the absence of this characteristic band for each addition of propargylamine when synthesising Fh•Fh•Fh•Fh.

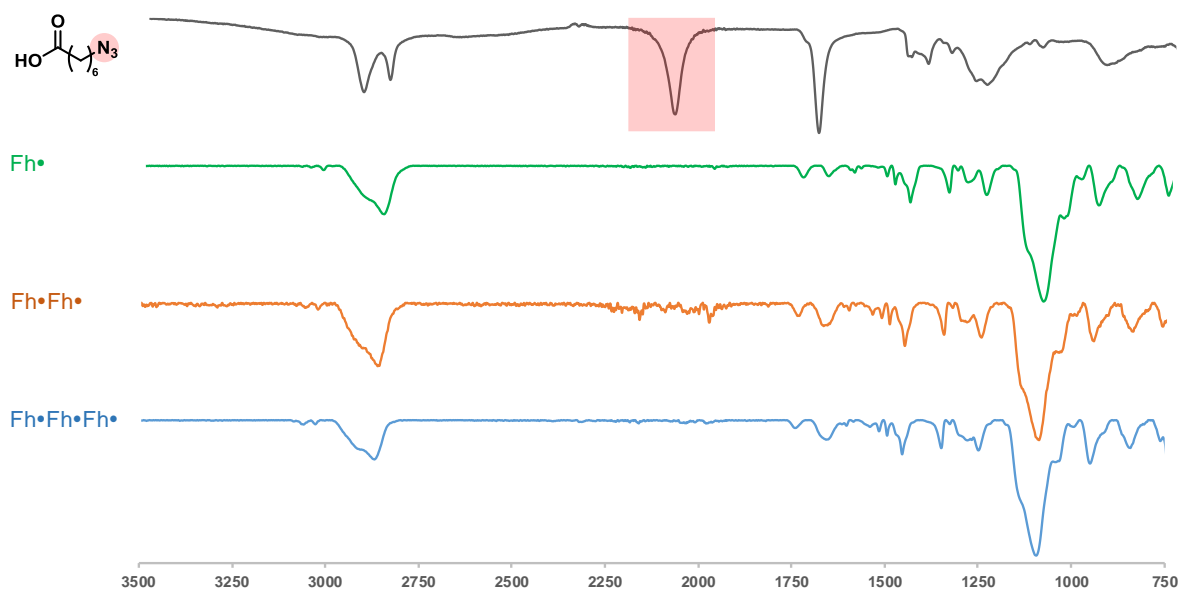


Figure II.8: FT-IR spectrum of 7-azidoheptanoic acid (top) with a red highlight on the characteristic azide absorbance band at 2100 cm⁻¹, overlaid with FT-IR spectra after each Huisgen cycloaddition reaction step for the synthesis of Fh•Fh•Fh•Fh.

Indicated in **Figure II.8**, the presence of the azide signal could be monitored up until the resolution of the IR spectrophotometer. However, peaks may get increasingly difficult to observe once the size of the oligomer during synthesis increased (decreasing the relative weight percentage of the azide group). The possibility that the azide group was present but indistinguishable from noise should be taken into account.

3.2. Approaches to improve reaction efficiency

3.2.1. Identification of the approaches of interest

Problems to afford complete reactions in solid-phase synthesis are common and as such many instances have been observed with appropriate solutions [II.19]. Considering Fmoc-based solid-phase synthesis, different parameters were considered to improve the reaction efficiency of each step of the synthesis.

One of the difficulties encountered in solid-phase peptide synthesis is the strong ability of peptides to form aggregates, phenomenon that can occur during the supported synthesis of peptides. While hydrogen bonding between peptide chains (intra and intermolecular) can lead to supramolecular association of peptide chains [II.19], the use of phenylalanine residues in the oligomer could intensify the aggregation due to the interactive contribution of the phenyl ring (*e.g.* π - π stacking). One approach to disrupt aggregation includes using different solvents, such as DMF, DMSO, NMP or DCM to optimise dispersion of the growing peptide chains as well as swelling parameters, so that at no point entry of

Chapter II: Preparation and characterisation of oligomers based on phenylalanine and aliphatic building blocks by solid-phase synthesis

the coupling reagents towards the reactive surface is hindered [II.20]. Additionally, fluorinated solvents can be used as a stronger hydrogen bonding donor, which may help to overcome any strong hydrogen bonding character of the growing peptide chain [II.21]. Originally, DMF had been used as a solvent for the synthesis, following earlier reported conditions [II.15]. However, using these conditions, incomplete reactions were observed. Another reason for the formation of aggregates is either through hydrophobic effects or a strong hydrogen bonding network [II.22-II,23], hindering the addition of new residues to the growing chain.

Usage of chaotropes such as salts (e.g. NaClO₄, KSCN, LiBr) [II.24-II.25] or detergents like Triton X-100 and Tween 20 [II.26] can also be considered. The principle behind the chaotrope lies in structure breaking properties of large low charge ions, based on Hofmeister effects. In protein structures, a chaotrope will affect the hydration shell around the aggregate. Ions, by showing interactions with the solute, may specifically encourage the hydration shell to associate more homogeneously with the solute [II.27]. Several polar solvents may act as chaotrope, such as DMF [II.20].

With this chaotrope effect in mind, commonly used during peptide synthesis is the so called 'magic mixture' which is a mixed solvent system of DCM/NMP/DMF 1/1/1 (by volume) along with 1% of Triton X-100 and 2N ethylene carbonate [II.28]. However, the usage of detergents may give additional difficulties while performing purification by high performance liquid chromatography (HPLC) and reduce signal intensities in mass spectrometry [II.29].

Crucial to the reaction behaviour is the environment which is introduced by the type of solid-phase resin that is chosen. Vaino and Janda argue that in essence solid-phase synthesis is analogous to solution phase, with main important parameters including effective concentration, swelling and hydrophobicity [II.30]. The first parameter is governed not only by the loading but also the ability for the reagents to disperse towards the reactive site of the growing peptide chain. The structure of any linkers or functionalization present between the polymeric core and the reactive site can improve the dispersion and resins like Tentagel® make use of this property [II.30]. The reactive group is connected to the polystyrene (PS) core by a poly(ethylene glycol) (PEG) chain, effectively making the reaction behaviour closer to that of a solution-phase coupling. Depending on the peptide structure, this may lead to improvements in the coupling behaviour. Related to that parameter is the swelling, as a higher swelling can improve the surface area of the beads significantly, allowing for an improved dispersion. Lastly, the hydrophobic or hydrophilic character of the resin may influence the solubilisation of the growing peptide chain and can also be a factor for the choice of solvents to be used during coupling [II.30].

Some of these approaches were investigated for the synthesis of phenylalanine-based oligomers and are discussed in the following sections.

Chapter II: Preparation and characterisation of oligomers based on phenylalanine and aliphatic building blocks by solid-phase synthesis

3.2.2. Results

In order to find the most optimal reaction conditions for the synthesis of a new library of oligomers, three different techniques mentioned in section 3.2. were evaluated: 1) pre-activation of the carboxylic acids for the amide bond formation steps to improve addition of the phenylalanine and aliphatic spacing units, 2) use of aggregate disrupters, and 3) use of a Tentagel® resin. Fh•Fh•Fh•Fh was used as model oligomer due to its relative small size, allowing convenient synthesis.

3.2.2.1. Pre-activation of the carboxylic acids for the amide bond formation steps

Before considering the use of additives or changing of resin the pre-activation of the carboxylic acid of Fmoc-Phe-OH and 6-azidohexanoic acid was considered in order to enhance the coupling step. To overcome this potential problem, all the reagents for **steps I** and **III** were premixed until their full dissolution before adding the solution to the reaction vessel containing the growing oligomer attached to the resin.

The absence of change of colour when conducting the Kaiser test at low temperature (< 110 °C) was observed for all **steps I** and **III** indicating the absence of primary amine. However, for the addition of the last 6-azidohexanoic acid, the purple dye was visible in the beads. The repetition of this step indicated the absence of primary amine, i.e. no colour change. When the Kaiser test was performed at higher temperatures (>110 °C), slight brown colourations were observed, possibly indicating presence of free amine.

Thusly, the above mentioned conditions did not lead to completion of the performed reactions. Synthesis steps were repeated once or twice if needed, allowing the disappearance of the brown colouration at higher temperature of the Kaiser test.

The synthesis of the final product did not lead to a significantly improved integration of the CH_2-N_3 peak relative to the aromatic peaks of the phenylalanine residues in comparison to oligomers synthesized using the “normal” conditions (1.31 as compared to 1.39, **Figure II.9**). It is however important to note that the presence of solvents in the second spectrum made the integration of this particular peak more difficult.

Chapter II: Preparation and characterisation of oligomers based on phenylalanine and aliphatic building blocks by solid-phase synthesis

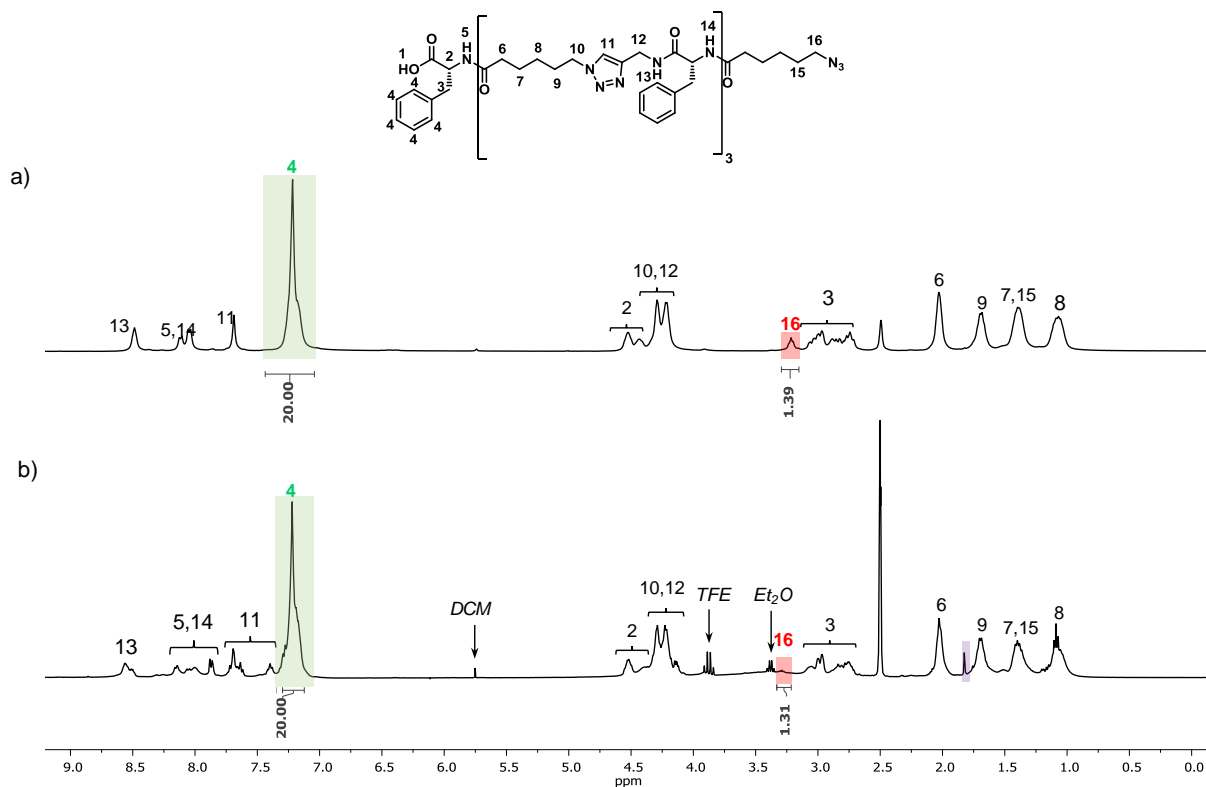


Figure II.9: ^1H NMR spectra in DMSO-d_6 of $\text{Fh}\cdot\text{Fh}\cdot\text{Fh}\cdot\text{Fh}$ synthesized (a) using normal conditions and (b) while performing pre-activation of the carboxylic acids (unidentified peaks in purple).

3.2.2.2. Use of aggregate disruptors

Various parameters, resin loading, use of chaotropic salt, nature of the solvent, have been investigated in order to decrease the tendency of the oligomer to form aggregates during the synthesis of $\text{Fh}\cdot\text{Fh}\cdot\text{Fh}\cdot\text{Fh}$. These parameters are summarised in **Table II.3**. As a general comment, all FT-IR measurements after **step IV** indicated a full depletion of the azide moiety, confirming no presence of said group beyond the observation limit of the FT-IR spectrometer. However, the products obtained after cleavage from the solid phase resin did not display the azide moiety on the FT-IR spectra clearly. It is for this reason that even though an absence of the azide peak on FT-IR may be observed, an amount of the group itself could still be present in the growing oligomer mixture.

Chapter II: Preparation and characterisation of oligomers based on phenylalanine and aliphatic building blocks by solid-phase synthesis

Table II.3: Overview of different reaction conditions used for the synthesis of Fh•Fh•Fh•Fh using a CTC resin and the results of the monitoring of the synthesis using the Kaiser test. All reactions went to completion after second coupling attempt.

Entry	Loading (mmol)	Conditions	Observations for the Kaiser test
1	0.94	“normal” conditions	Incomplete reaction for the addition of the second F
2	0.54	lower loading of the resin	Incomplete reaction for the addition of the second F
3	0.86	addition of TBAB (1 eq. relative to loading) [II.21]	Incomplete reaction for the addition of the second F
4	0.94	DMSO instead of DMF [II.17]	Incomplete reaction for the addition of the final h
5	0.90	DCM/DMF/NMP (1/1/1 v/v/v) instead of DMF [II.25]	Incomplete reaction for the addition of the final h

The first approach was to lower the loading concentration. To evaluate this parameter, a resin was functionalised with a lower density in phenylalanine residue (0.54 mmol per gram of resin as compared to 0.94 previously, **Table II.3, entry 2**). While performing the Kaiser test, evolution of brown colouration appeared once again at higher temperatures (>110 °C). The colouration appeared lighter, possibly due to the decreased loading density or through increased reaction efficiency. Synthesis steps were repeated once or twice if needed, allowing for the disappearance of the brown colouration and synthesis of the final product with improved integration of the CH_2-N_3 signal in comparison to oligomers synthesized using previous loading conditions (1.89 vs 1.39, **Figure II.10**).

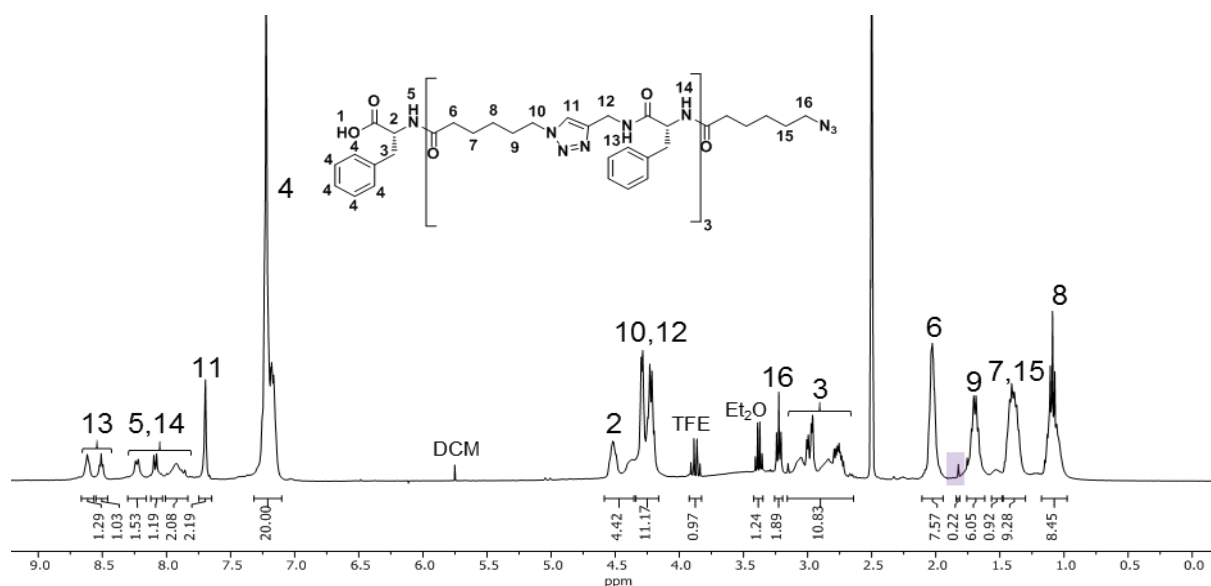


Figure II.10: ¹H NMR spectrum in DMSO-d₆ of Fh•Fh•Fh•Fh synthesised using a resin with a lower loading of 0.54 mmol per gram of resin. (unidentified peaks in purple).

The second approach is to add chaotropic salts such as tetrabutylammonium bromide (TBAB) (**Table II.3, entry 3**) to DMF to “break” these aggregates. While performing the Kaiser test, evolution of brown colouration appeared at higher temperatures (>110 °C), not significantly different from reaction conditions without salts. Thusly, it is likely that this approach did not lead to an improvement in

Chapter II: Preparation and characterisation of oligomers based on phenylalanine and aliphatic building blocks by solid-phase synthesis

reaction efficiency. Reactions were repeated once again 1-2 times until brown colouration was no longer observed, leading to no significant improvement of the integration values (1.41 vs 1.39, **Figure II.11**).

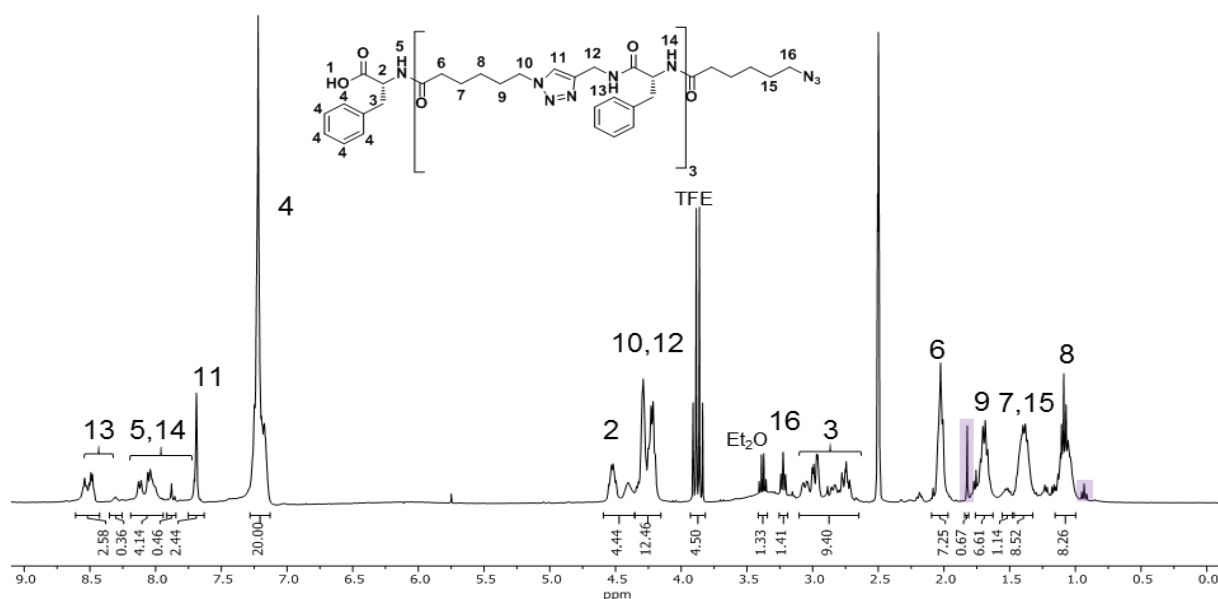


Figure II.11: ¹H NMR spectrum in DMSO-d₆ of Fh•Fh•Fh•Fh synthesised with addition of TBAB (unidentified peaks in purple).

The last approach considered replacing DMF by other solvents. DMSO was first used (**Table II.3, entry 4**). While performing the Kaiser test, a decrease in the brown colouration was observed in comparison to the initial solvent conditions, which disappeared after repetition of the coupling step. Better results however, were obtained when DMF was instead replaced by a mixture of dichloromethane, DMF and NMP in equal proportion (**Table II.3, entry 5**). While performing the Kaiser test, no more brown colouration was observed at any point after having performed the reactions. Thusly these conditions were found to be the most effective in increasing reaction efficiency. In **Figure II.12** an ¹H NMR spectrum is shown of Fh•Fh•Fh•Fh in which previously troublesome steps have been performed or even repeated using the mixed solvent system. The integration of the methylene next to the azide signal was improved, just as with lower loading conditions (1.80 vs 1.39).

Chapter II: Preparation and characterisation of oligomers based on phenylalanine and aliphatic building blocks by solid-phase synthesis

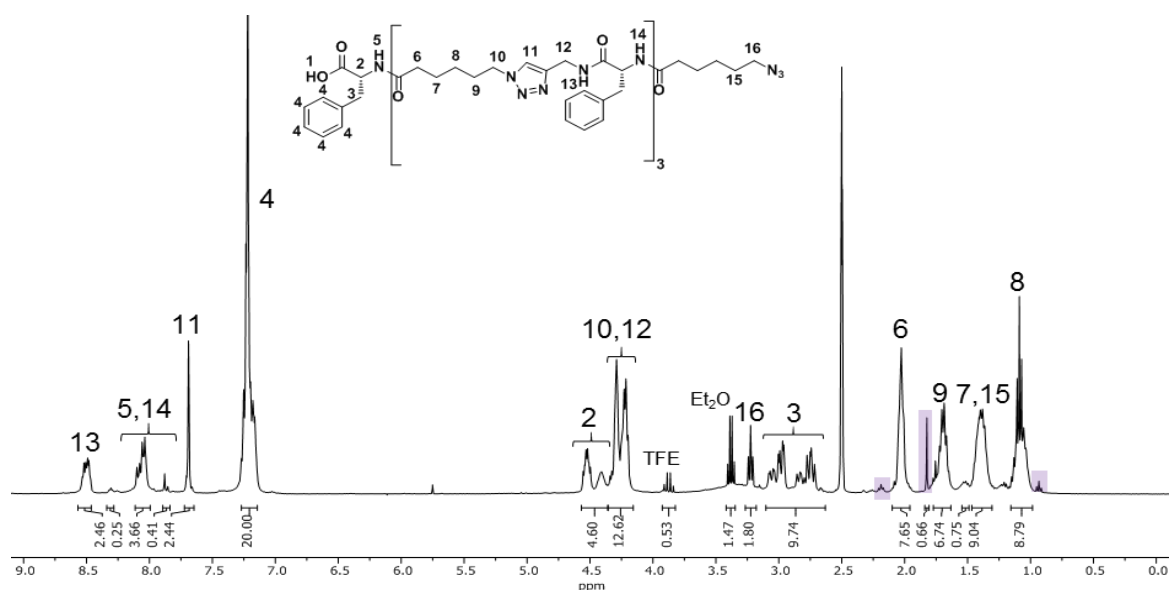


Figure II.12: ^1H NMR spectrum of Fh•Fh•Fh•Fh synthesised using mixed solvent system at select steps in DMSO-d_6 (unidentified peaks in purple).

In summary, from all these conditions investigated using monitoring tests and NMR spectroscopy, the use of a mixture of DCM, DMF and NMP as solvent for **steps I** and **III** or overall loading concentration (factor 2) permitted to have the most optimal conditions for the synthesis of Fh•Fh•Fh•Fh. However, it was observed for all the conditions tested that several coupling steps had to be repeated using the same conditions, showing the continued difficulties with the coupling of either the phenylalanine or aliphatic spacing residues.

3.2.2.3. Investigation of Tentagel[®] resin

A proposed solution to overcome these problems is to change the resin to a more hydrophilic resin. In our case, Tentagel[®] has been chosen due to commercial availability of a form pre-functionalised with Fmoc protected phenylalanine. This particular solid phase resin is a commercial product in which PEG chain with a molecular weight of $3000 \text{ g}\cdot\text{mol}^{-1}$ is grafted onto polystyrene beads with a low crosslinking density [II.31]. The linker is attached to the free extremity of the PEG chains. As discussed in Section 3.2, these types of resins are known to enhance the synthesis of difficult peptides providing to the reactive sites a kinetic reactivity as high as in solution. In this study, Fmoc Phe Tentagel[®]-S-PHB, as depicted in **Figure II.13** where PHB stands for the 4-hydroxybenzyl alcohol linker, was evaluated for the synthesis of Fh•Fh•Fh•Fh using the optimised conditions identified earlier. The loading density of the Tentagel[®] resin is lowered ($0.24 \text{ mmol per gram of resin}$) and DMF has been used as coupling solvent for phenylalanine and 6-azidohexanoic acid spacing units.

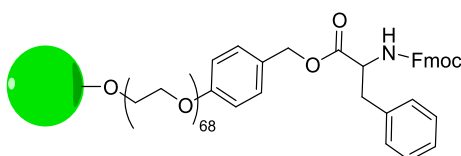


Figure II.13: Structure of Fmoc Phe Tentagel[®]-S-PHB (polystyrene resin represented as a green sphere).

Chapter II: Preparation and characterisation of oligomers based on phenylalanine and aliphatic building blocks by solid-phase synthesis

Indicated in **Figure II.14**, peaks corresponding to the oligomer have been found with appropriate integration values. Although the methylene next to the azide group was partially overlapping with the water signal, the integration value observed was improved over previous results with optimised conditions (2.18 vs 1.89 (lower loading) and vs 1.80 (mixed solvent system)). Furthermore, at no point during the synthesis did the Kaiser test indicated an incomplete reaction.

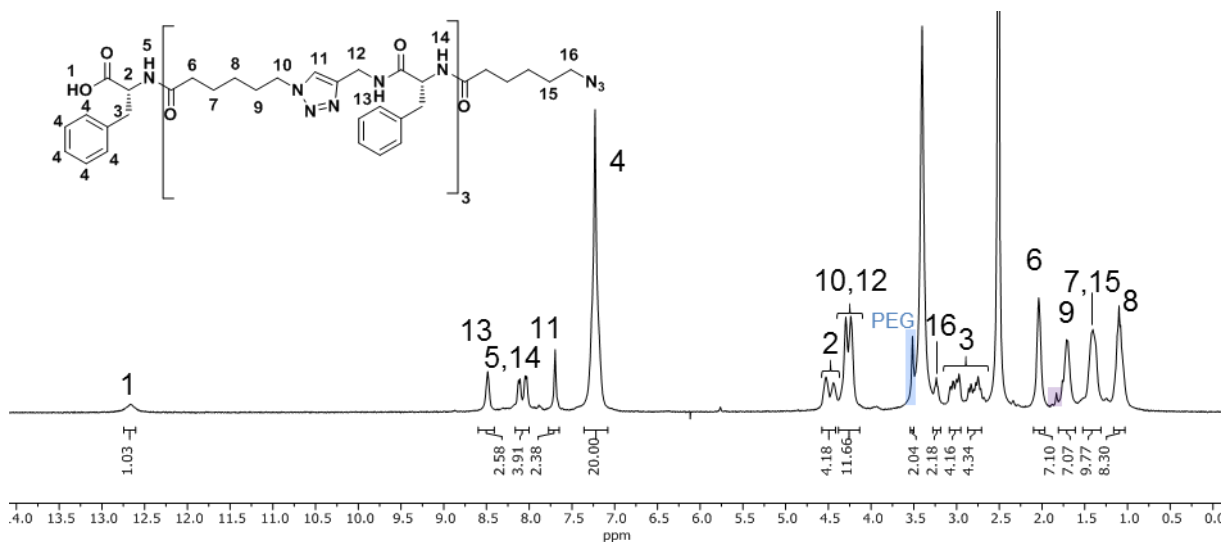


Figure II.14: ^1H NMR spectrum in DMSO-d_6 of $\text{Fh}\bullet\text{Fh}\bullet\text{Fh}\bullet\text{Fh}$ (PEG is highlighted in blue and unidentified peaks in purple).

In summary, the synthesis of $\text{Fh}\bullet\text{Fh}\bullet\text{Fh}\bullet\text{Fh}$ was optimised by replacing the CTC resin by a Tentagel[®] PHB resin.

3.2.3. Oligomers synthesised using the optimised conditions

After optimisation of the reaction conditions to obtain $\text{Fh}\bullet\text{Fh}\bullet\text{Fh}\bullet\text{Fh}$, a new library of oligomers was prepared using the Tentagel[®] resin (**Table II.4**). As for the library of oligomers previously synthesised (see **Table II.2**), various parameters have been considered to prepare this new library: 1) number of phenylalanine residues per reaction cycle, 2) length of the spacing unit used and 3) distribution of the phenylalanine and spacing units along the oligomer chain. It is noteworthy to mention that while performing the Kaiser test, a slight change in colouration was observed at the later steps (notably after the addition of the fifth phenylalanine residue and especially at the coupling of the last phenylalanine and 6-azidohexanoic acid spacing unit). This was mitigated using the earlier mentioned mixed solvent system of DCM, DMF and NMP (1/1/1) solvent for **steps I** and **III** and repeating the step until the colouration had completely disappeared.

Chapter II: Preparation and characterisation of oligomers based on phenylalanine and aliphatic building blocks by solid-phase synthesis

Table II.4: Library of oligomers synthesised using a Tentagel® PHB resin and considering four reaction cycles.

Parameters investigated	Oligomer composition	Yield (%)
Effect of the number of phenylalanine residues per cycles using an hexyl spacer	Fh•Fh•Fh•Fh	5
	FFh•FFh•FFh•FFh	19
	FFFh•FFFh•FFFh•FFFh	29
	FFFFh•FFFFh•FFFFh•FFFFh	22 (second batch: 28)
Effect of the length of spacer	FFFFb•FFFFb•FFFFb•FFFFb	35 (second batch: 31)
	FFFFv•FFFFv•FFFFv•FFFFv	17 (second batch: 29)
	FFFFu•FFFFu•FFFFu•FFFFu	23 (second batch: 26)
Effect of the distribution of phenylalanine and the use of different spacers	Fh•FFFh•Fh•FFFh	40
	Fh•FFFh•FFFh•Fh	26
	Fh•FFFu•FFFh•Fh	36

When comparing **Table II.2** and **Table II.4**, the yields obtained for the new library of oligomers were lower than those measured for the previous library (60-70%). This discrepancy could be attributed to the loading density of the solid phase resin, which was lowered by a factor in between two and five in respect to the loading done on CTC resin. This enabled to get a much finer powder during precipitation, which provided difficulty to be filtered or centrifuged. Weighing of concentrated crude mixture before the precipitation step with subsequent correction using NMR spectroscopy confirmed that the majority mass loss took place during the workup.

4. Characterisation of the synthesised phenylalanine-based oligomers

The structural integrity of the synthesised oligomers was evaluated by NMR spectroscopy and mass spectrometry (MALDI-ToF-MS, ESI-MS and tandem mass spectrometry (MS/MS)). As an example, the extensive description of the characterisation of FFFFv•FFFFv•FFFFv•FFFFv is proposed in this section. The characteristics of the other oligomers will be presented as a summary.

4.1. Example of FFFFv•FFFFv•FFFFv•FFFFv

4.1.1. Results of ¹H NMR spectroscopy

Using the optimised synthesis conditions allowed to obtain fine powders of the oligomers with minimal presence of solvent impurities, thanks to freeze drying procedures. The characteristic signals of FFFFv•FFFFv•FFFFv•FFFFv were once again observed on the ¹H NMR spectrum (**Figure II.15**).

Chapter II: Preparation and characterisation of oligomers based on phenylalanine and aliphatic building blocks by solid-phase synthesis

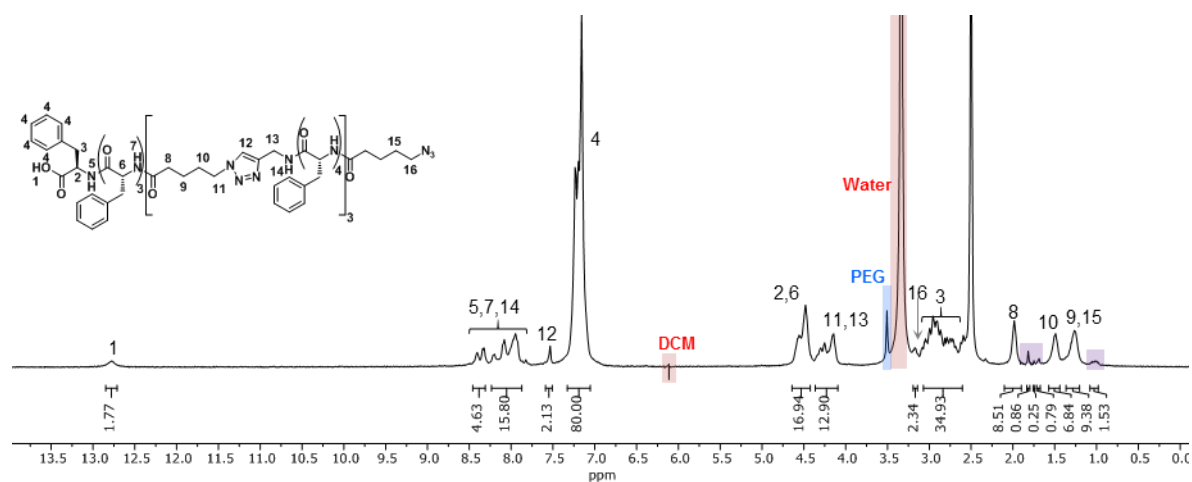


Figure II.15: ^1H NMR spectrum of FFFFv•FFFv•FFFv•FFFv in DMSO- d_6 (Residual solvents are highlighted in red, PEG in blue and unidentified peaks in purple).

When comparing the integration of the phenyl groups of the phenylalanine residues to the one of the terminal methylene next to the azide group on the ^1H NMR spectrum (**Figure II.15**), the ratio observed was 80 to 2.34 respectively, which was in better agreement with the ratio expected. The value might not be fully accurate due to the overlap with the methylene next to the phenyl (peak 3, 2.55-3.11 ppm) and the water peak (3.33 ppm). From this point of view, some improvements as compared to the synthesis performed previously (Section 2.3) have been achieved using the optimised conditions established.

However, the presence of impurities that were not present in the previous library of oligomers was noticeable. In fact, this sample contained residual DCM (5.76 ppm) as a consequence of insufficient drying. In a second batch, presence of THF (3.76 ppm) was also observed. The presence of the water signal at 3.33 ppm was expected due to the use of DMSO- d_6 as NMR solvent. DMSO being a hygroscopic solvent, it is not possible to differentiate between water which would be present in the sample and the water present due to moisture absorbed by DMSO. Furthermore, residual PEG was also identified on the ^1H NMR spectrum at 3.50 ppm. The presence of PEG was attributed to the use of Tentagel[®] resin as solid support for the synthesis as it is known from the literature that PEG leaching can occur during the cleavage of peptides from Tentagel[®] resins [II.32]. Other signals that could not be attributed were observed at 1.00, 1.69, 1.75, and 1.82 ppm.

4.1.2. Results of ^{13}C NMR spectroscopy

Considering the presence of various impurities as indicated by ^1H NMR spectroscopy, it is useful to also analyse the same oligomer using ^{13}C NMR spectroscopy, in order to obtain additional information. Additionally, considered was the usage of a ^{13}C NMR experiment using distortionless enhancement by polarisation transfer (DEPT) to discriminate primary and tertiary carbon atoms from secondary ones.

Chapter II: Preparation and characterisation of oligomers based on phenylalanine and aliphatic building blocks by solid-phase synthesis

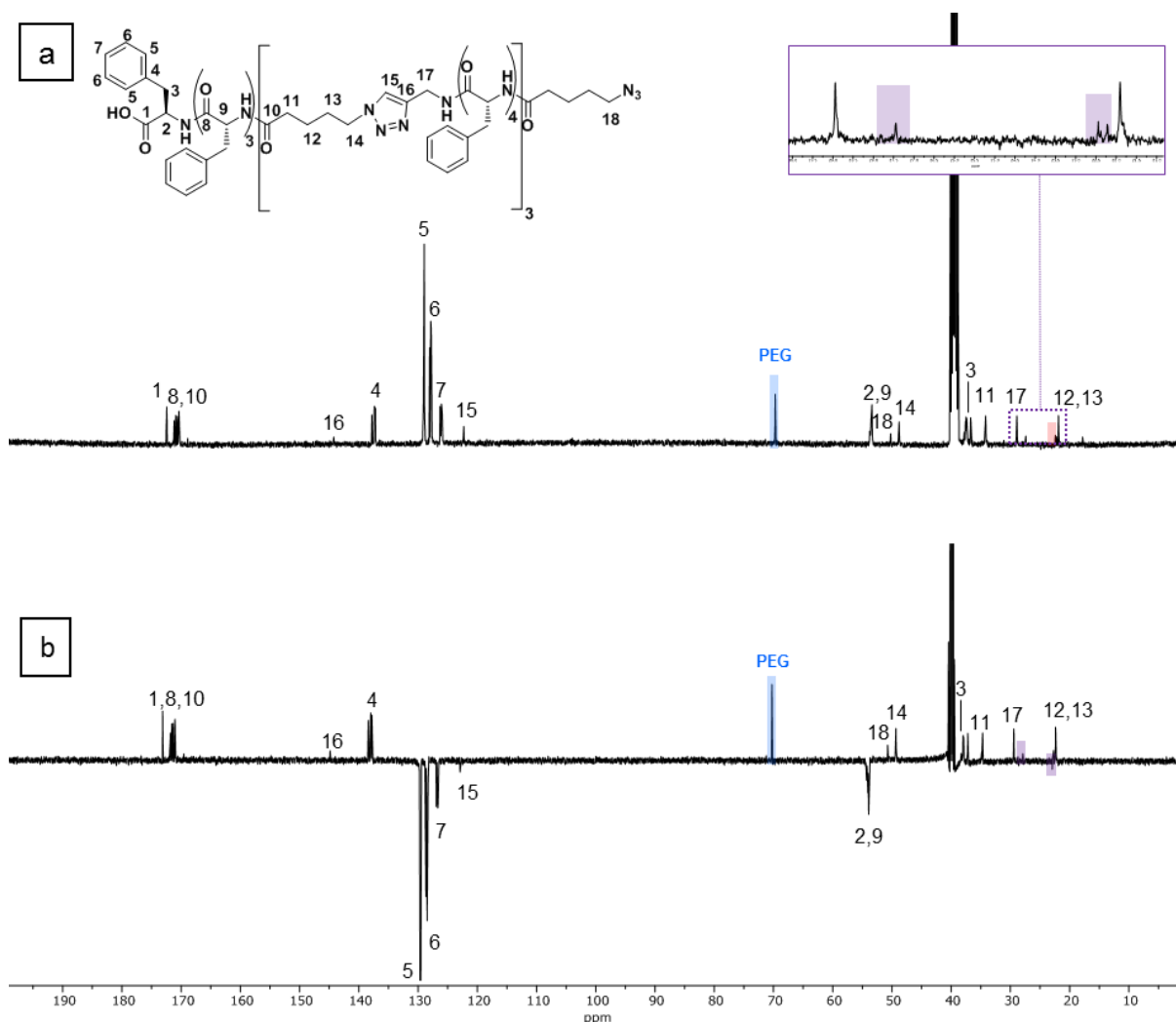


Figure II.16: ^{13}C NMR spectra of $\text{FFFFv}\cdot\text{FFFFv}\cdot\text{FFFFv}\cdot\text{FFFFv}$ in DMSO-d_6 (PEG is highlighted in blue and the unidentified impurities in purple): a) full spectrum (400 MHz) with a zoom from 20 to 30 ppm, and b) DEPT measurement (500 MHz).

As observed by ^1H NMR spectroscopy, the ^{13}C NMR spectrum (**Figure II.16**) revealed the presence of impurities in the sample. The PEG peak was clearly visible at 69.78 ppm, while three unidentified peaks were observed at 27.44, 22.44 and 22.21 ppm. The DEPT NMR experiment conducted on a 500 MHz spectrometer revealed the same impurities. Of these unidentified peaks, only the one at 22.44 ppm was pointing downwards indicating a carbon atom coupled to either a single or three hydrogen atoms, while the peaks at 22.21 and 27.44 ppm were pointing upwards corresponding to methylenes.

4.1.3. Results of 2D NMR spectroscopy

In order to get a better understanding of the nature of these unknown impurities, 2D NMR experiments such as heteronuclear single quantum correlation (HSQC) and heteronuclear multiple bond correlation (HMBC) experiments were conducted on this sample (**Figure II.17**).

Chapter II: Preparation and characterisation of oligomers based on phenylalanine and aliphatic building blocks by solid-phase synthesis

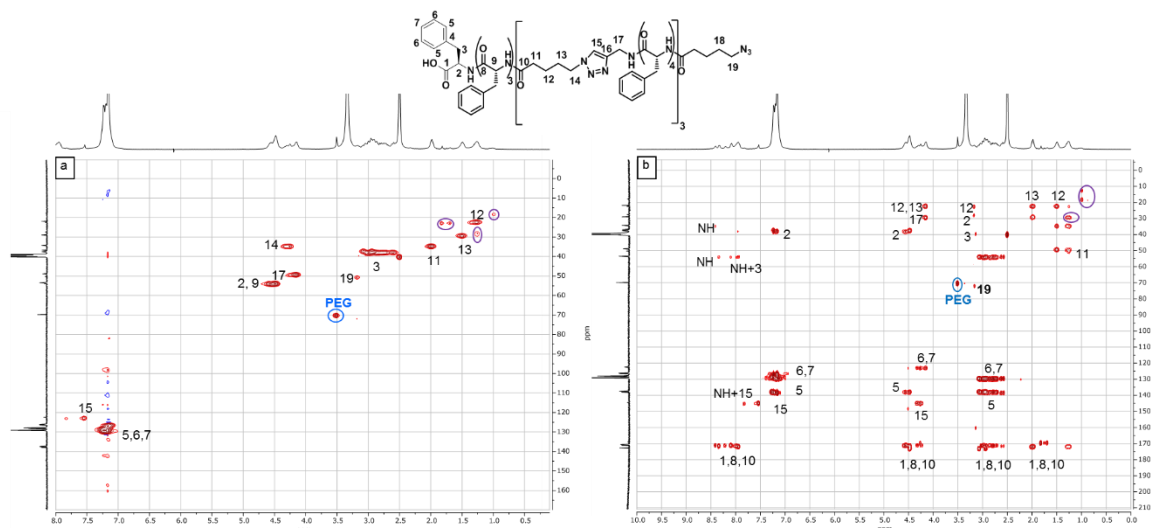


Figure II.17: 2D NMR spectra (500 MHz) of FFFFv•FFFVv•FFFVv•FFFVv in DMSO- d_6 (PEG marked with blue circles and unidentified impurities with purple circles): spectra of a) HSQC and b) HMBC experiments.

The impurities previously observed on the ^1H and ^{13}C NMR spectra were also present on the HSQC spectrum. Firstly, PEG was clearly seen with a chemical shift at 3.50 ppm on the ^1H signal and at 69.47 ppm on the ^{13}C signal (marked with a blue circle on **Figure II.17,a**). This band did not show any direct interaction with other bands confirming that the molecule corresponding to this band was not covalently linked to the synthesised oligomer. Besides, the three unassigned bands on the ^1H signal between 1.70 and 1.82 ppm (marked with the purple circle on the left on **Figure II.17,a**) corresponded to the same chemical shifts as those seen on the ^1H NMR spectrum of this sample (**Figure II.15**). These bands observed at 1.69, 1.75 and 1.82 ppm on the ^1H signal were correlated to the bands with a chemical shift of 21.74, 22.18 and 22.18 ppm respectively on the ^{13}C signal for the HSQC spectrum, which may relate to the bands at 22.28 and 2.42 ppm that were observed on the ^{13}C NMR spectrum (**Figure II.16**) due to their broadness. Showing overlap with the broad band at 1.00 ppm on the ^1H NMR spectrum, additional bands were visible at 1.00 and 1.27 ppm on the ^1H signal in the HSQC experiment with a correlation at 17.65 and 28.00 ppm respectively on the ^{13}C signal. The band with a chemical shift of 28.00 ppm on the ^{13}C signal may overlap with the one observed at 27.49 ppm on the DEPT experiment (**Figure II.16,b**), which could correspond to the same band. Due to the difficulty to observe direct interactions between the bands, the nature of these impurities relative to the oligomers was not established from the HSQC experiment.

When analysing the spectrum obtained from the HMBC experiment (**Figure II.17,b**), in a similar manner, the presence of PEG with a ^1H signal at 3.50 ppm and a ^{13}C signal at 69.82 ppm was confirmed. The earlier mentioned bands in the HSQC spectrum at a chemical shift of 1.00 and 1.24 ppm on the ^1H signal were also seen and correlated with a chemical shift of 18.05 and 29.36 ppm on the ^{13}C signal. The differences in chemical shifts could be associated with the broadness of the peaks. Considering the band of the impurity having a ^1H signal at 1.00 ppm and a ^{13}C signal at 18.05 ppm, this band was

Chapter II: Preparation and characterisation of oligomers based on phenylalanine and aliphatic building blocks by solid-phase synthesis

correlated to those at 0.87, 0.90 and 1.00 ppm with a chemical shift on the ^{13}C signal at 18.05, 18.05 and 12.50 ppm respectively. Considering the band of the impurity having a ^1H signal at 1.24 ppm and a ^{13}C signal at 29.36 ppm, a line could be drawn directly to the bands corresponding to the assignment of C12 and C13, but also to those of C1, C8 and C10 on the HMBC spectrum. It was unclear whether this was an indication of a direct bond between said impurities and any of the carbon atoms in the 1-2 ppm range on the ^1H spectrum as overlap with the aliphatic hydrocarbons could be seen in the signal.

4.1.4. Results of mass spectrometry

The sample was characterised by ESI-MS in positive mode by the group of Laurence Charles (Institut de chimie radicalaire) at the University of Marseille and the spectrum obtained is depicted in **Figure II.18**. The molecular ion peak was not observed as $[\text{M}+\text{H}]^+$, $[\text{M}+2\text{H}]^{2+}$ and $[\text{M}+3\text{H}]^{3+}$ were expected for a m/z value of 3037.48, 1519.25 and 1013.17 respectively.

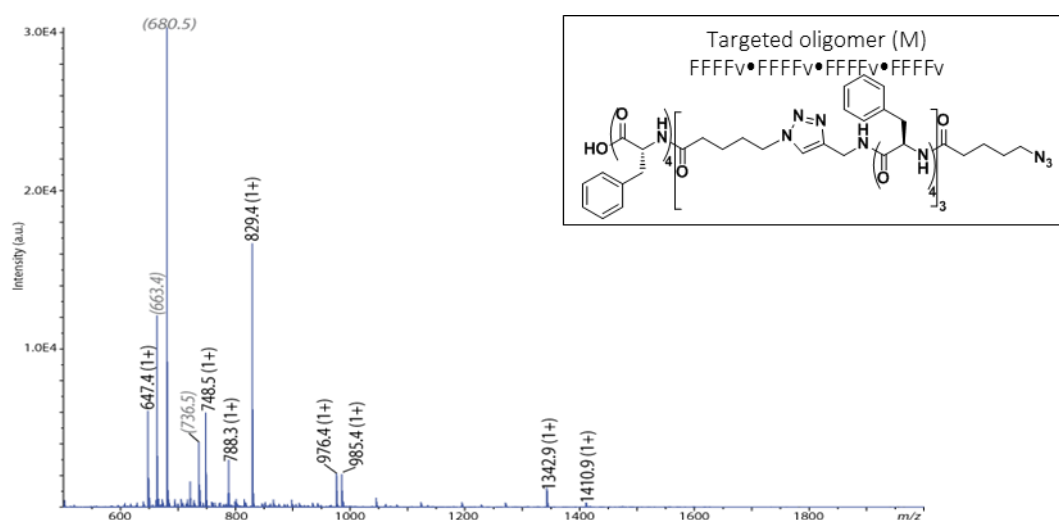


Figure II.18: ESI-MS spectrum of FFFFv•FFFFv•FFFFv•FFFFv (monoisotopic mass of FFFFv•FFFFv•FFFFv•FFFFv calculated from $\text{C}_{173}\text{H}_{189}\text{N}_{31}\text{O}_{21}$: $3036.47 \text{ g mol}^{-1}$).

A small Gaussian curve was observed for m/z between 600 and 800 corresponding to a quadruply charged ion. This Gaussian distribution suggested the presence of a polymer. Considering the NMR analysis reported in the previous sections, the presence of residual PEG was noticed and attributed to the use of Tentagel[®] resin, which possesses PEG chains having a molecular weight of $3000 \text{ g}\cdot\text{mol}^{-1}$. ESI-MS confirmed the presence of PEG with a molecular weight ranging from 2400 to $3200 \text{ g}\cdot\text{mol}^{-1}$.

Considering that one reaction cycle could be missing, the molecular ion peaks would be expected for m/z values of 2269.10, 1135.05 and 757.04 for $[\text{M}+\text{H}]^+$, $[\text{M}+2\text{H}]^{2+}$ and $[\text{M}+3\text{H}]^{3+}$ respectively, which were not observed. Similarly, if two reaction cycles were missing, the expected m/z values would have been 1500.73, 750.87 and 500.91. A more thorough analysis of the deletion sequences may be necessary to assign to peaks observed by ESI-MS. However, some of the observed peaks indicated in brackets were not structurally correlated to the targeted oligomer.

Chapter II: Preparation and characterisation of oligomers based on phenylalanine and aliphatic building blocks by solid-phase synthesis

Another batch of the oligomer FFFV•FFFFV•FFFFV•FFFFV was synthesised. The NMR characterisation of this sample was similar to the spectra presented in the previous section. The sample was further characterised by MALDI-ToF mass spectrometry (**Figure II.19**). This measurement was performed by Jean-Marc Strub (Institut pluridisciplinaire Hubert Curien) at the University of Strasbourg. The molecular ion peak $[M+H]^+$ (expected m/z value of 3037.48) was not observed or difficult to distinguish from the baseline. A large number of peaks was observed on the spectrum. Indicated in **Figure II.19**, amongst these peaks, oligomers with varying combinations of sequence deletions were observed and listed.

Chapter II: Preparation and characterisation of oligomers based on phenylalanine and aliphatic building blocks by solid-phase synthesis

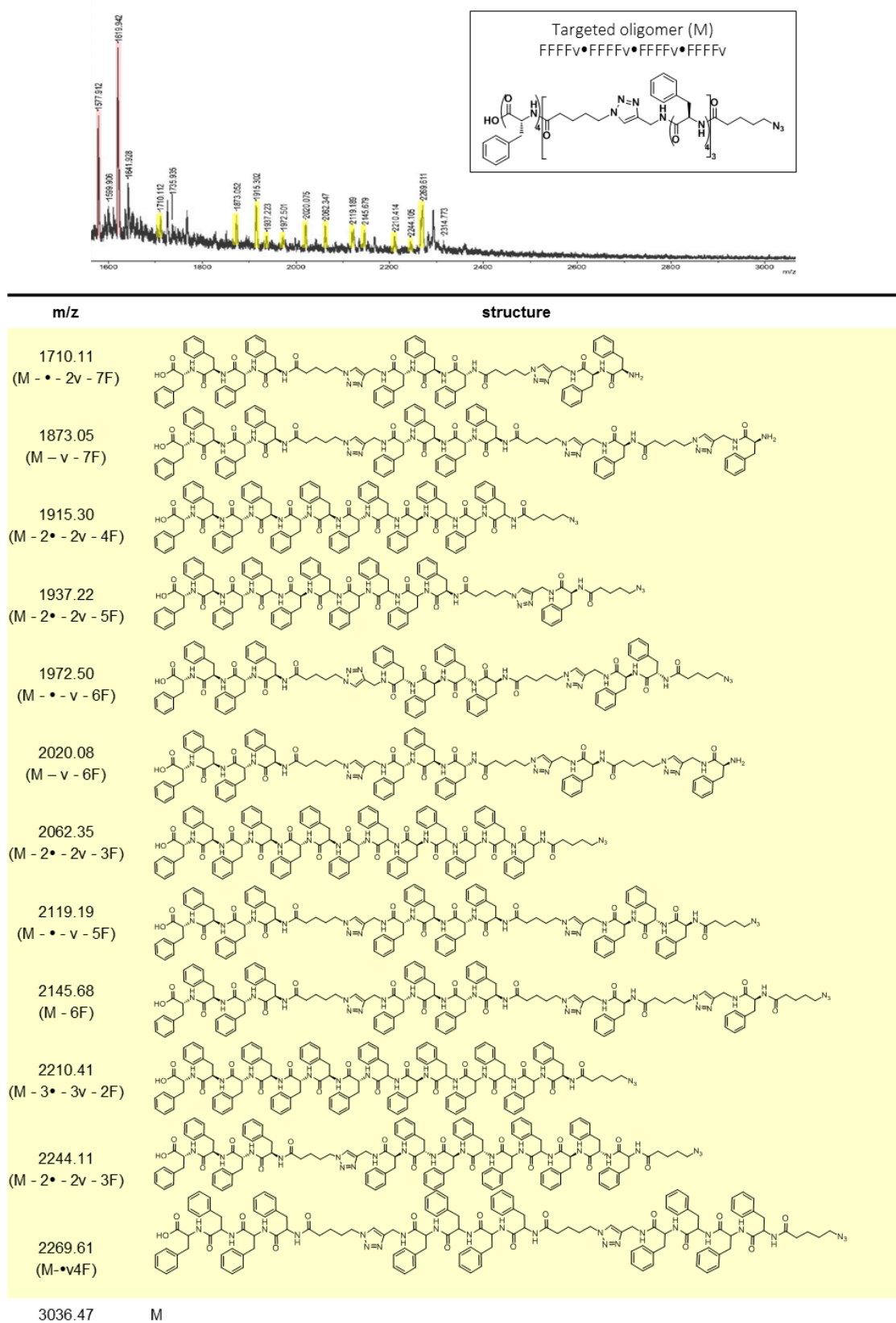


Figure II.19: MALDI-ToF spectrum of the second batch of FFFFv•FFFFv•FFFFv•FFFFv synthesised. The peaks listed correspond to oligomers with deletion sequences (in yellow), while others remained unidentified (in red). The molecular weight of F, v and • are 147.07, 126.07 and 54.03 g·mol⁻¹ respectively. Main mass peak (M) was not observed.

4.2. Evaluation of impurities potentially attributed to the use of a Tentagel[®] resin by ¹H NMR spectroscopy

NMR spectra revealed the presence of PEG due to leaching from Tentagel[®] resin. However, the use of this resin could be the source of other impurities. As the supplier recommends washing the Tentagel[®] resin with DCM, DMF, toluene and methanol before handling to remove possible impurities, it is possible that some of these impurities can be explained as naturally being present on 'unwashed' Tentagel[®] resin. Our experimental procedures did not involve any washing cycles involving toluene or methanol and so some of these impurities may be attributed to this fact.

A cleavage test on the Fmoc Phe Tentagel[®] PHB resin used was thus conducted. After washing cycles first with DMF and following DCM, the resin was treated with the cleavage solution (i.e. TFA/water/TIPS 95/2.5/2.5 v/v/v) for 2 h and the concentrated filtrate was characterised by ¹H NMR spectroscopy (**Figure II.20**).

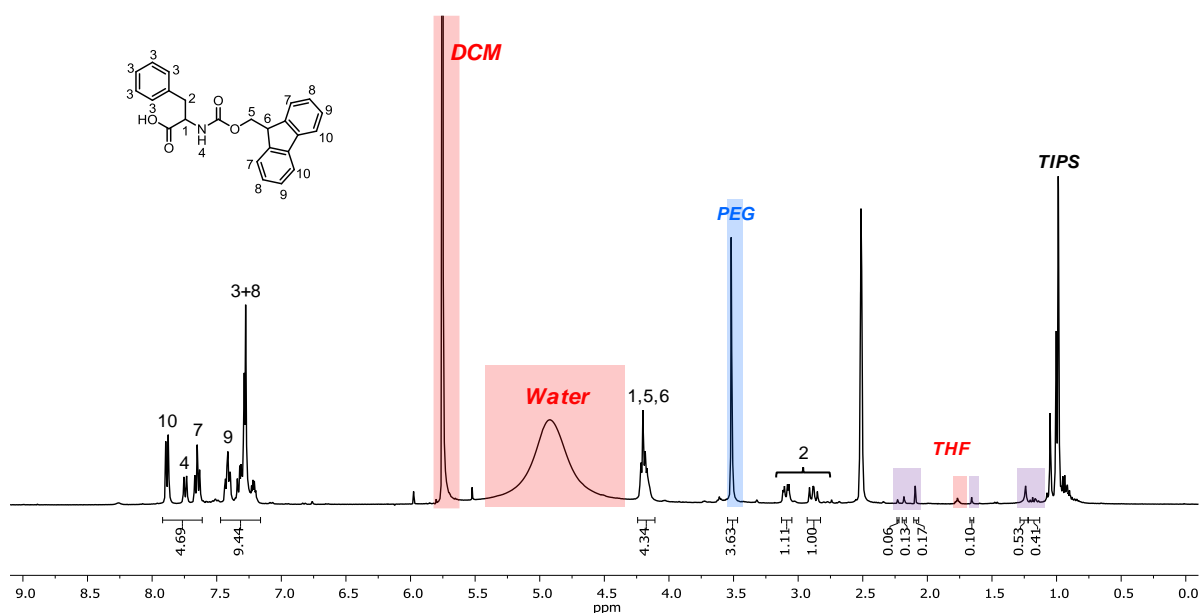


Figure II.20: ¹H NMR spectra in DMSO-d₆ of the filtrate obtained after treating Fmoc Phe Tentagel[®] PHB resin with the cleavage solution (residual solvents are highlighted in red, PEG in blue and unidentified peaks in purple): a) full spectrum and b) zoom on the 1.10-1.45 ppm region.

The presence of residual triisopropylsilane (TIPS, 0.97 ppm) was associated to the cleavage solution used, while the one of PEG at 3.50 ppm was due to PEG leaching from the Tentagel[®] resin [II.32]. The presence of solvents was expected due to the short duration of drying of the sample. Furthermore, other smaller impurity signals were present at 1.23, 1.64, 2.08, 2.17 and 2.22 ppm.

The signal at 1.23 ppm was present as one of the unidentified signals on some of the spectra (FFFFb•FFFFb•FFFFb•FFFFb and FFFFh•FFFFh•FFFFh•FFFFh) of oligomers synthesized using Tentagel[®] resin, allowing it to be related to the use of this resin. In a similar reasoning, the signal at 1.75 ppm, found on the spectrum of FFFFh•FFFFh•FFFFh•FFFFh synthesized using CTC resin (**Figure II.4**) has its origin excluded from the Tentagel[®] resin due to the lack of its presence in **Figure II.20**. This signal may

Chapter II: Preparation and characterisation of oligomers based on phenylalanine and aliphatic building blocks by solid-phase synthesis

be related in some way or another due to the synthesis technique (reagents or side reactions, for example). Unfortunately, it was not possible to relate any of the above mentioned signals (**Figure II.20**) to a molecular structure.

4.3. Summary on all the phenylalanine-based oligomers synthesised from a Tentagel® resin

To summarise, ten oligomers with different phenylalanine blocks, spacers and composition have been synthesised using Tentagel® resin, as indicated in Section 3.2.3. Despite optimisation of the synthetic procedure and subsequent increased reaction efficiency, impurities related to deletion sequences and unknown factors were still present. Similar to the example of FFFFv•FFFFv•FFFFv•FFFFv in Section 4.1, FFFFb•FFFFb•FFFFb•FFFFb, FFFFh•FFFFh•FFFFh•FFFFh and FFFFu•FFFFu•FFFFu•FFFFu synthesised using Tentagel® resin have also been extensively analysed and compared regarding their purity. An overview recording the impurities present and their integration values, is given in **Table II.5**. All the ¹H NMR spectra have been normalised based on the phenyl protons at 7.02-7.35 ppm, i.e. the integration value of the phenyl protons was set to 80.

Chapter II: Preparation and characterisation of oligomers based on phenylalanine and aliphatic building blocks by solid-phase synthesis

Table II.5: A list of impurities of four oligomers synthesized using Tentagel® (oligomers ending with T) and CTC (oligomer ending with C) resin. The values indicated in brackets are the values of the integration for the signals considered.

Impurity chemical shift	FFFFb•FFFFb•FFFFb•FFFFb-T		FFFFv•FFFFv•FFFFv•FFFFv-T		FFFFh•FFFFh•FFFFh•FFFFh-T		FFFFu•FFFFu•FFFFu•FFFFu-T		FFFFu•FFFFu•FFFFu•FFFFu-C
	Batch 1	Batch 2	Batch 1	Batch 2	Batch 1	Batch 2	Batch 1	Batch 2	
PEG (Tentagel® leaching) 3.50 ppm (¹ H NMR) 69.77 ppm (¹³ C NMR)	Yes (2.05)	Yes (7.20)	Yes (4.03)	Yes (8.40)	Yes*	Yes (7.80)	Yes (8.07)	Yes (7.30)	N/A
THF: 3.60 ppm (¹ H NMR) 67.03 ppm (¹³ C NMR)	No	Yes (0.40)	No	Yes (1.00)	No	No	No	Yes (4.70)	No
DCM: 5.75 ppm (¹ H NMR) 54.84 ppm (¹³ C NMR)	No	No	No	Yes (1.00)	No	No	Yes (0.34)	Yes (1.18)	No
Unidentified: 2.45/2.33 ppm (¹ H NMR) 21.65/25.12/24.63 ppm (¹³ C NMR)	No	No	No	No	Yes (0.97)	No	Yes (0.61)	No	Yes (0.42)
Unidentified: 1.82 ppm (¹ H NMR) 22.27 ppm (¹³ C NMR)	Yes*	Yes*	Yes (1.14)	Yes (1.15)	Yes (0.52)	Yes (0.74)	Yes (1.15)	Yes (1.02)	Yes (0.13)
Unidentified: 1.75 ppm (¹ H NMR) 22.10 ppm (¹³ C NMR)	Yes (0.38)	Yes (0.66)	Yes (0.47)	Yes (1.63)	No	Yes (0.80)	No	Yes*	No
Unidentified: 1.69 ppm (¹ H NMR) 20.48 ppm (¹³ C NMR)	Yes (0.80)	Yes (1.45)	Yes (0.89)	Yes (1.69)	No	Yes*	No	Yes*	Yes*
Unidentified: 1.55 ppm (¹ H NMR) 24.22 ppm (¹³ C NMR)	Yes (0.75)	Yes (0.60)	No	No	No	No	Yes (1.02)	No	Yes (0.36)
Unidentified: 1.30 ppm (¹ H NMR) 24.85 ppm (¹³ C NMR)	Yes**	No	Yes*	Yes*	No	No	No	No	No
Unidentified: 1.27 ppm (¹ H NMR) 28.00 ppm (¹³ C NMR)	No	No	Yes*	Yes*	No	No	No	No	No
Unidentified: 1.24 ppm (¹ H NMR) 29.36 ppm (¹³ C NMR)	No	No	Yes*	Yes*	No	No	No	No	No
Unidentified: 1.23 ppm (¹ H NMR) 28.57 ppm (¹³ C NMR)	Yes (0.11)	Yes (1.36)	No	No	No	Yes (0.50)	No	No	No
Unidentified: 0.87-1.00 ppm (¹ H NMR) 12.13-18.03 ppm (¹³ C NMR)	Yes (1.08)	No	Yes (1.67)	No	No	No	No	No	No
Possibly related to the use of RPC: 4.00 ppm (¹ H NMR) ? ppm (¹³ C NMR)	No	No	No	No	No	No	No	Yes (3.60)	No

*Overlap with other peaks complicated measuring integration value, **Not visible on ¹H NMR spectrum, chemical shift determined by HSQC

Concluding from this overview, it is clear that the recurring impurity at 1.82 ppm on the ^1H NMR spectrum was present for all the samples. The presence of signals at 1.75, 1.69, 1.55, 1.30 and 1.23 ppm seemed more sporadic, with only the 1.69 ppm signal visible on the oligomer synthesised using CTC resin. Interestingly, presence of signals at 1.30, 1.27 and 1.24 ppm seemed confined to only the oligomers containing valeric acid spacing units. The presence of several signals around 1.00 ppm seemed confined only to the first batches of oligomers synthesised using butyric acid spacing units. The second batch of FFFFu•FFFFu•FFFFu•FFFFu showed an impurity at 4.00 ppm uniquely. It is likely that this is the result of preliminary purification attempted for this batch using reverse phase column chromatography (silica bonded DSC18, 56 μm particle size, 0.007 μm porosity). The solvent gradient (60/25/15 to 85/0/15 acetonitrile/ H_2O /concentrated HCl) likely caused partial degradation of the column, although it was unclear what this particular peak in ^1H NMR represented.

5. Attempts at purifying the synthesised oligomers

As discussed in the previous sections some of the impurities could be assigned to oligomers with deletion sequences, but also other sources such as the use of a Tentagel[®] resin. Furthermore, even though the reaction conditions have been improved, impurities remained, leading to the investigation of a technique to purify the oligomer.

5.1. Identification of the potential techniques for the purification of the oligomers

Deletions and side reactions during solid-phase synthesis are commonly observed in peptide synthesis, despite the usage of synthetic techniques as described in Section 3.1.1 [II.19]. For that reason, purification of peptides is routinely performed after synthesis by preparative HPLC. Keeping these factors in mind and not being able to pinpoint with some certainty the purity of the desired oligomers, it seems necessary that the crude mixtures should be further purified.

Two techniques were considered here for purification of the oligomers: preparative HPLC and centrifugal partition chromatography (CPC). Both techniques rely on the usage of a stationary and mobile phase to separate the different components of the reaction with the difference that HPLC utilises a stationary phase which is solid, while it is liquid in CPC. A limiting factor for the purification using either HPLC or CPC is related to the conditions of the apparatus. Solvents and reagents used in HPLC should not degrade the solid column material used and the compounds themselves need to be completely dissolved in order to allow recovery. In CPC additionally a biphasic system is necessary of two non-miscible solvents both able to solubilise the crude mixture.

5.2. Evaluation of the solvent miscibility of synthesised oligomers

As had been made evident during the synthesis of the oligomers, they showed significant difficulties to be solubilised in regular organic solvents such as DCM and ethyl acetate. The problems of solubilisation are likely related to the hydrophobic nature and the tendency to form aggregates via

hydrogen bonding and π - π interactions. The problem was significant and limited the conditions for workup and purification. Therefore, in order to find suitable conditions for purification of the oligomers, solubility parameters can be considered.

Solubilisation tests have been performed on FFFFu•FFFFu•FFFFu•FFFFu synthesised using a CTC resin (**A**) and FFFFh•FFFFh•FFFFh•FFFFh synthesised using a Tentagel® resin with the optimised reaction conditions (**B**). Although the solubility experiments were done on two different oligomers, it could be expected that the main parameter to the solubility was the contribution of the phenylalanine hydrophobicity. It is therefore likely that the two oligomers were similar in this nature. For these experiments, 0.5 mg of oligomer per mL of solvent was used and unless mentioned otherwise slight heating (50 °C) was used to assist in the solubilisation. The use of adducts, i.e. concentrated HCl and TBAB, was considered to break the aggregates formed by the oligomers. In the case of the concentrated HCl, the main purpose was to break apart possible hydrogen bonding networks that may make dissolution unfavourable. The concentrated HCl could freely be swapped to other acids such as H₂SO₄. The addition of 10-15% of acid solution was experimentally found necessary to facilitate dissolution. The only exception was found in the usage of TFA in acetonitrile, where 5-10 vol% of acid was found to be enough to facilitate dissolution. The role of TBAB was that of a chaotrope, a molecule intended to break up aggregates [II.23]. One to two equivalents relative to the number of moles of oligomer was used as a starting point as it provided fast enough dissolution. However, smaller amounts of the chaotrope may also facilitate the dissolution. The results are summarised in **Table II.6** and the solvents are listed in order of solubility.

Table II.6: Overview of solubility of FFFFu•FFFFu•FFFFu•FFFFu-C (**A**) and FFFFh•FFFFh•FFFFh•FFFFh-T (**B**) in different solvents, including adducts (++ indicates a complete dissolution, + the visible breaking up of aggregates or slight dissolution, and - no dissolution).

Oligomer	Solvent	No adduct	+ 5-15 vol% conc. HCl _(aq)	+ 1-2 eq.TBAB
B	4-Methyl-2-pentanone*	++		
A and B	TFA	++		
A and B	Dimethylsulfoxide	++		
B	Dimethylacetamide	++		
A	<i>N</i> -Methylpyrrolidone	++		
A and B	Dimethylformamide	++		
B	Benzaldehyde	++		
A and B	TFA/dichloromethane 1/3	++		
A and B	Acetonitrile	+	++	++
A and B	Tetrahydrofuran	+	++	++
B	2-Butanol	+	++	+
B	2-Propanol	+	++	+
B	Butyl acetate	-	++	-
B	Diacetyl	-	++	-
B	3-Hexanol	-	++	-
B	1,2-Propanediol	-	++	-
A and B	Tetrahydrofuran/water 3/1	-	++	
B	Dichloroethane	+	+	++
A and B	Acetone	-	-	++
B	<i>m</i> -Xylene	-		++
B	<i>o</i> -Xylene	-		++
A and B	Dichloromethane	+		
A	Chloroform	+		
A	Carbon tetrachloride	+		
A	Toluene	-		
A and B	Methanol	-		
A	Pentane	-		
A	Cyclohexane	-		
A	Dioxane	-		
A	Ethanol	-		
A	Ethyl acetate	-		
A	Heptane	-		
A and B	Acetonitrile/water 1/1	-		
A and B	Acetic acid	-		
A and B	Water	-	-	-
A and B	Diethyl ether	-		

*Immediate dissolution without heating

4-Methyl-2-pentanone was the only solvent which immediately dissolved **B** without the need of heating. In particular, acetonitrile and THF performed well as solvents when adducts were used. 1/9 concentrated HCl_(aq)/THF was particularly convenient thanks to its volatility, allowing for a full recovery of the oligomer from solution if needed. Despite this, since acetonitrile allowed for the lowest amount of necessary acid (5% TFA) it was continuously used as a model solvent system for coating applications of the oligomers (Chapter III).

Only one biphasic system was able to be found to be potentially used for CPC using this solubility data: a 1/1 mixture of 15% concentrated HCl in 3-hexanol with DMSO. This greatly limited the ability to

perform purification using CPC. Additionally, in order to perform CPC accurately, analysis by HPLC was a necessity. For these reasons HPLC was considered.

5.3. Analysis of some oligomers by HPLC

In order to assess the ability to purify the oligomers, two of the oligomers synthesised using Tentagel® resin were considered: FFFFh•FFFFh•FFFFh•FFFFh and FFFFu•FFFFu•FFFFu•FFFFu. These oligomers were sent to the company Altergen [II.33] who kindly accepted to make a characterisation by analytical HPLC using a reverse phase HPLC column (Knauer, Eurosphere 100-5, C18, 250 x 4 mm). The different components of the impure mixture were able to be visualised in the used conditions (acetonitrile with 1% of TFA) on the chromatograms (**Figure II.21**).

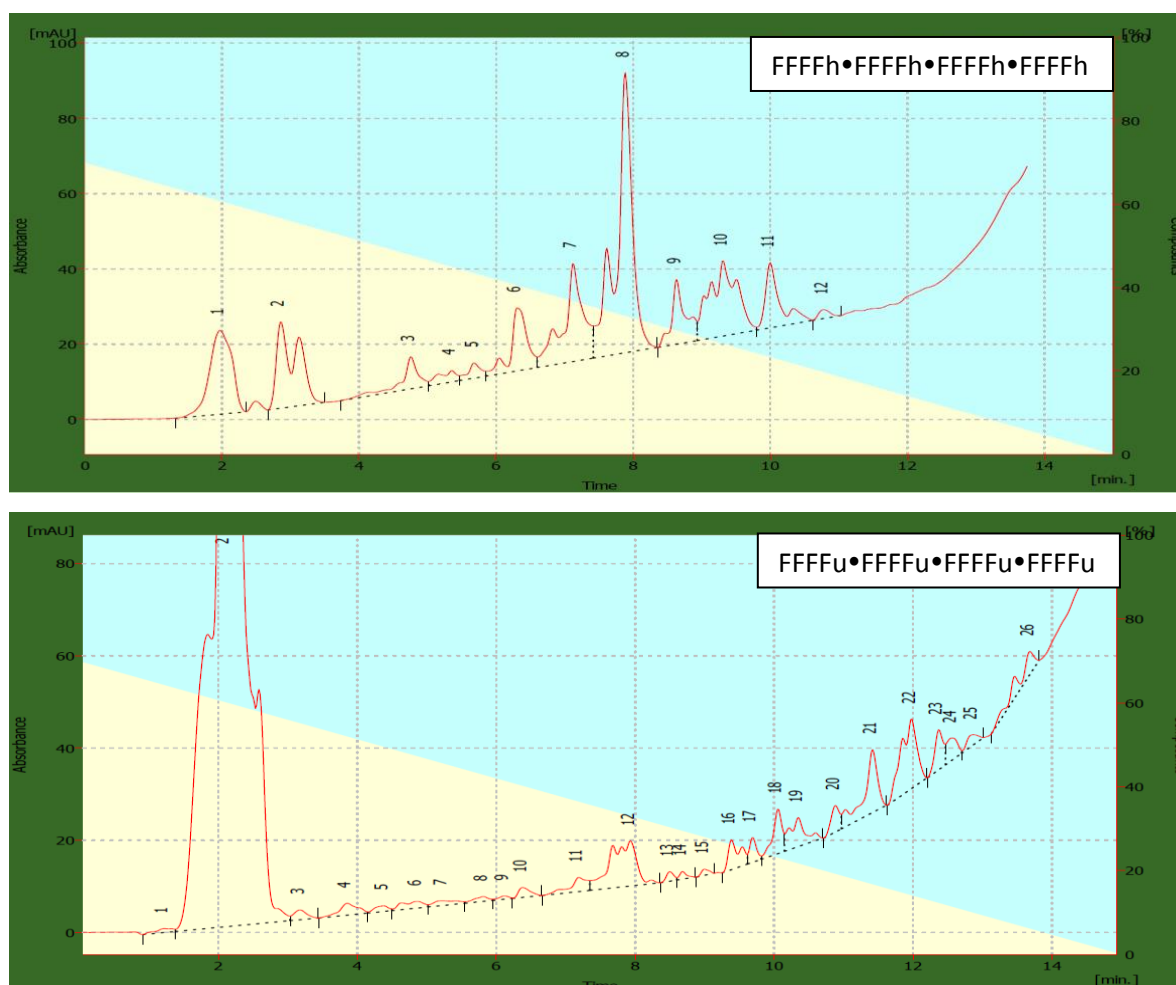


Figure II.21: HPLC chromatograms of FFFFh•FFFFh•FFFFh•FFFFh and FFFFu•FFFFu•FFFFu•FFFFu.

For FFFFh•FFFFh•FFFFh•FFFFh the largest peak was peak 8 eluting at 7.88 min, which may correspond to the desired product. The surface area of this peak indicated that it represented 28.4% of the total surface area, with the other peaks ranging in between 0.6 and 12.8%.

For FFFFu•FFFFu•FFFFu•FFFFu, the largest peak was peak 2 eluting at 2.10 min. It is possible that this peak corresponded to one of the impurities present in the mixture as the early and broad appearance could indicate a highly polar fraction of varying molecular weight while the oligomers themselves were

expected to be less polar. If the surface area was renormalized without peak 2, peaks 12 (7.93 min), 21 (11.42 min) and 22 (11.98 min) seemed to be the biggest peaks with respectively surface areas of 16.7, 12.1 and 15.2% of the total surface area.

It is therefore likely that the purity of FFFFu•FFFFu•FFFFu•FFFFu may be decreased in respect to FFFFh•FFFFh•FFFFh•FFFFh and harder to purify. More efforts need to be made to fully evaluate the purification procedure of these oligomers and whether or not a significant amount of the oligomer of interest can be recovered using preparative HPLC techniques.

6. Summary and future outlooks

Using the synthetic approach reported previously [II.15] a library of nineteen oligomers based on phenylalanine and aliphatic building blocks was synthesized using CTC resin. The presence of oligomers with deletion sequences led to investigate the optimisation of the reaction conditions. Various parameters have been considered including the pre-activation of the carboxylic acids during the steps leading to the formation of amide bonds, the use of additives to break aggregates that could form during the synthesis and the use of a resin other than the CTC one. Improved conditions have been identified in this work as using Tentagel® resin as solid support and using a mixture of solvents (DCM, DMF and NMP in equal volume). With these conditions a library of ten new oligomers was prepared and extensively characterised. While the oligomers obtained were still a mixture of the targeted oligomer with oligomers containing deletion sequences and several identified and yet unidentified impurities as indicated by mass spectrometry, some improvements were observed by ¹H NMR spectroscopy. When comparing the integration value of the peak corresponding to the methylene next to the terminal azide group to the one of the phenylalanine residues the values obtained were closer to the expected values.

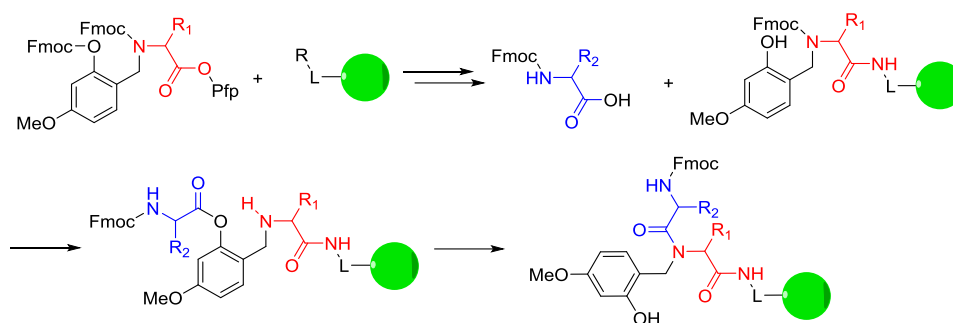
To obtain oligomers of higher purity two routes could be considered: (i) optimisation of the synthesis and (ii) identification of the best technique to purify the crude products obtained. Few approaches are discussed in the following sections.

6.1. Prospects of optimising synthesis

The first considerations to improve the reaction efficiency would consider the optimised conditions established in this chapter and modify some parameters by (1) using different coupling agents, such as *N,N'*-dicyclohexylcarbodiimide, (1-[bis(dimethylamino)methylene]-1*H*-1,2,3-triazolo[4,5-*b*]pyridinium 3-oxid hexafluorophosphate, and O-(benzotriazol-1-yl)-*N,N,N',N'*-tetramethyluronium tetrafluoroborate [II.34], and (2) increasing temperature either classically [II.35] or by microwave irradiation [II.36].

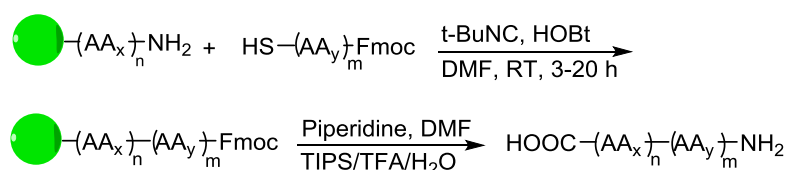
The synthesis itself may also be selectively modified. One example is the use of specific protective groups. For Fmoc-based solid-phase synthesis, the usage of an ortho-hydroxybenzyl (Hmb) protecting

group on the Fmoc protected *N*-terminus of the growing amino acid chain has been used with some success. The coupling reactions are performed with an alternative mechanism, which makes use of intramolecular hydrogen bonding interactions and *N*-acyl transfer so that usual inhibiting factors (e.g. H-bonding, aggregation) may be circumvented (**Scheme II.4**). Hmb-protected amino acids may be used at key difficult steps at any point during the synthesis. The Hmb protective group remains on the peptide backbone and can be cleaved at the final step in acidic conditions [II.37].



Scheme II.4: Amino acid coupling procedure using Hmb protective group [II.37].

Another common solution for larger peptides has been to perform the synthesis as a fragmented approach, meaning the synthesis of one specific peptide is split into separate syntheses of smaller fragments which do not show the same problems during reaction steps and once purified, the different fragments are coupled to obtain the final product [II.19]. This approach may be useful for any synthesis that requires the coupling of multiple repeating units. The final couplings can be performed with standard coupling chemistry or native chemical ligation and this step is not necessarily limited by the solid-phase constraints and can therefore be done in solution if needed [II.19]. One example is the use of isonitrile-mediated ligation, which allows the coupling of blocks of amino acids after an amidation reaction on a reactive thioacid [II.38].



Scheme II.5: Solid-phase ligation procedure of amino acid blocks using isonitrile chemistry [II.38]

Although both CTC and Tentagel® resins have been reviewed for synthesis, there exist other types of solid-phase resins, a list of which can be found in **Table II.7**. Several of the solid phase resins listed below are convenient for long peptide sequences or reaction steps showing difficulties, which may help synthesise the phenylalanine-based oligomers with higher reaction efficiency and fewer side products. Potential reasons for incomplete reactions included hydrophobic effects, which may be mediated with a PEG-based solid phase resin, such as ChemMatrix, PEGA or CLEAR. If alternative

reaction conditions are considered, JandaJel resin may be another viable option. Linker choice may also be selectively modified in order to mediate potential aggregation of the growing peptide chain.

Table II.7: Overview of some solid-phase resins used for peptide synthesis and some of their characteristics.

Composition	Resin	Linkers	Loading (mmol·g ⁻¹)	Application
Styrene crosslinked with divinylbenzene	Polystyrene	CTC [II.39-II.40] PHB [II.40] Amine Rink amide [II.40]	0.5 - 1.0	For routine and large scale synthesis
Styrene crosslinked with 1,6-bis(4-vinylphenyl)hexane	JandaJel [II.41]	Amine Hydroxide Chloride	0.45 - 1.2	For solid phase organic synthesis
PEG grafted on crosslinked polystyrene	Tentagel [II.31]	PHB [II.40] Rink amide [II.40]	0.15 - 0.6	For short biomolecules
	NovaGel [II.42]	PHB [II.40] Amine	0.6 - 0.8	For medium-length peptide
	NovaSyn [II.43]	PHB [II.40] Amine	0.2 - 0.3	For medium to long peptides
Crosslinked PEG	ChemMatrix [II.31]	Amine	0.4 - 0.6	For long and difficult peptide sequences
Crosslinked polyacrylamide-PEG	PEGA [II.31, II.44]	Amine	0.2 - 0.4	For peptide libraries and on-bead enzyme assay
Crosslinked PEG and ethacrylate	CLEAR [II.45]	PHB [II.40] Amine Rink amide [II.40]	0.2 - 0.6	For difficult peptide sequences

6.2. Prospects of purification

Existing purification techniques can be combined with a variety of labelling and addition of functional moieties during synthesis. One example is the use of acetylation steps after the coupling reactions are performed. The high reaction rate of the acetylation allows for a complete quenching of any reactive groups, preserving the structure of the smaller peptide. As a result, the final crude mixture will contain an improved distribution of the desired compound and deletion containing peptides, allowing easier purification [II.46].

Another strategy is to use ‘capping’ type reactions that react only with unreacted growing peptide chains. The capped chains, thanks to their polarity difference, allow for an easier purification after the final cleavage step [II.47].

Another approach involves the addition of tags to improve solubilisation. Two commonly used examples are PEG [II.46] or glycosyl [II.48] tags, which can be introduced as a sidechain during the reaction. These tags make it possible to use more hydrophilic solvents both during synthesis and purification gradients in HPLC, which may improve separation of the chromatography peaks. Similarly, peptide tags, such as an oligohistidine, lysine or arginine tags can also be used and coupled to the final reactive group of the peptide.

This allows the peptides that managed to couple to the tag to easily be purified from any peptides which did not, which could be peptides showing deletions. After purification the tag can be removed by separate cleavage [II.49-II.50].

CHAPTER III

Evaluation of the synthesised oligomers as potential interfacial agents for Kevlar fibre-reinforced polypropylene materials

Chapter III: *Evaluation of the synthesised oligomers as potential interfacial agents for Kevlar fibre-reinforced polypropylene materials*

1. Introduction

The library of oligomers based on phenylalanine and aliphatic building blocks described in Chapter II and listed in **Table II.4** was designed as potential compatibilizers for aramid fibre-reinforced polypropylene-based composite materials. Chapter III will focus on investigating their potential for this application including thermal stability, their adsorption properties onto aramid fibres and preliminary studies of aramid fibre reinforced composite materials. A selection of synthesised oligomers were considered using the Tentagel® resin focusing on two parameters (**Table III.1**): 1) the number of phenylalanine residues per reaction cycles and 2) the length of the spacer. The first parameter aimed at understanding if the presence of multiple phenylalanine residues would enhance the adsorption of the molecule on Kevlar fibres. Furthermore, as the space constraints of molecules to orient themselves along an interactive surface may be a relevant factor, spacing units in between interactive groups were introduced in the form of aliphatic chains, which are known for their highly flexible characteristics [III.1]. To have a better understanding of the interactions involved between the molecules and Kevlar fibres, some model molecules (commercially obtained) were also used. The contribution of the triazole moiety will be investigated by studying molecules without this functional group (molecules prepared by the Laboratoire Altergen). As phenylalanine could adsorb on Kevlar fibres through hydrogen bond interactions, π interactions or both, three model molecules were also used to discriminate these interactions: oligoglycine, polystyrene and oligophenylalanine respectively. Thusly, the molecules considered in this study were distinguishable in four categories: 1) commercially available standards (tetraphenylalanine (FFFF), tetraglycine (GGGG), polystyrene (PS)) having constrained freedom of movement in between the interactive subunits (F, G, styrene), 2) oligomers containing a single residue of phenylalanine per block with freedom of movement governed by spacing units (b,v,h) between the residues, 3) oligomers containing a single residue of phenylalanine per block with freedom of movement governed by hexanoic (h) spacing unit between the residues and triazole moieties, and 4) oligomers containing four residues of phenylalanine per block, freedom of movement also governed by spacing units (b,v,h,u) and triazole moieties between the blocks of phenylalanine residues.

Chapter III: Evaluation of the synthesised oligomers as potential interfacial agents for Kevlar fibre-reinforced polypropylene materials

Table III.1: Molecules considered in this study (the groups promoting π interactions are in blue, while those in red contribute in hydrogen bonding interactions).

Parameter considered	Molecule	Molecular weight (g·mol ⁻¹)
Synthesised oligomers	Fh•Fh•Fh•Fh	1327.71
	FFFFb•FFFFb•FFFFb•FFFFb	2980.40
	FFFFv•FFFFv•FFFFv•FFFFv	3036.47
	FFFFh•FFFFh•FFFFh•FFFFh	3092.53
	FFFFu•FFFFu•FFFFu•FFFFu	3372.84
Oligomers without triazole moiety	FbFbFbFb	946.46
	FvFvFvFv	1002.50
	FhFhFhFh	1058.53
Oligophenylalanine (π and hydrogen bonding interactions)	Tetraphenylalanine (FFFF)	606.28
Oligoglycine (hydrogen bonding interactions only)	Tetraglycine (GGGG)	246.46
Polystyrene (π interactions only)	Polystyrene (PS)	2100

2. Thermal stability

For many industrial processes elevated temperatures are not just occasional, but a necessity. In composite material, commonly used compound techniques include thermal injection moulding, which oblige to melt the resin material to be used. Given in **Table III.2** is an overview of thermal behaviour of resins commonly used in industrial environments (in particular automotive industry). Considering that the aim of this project is to prepare Kevlar fibre-reinforced polypropylene-based composite materials, the molecules used as interfacial agents should be stable, and thus not degrade, at the processing temperature, which correspond to 30 °C above the melting temperature of the polymer matrix. The polymer matrix consider was a copolymer of polypropylene and ethylene for convenient handling (Aceso®Lumicene® MR10MM0) and has thusly a lowered melting temperature of 137 °C. Therefore, the interfacial agents used should not degrade below 167 °C. An extensive thermal analysis of these molecules is proposed. Thermogravimetric analysis (TGA) and pyrolysis gas chromatography-mass spectrometry (GC-MS) results are presented in Sections 2.1 and 2.2. Another noted factor for compounding is crystallinity, notably in the form of the transcristalline effect previously mentioned in Chapter I [III.2-III.4]. For this reason, differential scanning calorimetry (DSC) results are presented in Section 2.3.

Table III.2: Thermal characteristics of commonly used thermoplastic resins: polypropylene (PP), polyamides (PA) and low density polyethylene (LDPE) [III.5-III.6].

Polymer	Melting point (°C)	Glass transition temperature (°C)
PP	174	-3
PA6	260	41-60
PA6,6	270	46-80
LDPE	138	-35

As a side note, the used aramid fibres (Kevlar® K29) are expected to be hygroscopic and likely to show a presence of water. At production, the expected water content is up to 7 wt%, while at equilibrium, this is expected to be 4.5 wt% [III.7]. In order to verify this, a thermogram has been taken of the aramid fibres (**Figure III.1**). Using thermogravimetry, a weight change of 4.1% was seen between 50 and 150 °C and could be solely attributed to the presence of water.

Chapter III: Evaluation of the synthesised oligomers as potential interfacial agents for Kevlar fibre-reinforced polypropylene materials

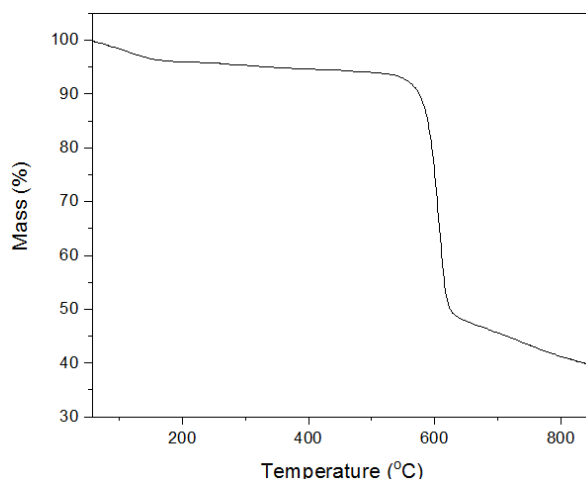
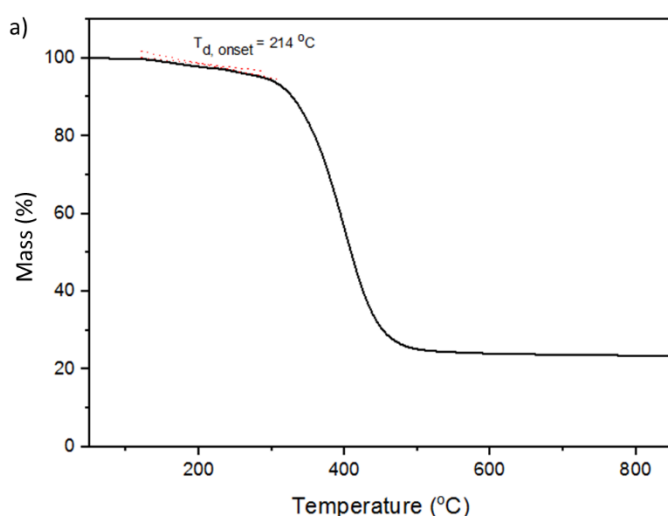


Figure III.1: Thermogram of aramid fibres (N_2 , flow rate: $10\text{ cm}^3\cdot\text{min}^{-1}$, heating rate: $50\text{ °C}\cdot\text{min}^{-1}$).

2.1. Thermogravimetric analysis of the molecules considered

Thermogravimetric analysis allows for the evaluation of weight loss over given temperatures and gives a characteristic degradation profile as well as the initial point of degradation ($T_{d, \text{onset}}$). These measurements were performed for all the molecules mentioned in **Table III.1** excluding polystyrene. TGA graphs for all synthesised oligomers showed similar profiles including initial degradation temperature. Roughly, three regions of degradation were observed: 1) until 300 °C with less than 10% of mass loss, 2) from 300 to 450 °C with a rapid decrease in mass until ca. 25% of weight remained, and 3) from 450 °C to 850 °C with no more mass loss. As example, the thermogram for $\text{FFFFh}\cdot\text{FFFFh}\cdot\text{FFFFh}\cdot\text{FFFFh}$ is depicted in **Figure III.2** (the thermogram of all other molecules can be found in Appendix A). The graph showed an onset of degradation ($T_{d, \text{onset}}$) starting at a temperature of 214 °C . This value was not calculated but rather estimated visually and pinpointed with tangent lines. Using this method, it was possible to record initial degradation temperatures for all the applicable molecules for the adsorption study (**Figure III.2b**).



Oligomer	$T_{d, \text{onset}}\text{ (°C)}$
Polystyrene	375*
GGGG	282
FFFF	232
FbFbFbFb	134
FvFvFvFv	139
FhFhFhFh	134
Fh•Fh•Fh•Fh	214
FFFFh•FFFFh•FFFFh•FFFFh	214
FFFFb•FFFFb•FFFFb•FFFFb	226
FFFFv•FFFFv•FFFFv•FFFFv	215
FFFFu•FFFFu•FFFFu•FFFFu	230

Figure III.2: TGA analyses: a) thermogram of $\text{FFFFh}\cdot\text{FFFFh}\cdot\text{FFFFh}\cdot\text{FFFFh}$ (N_2 , flow rate: $10\text{ cm}^3\cdot\text{min}^{-1}$, heating rate: $50\text{ °C}\cdot\text{min}^{-1}$) and b) $T_{d, \text{onset}}$ values for the molecules used for adsorption studies (* from Seleem *et al.* [III.8]).

Chapter III: Evaluation of the synthesised oligomers as potential interfacial agents for Kevlar fibre-reinforced polypropylene materials

Considering the impurities presented in Chapter II, it was difficult to make a prediction of the degradation behaviour. However, it is known from literature that the peptide bond of phenylalanine by itself degrades starting at roughly 291 °C [III.9-III.10]. Knowing this, it may be possible that the region of degradation before the sharp decrease of mass was related to extremities (COOH and N₃) and the terminal linker unit. A possible reason for the plateau region above 450 °C could be the partial formation of a product that does not degrade under nitrogen atmosphere, for example graphite from the phenyl moieties. A difference in the final mass can then be related to how easy this product is formed depending on the structure, although it may not be straightforward to predict which factors lead to more or less formation. Although the final mass of the degraded oligomers may differ ($\pm 10\%$), it is unclear what could be the cause of this difference.

2.2. Pyrolysis GC-MS results of the synthesised oligomers

Using the data obtained by thermogravimetric analysis (Section 2.1), distinct steps in the degradation behaviour were identified. By wisely selecting pyrolyser temperatures, results from pyrolysis GC-MS experiments can act complementary to the TGA results. The chromatogram delivered continuous mass spectra of degradation products at variable time and temperature, which were analysed by comparing to known spectra in the NIST library [III.11]. Two different methods were used to express similarities: *For(ward)* and *Rev(erse)*, indicating a similarity and absence of dissimilarity respectively. The following four temperatures were chosen: 230 °C as initial temperature for the start of degradation, 320 °C as temperature at which the initial less steep 'bump' in the TGA graph finished, 480 °C as temperature at which the steep curve in the TGA graph finished, and 750 °C as temperature at which no further loss of mass was observed. Pyrolysis GC-MS spectra were recorded for FFFFh•FFFFh•FFFFh•FFFFh at different temperatures (**Figure III.3**). The early region of degradation at 230 °C was related to the degradation of the oligomer extremities (COOH, N₃), which was confirmed as the chromatogram did not show any peaks other than oxygen and carbon dioxide gas (CO₂ at 1-2 min, oxygen and nitrogen in the baseline). At first glance, the chromatogram at 320 °C appeared similar to that of 230 °C, as no peaks were visible in the chromatogram. However, with careful probing a mass spectrum recognised by the NIST library was obtained. In the region of 14-15 min, degradation products were visible (pyrimidine and cis-acetonic anhydride). This observation supported the hypothesis made from TGA results in the region in between 230-320 °C on the degradation of the terminal spacing unit together with the nitrogen from triazole moieties. Unfortunately, as the peaks at 13.58 and 14.59 min were not distinct from the noise the mass spectrum was hard to compare to the NIST library [III.11], and thus to confirm this hypothesis. Other products at 480 °C, notably toluene (4.23 min), styrene (7.74 min) and dibenzyl (18.03 min), were attributed to the characteristic degradation of phenylalanine, which is expected starting at ca. 290 °C [III.9-III.10, III.12]. However, the peak at 14.59 min was not present in the chromatogram of phenylalanine and was associated with one of the other building blocks

Chapter III: Evaluation of the synthesised oligomers as potential interfacial agents for Kevlar fibre-reinforced polypropylene materials

constituting the oligomer. According to the NIST library, this peak was assigned to caprolactam corresponding thus to the degradation product from the hexyl spacing unit. Its small abundance was attributed to its rapid combustion into other degradation products.

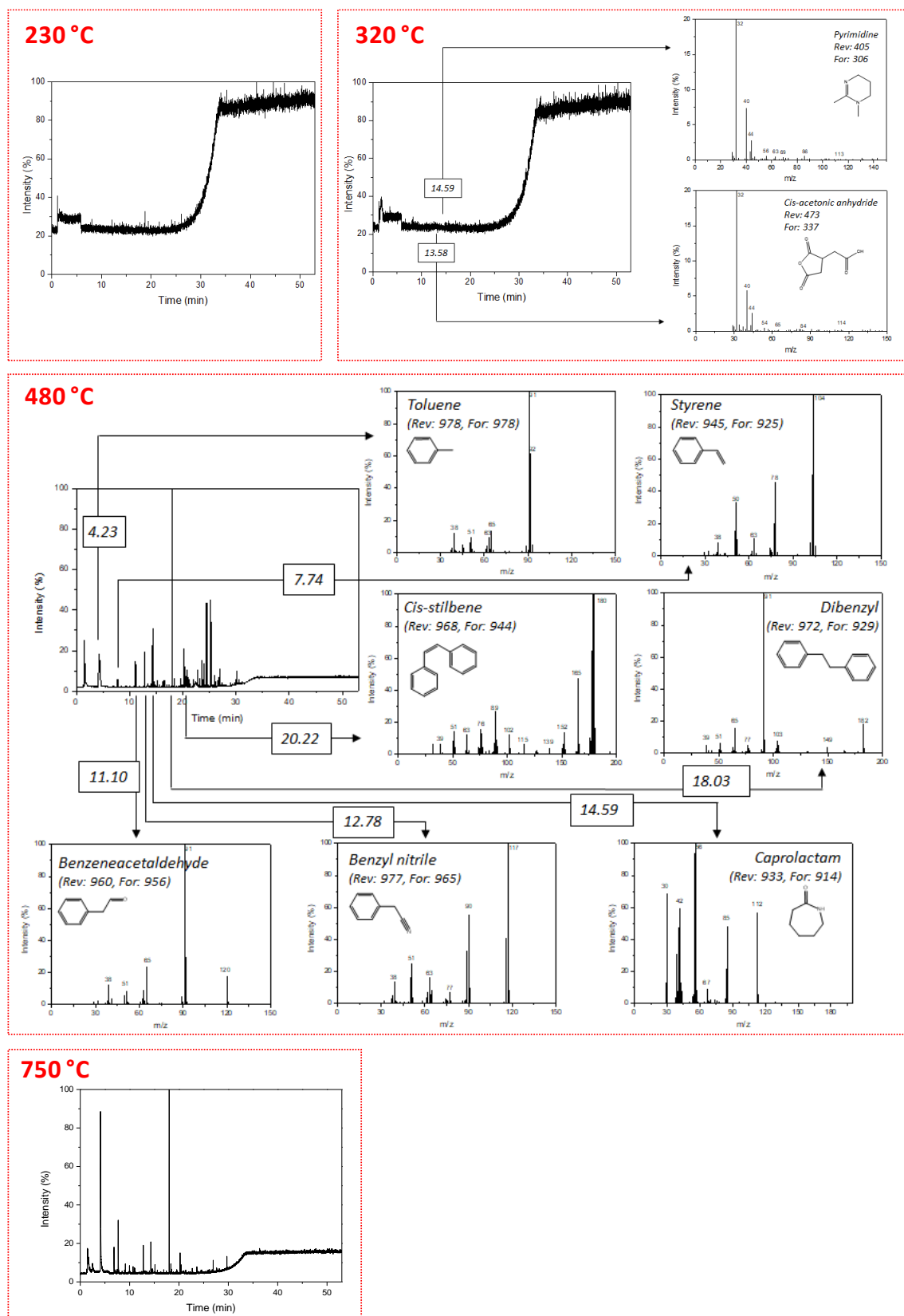


Figure III.3: Gas chromatograms of FFFFh•FFFFh•FFFFh•FFFFh at 230, 320, 480 and 750 °C.

2.3. Differential scanning calorimetry analysis

Differential scanning calorimetry studies allows the analysis of any semi-crystalline behaviour including the recording of a glass transition temperature (T_g). DSC studies were performed for all molecules mentioned in **Table III.1**, excluding polystyrene. Example graphs can be seen for FFFFh•FFFFh•FFFFh•FFFFh and FvFvFvFv in **Figure III.4**. All DSC thermograms followed a similar shape to these examples, data of which can be found in Appendix A. T_g determination was done by considering the crossing point between the half distance dotted tangent lines and the curve (dQ/dT). Since T_g is an out of equilibrium transition, value depending on cooling or heating rate (dT/dt), an extrapolated value at $dT/dt = 0$ is given for a sake of comparison. For FvFvFvFv the extrapolated T_g was 80 °C. The decrease in T_g with decreasing heating rate was expected considering physical properties [III.6].

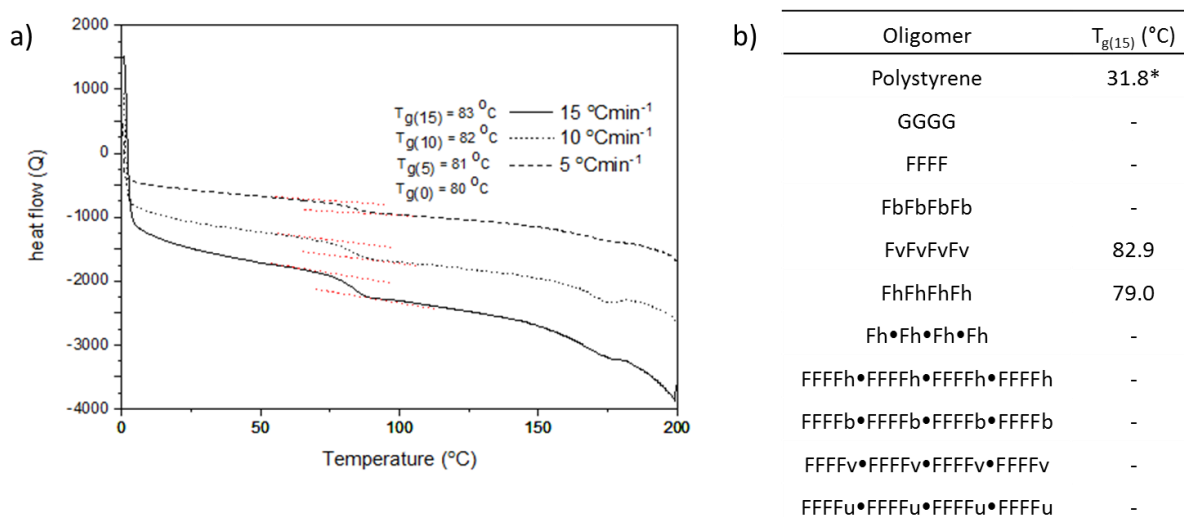


Figure III.4: DSC results: heating curves for oligomer a) FvFvFvFv (N_2 , flow of $10\text{ mL}\cdot\text{min}^{-1}$) and b) summary of the T_g values for the molecules considered for the study (*Determined by Rugin and Burgin using a heating rate of $17.9\text{ }^\circ\text{C}\cdot\text{min}^{-1}$) [III.13]).

The oligomers synthesised were seemingly lacking in a T_g in the range 0-200 °C temperature range. The impurities that are present in the molecules can affect the results in several ways, acting as a plasticizer. In the more specific case of oligomers containing deletions, it is possible that the size of the oligomer was associated with a different T_g . As a result, the transition itself was less well defined and as a result harder to determine. To overcome this issue, modulated temperature DSC (MTDSC) was attempted, where rather than a linear heating program, a stepwise heating gradient was applied. This allowed to more accurately take into account some relaxation issues. As can be seen in the curve in **Figure III.5** the presence of a T_g for FFFFh•FFFFh•FFFFh•FFFFh was not able to be confirmed using this method.

2.4. Concluding remarks

Coating molecules were characterised by TGA, pyrolysis GC-MS and DSC techniques. TGA thermograms showed a large overlap in degradation behaviour, with most onset degradation temperatures above

Chapter III: Evaluation of the synthesised oligomers as potential interfacial agents for Kevlar fibre-reinforced polypropylene materials

the melting points of thermoplastic matrices of interest, including polypropylene, with the exception of purchased peptide products FbFbFbFb, FvFvFvFv and FhFhFhFh. The other coatings compounds should be suitable for use as interfacial agents on fibres in composites fabricated using thermal injection moulding. Using pyrolysis GC-MS in conjunction with TGA allowed for the confirmation of specific phenylalanine degradation regions and possible degradation regions of molecule extremities. By DSC a T_g was determined for some compounds. However, a large influence of the cooling rate was noticed. The relaxation of the oligomers had a large influence in the thermal behaviour so care must be taken to pick a certain cooling rate. With MTDSC no improvement over the visualisation of the gradients over regular DSC was observed. It is important to also mention that since the purity of the oligomers cannot be guaranteed, it is difficult to take any value in trends seen in the DSC measurements.

3. Coating procedures

As mentioned in Chapter I, various fibre treatments for composite materials are commonly performed in industry, one of which is the application of 'sizing', a fibre coating which may include various additives of which compatibilizers can be a part. In industry, two coating techniques frequently used for applying sizings from solution onto fibres are dip coating and spray coating.

3.1. Dip coating

Background. Dip coating is a popular technique for large scale industrial production of various products, including optical filters, coated glass, and various photovoltaic devices [III.21]. The procedure follows in two steps: first the application of the solvated molecule onto the fibre surface and then removal of the solvent via evaporation, leaving the solid sizing layer. This sizing thickness can be controlled and is typically within a range of a few nanometers to approximately 200 nm for oxide coatings prepared from solutions of metal salts, up to 1 μm for colloidal systems coatings and several microns for inorganic-organic hybrid materials [III.14].

Protocol used. The dip coating procedure was adapted to apply the chosen coating molecules as treatments for aramid fibres (**Figure III.5**) and allow subsequent analysis. For this procedure, short fibres of aramid (SFA, average diameter of 12 μm , average length of 50 mm) were held in place by using PTFE or PTFE-coated tweezers. Due to the dimensions of the fibres, it proved to be very difficult to hold a single fibre in place. Five to ten fibres were thusly used for each coating experiment and was referred to as a 'fibre bundle'. A 1 $\mu\text{mol}\cdot\text{mL}^{-1}$ solution (unless mentioned otherwise) of the coating molecule in trifluoroacetic acid (TFA)/acetonitrile (ACN) 5/95 v% was made, which was poured into a glass Petri dish (diameter of 35 mm, height of 10 mm). In the case of polystyrene, the solvent was changed to toluene. The fibre bundle was then fully submerged into the solution. By either manually holding the tweezers into place or using glass vials as a wedge, the fibre bundle was left static in the

Chapter III: Evaluation of the synthesised oligomers as potential interfacial agents for Kevlar fibre-reinforced polypropylene materials

solution for 5 min. Then, the fibre bundle was removed from the solution perpendicularly to the basin, after which drying took place. This was done still on the tweezers in air for ca. 3 h.

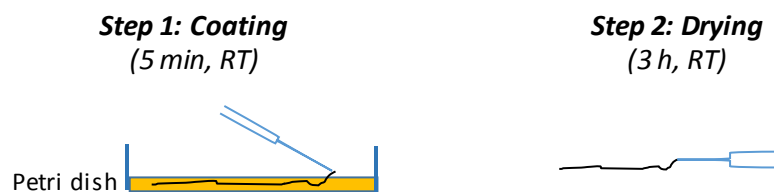


Figure III.5: Adapted dip coating procedure.

3.2. Spray coating

Background. As mentioned in Section 3.1., dip coating often allows for a controllable thickness of the applied sizing. However, this technique also has some disadvantages, requiring a relatively high volume of solvent and the need of voluminous basins. Furthermore, the withdrawal speeds can often range in a few $\text{cm}\cdot\text{min}^{-1}$, giving rise to a long processing time [III.14]. For these reasons, spray coating can be a viable alternative, involving nebulizing the solution using a ‘spray gun’, which allows droplets at micrometer scale to hit the fibre surface. In an industrial setting, this is performed in a closed compartment so that droplets not hitting the fibre surface can be recovered [III.14]. Depending on the solute and substrate and the necessity for certain droplet size distributions, a setup involving atmospheric conditions [III.15], vacuum [III.16], variable temperature [III.17], electrochemistry [III.18] or ultrasonic conditions [III.19] may be preferred. The spray coating process in general involves three separate steps: generation of droplets, attachment of droplets on the fibre surface and subsequent drying.

Protocol used. A $10\ \mu\text{mol}\cdot\text{mL}^{-1}$ solution of the coating molecule in TFA/ACN 5/95 v% was made and left inside the glass vial used for dissolution. The plunger of a disposable HDPE spray head was placed in the solution and the trigger allowed suction and subsequent spraying (**Figure III.6**). By carefully manoeuvring around the fibre bundle held in place by PTFE or PTFE-coated tweezers, spraying was performed around the surface of the fibres. The fibre bundle was subsequently dried for ca. 3 h in air still on the tweezers.

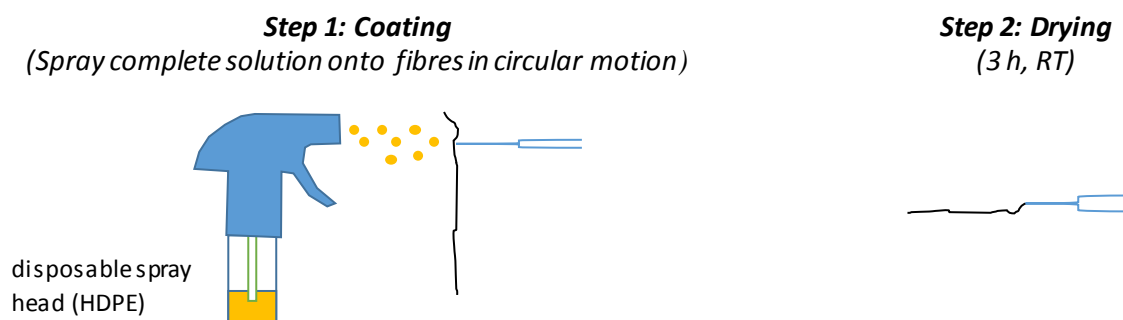


Figure III.6: Adapted spray coating procedure.

4. Preliminary SEM/EDS studies

4.1 SEM/EDS studies: introduction

Scanning electron microscopy (SEM) was used to analyse our coatings (see Kapustin *et al.* for polymer-based coatings [III.20] observed by SEM). A schematic overview of the SEM/EDS characterisation areas is given in **Figure III.7**. Any sample to be analysed was placed on a substrate which was loaded into a vacuum chamber of the microscope. This allowed an electron beam to hit the surface of the sample without disturbances of the environment. Depending on the amount of energy used, different regions of the volume of the substrate can be reached. The upper layers (5-50 nm) generate secondary electrons when hit by the beam and can be used to obtain a topographical contrast, leading to a high resolution image, a secondary electron image (SEI, **Figure III.7b**). In a range from 50 to 450 nm, backscattered electrons are generated and higher energies are required, leading to a Backscattered Electron Image (BEI, **Figure III.7c**). Although surface detail may decrease, additional information about the composition may be obtained and more detail in regions below the surface layer can be visualised [III.21]. In 50-450 nm range, X-rays will be generated on top of the backscattered electrons, which may be selectively detected using a probe to obtain information on the atomic composition of this volume. However, as can be seen in **Figure III.7**, X-rays can also be generated beyond this volume. As this X-ray analysis is a semi-quantitative technique, results need to be normalised around an internal standard. In our case, such functions were built in to the EDS analysis software (Oxford instruments Aztec) [III.22].

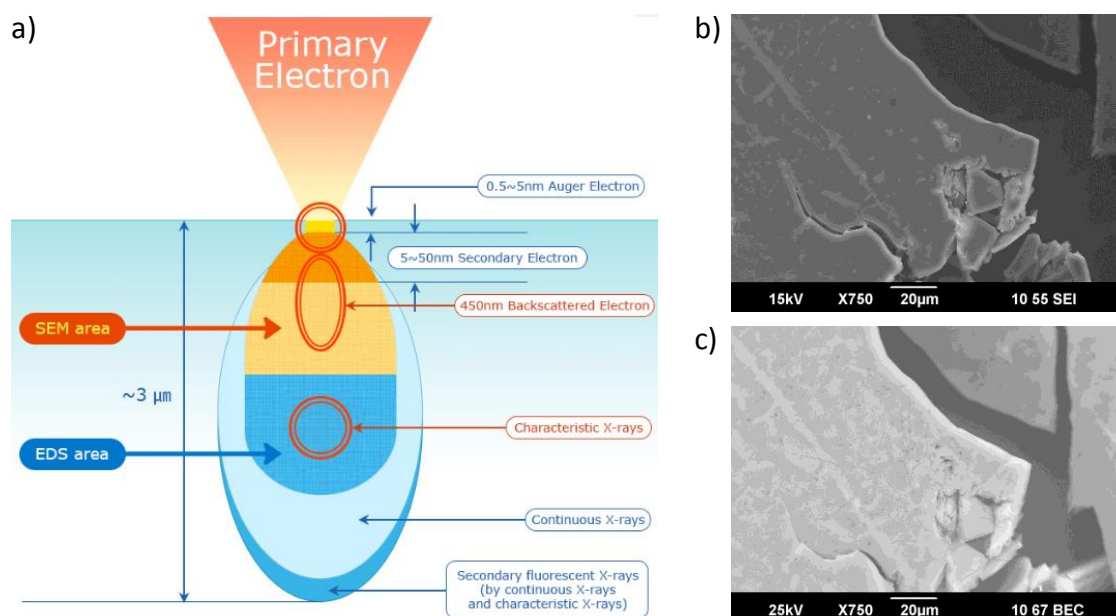


Figure III.7: SEM/EDS measurements: a) overview of the different characterisation areas associated generation of electrons/X-rays [III.21], b) SEI topographical image and c) BEI compositional image of solid Fh•Fh•Fh•Fh.

All samples were analysed using a JEOL JSM6490LV (max resolution: 3 nm) microscope equipped with an Oxford instruments AZTEC (lateral resolution: 200 nm) or X-Max (lateral resolution: 30 nm) energy dispersive X-ray spectroscopy (EDS) module. The source of X-rays was a W Filament. For preparation

Chapter III: Evaluation of the synthesised oligomers as potential interfacial agents for Kevlar fibre-reinforced polypropylene materials

of SEM samples, an Emitech K575 sputter coater was used with the following settings: platinum as metal with a pressure of 10^{-3} mbar, a current of 65 mA, and a sputter distance of 3 cm. Measurements were taken under a pressure of ca. 10^{-5} mbar with a voltage of 15 kV. Preparation of the samples for proper analysis was not always straightforward and the steps taken to eliminate known charge buildup, movements of samples and the geometry of the sample surface [III.23] are elaborated in Sections 4.2. and 4.3.

4.2. Preparation of substrate

Owing to the lightweight and nonconductive nature of the aramid fibres, preparation of substrates for SEM/EDS analysis required additional efforts. The low mass of the individual fibres allowed the fibres to move in the vacuum chamber when hit with the electron beam, causing both trouble with generating images as well as X-ray spectra [III.22]. Additional movements may be inferred from charge buildup caused by the lack of conductivity. For these reasons, the substrate was prepared by spreading the fibres between two adhesive substrates (**Figure III.8**). The reason was threefold: 1) stretching out the fibres across the two substrates for a minimal height difference and freedom of the fibre to move around in the vacuum chamber, 2) a minimal contact between the carbon substrate and the fibres since the adhesive on the substrate may disturb the coating layer, and 3) diminishing X-rays generated from the carbon substrate. For the latter case, owing to the atomic composition of the carbon substrate, notably in carbon and oxygen, the carbon substrate will interfere with the spectra of the (treated) fibre surface. A similar overlap was not found for the metal support, owing to the critical excitation energy needed to generate X-rays, which means X-ray spectra on the fibre surface can be generated in the area between the two carbon substrates without any significant interference. Finally, to eliminate the conductivity problems, the substrate was treated with platinum sputter coating (thickness $<10\text{nm}$).

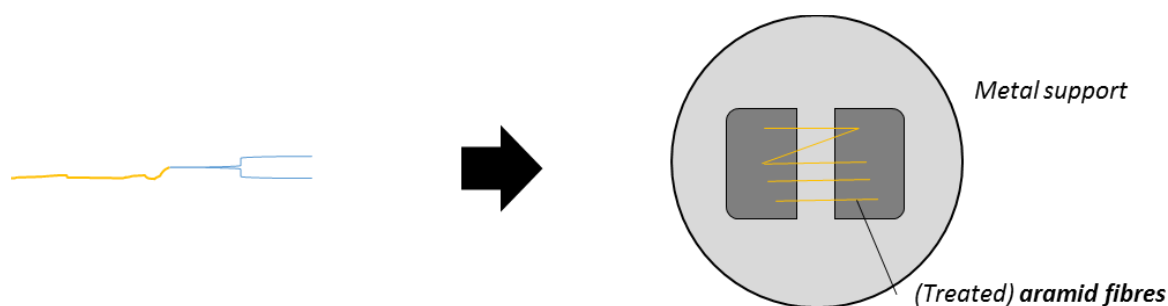


Figure III.8: Application of treated Kevlar® fibres onto metallic substrate.

4.3. Angle and morphology effect

Proper collection of EDS spectra relies on the angle of the generated backscattered X-rays from the electron beam. Accurate spectra can thus best be generated from flat surfaces [III.22]. However, since the aramid fibres are cylindrical in shape, selection of the area at which the EDS spectrum is obtained is a crucial factor (**Figure III.9**). Spectrum 8 was obtained by collecting X-rays emitted by a zone

Chapter III: Evaluation of the synthesised oligomers as potential interfacial agents for Kevlar fibre-reinforced polypropylene materials

delimited by the long rectangle placed on the edge of the fibre image. Each transition energy peak identified an atomic element (ideally). On spectrum 8, Pt from sputtering, C, O, N from the aramid fibre were detected. A peak attributed to aluminium was also detected. These X-rays must have been generated by the aluminium of the substrate and were not expected. Spectrum 6 was obtained by collecting X-rays emitted by a larger rectangular zone in the middle of the fibre image. C, O, N from the aramid fibre were once more detected as well as platinum from sputter coating. Overall, the resolution of the spectrum increased, with additional numbers of received X-rays (coups). To finally obtain the proper C, O and N atomic ratios, the peaks were renormalized to obtain the values as listed in the table. Following this, differences were noted between the two spectra, with spectrum 8 having a higher O% and lower C%. Comparing the two to the theoretical value of the aramid fibre, a notable difference was obtained, with spectrum 6 being a closer approximation. It can therefore be argued that the curved surface of the fibre gave trouble, possibly due to the angle with which X-rays were generated, inhibiting the collection of data.

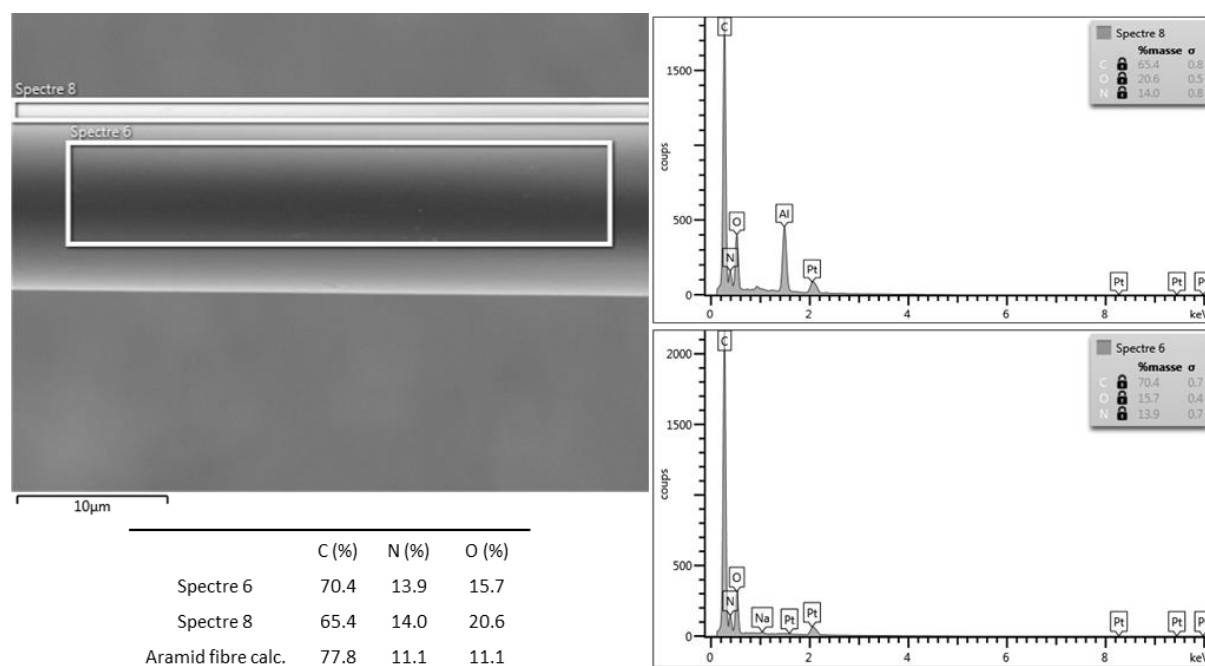


Figure III.9 SEM image of the aramid fibre surface with highlighted areas for EDS spectra.

Despite this, likely due to the semi-quantitative nature of EDS, overlap with the calculated atomic values was not observed [III.22]. A notable increase in atom% of oxygen was obtained for both measured spectra. One of the reasons for this increase is that due to the hygroscopic nature of the fibres, the presence of water of 4.5 wt% at equilibrium was expected [III.6]. Indeed, as TGA results have indicated (Section 1.2.1), 4.1 wt% of water was present. It is for this reason that comparisons were only made between different experimental datasets, *e.g.* untreated aramid fibre, individual solid coatings and applied coatings, given in Section 5.3.

Chapter III: Evaluation of the synthesised oligomers as potential interfacial agents for Kevlar fibre-reinforced polypropylene materials

4.4. Determination of coating solution concentration and influence of spray coating

A series of different concentrations of the simplest (and most readily available) coating molecule, GGGG, was applied using spray coating. The overview of different morphologies observed in spots that showed coating via SEM is given in **Figure III.10** [III.24-III.26]. Increasing the amount of GGGG present in the coating solution led to a roughening of the surface, detected with a solution concentration of $0.01 \text{ mmol}\cdot\text{mL}^{-1}$, then appearance of different shapes, including droplets, above this concentration.

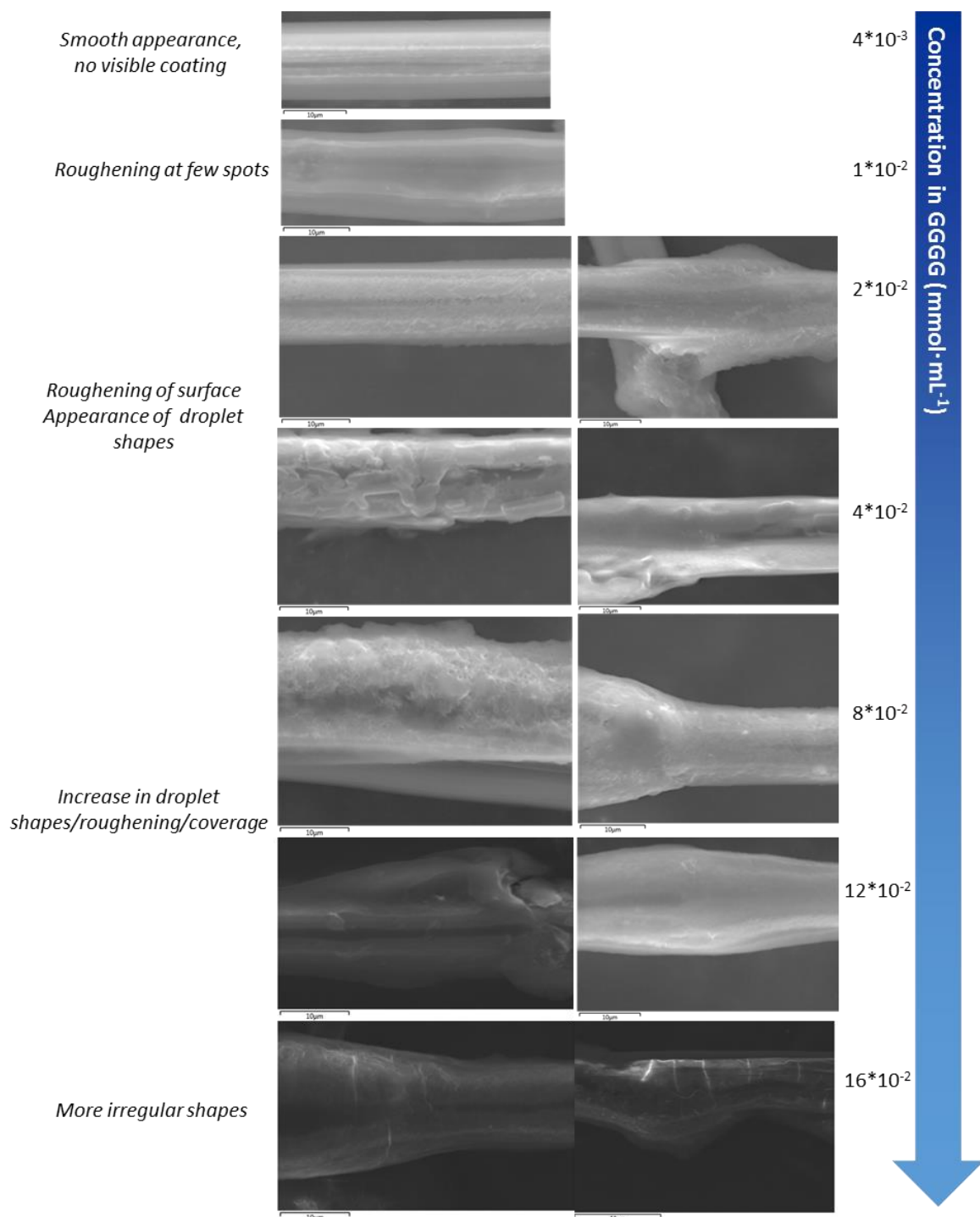


Figure III.10: Coating morphologies obtained by spray coating varying concentrations of GGGG. Length of bar scale is 10 μm for all images.

Chapter III: Evaluation of the synthesised oligomers as potential interfacial agents for Kevlar fibre-reinforced polypropylene materials

The concentration of $0.01 \text{ mmol}\cdot\text{mL}^{-1}$ was chosen as a starting point for the qualitative analysis of coating morphologies. First observations of dip and spray coating with a $0.01 \text{ mmol}\cdot\text{mL}^{-1}$ concentrated solution immediately showed strong morphological differences between the two coating methods, exemplified in **Figure III.11**. Both treated fibres showed the presence of a coating. The adsorbed quantity was much larger for dip coated fibres, leading to the formation of morphologies such as films between fibres (**Figure III.11**). As the study was concerned with fibre-compatible interactions, these morphologies (compatibilizer-compatible interactions) were an undesirable effect. To reduce their presences, final concentration was lowered to $1 \mu\text{mol}\cdot\text{mL}^{-1}$ for dip coating.

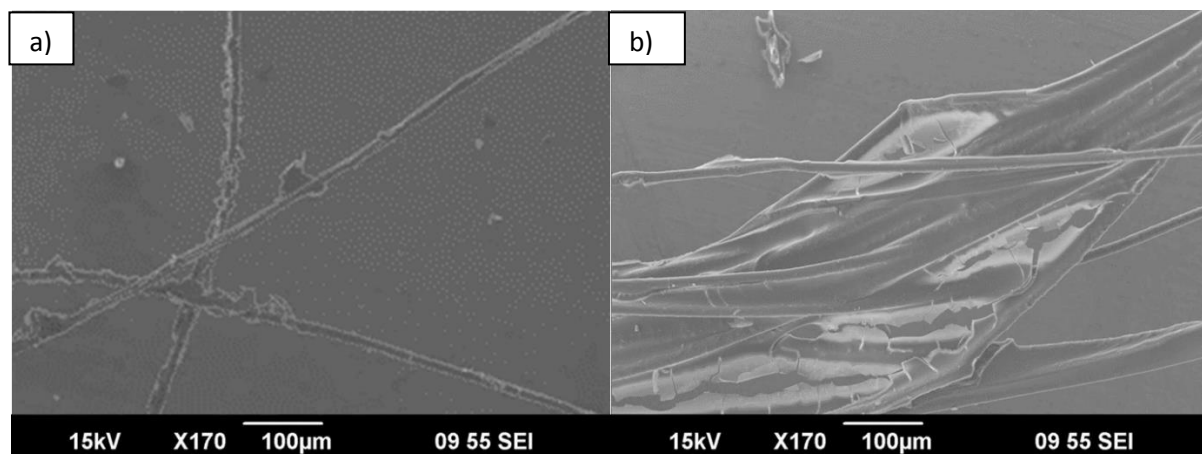


Figure III.11: Coating morphologies as observed by SEM for aramid fibres a) spray and b) dip coated using a $0.01 \text{ mmol}\cdot\text{mL}^{-1}$ solution of FhFhFhFh.

5. SEM/EDS qualitative analysis of dip and spray coating

5.1. Dip coating results

Dip coating with commercial molecules allowed for a rapid overview of the effects of altering between hydrogen bonding and π -interactions to govern adsorption. As can be seen in **Figure III.9**, the regular appearance of aramid fibre was smooth, with few loose individual filaments, but changes in morphology were discerned when the fibres were treated with $1 \mu\text{mol}\cdot\text{mL}^{-1}$ of coating solution.

5.1.1. Dip coating of commercial molecules affording the distinction between hydrogen bonding and π interactions

5.1.1.1. Tetraglycine, GGGG

As can be seen in **Figure III.12a**, most of the fibre treated with GGGG appeared as showing smooth fibre surface, however a few select spots showed aggregation (**Figure III.12b**). The aggregates themselves showed a dewetting effect in numerous locations, indicating the unpreferred interaction with the aramid surface. After dip coating, the fibre surface itself was mostly undisturbed by GGGG (**Figure III.12c**). The EDS spectrum 82 showed atomic values deviating by less than 2% compared with the values measured on untreated Kevlar fibres. On the contrary, the surface seen between the fibres on this figure, is characterized by spectrum 83 which more closely fits GGGG atomic ratios.

Chapter III: Evaluation of the synthesised oligomers as potential interfacial agents for Kevlar fibre-reinforced polypropylene materials

There was a deviation seen within the oxygen and nitrogen values. However, it could be attributed to the nonflat surface and angle effects as mentioned in Section 4.3. Considering these results, it was likely that although GGGG was adsorbed onto the fibre surface, the interactions it had with the surface are not strong enough to warrant a large coverage and consequently show a dewetting effect.

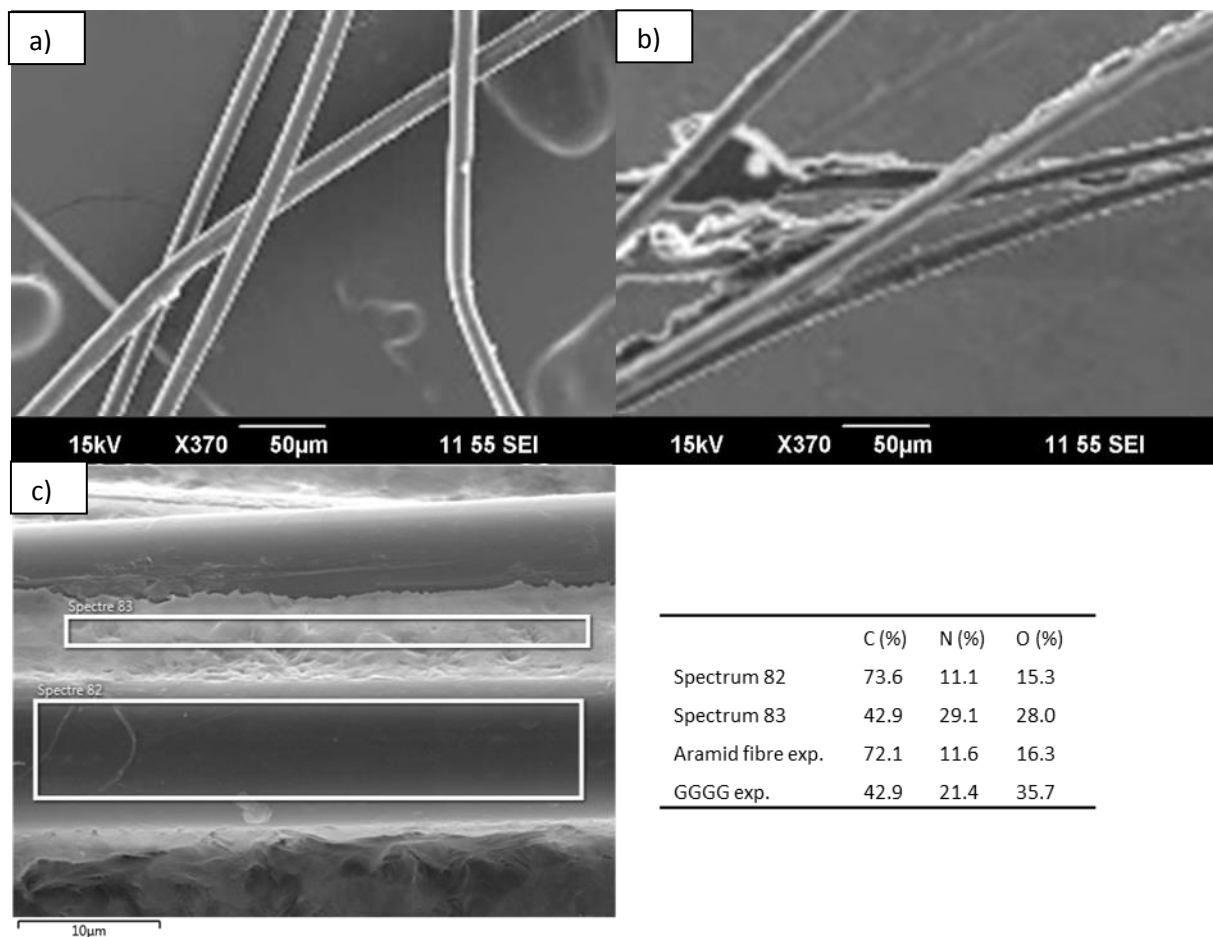


Figure III.12: Coating morphologies of aramid fibres treated with solutions of GGGG. a): Smooth appearance (concentration: $1 \mu\text{mol}\cdot\text{mL}^{-1}$) b) visible aggregates (concentration: $1 \mu\text{mol}\cdot\text{mL}^{-1}$), c) close up on aggregate shapes, showing dewetting effect (concentration: $0.01 \text{ mmol}\cdot\text{mL}^{-1}$) and relevant EDS results.

5.1.1.2. Polystyrene

Owing to the low solubility in TFA/ACN, toluene was used exceptionally as a solvent for dip coating experiments using polystyrene. The polystyrene treated fibres similarly showed the presence of coating (**Figure III.13**). However, by comparing morphology between polystyrene and GGGG treated fibres, differences were observed: an increased coverage of the aramid fibre with polystyrene; a decreased formation of polystyrene aggregates. Local dewetting of the polystyrene layer shows the aramid neat fibre, the chemical natures of those two regions being confirmed by EDS (spectra 37 and 38), with spectrum 37 deviating less than 3% from the experimental values of the untreated aramid fibre while spectrum 38 showed a large increase in atom% of carbon and decrease in both nitrogen and oxygen values, corresponding to an increased presence of polystyrene.

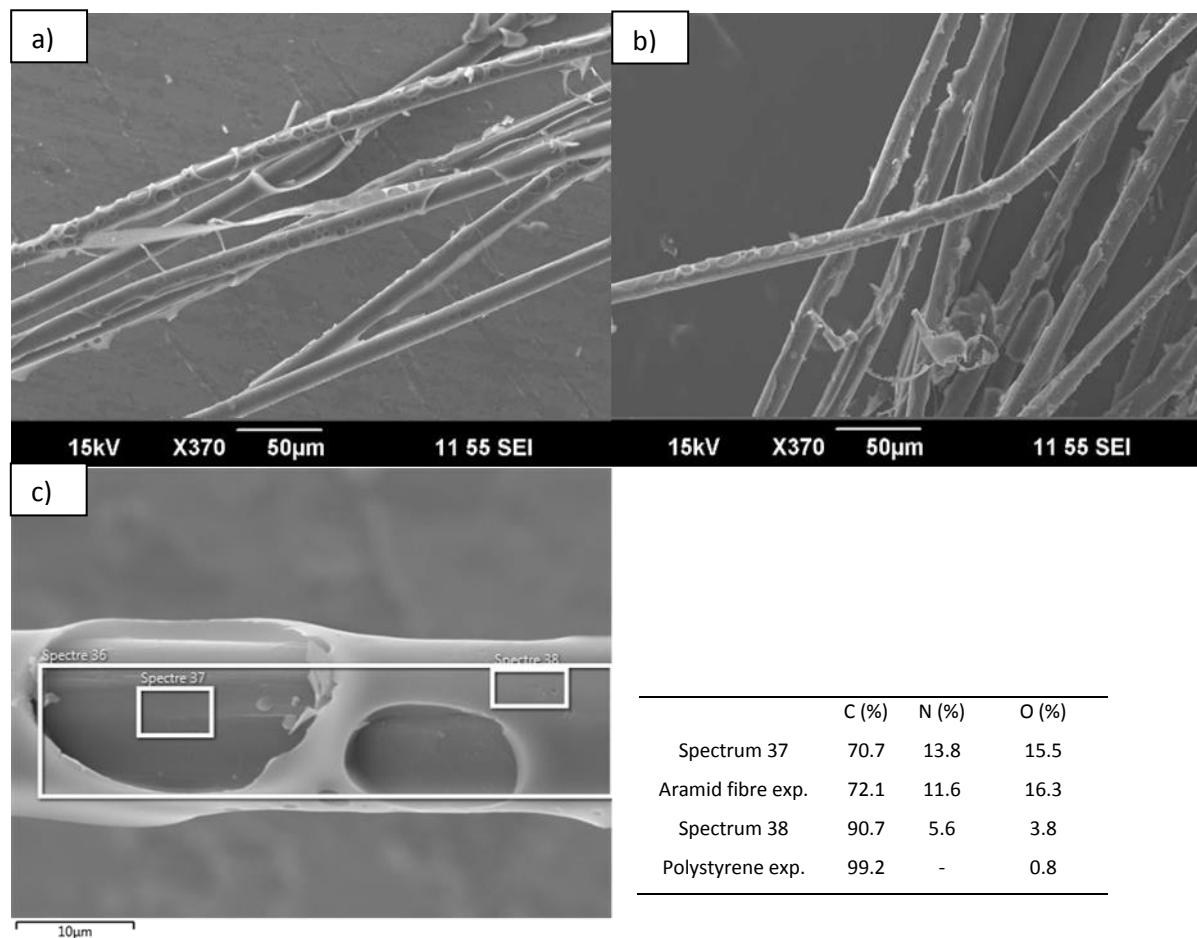


Figure III.13: Coating morphologies of aramid fibres treated with a $1 \mu\text{mol}\cdot\text{mL}^{-1}$ solution of polystyrene. a), and b) overall appearance, c) close up showing partial dewetting effect and relevant EDS results.

5.1.1.3. Tetraphenylalanine, FFFF

The amount of covered surface was increased when FFFF was used as a coating (**Figure III.14**), with regular roughening of the fibre surface and full coverage of the fibre itself. Similarly, to the results obtained with GGGG, few spots of the FFFF treated aramid fibres showed the presence of aggregates on the fibre surface.

Chapter III: Evaluation of the synthesised oligomers as potential interfacial agents for Kevlar fibre-reinforced polypropylene materials

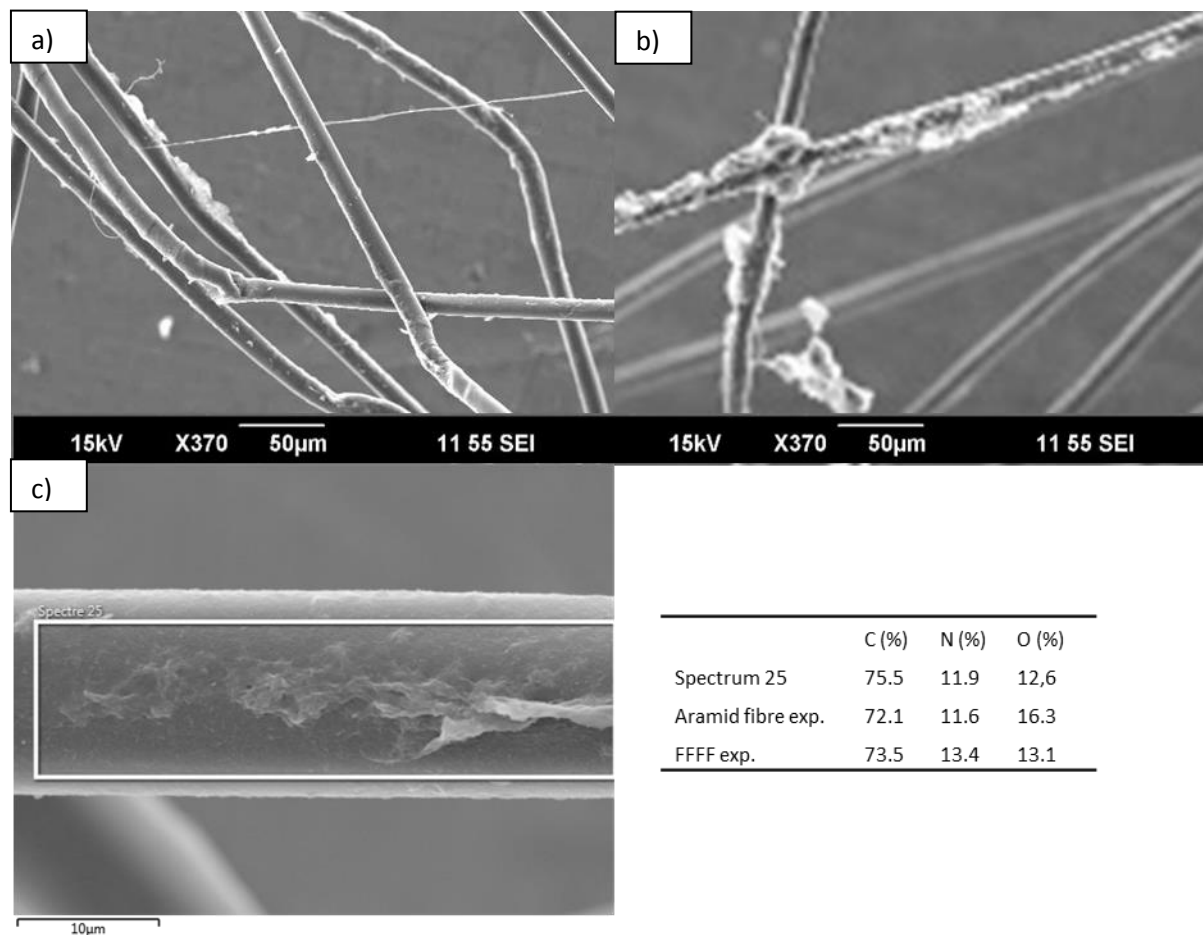


Figure III.14: Coating morphologies of aramid fibres treated with solutions of FFFF. a): Overall appearance, b) visible aggregates (concentration: $1 \mu\text{mol}\cdot\text{mL}^{-1}$), c) close up on aggregate shapes, showing dewetting effect (concentration: $0.01 \text{ mmol}\cdot\text{mL}^{-1}$) and relevant EDS results.

5.1.1.4. Summary

Three model molecules were investigated for their adsorption morphologies onto aramid fibre using either only π (polystyrene) or hydrogen bonding (GGGG) or both interactions (FFFF) as the main driving factor for adsorption. Key differences were found regarding wetting behaviour, surface roughness and the formation of aggregate forms, which are summarised below (**Figure III.15**).

Chapter III: Evaluation of the synthesised oligomers as potential interfacial agents for Kevlar fibre-reinforced polypropylene materials

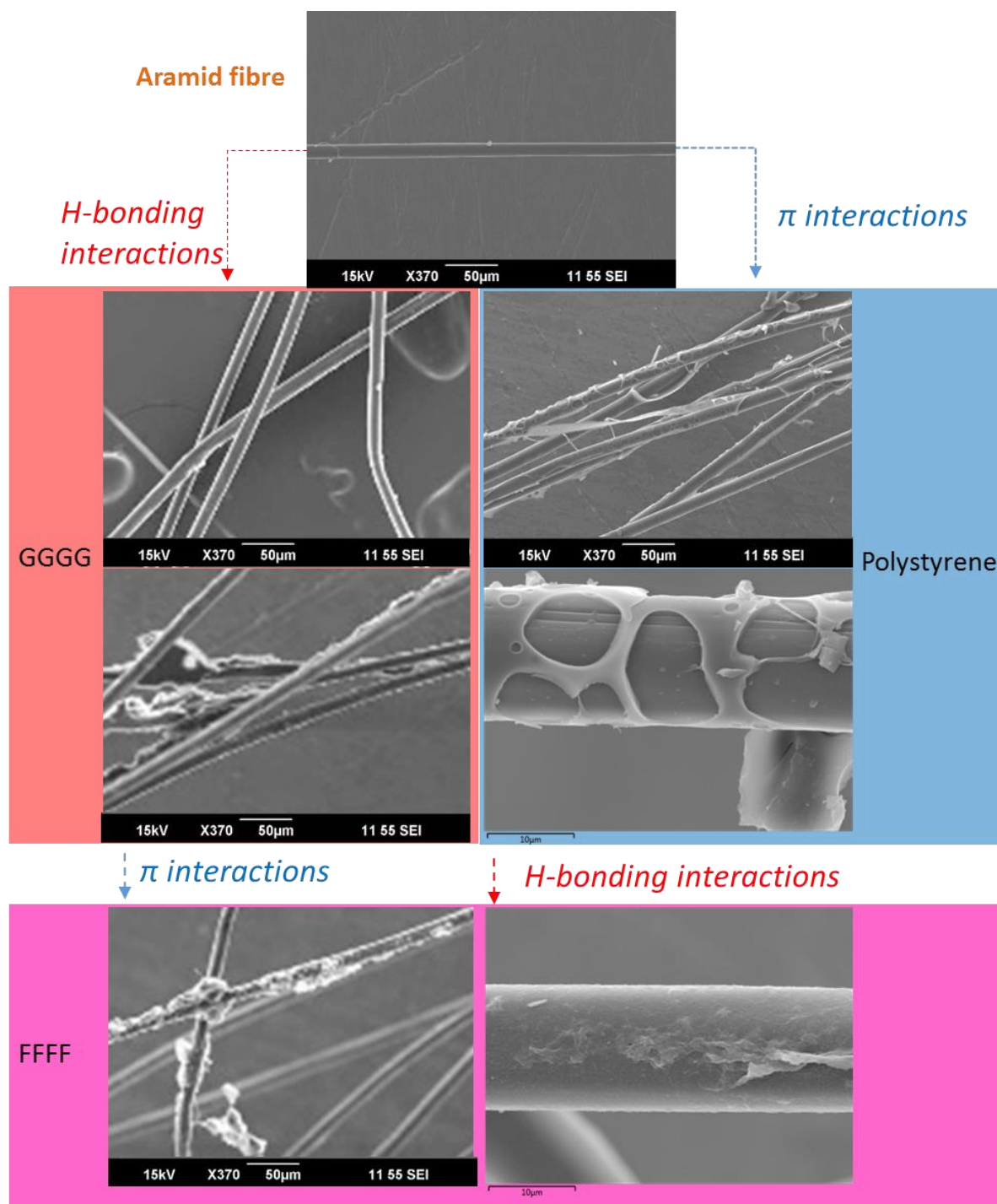


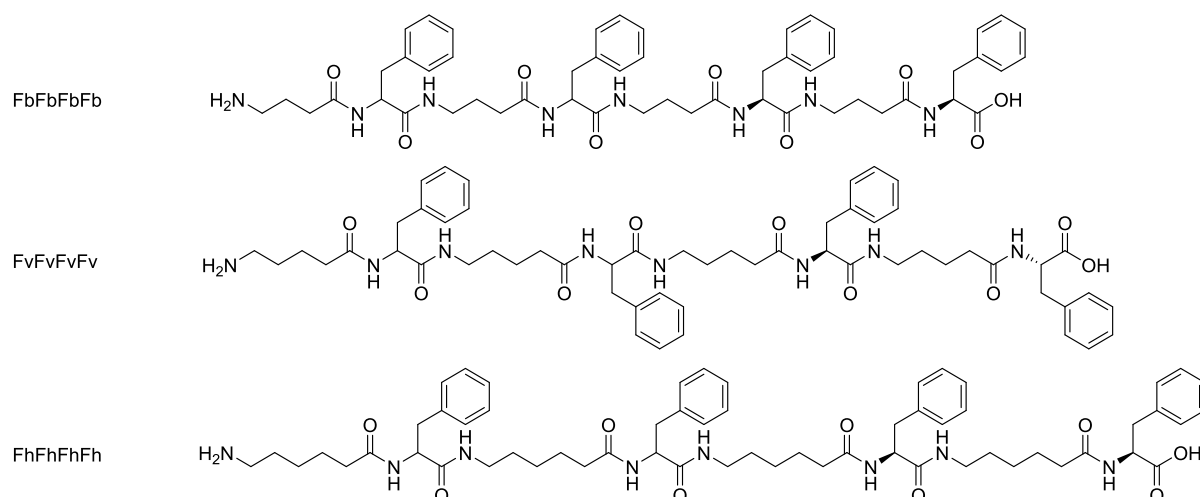
Figure III.15: Overview of coating morphologies seen for aramid fibres dip coated with $1 \mu\text{mol}\cdot\text{mL}^{-1}$ of polystyrene, GGGG and FFFF.

5.1.2. Dip coating of oligomers with single phenylalanine unit per block

As discussed in Section 1, the orientational behaviour of the interactive units per molecule on a surface can potentially be governed by spacing units in the form of aliphatic chains. In this section, three molecules with variable spacing between single phenylalanine residues (FbFbFbFb, FvFvFvFv and FhFhFhFh) will be discussed regarding their dip coating morphologies. Lastly, one of the synthesised oligomers will be considered for the effect of the triazole unit (Fh●Fh●Fh●Fh). Although the amount

Chapter III: Evaluation of the synthesised oligomers as potential interfacial agents for Kevlar fibre-reinforced polypropylene materials

of phenylalanine units remained the same, the quantity and roughness of coating on the fibres increased with respect to FFFF-coated fibres (**Figure III.16**). The coating surface showed differences in micro scale roughness, with FbFbFbFb and FhFhFhFh appearing smoother than FvFvFvFv. This difference may be caused by symmetry of the phenylalanine residues in respect to each other. With an even amount of atoms added by the spacing unit (butyric or hexanoic spacing) the phenylalanine residues were expected to orient in the same direction. However, when an uneven amount of atoms was added by the spacing, the orientation of the phenylalanine residues was expected to be alternating (**Scheme III.1**).



Scheme III.1: Molecular structures of FbFbFbFb, FvFvFvFv and FhFhFhFh.

Synthesised oligomer Fh●Fh●Fh●Fh appeared different from the commercial products and showed presence of both droplet shapes and films between fibres as well as a decreased surface roughness in comparison to FhFhFhFh. Droplet shapes showed a significant increase in coating thickness where an increase of two to three times the original fibre diameter was commonly observed. The inclusion of the triazole moiety may therefore be responsible for introducing additional flexibility for the molecule to orient itself on the surface of the aramid fibre, on top of the spacing units.

Chapter III: Evaluation of the synthesised oligomers as potential interfacial agents for Kevlar fibre-reinforced polypropylene materials

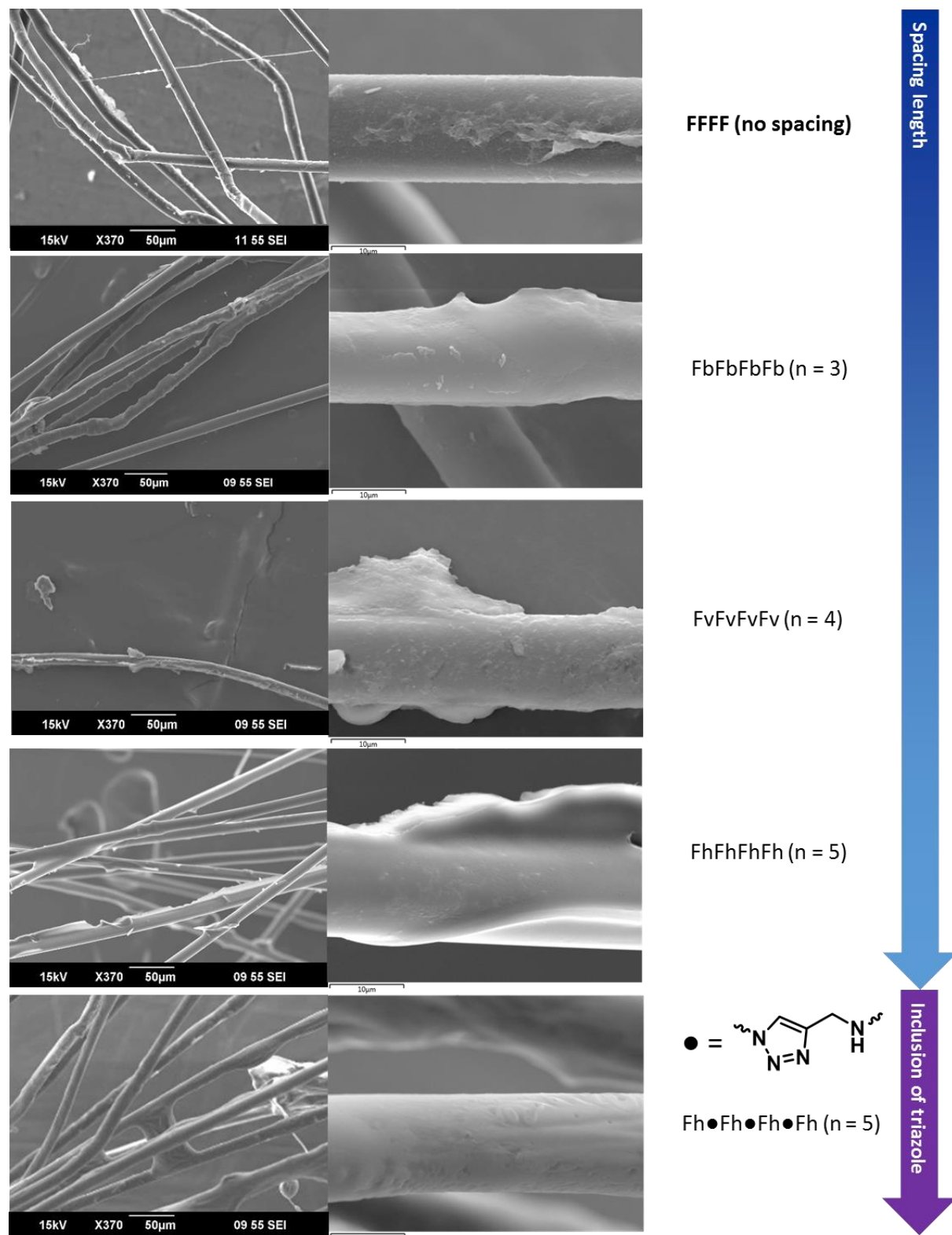


Figure III.16: Overview of coating morphologies seen for aramid fibres dip coated with $1 \mu\text{mol}\cdot\text{mL}^{-1}$ of FbFbFbFb, FvFvFvFv, FhFhFhFh and Fh●Fh●Fh●Fh. n denotes the amount of carbon atoms present between the carbonyl and amide parts of the spacing.

Chapter III: Evaluation of the synthesised oligomers as potential interfacial agents for Kevlar fibre-reinforced polypropylene materials

5.1.3. Dip coating of oligomers with four phenylalanine units per block

When increasing the amount of phenylalanine residues in the oligomer, the amount of interactive units increased and may give rise to additional adhesion. Here, synthesised oligomers are discussed with four variable spacings between four phenylalanine residues. As can be seen from **Figure III.17**, the coating morphologies changed once more in regards to the commercial peptide products. In any case an increased surface coverage was obtained and the micro-roughness of the surface showed unique differences with FFFFb●FFFFb●FFFFb●FFFFb and FFFFh●FFFFh●FFFFh●FFFFh having a smoother appearance than FFFFv●FFFFv●FFFFv●FFFFv and FFFFu●FFFFu●FFFFu●FFFFu. As can be seen, large differences in the morphologies of equimolar coatings of different molecules were observed. The roughness differences of Section 5.1.2., possibly in regards to the even or uneven spacing seem increased. Cracked films are notable visible for FFFFv●FFFFv●FFFFv●FFFFv, which also contains the most aggregation.

Chapter III: Evaluation of the synthesised oligomers as potential interfacial agents for Kevlar fibre-reinforced polypropylene materials

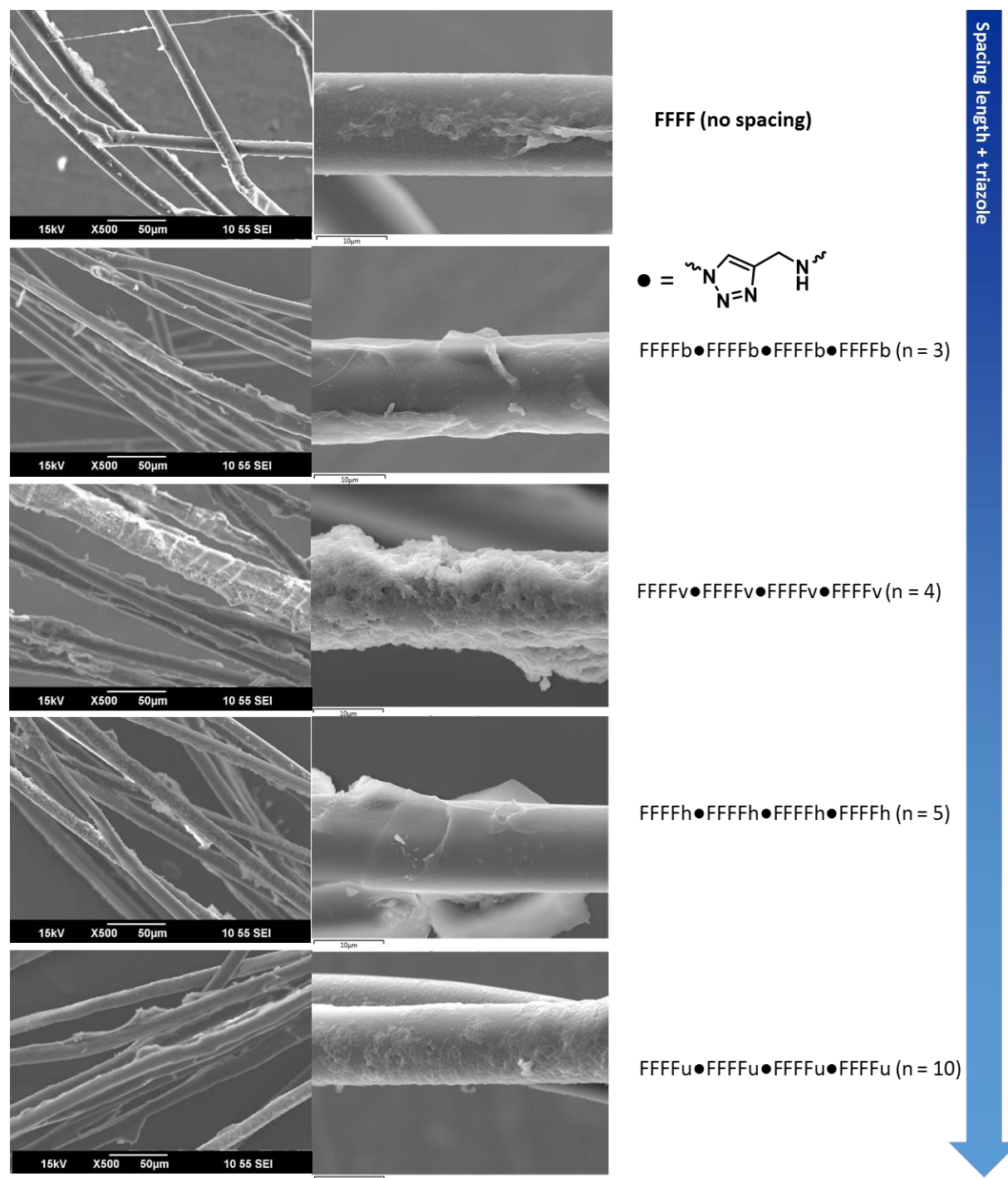


Figure III.17: Coating morphologies for aramid fibres dip coated with $1 \mu\text{mol}\cdot\text{mL}^{-1}$ of FFFFb•FFFFb•FFFFb•FFFFb, FFFFv•FFFFv•FFFFv•FFFFv, FFFFh•FFFFh•FFFFh•FFFFh and FFFFu•FFFFu•FFFFu•FFFFu. n denotes the amount of carbon atoms present between the carbonyl and amide parts of the spacing.

5.2. Spray coating

Like dip coating, spray coating also allowed for a rapid overview of the effects of altering between hydrogen bonding and π -interactions to govern adsorption. Similar effects as with dip coating were observed, which will be discussed below. Due to the disposable spray head consisting of HDPE, toluene was not able to be used as a solvent, as it would cause degradation and possible contamination. As a result, spray coating of polystyrene was not possible. Similarly, owing to the necessity of a higher

Chapter III: Evaluation of the synthesised oligomers as potential interfacial agents for Kevlar fibre-reinforced polypropylene materials

concentration ($0.01 \text{ mmol}\cdot\text{mL}^{-1}$) and the scarcity of FFFFu●FFFFu●FFFFu●FFFFu, it was not possible to spray coat this.

5.2.1. Spray coating of commercial molecules

5.2.1.1. Tetraglycine, GGGG

Spray coating of GGGG showed analogous results to Section 5.1.1.1, with most fibres showing no visible or small amounts of coating while a few spots showed presence of aggregates.

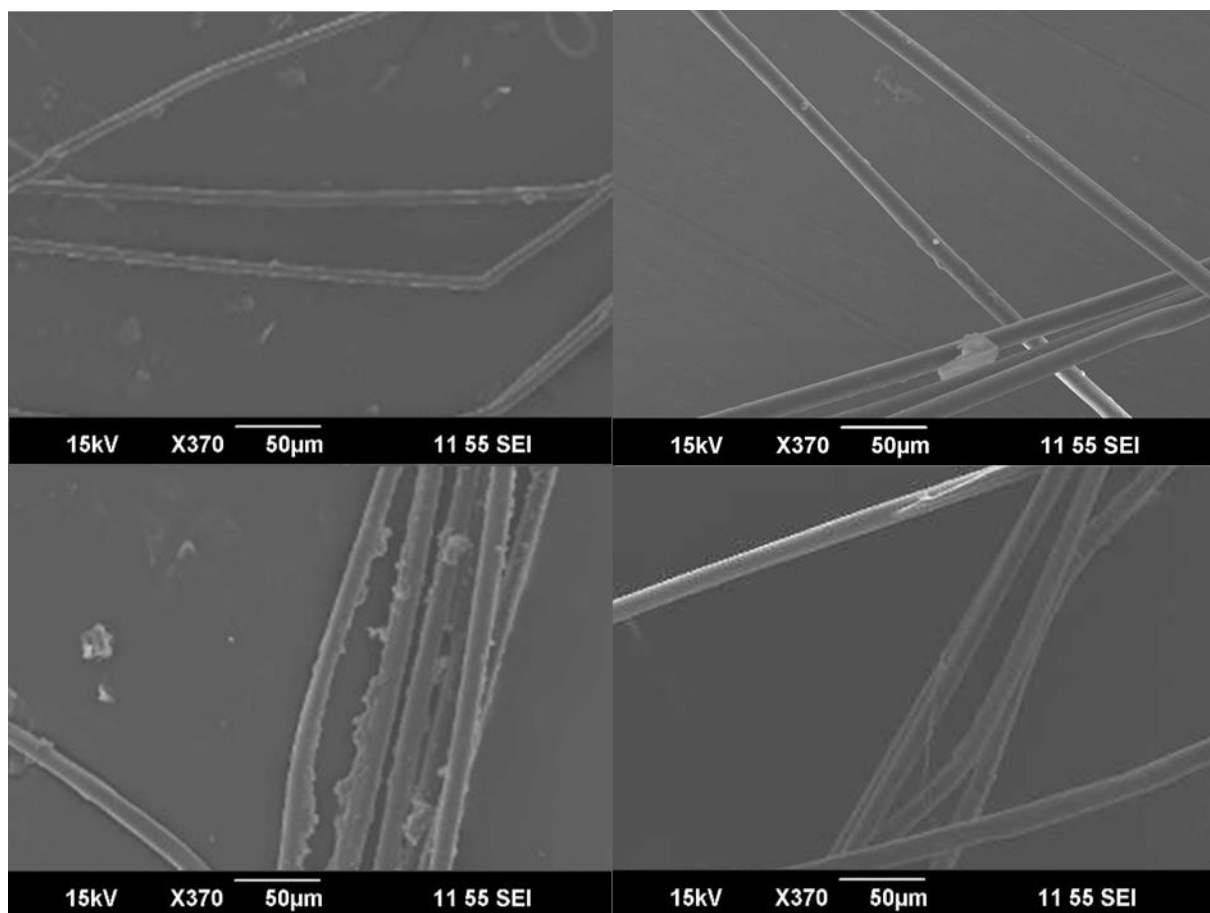


Figure III.18: Coating morphologies of aramid fibres treated with a $0.01 \text{ mmol}\cdot\text{mL}^{-1}$ solution of GGGG.

5.2.1.2. Tetraphenylalanine, FFFF

Aramid fibres treated with FFFF spray coating showed an increase in surface roughness and overall presence of coating with a few aggregate shapes relative to the GGGG treated aramid fibres, similar to the results discussed in Section 5.1.1.3.

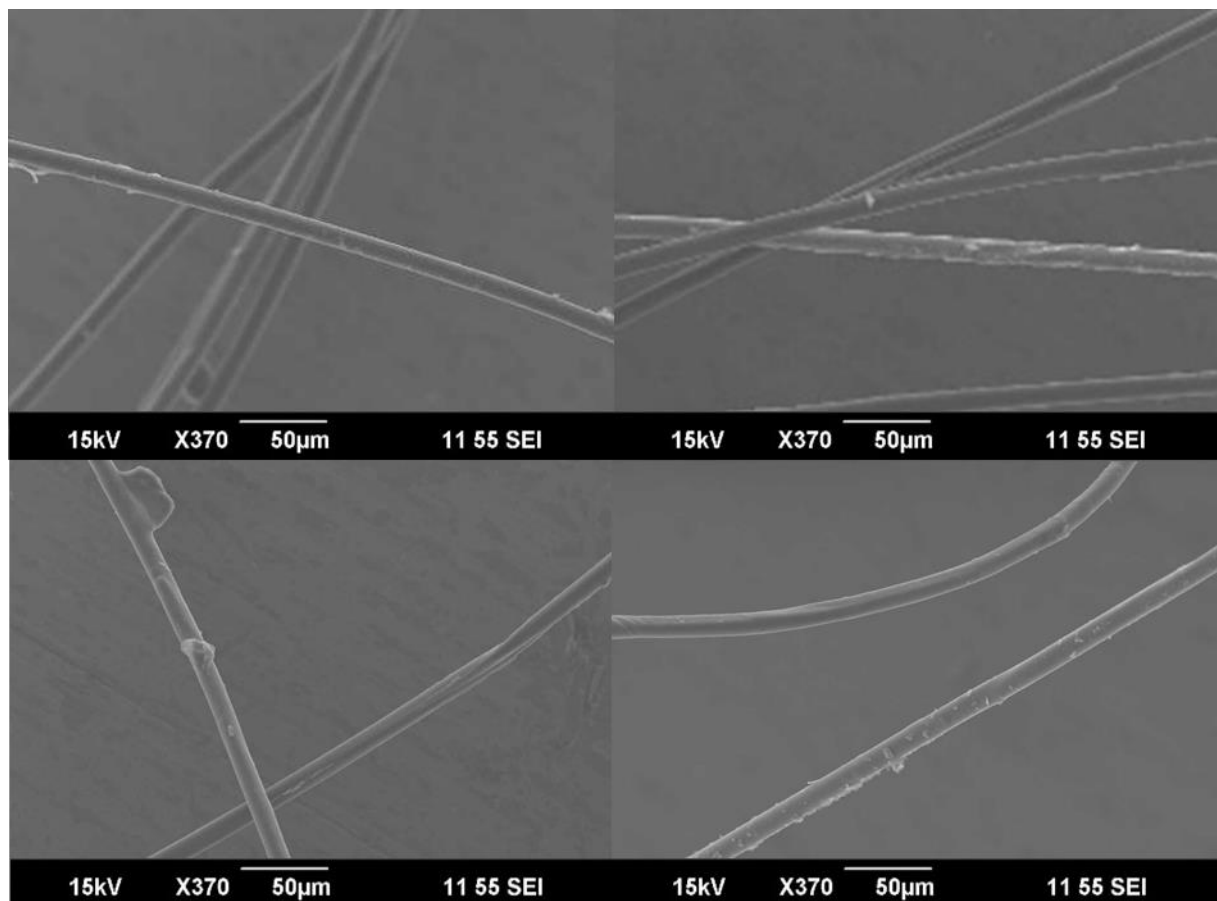


Figure III.19: Coating morphologies of aramid fibres treated with a $0.01 \text{ mmol}\cdot\text{mL}^{-1}$ solution of FFFF.

5.2.1.3. Summary

Two model molecules were investigated for their adsorption morphologies onto aramid fibre using either only hydrogen bonding (GGGG) or hydrogen bonding and π -interactions (FFFF) as the main driving factor for adsorption. Similar differences in coatings were visible as for dip coating with GGGG coatings sparsely visible aside from a few aggregates, showing a clear dewetting effect and FFFF showing an increased coverage.

Chapter III: Evaluation of the synthesised oligomers as potential interfacial agents for Kevlar fibre-reinforced polypropylene materials

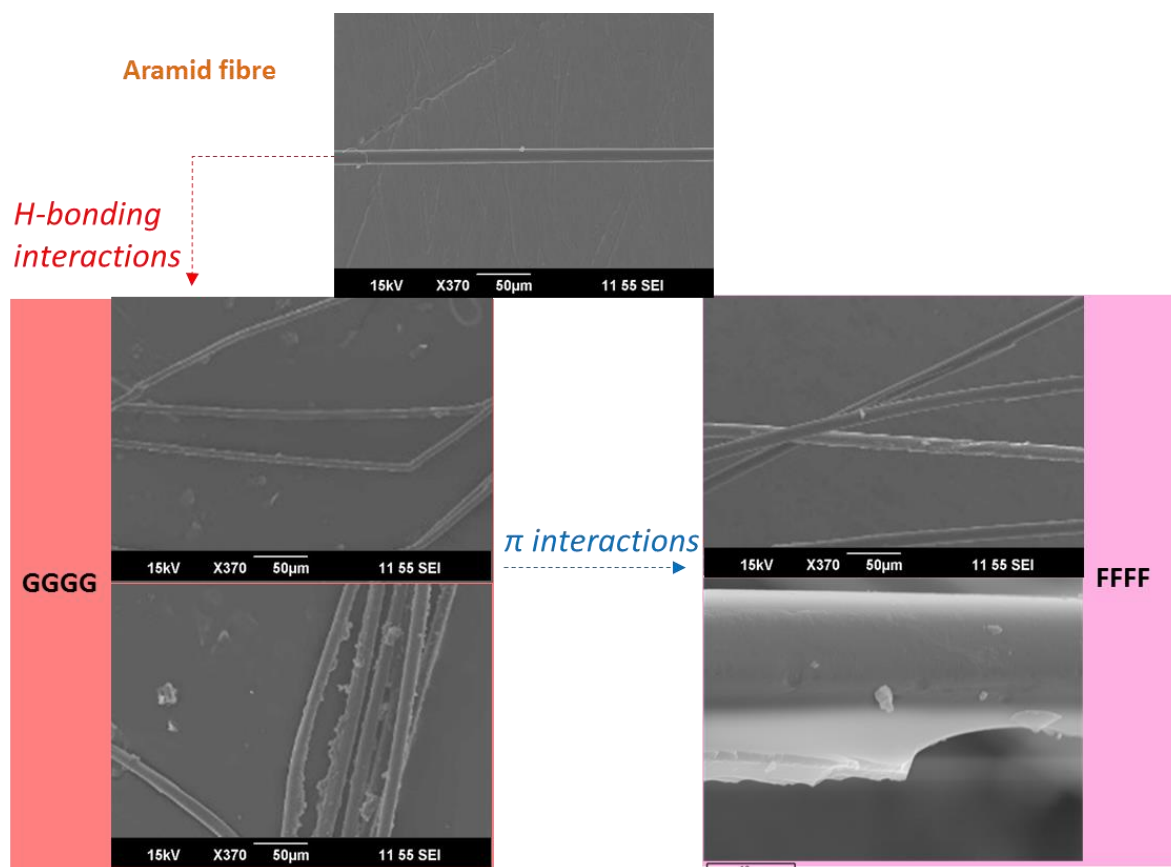


Figure III.20: Coating morphologies for aramid fibres spray coated with GGGG and FFFF at $0.01 \text{ mmol}\cdot\text{mL}^{-1}$.

5.2.2. Spray coating of oligomers with a single phenylalanine unit per block

Analogous coating behaviour to the dip coating treatments was also found with the commercial peptidic products (Section 5.1.2). In all cases a near uniform coating was obtained with various degrees of roughness. However, differences between surface roughness were changed, with FbFbFbFb and FhFhFhFh showing a relatively rougher surface than FvFvFvFv. However, FvFvFvFv also showed distinctive droplet shapes with unique 'folding behaviour'. These differences may again be related to the even/uneven effect as illustrated in **Scheme III.1**, where the ability for coating containing microdroplets to disperse along the surface after initial contact is affected in some way by the spacing.

Chapter III: Evaluation of the synthesised oligomers as potential interfacial agents for Kevlar fibre-reinforced polypropylene materials

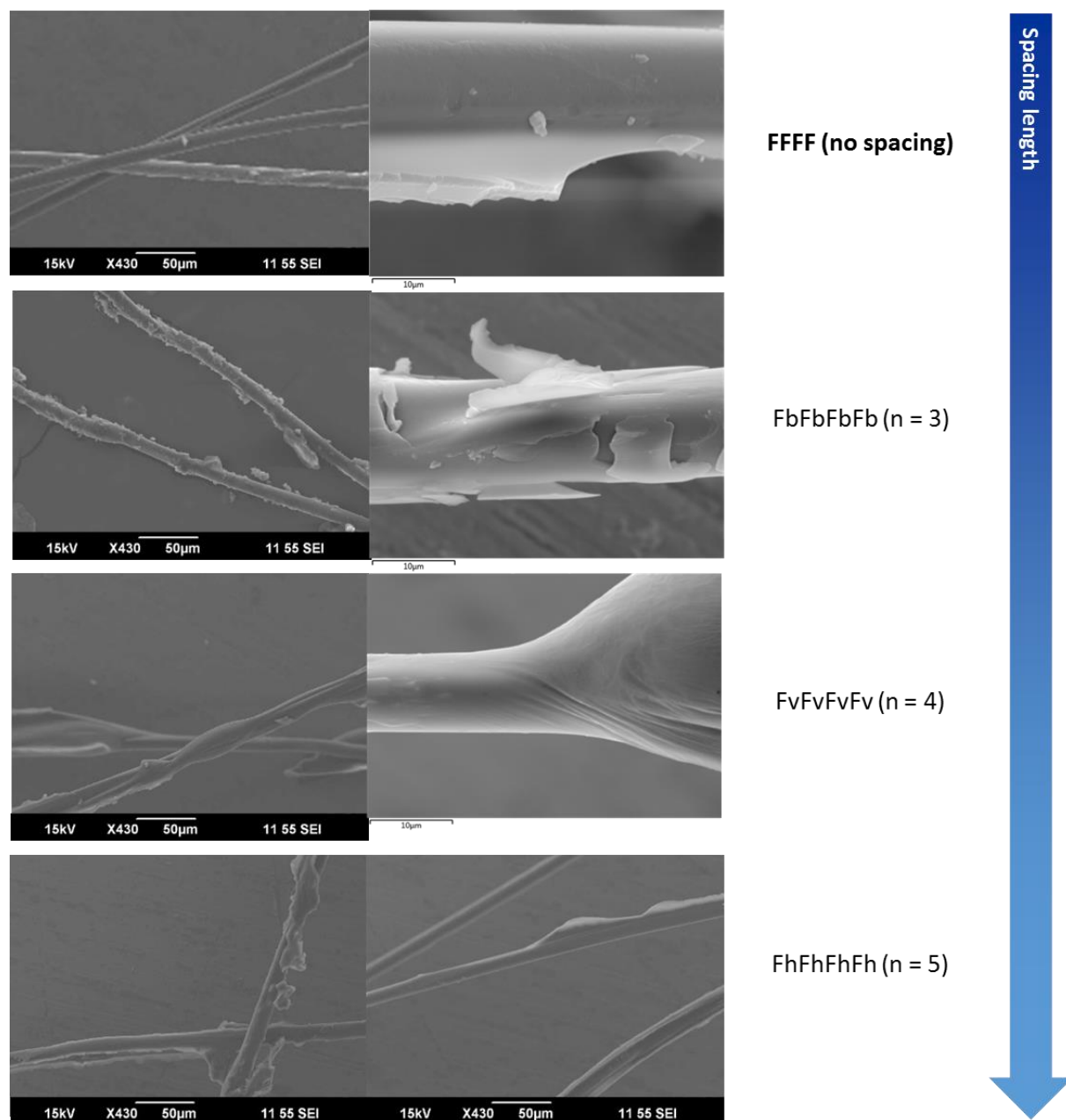


Figure III.21: Overview of coating morphologies seen for aramid fibres spray coated with $0.01 \text{ mmol} \cdot \text{mL}^{-1}$ of FbFbFbFb, FvFvFvFv and FhFhFhFh. n denotes the amount of carbon atoms present between the carbonyl and amide parts of the spacing.

5.2.3. Spray coating of oligomers with four phenylalanine units per block

Similarity was once again observed with the dip coating treatment of oligomers containing four phenylalanine residues (Section 5.1.3). The surface roughness was again decreased although showing full coverage. However, the shapes of aggregations were changed compared to coating on the fibres treated by dip coating. While FFFFb•FFFFb•FFFFb•FFFFb showed larger aggregates, FFFFv•FFFFv•FFFFv•FFFFv mostly showed aggregates in the form of droplets shapes and FFFFh•FFFFh•FFFFh•FFFFh and FFFFu•FFFFu•FFFFu•FFFFu showed a large decrease in aggregate shapes.

Chapter III: Evaluation of the synthesised oligomers as potential interfacial agents for Kevlar fibre-reinforced polypropylene materials

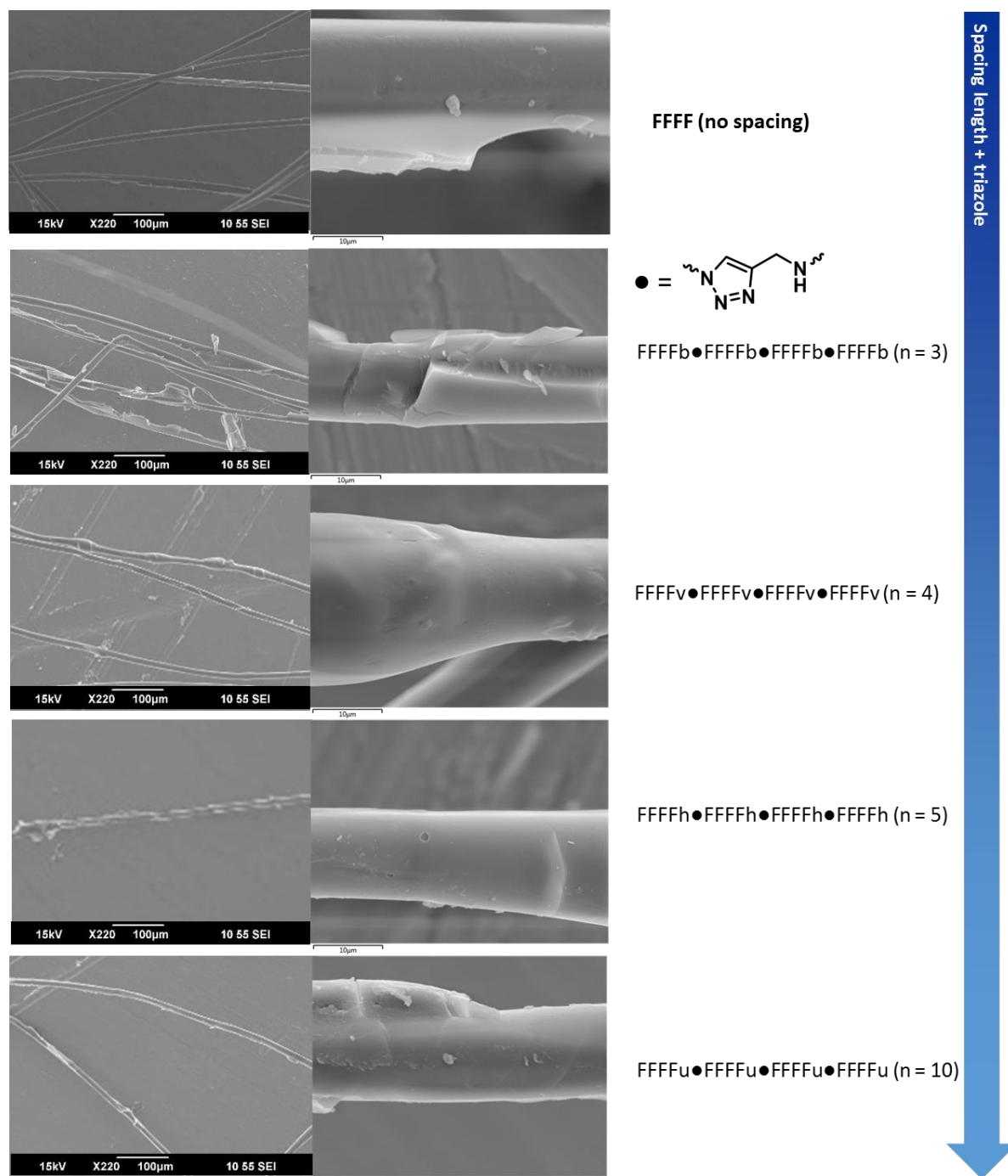


Figure III.22: Coating morphologies for aramid fibres spray coated with $0.01 \text{ mmol}\cdot\text{mL}^{-1}$ of FFFFb●FFFFb●FFFFb●FFFFb, FFFFv●FFFFv●FFFFv●FFFFv, FFFFh●FFFFh●FFFFh●FFFFh and FFFFu●FFFFu●FFFFu●FFFFu. n denotes the amount of carbon atoms present between the carbonyl and amide parts of the spacing.

5.3. EDS analysis of fibre surface

EDS was used to confirm the identity of the coatings observed by SEM topography. As mentioned in Section 4, relative comparisons were made due to the semi-quantitative nature of EDS and observed differences with theoretical values. It was therefore necessary to take blank measurements of both the fibres and the applied coatings. Owing to the precautions listed in Sections 4.2 and 4.3, the coatings in powder form were first compressed into a solid shape using hydraulic press. This prevented

Chapter III: Evaluation of the synthesised oligomers as potential interfacial agents for Kevlar fibre-reinforced polypropylene materials

movement of individual powder particles under the influence of the electron beam. The EDS analysis of the untreated aramid fibres, compressed solid coating molecules (compounds) and finally treated fibres are given as average measured values. Full analysis can be found in Appendix B.

5.3.1. Untreated aramid fibre

For the aramid fibre reference measurements, two sets of nine measurements were taken, one for EDS probe AZTEC and the second for EDS probe X-MAX (upgrade of the instrument during the thesis). The comparison of the measured atomic composition of untreated aramid fibres is given in **Table III.5**. The absolute difference $|\Delta\alpha_i|$ between the experimental and theoretical atomic composition values may be described by using the absolute total difference of each atom considered (C, N and O):

$$|\Delta\alpha_i| = |\Delta\alpha_{i,C}| + |\Delta\alpha_{i,N}| + |\Delta\alpha_{i,O}|$$

Going by this value, the accuracy of the X-MAX probe was increased in respect to the AZTEC probe, which may be attributed to an increase in resolution. Depending on which probe was used for the coated fibres, either of the results in the table has been chosen as a reference point. Despite these differences, the standard deviations were increased for the X-MAX probe for both carbon and nitrogen, while a decrease was seen for oxygen. For both probes, the differences with the calculated values were higher for oxygen and carbon than nitrogen.

Table III.5: Atomic composition of untreated aramid fibres given by EDS analysis over nine measurements

	Probe	%C	%N	%O	%C/%N	%C/%O
Calculated	N/A	77.77	11.11	11.11	7.00	7.00
Composition	AZTEC	69.31	12.67	18.03	5.47	3.84
Standard deviation	AZTEC	1.72	1.17	0.95	0.67	0.26
$\Delta\alpha$	AZTEC	-8.47	1.56	6.92	-1.53	-3.16
Composition	X-MAX	72.12	11.58	16.31	6.23	4.42
Standard deviation	X-MAX	1.94	1.41	0.62	1.00	0.27
$\Delta\alpha$	X-MAX	-5.66	0.47	5.20	-0.77	-2.58

$$|\Delta\alpha_{\text{AZTEC}}| = 16.95 \quad |\Delta\alpha_{\text{X-MAX}}| = 11.33$$

5.3.2. Coating molecule compounds

Due to time constraints, coating molecule compounds were only analysed using the AZTEC probe. The differences observed with the calculated values were once again observable, with 0.80 to ca. 8% of difference depending on the atom measured and the sample. Given below in **Table III.6** is an overview of the total absolute atomic difference with the calculated composition values of each of the molecules ($|\Delta\alpha|$), which should be an indication of how much reflective the experimental data is of the true value.

Chapter III: Evaluation of the synthesised oligomers as potential interfacial agents for Kevlar fibre-reinforced polypropylene materials

Table III.6: Overview of absolute differences in atomic composition of coating molecule compounds with theoretical values

Molecule	$ \Delta\alpha $
Polystyrene	1.60
GGGG	12.59
FFFF	12.88
FbFbFbFb	14.07
FvFvFvFv	18.43
FhFhFhFh	20.72
Fh●Fh●Fh●Fh	13.13
FFFFb●FFFFb●FFFFb●FFFFb	10.22
FFFFv●FFFFv●FFFFv●FFFFv	8.49
FFFFh●FFFFh●FFFFh●FFFFh	10.03
FFFFu●FFFFu●FFFFu●FFFFu	10.30

5.3.3. Treated fibres

In order to evaluate the treated fibres, fifteen spots were taken for analysis of each. Then the average value of C, O and N atom% was compared individually with both untreated aramid fibre and the relevant coating molecule compound. By adding up the absolute differences, a single value was obtained which expresses the similarity in atomic composition ($|\Delta A|$), where the lower value denotes a more similar composition. It is now possible to review whether in the volume measured by the EDS there was more or less presence of coating. By comparing whether the absolute difference between the treated fibre and coating compound ($|\Delta A_{\text{compound}}|$) or the absolute difference between the treated fibre and untreated fibre ($|\Delta A_{\text{aramid}}|$) was smaller, presence may be confirmed using EDS. As can be seen in **Table III.7**, despite visual presence indicated in Section 5, several of the treated fibres showed an EDS composition more similar to the untreated aramid fibres than the coating molecule compounds. Owing to the dewetting effect and selection of the spots, the EDS composition may not be a fully accurate indication of the presence of coating.

Chapter III: Evaluation of the synthesised oligomers as potential interfacial agents for Kevlar fibre-reinforced polypropylene materials

Table III.7: Relative total atomic composition differences with both the untreated aramid fibre and the coating compound for treated fibres

Molecule	Dip coated		$ \Delta A_{\text{compound}} < \Delta A_{\text{aramid}} $	Spray coated		$ \Delta A_{\text{compound}} < \Delta A_{\text{aramid}} $
	$ \Delta A_{\text{aramid}} $	$ \Delta A_{\text{compound}} $		$ \Delta A_{\text{aramid}} $	$ \Delta A_{\text{compound}} $	
Polystyrene	21.21	18.51	Y	-	-	-
GGGG	6.24	52.21	N	6.44	54.28	N
FFFF	5.16	3.84	Y	3.20	5.62	N
FbFbFbFb	1.78	8.53	N	4.01	7.10	N
FvFvFvFv	1.42	10.93	N	4.82	9.41	N
FhFhFhFh	1.80	10.69	N	5.44	12.90	N
Fh●Fh●Fh●Fh	1.98	19.62	N	-	-	-
FFFFb●FFFFb●FFFFb●FFFFb	5.51	5.52	N	6.53	1.22	Y
FFFFv●FFFFv●FFFFv●FFFFv	8.58	3.18	Y	6.34	3.78	Y
FFFFh●FFFFh●FFFFh●FFFFh	6.05	2.73	Y	13.56	5.46	Y
FFFFu●FFFFu●FFFFu●FFFFu	6.59	1.15	Y	10.35	0.65	Y

5.4. Conclusion

Various non-covalent coatings for aramid fibres were analysed for morphology using SEM/EDS. Notable morphological differences between coatings were able to be pinpointed, including coverage, surface roughness and appearance of certain shapes, showing similarity between the two coating methods used (dip and spray coating). EDS analysis showed instances of characteristic differences between the untreated and treated fibres, based on relative comparisons. Unfortunately, the morphological differences and selection of spots may make the technique difficult to use as a supplement to SEM topography.

Considering these results, coating morphology may be influenced by the properties of the molecules, notable the presence of the spacing unit and the even or uneven nature of the amount of carbon atoms as well as the nature of the interactive subunit (G vs F).

6. Preliminary quantification of coatings

Although the qualitative results of Section 5 gave an indication that the ability of the coatings to perform adsorption may be governed by their molecular structure, the section by itself it only provided visual results. In order to have concrete data on the amount adsorbed, quantitative measurements are necessary. Several approaches to quantify the coating behaviour are described below: spectroscopic quantification using EDS (Section 6.1), quantification using weight differences of fibre bundles (Section 6.2), and quantification using UV-Vis absorption (Section 6.3).

6.1. Quantification by EDS

From EDS experiments, the difference between average experimental oxygen values of the aramid fibres and GGGG was the largest ($\%O_{GGGG} = 35.73, \%O_{aramid} = 18.03$) and thusly a significant contrast of GGGG and aramid regions was found ($|\Delta A_{compound,O}| - |\Delta A_{aramid,O}|$). For this reason, initial quantification trials were performed using EDS characterisations of fibres spray coated with different concentrations GGGG and compared to solid GGGG compound and untreated aramid fibre EDS results which are given in Section 5.3. Averages were again calculated from fifteen spots (**Figure III.23**). Although a linear trend was observed, there was a significant increase in standard deviations, making the trend line unreliable. An explanation for this was found in the broad morphology differences as described in Section 4.3., where more dissimilar shapes and aggregations were found for increasing concentrations. These aggregates could directly influence the ability to properly generate X-rays (Section 4.3). Owing to this effect and manual selection of sample areas, the technique was not suitable for precise quantification.

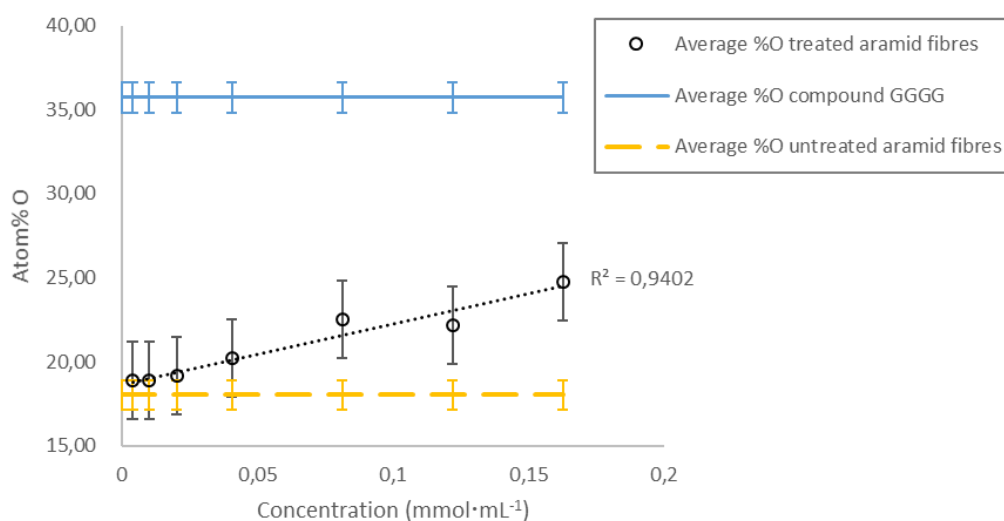


Figure III.23: EDS analysis of oxygen atom% of coated fibre surfaces compared to untreated aramid fibre and GGGG compound.

6.2. Quantification by gravimetry using fibre bundles

Although spectroscopy can potentially be a precise and reliable technique to obtain information about the quantification of coatings, another method is by differentiating mass before and after coating. For this purpose, a vibration- and temperature-stabilised analytical balance was used. Unfortunately, the aramid fibres were not homogenous in shape, but rather delivered as a distribution with diameters between 10 and 15 μm and maximum lengths of 5 cm due to the manufacturing process. The measurement of the initial fibre weight was first detailed (**Table III.8**) considering one fibre as one of the full 5 cm (if the fibre used was half that size it will be considered as 0.5 fibre).

Chapter III: Evaluation of the synthesised oligomers as potential interfacial agents for Kevlar fibre-reinforced polypropylene materials

A simple average measurement of the coating adsorbed on the fibres was proposed thanks to weight increase of the aramid fibres.

Table III.8: Mass measurements of bundles of three SFA A fibres (expected instrumental standard deviation of $\pm 1 \mu\text{g}$)

Sample	m (mg)
1	0.030
2	0.030
3	0.024
4	0.030
5	0.026
6	0.027
7	0.019
8	0.018
Average on three fibres	0.026
Average on one fibre	0.009

Polystyrene was used as model molecule owing to its abundance. First attempts at quantification of the mass present on the fibres using the dip coating procedure described in Section 3.1 was done using fibre bundles of a few fibres. The results are given in **Table III.9**, where $m_{\text{polystyrene}}$ and $C_{\text{Polystyrene}}$ denote respectively the mass of polystyrene weighted for and concentration of the coating solution, while m_i and m_f denote the mass of the fibres before and after coating and Δm ($m_f - m_i$) the mass of polystyrene present at the surface of the fibres.

Table III.9: Mass measurements of bundles of aramid fibres dip coated with $10 \mu\text{mol}$ of polystyrene and dried overnight (expected instrumental standard deviation of $\pm 1 \mu\text{g}$).

	$m_{\text{polystyrene}}$ (mg)	$C_{\text{Polystyrene}}$ (mmol·mL ⁻¹)	number of fibres	m_i (μg)	m_f (μg)	Δm (μg)
1	21.29	10.1	3	28	44	16
2	21.32	10.2	2	18	27	9
3	21.35	10.2	3	27	39	12
4	21.28	10.1	2.5	21	36	15
Average	21.31	10.1	-	36.5	23.5	13
Standard deviation	0.03	$1.51 \cdot 10^{-2}$	-	7.14	4.8	3.16
Ratio (%)	0.15	0.15	-	19.57	20.41	24.33

As can be seen, despite correcting for the amount of fibres present, the standard deviation ($8.9 \mu\text{g}$) approached the instrumental deviation ($1 \mu\text{g}$), which may cause the wide distribution of masses inferred. Visually, the bundles appeared to be different in form and did not 'stick together' in the same fashion, allowing for different surfaces of the coatings to adhere to. Therefore, the mass quantification with individual fibres was likely unreliable.

6.3. Quantification by UV-visible spectroscopy

Owing to the difficulties observed with mass quantification above, an alternative approach is the re-dissolution of the coatings from the fibres and determination of the concentration using absorption of UV-visible (UV-Vis) spectroscopy. However, as the expected amount of deposited content and the emission coefficients of the used coating molecules were unknown, trendlines were necessary to setup. The classical approach was by measuring a dilution series from stock concentration to obtain a calibration curve. Owing to the well described absorption, polystyrene was used as an example (**Figure III.24**). The absorption spectra of the polystyrene were in good accordance with literature [III.27], showing two distinctive absorption peaks at 262 and 269 nm. The first peak was a result of primary aromatic absorption and the later of π -interactions [III.27].

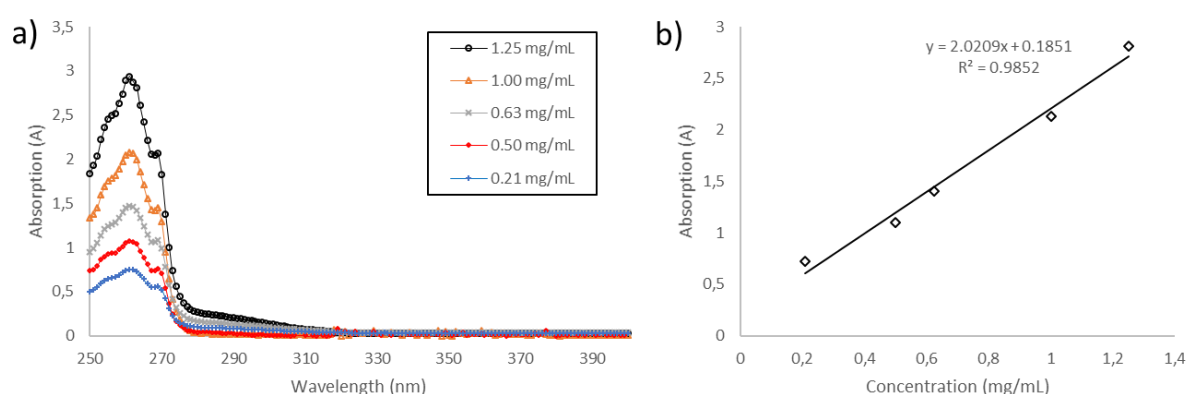


Figure III.24: a) Absorption curves of dilution series of polystyrene (average of three) b) trend line as a result of absorption peaks of a) at 261 nm.

As a preliminary quantification test by UV-Vis spectroscopy, the four different samples of fibre bundles dip coated mentioned in Section 6.2 were taken and soaked overnight in 2 mL of 95/5 ACN/TFA to allow the coating to re-dissolve (**Figure III.25**). The 2 mL of volume was chosen with the volume of the cuvettes in mind, but since the original concentration was made in 1 mL, this meant the concentration was effectively halved and corrected for appropriately by multiplying the mass value in the trendline value times two.

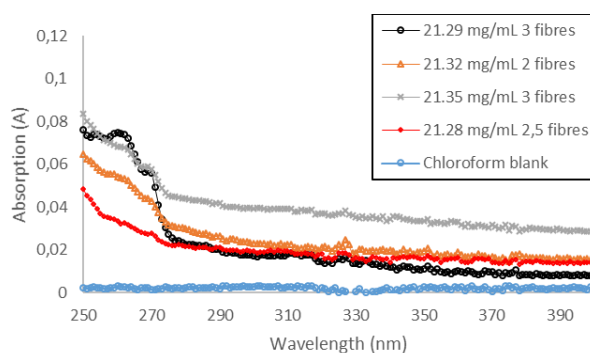


Figure III.25: UV-vis spectra of fibre bundles dip coated with 0.01 mmol polystyrene.

Chapter III: Evaluation of the synthesised oligomers as potential interfacial agents for Kevlar fibre-reinforced polypropylene materials

As can be seen from **Figure III.25** and **Table III.10**, the absorption curves and values showed variation despite relatively consistent masses of the polystyrene used for treatment. Furthermore, the calculated values of masses were negative. One possible explanation was that the absorption values fell outside of the range of the trendline equation of **Figure III.25**, not guaranteeing its accuracy.

Table III.10: Absorption values and calculated mass of fibre bundles dip coated with 0.01 mmol polystyrene based on the baseline formula of **Figure III.24**.

	$m_{\text{polystyrene}}$ (mg)	$C_{\text{Polystyrene}}$ ($\mu\text{mol}\cdot\text{mL}^{-1}$)	#Fibres	Absorption (A, 261 nm)	Δm_{calc} (mg)	$\Delta m_{\text{calc.}}/\text{fibre}$ (mg)
1	21.29	10.1	3	$7.40\cdot 10^{-2}$	$-5.48\cdot 10^{-2}$	$-1.83\cdot 10^{-2}$
2	21.32	10.2	2	$5.30\cdot 10^{-2}$	$-6.51\cdot 10^{-2}$	$-3.25\cdot 10^{-2}$
3	21.35	10.2	3	$6.80\cdot 10^{-2}$	$-5.79\cdot 10^{-2}$	$-1.93\cdot 10^{-2}$
4	21.28	10.1	2.5	$3.20\cdot 10^{-2}$	$-7.56\cdot 10^{-2}$	$-3.03\cdot 10^{-2}$
Average	21.31	10.1	2.63	$5.70\cdot 10^{-2}$	$-6.34\cdot 10^{-2}$	$-2.51\cdot 10^{-2}$
Standard deviation	0.03	$1.51\cdot 10^{-2}$	0.48	$1.87\cdot 10^{-2}$	$9.23\cdot 10^{-3}$	$7.34\cdot 10^{-3}$
Ratio (%)	0.15	0.15	18.24	32.73	-14.58	-29.28

6.3. Discussion and conclusion

Although theoretically it may be possible to relate the EDS results to a certain average thickness of coating, large standard deviations, angle or morphology effects and manual selection of spots made this method not suitable. This technique also proved difficult to set up, requiring numerous spectra before a proper average could be determined. It is for these reasons that EDS was not considered suitable enough for quantitative analysis. Preliminary mass tests were thus set up using fibre bundles. However, the results were inconsistent and unreliable, owing to the shape and irregularities of the fibre material. In order to more accurately measure adsorbed amounts, UV-Vis spectroscopy was used. Although absorption baselines for several compounds were able to be set up using UV-Vis spectroscopy, quantification of adsorbed coatings on treated fibre bundles proved difficult due to the low absorption values. Additionally, the values showed a large dispersion despite normalisation with the amount of fibres, which may be a result of the distribution in both lengths and diameters of the fibres used. For the reasons mentioned above, there was a need to develop a quantification method which could reliably and conveniently give results.

7. Quantification by gravimetry using fibre pellets

In order to achieve a reliable distribution of aramid fibre surface available for quantification experiments, there was a necessity to have samples with a homogenous shape, volume and convenient handling. As has been seen in Section 6.2, individual fibres are delivered with a distribution in dimensional parameters, leading to a variable surface area and uncontrolled adsorption. Additionally, owing to the low weights of the fibres, individual handling was a delicate endeavour and slight

Chapter III: Evaluation of the synthesised oligomers as potential interfacial agents for Kevlar fibre-reinforced polypropylene materials

disturbances in the atmosphere (turbulence of the wind or static charge) may move the fibres in an uncontrolled fashion.

7.1. Dip coating procedure using fibre pellets

In order to eliminate the problems mentioned above and allow convenient handling, aramid fibre 'pellets' were used, fabricated through compressing a set amount of aramid fibres into a set shape via hydraulic press. The dip coating procedure is described in **Figure III.26**. The pellet did not significantly deform after treatment, allowing the convenient use for coating procedures and subsequent determination of masses.

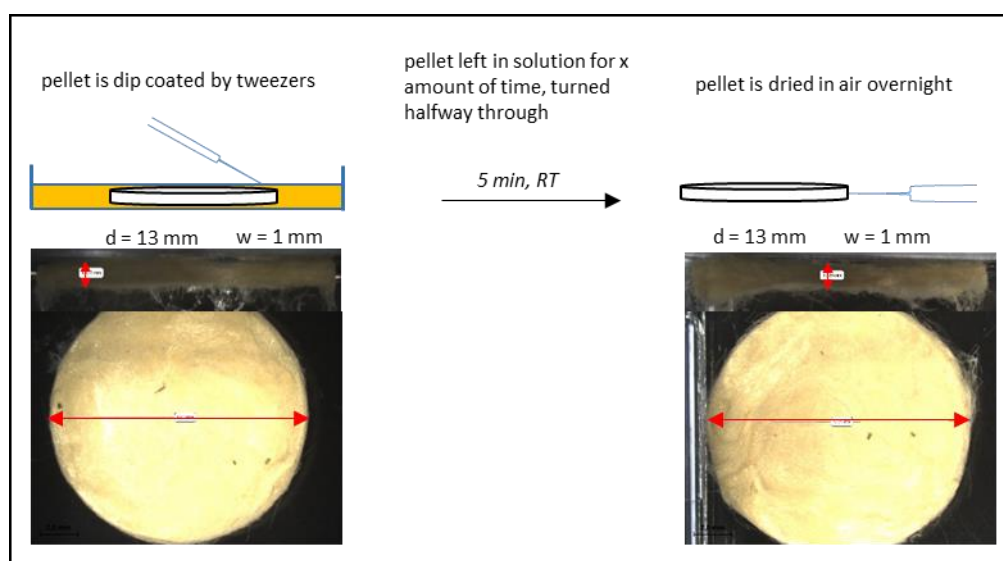


Figure III.26: Dip coating procedure of aramid fibre pellets. Photos illustrate the pellet before and after treatment with $1.07 \cdot 10^{-3} \text{ mmol} \cdot \text{mL}^{-1}$ solution of polystyrene.

7.2. Dimensional considerations

Dimensions of the pellets (mass, diameter, thickness) were taken on twelve samples, six of which (1 to 6) were untreated and six (7 to 12) were treated with $1.00 \mu\text{mol} \cdot \text{mL}^{-1}$ polystyrene in toluene through dip coating. The distributions can be seen in **Table III.11**, where m_{pellet} denotes the mass of the pellet, d and h the diameter and height. Considering the relatively low ratios of standard deviation over measured values, it can be concluded that the formation of the aramid pellets via hydraulic press was relatively consistent, as can be seen for Entries 1-6. Following treatment, the consistency remained for both the weight and diameter with both minimal changes in values and similar standard deviations. However, the height of the pellet was subjected to a change with an increase in the standard deviation.

Chapter III: Evaluation of the synthesised oligomers as potential interfacial agents for Kevlar fibre-reinforced polypropylene materials

Table III.11: Mass, diameter and thickness measurements of SFA pellets (expected instrumental standard deviation of $\pm 1 \mu\text{g}$)

Entry	m_{pellet} (mg)	d (mm)	h (mm)
1	75.05	13.32	1.13
2	74.21	13.51	1.20
3	74.56	13.38	1.14
4	74.58	13.38	1.15
5	74.16	13.48	1.11
6	74.22	13.14	1.16
Average	74.46	13.37	1.15
Standard deviation	0.34	0.13	0.03
Ratio (%)	0.46	0.99	2.67
7	75.14	13.71	1.04
8	75.32	13.89	1.23
9	75.23	13.73	1.77
10	74.84	13.57	1.62
11	74.54	13.73	1.39
12	74.78	13.41	1.20
Average	74.98	13.67	1.38
Standard deviation	0.30	0.16	0.28
Ratio (%)	0.40	1.20	20.05
Average difference	0.51	0.30	0.23

Considering that the dimensions of the pellet were known, various dimensions can be extrapolated. In a first approximation the volume of the pellet (substrate) followed from the dimensions of a cylinder:

$$V_s = \pi r^2 h = 0.13 \text{ mL} \quad (3.1)$$

However, as the pellet itself was a porous structure, the entire volume V_s was not occupied by aramid fibres. To obtain the free volume available for coatings, the volume of the aramid fibres was subtracted from the volume of the substrate:

$$V_\phi = V_s - V_{KF} = V_s - \frac{m_f}{\rho} = 0.08 \text{ mL} \quad (3.2)$$

with m_f the mass of the fibres inside the pellet and $\rho = 1.44 \cdot 10^6 \text{ mg} \cdot \text{m}^{-3}$ the density of aramid fibre [III.6].

As the pellet was plunged in a given volume of coating solution V_L (e.g. 2 mL), three different results can occur depending on the effectiveness of the coating:

1) there was no net interaction between coating and fibres. In equilibrium state during the coating procedure, the concentration of the solution inside the free volume of the pellet and outside will be equal, leading to a proportional adsorption and thusly the percentage of the original concentration adsorbed ($|\Delta C|$) will be the percentage of the coating solution volume occupied by the free volume of the pellet. For example, if the total volume was 2 mL, the free volume inside the pellet was 4% of the total volume. In this situation, 4% of the coating will be adsorbed by the pellet.

Chapter III: Evaluation of the synthesised oligomers as potential interfacial agents for Kevlar fibre-reinforced polypropylene materials

2) there was a net attractive interaction between coating and fibres, leading to an equilibrium state with increased concentration inside the free volume of the pellet. For example, assuming previous variables, >4% of the coating will be absorbed by the pellet.

3) there was a net repulsive interaction between coating and fibres, leading to an equilibrium state with decreased concentration inside the free volume of the pellet. For example, assuming previous variables <4% of the coating will be absorbed by the pellet.

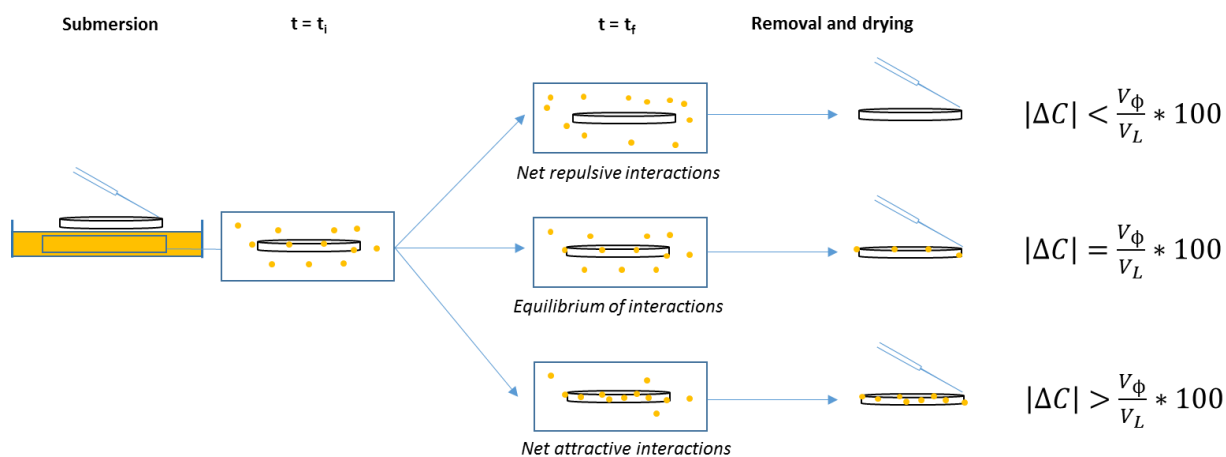


Figure III.27: Possible scenarios of adsorption depending on the interactive properties of the solute.

7.3. Drying process evaluation

Dip coating was performed using 2 mL 95/5 ACN/TFA as a blank solvent test. Three sets of pellets were treated. The pellets were weighed before, to give the initial mass (m_i) and 16-18 hours after treatment to give the final mass (m_f) in triplicate to obtain average values for mass differences (**Table III.12**). The weighted mass of the pellet (m_i) showed relative consistency and justified the choice of the pellet over the original fibre bundle as described in Section 6.2. However, observed was a systematic mass increase averaging at 0.41 mg (m_s), 0.55% of the original average mass of the pellet. However, this mass increase showed a significant standard deviation. The mass increase can be explained due to insufficient drying, resulting in a solvent left behind in the pellet.

Chapter III: Evaluation of the synthesised oligomers as potential interfacial agents for Kevlar fibre-reinforced polypropylene materials

Table III.12: Mass of pellets before and after treatment with blank solvent

Pellet label	m_i (mg)	m_f (mg)	Δm (mg)
1A	73.98	74.31	0.33
1B	74.17	74.41	0.24
1C	74.26	74.76	0.50
2A	74.59	75.02	0.43
2B	74.46	74.85	0.39
2C	74.55	74.64	0.09
3A	74.59	74.98	0.39
3B	74.77	75.18	0.41
3C	74.85	75.73	0.88
Average	74.43	74.84	0.41
Standard deviation	0.26	0.38	0.18
Ratio (%)	0.35	0.50	44.56

Ratio difference/initial weight: $\left(\frac{\langle \Delta m \rangle}{\langle m_i \rangle}\right) * 100$: 0.55%

In order to verify this, the pellets may be treated with a heating step. However, from literature it is known that aramid fibres are relatively hygroscopic with up to 7 wt% of water content possible to be present on the surface of K29 fibres after production and ca. 4.5% of expected water content at equilibrium [III.6]. Therefore, removal of solvent by heating may lead to partial removing of this water content and an assumption was made: the average value from **Table III.12** (0.41 mg) can be taken as a constant amount of solvent which was always present within the fibre after treatment and drying of 16-18 h and can be freely removed from any values as a linear correction.

7.4. Preliminary quantification tests

As a preliminary test, aramid fibre pellets were subjected to $1 \mu\text{mol}\cdot\text{mL}^{-1}$ of FFFFu●FFFFu●FFFFu●FFFFu using the dip coating treatment for 5 min in 2 mL of TFA/ACN (5/95 v%). The resulting treated pellets were weighed for difference and analysed using SEM. As can be seen from **Figure III.28a** below, the surface of the aramid fibre pellet showed minor coating at few spots (notably on the top left) indicated by roughened areas. However, the amount of these areas was vastly decreased in comparison to the results given in Section 5.1.3, which was expected due to the large increase in amount of fibres (ca. 5-10 vs ca. 8000). Some regions on the pellet appeared as illustrated on **Figure III.28b**, showing a flattened area in which it was more difficult to discern any coating.

Chapter III: Evaluation of the synthesised oligomers as potential interfacial agents for Kevlar fibre-reinforced polypropylene materials

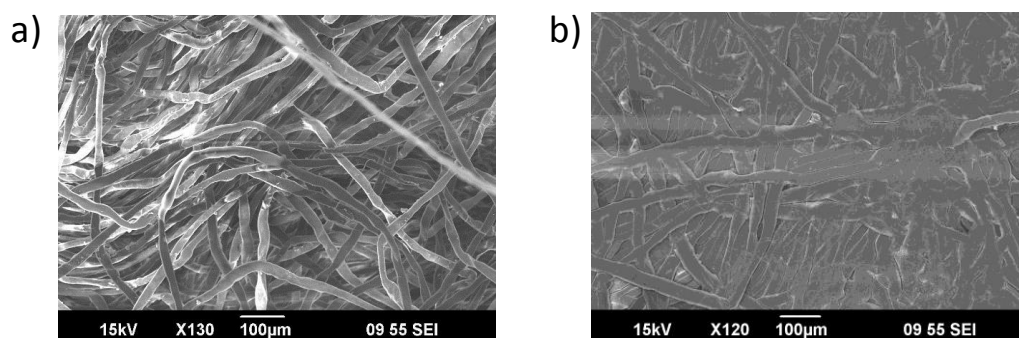


Figure III.28: SEM image of the surface morphologies present on aramid fibre pellets prepared using manual hydraulic press dip coated with $1 \mu\text{mol}\cdot\text{mL}^{-1}$ FFFFu•FFFFu•FFFFu•FFFFu. a) overview of general surface area b) flattened area.

Relative adsorption was calculated by noting the mass difference before and after treatment (Δm), corrected for solvent mass (m_s). The amount of adsorbed moles of oligomer per gram fibres (κ) now is the ratio of adsorbed oligomers in solution with and is given by:

$$\kappa = \frac{\Delta m_{\text{oligomer}} - m_s}{m_{\text{oligomer}}} * \frac{1}{m_i} = \frac{\Delta n_{\text{oligomer}}}{n_{\text{oligomer}}} * \frac{1}{m_i}$$

However, following the results of Section 7.3, the average mass of the pellet can be approximated to be constant giving the adsorption (in $\text{mg}\cdot\text{mL}$) ($\frac{1}{\langle m_i \rangle} = \frac{1}{74.46 \pm 0.34}$)

Considering the small size of this value, the adsorption can be approximated by taking the mass ratio.

$$\kappa^* (\%) = \frac{\Delta n_{\text{oligomer}}}{n_{\text{oligomer}}} * 100$$

Results are given in **Table III.13**. On average 24% of the original concentration was absorbed, indicating net attractive forces as discussed in Section 7.2. Even when the standard deviation was subtracted a non-zero value was obtained. These results therefore showed promise to gain information about the effect of supramolecular interactions on quantitative adsorption.

Table III.13: Mass of pellets before and after treatment with FFFFu•FFFFu•FFFFu•FFFFu ($1 \mu\text{mol}\cdot\text{mL}^{-1}$) as oligomer.

	m_{oligomer} (mg)	m_i (mg)	m_f (mg)	Δm (mg)	$\Delta m - m_s$ (mg)	κ ($1\cdot\text{mg}^{-1}$)	κ^* (%)
1	6.80	74.68	76.26	1.58	1.17	0.23	17.17
2	6.76	74.50	76.18	1.68	1.27	0.25	18.75
3	6.81	74.26	75.88	1.62	1.21	0.24	17.73
Average	6.79	74.48	76.11	1.63	1.22	0.24	17.88
Standard deviation	$2.65 \cdot 10^{-2}$	0.21	0.20	$5.03 \cdot 10^{-2}$	$5.03 \cdot 10^{-2}$	0.01	0.80
Ratio (%)	0.39	0.28	0.26	4.13	4.13	4.55	4.48

7.5. Quantitative analysis of coating behaviour of GGGG

7.5.1. Concentration effect

In order to obtain the influence of the concentration of coating solution onto the quantitative coating behaviour, the adsorption of different concentrations of GGGG on aramid fibre pellets was evaluated as a model molecule. Owing to the results of Section 7.4, a triplicate series of mass measurements was done before and after treatment to give the relative amount of the initial concentration adsorbed onto the pellet (κ) in mg·mL. In **Figure III.28a**, results of adsorption experiments with varying concentrations can be seen and in **Figure III.28b** the average values of each concentration are given including trendline. On the y axis, the values represent the adsorption (κ). The x axis is the concentration of the solution used. As can be seen from the value of R^2 , the exponential trendline was likely reflective the adsorption behaviour. Notably, one would expect the amount of adsorption to exponentially increase with decreasing concentration, owing to **Figure III.29**.

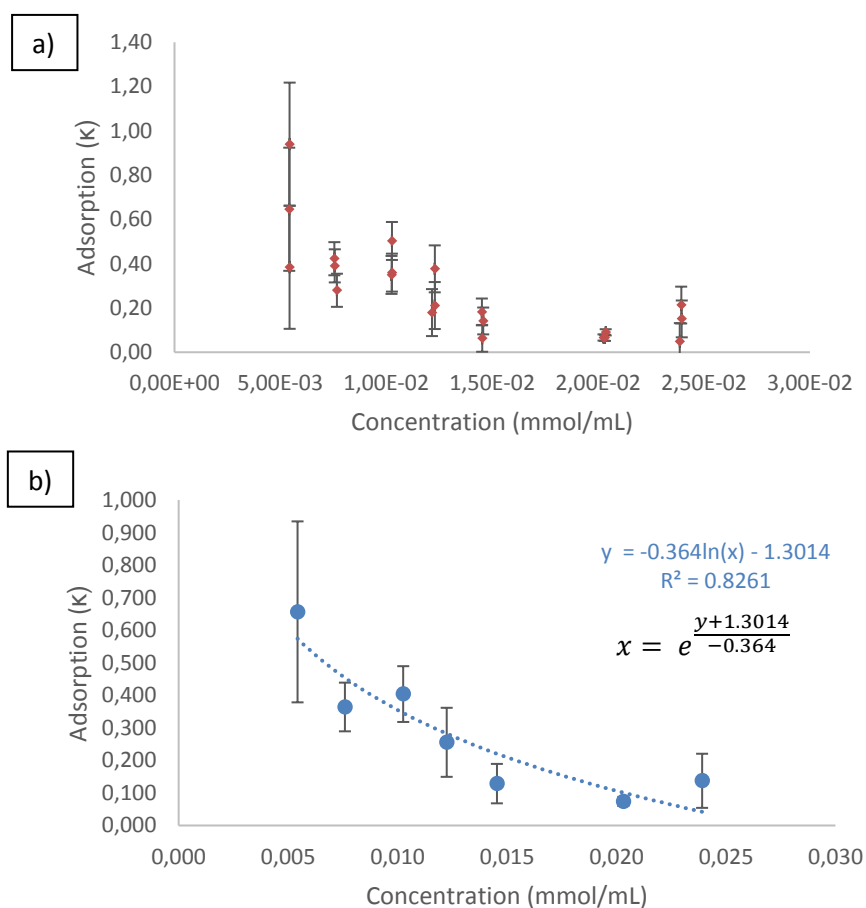


Figure III.29: a) Adsorption profile (in mol% of the original concentration adsorbed) of GGGG absorbed by aramid fibre pellet with varying concentration, b) average values of adsorption

However, at a concentration of $1 \mu\text{mol}\cdot\text{mL}^{-1}$, the adsorption became more difficult to measure, with negative values possible to be found (**Table III.14**). This negative mass difference fell within the sum of standard deviations of m_s and Δm ($1.83 \cdot 10^{-1}$) and was therefore negligible. It can be concluded that at

Chapter III: Evaluation of the synthesised oligomers as potential interfacial agents for Kevlar fibre-reinforced polypropylene materials

this concentration, no suitable relative comparisons can be made between adsorption of GGGG and other compounds.

Table III.14: Mass measurements of aramid fibre pellets dip coated with $1 \mu\text{mol}\cdot\text{mL}^{-1}$ GGGG and dried overnight (expected instrumental standard deviation of $\pm 1 \mu\text{g}$).

Sample	m_{GGGG} (mg)	m_i (mg)	m_f (mg)	$\Delta m - m_s$ (mg)	$[(\Delta m - m_s)/Mw_{\text{GGGG}}]/M_i$ (mol·g)	κ ($1\cdot\text{mg}^{-1}$)
1	0.56	73.31	73.69	-0.03	$-1.67\cdot 10^{-6}$	-0.07
2	0.55	73.98	74.31	-0.09	$-4.68\cdot 10^{-6}$	-0.21
3	0.56	73.97	74.30	-0.08	$-4.51\cdot 10^{-6}$	-0.20
Average	0.55	73.76	74.10	-0.07	$-3.80\cdot 10^{-6}$	-0.16
Standard deviation	$6.81\cdot 10^{-3}$	0.38	0.35	$3.09\cdot 10^{-2}$	$1.69\cdot 10^{-6}$	0.08
Ratio (%)	1.23	0.52	0.48	-44.71	-44.39	-50.00

7.5.2. Time effect

In order to get an idea about the effect of time on the adsorption behaviour, a 0.02 mmol solution of GGGG was applied to aramid fibre pellets for varying amounts of time. The time at which the adsorption process was expected to start ($t = 0$) was set as the point where the pellet was fully submerged. Thusly, we can expect that at this moment, the amount of adsorbate present in the free volume was proportional to this free volume (the flux was 0). For this case, since the free volume constituted 0.04 mL (as determined in Section 7.2) and the concentration was 0.02 mmol in 2 mL, this expected concentration at $t = 0$ constituted $5.39\cdot 10^{-6}$ mmol GGGG·mg⁻¹ aramid fibre. In **Figure III.30**, both results of adsorption as well as the average results are given. Between 1 and 5 min the amount absorbed increased, after which a plateau was likely obtained around the 5 min mark, after which any positive change in adsorbed amount of solute may be due to the volatile nature of the solvent. It was possible to fit these values in a logarithmic trend line.

Chapter III: Evaluation of the synthesised oligomers as potential interfacial agents for Kevlar fibre-reinforced polypropylene materials

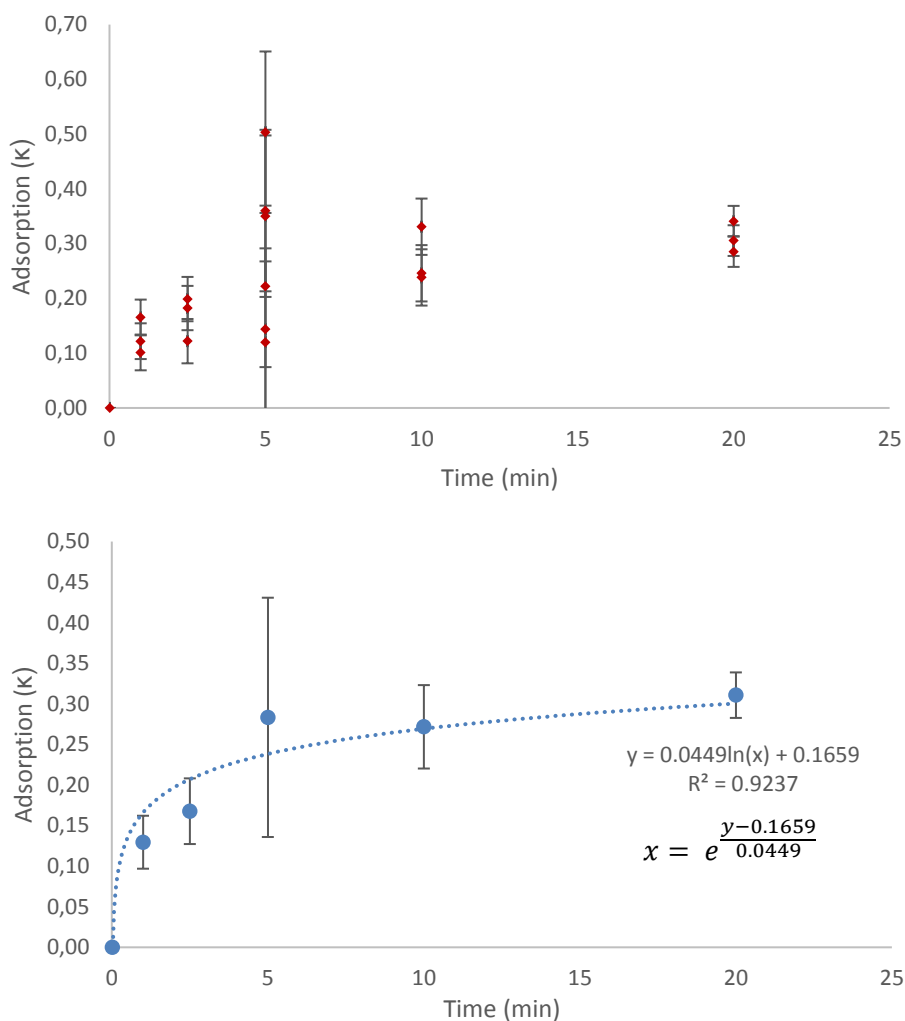


Figure III.30: Adsorption profile (in mol% of the original concentration) of GGGG adsorbed by aramid fibre pellet with varying treatment time.

7.6. Results of quantification of coating performed on fibre pellets

For the purpose of making a comparison between the different coating compounds listed in Section 1, the following parameters were chosen: 1) 5 min coating time considering the results from Section 7.5.2, 2) a concentration of $1 \mu\text{mol}\cdot\text{mL}^{-1}$ considering the results of Section 4.4 3) at minimum a triplicate series of measurements considering the results of Section 7.4. Adsorbing behaviours of the different coating compounds were then compared by using the average adsorption values. These were calculated using the relative mmol% of the original concentration adsorbed relative to the mass of the aramid fibre pellet re-multiplied by the average mass of the aramid fibre pellet. A full overview of the results is given in Appendix C.

Chapter III: Evaluation of the synthesised oligomers as potential interfacial agents for Kevlar fibre-reinforced polypropylene materials

7.6.1. Quantification of coating behaviour commercial molecules affording the distinction between hydrogen bonding and π interactions

The quantification was first conducted on the model molecules permitting the contribution between hydrogen bonding and π interactions, i.e polystyrene, GGGG and FFFF (**Table III.15**). The three different commercial standards gave differences in adsorption values. As indicated in Section 7.5.1., it was assumed that GGGG showed no significant adsorption with respect to the free volume (<4% adsorption) and showed a net repelling effect from the fibre pellet. This idea was reinforced with the results from the fibre morphologies on a ten times higher concentration as observed by SEM, showing a low coverage on the fibre surface and a dewetting effect. Interestingly, the adsorption was significant for FFFF and polystyrene, which showed a percentage adsorbed above 4%. Furthermore, it was possible to differentiate between the two, noting two different relative amounts of mmol adsorbed. As can be seen, the adsorption was increased for FFFF, giving an indication that the interactive properties were better exploited here.

Table III.15: Adsorption values for commercial standards

Compound	number of sites for specific interactions		κ^* (%)
	hydrogen bonding	π -interactions	
GGGG	8	-	0
Polystyrene	-	17-18	5.3
FFFF	8	4	9.2

7.6.2. Quantification of coating behaviour for oligomers with a single phenylalanine unit per block

Oligomers with one phenylalanine residue and variable spacing were then evaluated (**Table III.16**) and showed an increase in adsorption compared to the commercial standards described in Section 7.6.1. by a factor of more than two despite the doubled amount of H-bonding interactions. It can be seen that oligomer FvFvFvFv adsorbed by far the most, with more than 55% of the original solution contained within the pellet. These results were consistent with qualitative observations seen in Section 5, noting the increased roughness surfaces covered with FvFvFvFv or the appearance of droplet shapes unique to this compound compared to FbFbFbFb and FhFhFhFh which show a relatively similar morphology. Exceptionally, Fh●Fh●Fh●Fh, while the adsorption values were likely within the range of FbFbFbFb and FhFhFhFh, showed a much rougher surface profile, similar to that of FvFvFvFv.

Chapter III: Evaluation of the synthesised oligomers as potential interfacial agents for Kevlar fibre-reinforced polypropylene materials

Table III.16: Adsorption values for oligomers with a single phenylalanine unit per block.

compound	number of sites for specific interactions		κ^* (%)
	hydrogen bonding	π -interactions	
FbFbFbFb	16	4	23.9
FvFvFvFv	16	4	56.4
FhFhFhFh	16	4	26.1
Fh●Fh●Fh●Fh	16	4	29.0

7.6.3. Quantification of coating behaviour for oligomers with four phenylalanine units per block

The quantification was finally conducted on the oligomers with four phenylalanine units per block (**Table III.17**). The oligomers showed comparative adsorption behaviour, with FFFFv●FFFFv●FFFFv●FFFFv and FFFFu●FFFFu●FFFFu●FFFFu having an increase in adsorption over the other two oligomers. However, despite an increase in supramolecular interactions in comparison to tetraphenylalanine of a factor >4 the adsorption is not proportionate.

Table III.17: Adsorption values for oligomers with four phenylalanine units.

compound	number of sites for specific interactions		κ^* (%)
	hydrogen bonding	π -interactions	
FFFFb●FFFFb●FFFFb●FFFFb	39	16	16.4
FFFFv●FFFFv●FFFFv●FFFFv	39	16	19.2
FFFFh●FFFFh●FFFFh●FFFFh	39	16	14.2
FFFFu●FFFFu●FFFFu●FFFFu	39	16	17.9

7.6.4. Relative comparison of coating behaviour

Considering phenylalanine as an interactive unit, the adsorption values were compared relatively using tetraphenylalanine as a point of comparison. **Table III.18** now lists all the relative adsorption values. For GGGG, owing to the negative values, it was assumed that this adsorption was zero. Corresponding to three categories of the coating molecules, three ranges of adsorption quantity can now be distinguished. The commercial products showed the least adsorption, with GGGG showing no significant presence on the pellet, polystyrene likely very weak interactions and FFFF a limited presence. The adsorption was increased by roughly a factor of two for the synthesised oligomers of Chapter II despite the large increase in supramolecular interactions while the last category of the oligomers with spacing between single phenylalanine residues showed the highest relative adsorption, with differences observed depending on the spacing. Seeing that the adsorption does not follow any pattern related to the amount of H-bonding or π -interactions, it can be more reasonably assumed that the spacing between the interactive subunits is an important factor owing to the ability to manage

Chapter III: Evaluation of the synthesised oligomers as potential interfacial agents for Kevlar fibre-reinforced polypropylene materials

orientational parameters of the molecules on the fibre surface, where small differences in spacing can cause an optimization in molecular orientation. This may explain why FvFvFvFv can adsorb far more than other tested molecules.

Table III.18: Relative adsorption values for all the molecules considered in this study (*imposed value).

compound	number of sites for specific interactions		relative adsorption vs
	hydrogen bonding	π -interactions	FFFF
GGGG	10	-	0*
polystyrene	-	17-18	0.54
FFFF	10	4	1.00
FbFbFbFb	17	4	2.46
FvFvFvFv	17	4	5.85
FhFhFhFh	17	4	3.00
Fh●Fh●Fh●Fh	16	4	2.92
FFFFb●FFFFb●FFFFb●FFFFb	40	16	1.69
FFFFv●FFFFv●FFFFv●FFFFv	40	16	2.00
FFFFh●FFFFh●FFFFh●FFFFh	40	16	1.46
FFFFu●FFFFu●FFFFu●FFFFu	40	16	1.92

8. Preliminary results composites

Since the coatings that have been observed were based primarily on supramolecular interactions for their adhesion, it was uncertain how they behaved in composite conditions. Two preliminary tests were selected: analysis of fractured composites to assess presence of compatibilizer on the fibre surface after moulding conditions and pullout tests to assess shear force differences between treated and untreated fibres with the polymer matrix. For this purpose, aramid fibre-reinforced polypropylene ethylene copolymer was studied. Preliminarily, aramid fibre-reinforced polypropylene polyethylene copolymer was studied.

8.1. Fracture test results

8.1.1. Protocol

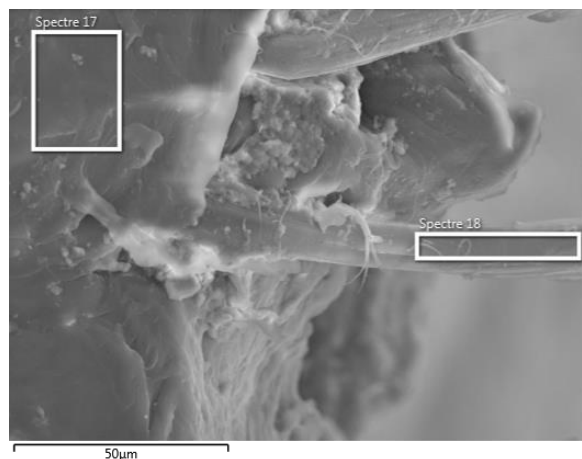
For this purpose, aramid fibre was sandwiched between layers of propylene ethylene copolymer spheres which were melted by oven at a constant temperature ($T = 180\text{ }^{\circ}\text{C}$). After cooling, the composite was then removed and fractured, leaving fragments which can be attached to a carbon substrate for SEM/EDS analysis. Since fracturing of the compound gave fragments with various shapes

Chapter III: Evaluation of the synthesised oligomers as potential interfacial agents for Kevlar fibre-reinforced polypropylene materials

and angles, it was necessary to manually correct for this in the SEM chamber by rotating and tilting the sample holder.

8.1.2. Blank aramid fibre in matrix

The first composite prepared considered untreated Kevlar fibres in polypropylene (**Figure III.31**). Fibres were observed as embedded into the polypropylene matrix and showed a relatively clean exit with little wetting of the polypropylene onto the fibre. This was reflected in the EDS results, showing only a small increase in the carbon percentage value measured on the aramid fibre surface.



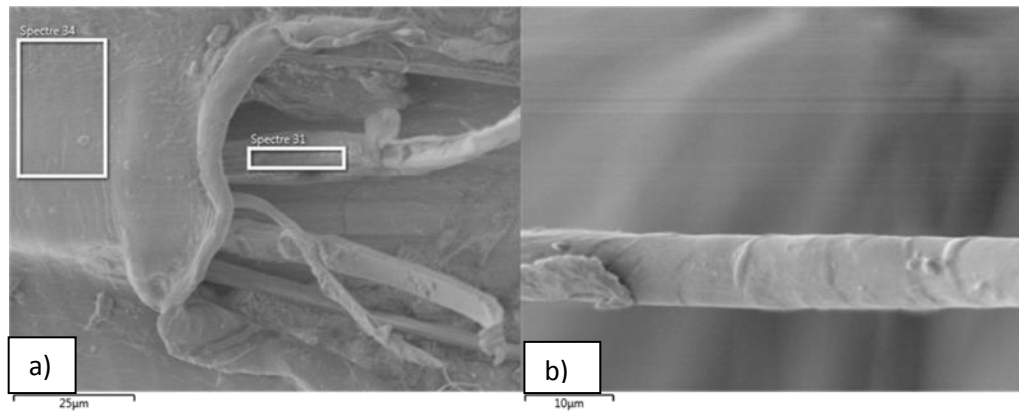
	C (%)	N (%)	O (%)
Spectrum 17	97.8	-	2.2
Spectrum 18	75.6	11.3	13.1
Aramid fibre exp.	72.1	11.6	16.3
PP calc.	97.4	-	2.7

Figure III.31: Morphology of aramid fibre-reinforced polypropylene and EDS results.

8.1.3. FFFFv•FFFFv•FFFFv•FFFFv coated aramid fibre in matrix

As a preliminary coating to evaluate, FFFFv•FFFFv•FFFFv•FFFFv was chosen. Of the synthesised oligomers, it showed the roughest surface and highest quantity of aggregates, making it the most likely to be able to be discerned from both the aramid fibre and polypropylene surfaces. An example of the coated fibre reinforced composite is given in **Figure III.32**. The fibre surface showed significant differences with those in **Figure III.31**, showing a covered surface. When the composite was analysed using EDS, the aramid fibre surface showed an increase in atom percentages for carbon and decrease in both nitrogen and oxygen, likely as a result of polypropylene on the surface.

Chapter III: Evaluation of the synthesised oligomers as potential interfacial agents for Kevlar fibre-reinforced polypropylene materials



	C (%)	N (%)	O (%)
Spectrum 31	89.4	3.7	6.9
Spectrum 34	94.8	-	5.2
Aramid fibre exp.	72.1	11.6	16.3
PP calc.	97.4	-	2.7

Figure III.32: Morphology of a) coated aramid fibre-reinforced polypropylene and EDS results, b) an individual covered fibre surface.

8.2. Pullout test results

8.2.1. Protocol

Here, aramid fibres were embedded in single propylene-ethylene copolymer spheres by controlled melting on heating element. The fibres can then be removed by pullout test on loading blade, where the shear force can be determined following:

$$\tau_{app} = \frac{F_{max}}{\pi \cdot d_f \cdot l_e} \Rightarrow \tau_{app} \propto F_{max}$$

With τ_{app} as the applied shear force, F_{max} the maximum force before breakage of the fibre from matrix, d_f and l_e the diameter and length of the embedded part of the fibre. In total, 27 pullout tests were performed on untreated aramid fibres and 26 on treated aramid fibres.

8.2.2. Comparison pullout test FFFFv•FFFFv•FFFFv•FFFFv treated vs untreated aramid fibre in matrix

Despite a difference in morphology observed in Section 8.1, the observed average shear strengths do not significantly differ. This can be explained by a possible lack of interlocking/mechanical adsorption between the polymer matrix and the oligomer layer. Although the adsorption of the oligomer on the aramid fibre seems maintained in the composite, the interactions with the polymer matrix are not improved over untreated aramid fibre.

Chapter III: Evaluation of the synthesised oligomers as potential interfacial agents for Kevlar fibre-reinforced polypropylene materials

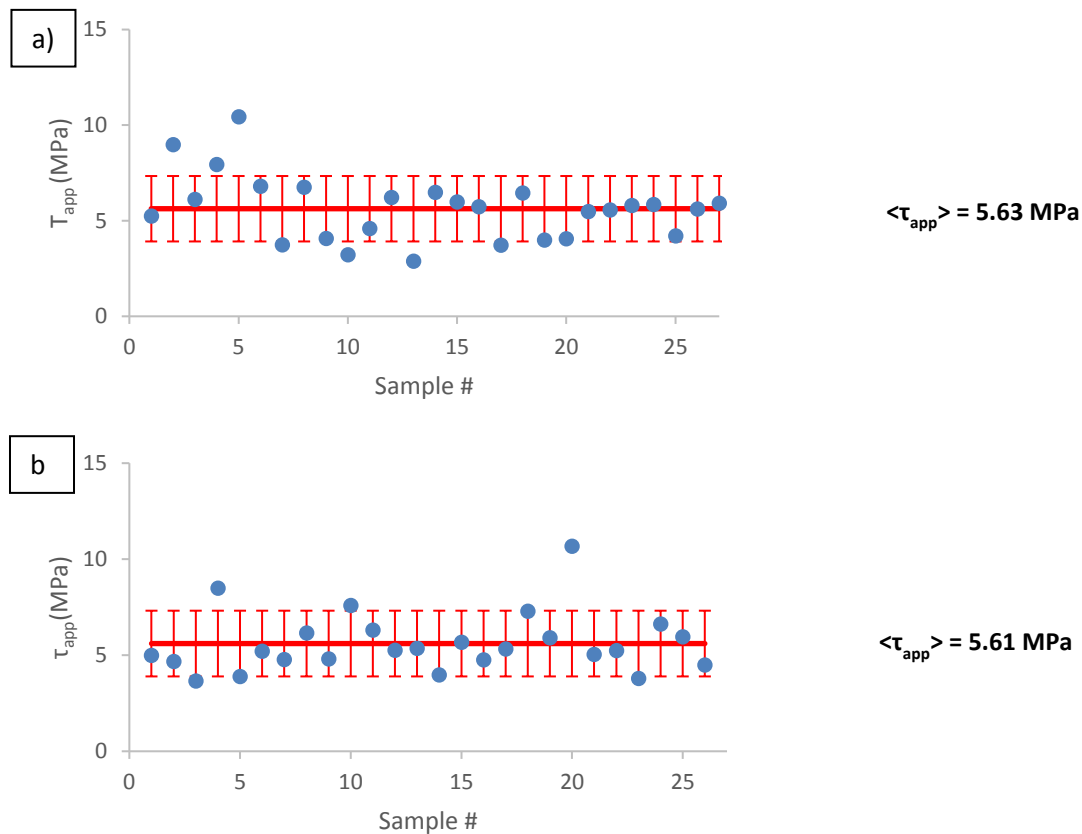


Figure III.33: Overview of shear strength measured between a) untreated and b) aramid fibres dip coated with $1 \mu\text{mol}\cdot\text{mL}^{-1}$ FFFFv•FFFFv•FFFFv•FFFFv in polypropylene ethylene matrix.

9. Interpretation of the results

Important toolboxes to determine the reasons for the behaviour of the coating molecules are physical models. Here, two parts will be described: the effect of the coating method onto the morphology and a description predicting molecular transport into fibrous material to approximate the aramid fibre pellet.

9.1. Description of coating processes

9.1.1. Dip coating

The dip coating process can be roughly described in three steps. The first step involves moving the fibre or fibrous material into a basin of liquid after which a liquid layer is formed on the surface. As described by Puetz and Aegerter: “The formation of this layer is based on fluid mechanical equilibrium between the entrained film and receding coating liquid (solvent + solute). The two regimes are divided by a stagnation line, above which the liquid is constrained by the substrate whereas the liquid below is retained in the basin. The equilibrium is governed by several forces, including viscous drag, gravity, surface tension, inertial force and disjoining pressure” [III.28]. Landau, Levich and Derjaguin described an exact solution for the formation of a liquid layer on a surface as it is withdrawn from a liquid basin in the following way:

Chapter III: Evaluation of the synthesised oligomers as potential interfacial agents for Kevlar fibre-reinforced polypropylene materials

$$h = 1.34r\left(\frac{\eta V}{\gamma}\right)^{\frac{2}{3}} \quad (3.8)$$

with h the thickness of the liquid layer, r the radius of the fibre pulled from solution, η is the viscosity of the liquid, V the velocity of the coating procedure and γ the surface tension of the liquid vs air. The equation is only valid for relatively low velocities ($\leq 1 \text{ cm}\cdot\text{s}^{-1}$) and the thickness of the fibre coating should be an order of magnitude smaller than the fibre radius itself, meaning that the term $\left(\frac{\eta V}{\gamma}\right)$ should not exceed 0.64 [III.29-III.30].

The second step of the dip coating procedure involves evaporation of the solvent. The fluid film on a fibre is unstable following the Plateau-Rayleigh instability [III.31]. As more and more solvent is removed, the surface tension and viscosity properties of the sizing will start to dominate the layer. Depending on these properties, the resulting film may either gradually reduce its thickness to form a smooth coating, but if the interactive forces are strong enough, the liquid layer can spontaneously fall apart into periodic arrays of droplets [III.31]. These droplets will show a variety in the contact angles depending on the material used and this is governed by a pressure balance. According to Quéré "In the absence of gravity, the Laplace pressure must be a constant. The drops can then have an unduloidal (asymmetric spherical) shape that conserves axisymmetry. Furthermore, in wetting situations, the profile has generally an inflection point since the drop must join the fibre with a small contact angle" [III.29].

Finally, when the material present on the fibre has fully solidified, stresses can no longer be relieved by flow and tensile stresses develop in the plane of the substrate, which can lead to visible cracks in the sizing film surface if the thickness of the film is above a critical value (typically $h_c \approx 0.5\text{-}1 \mu\text{m}$) [III.32].

The critical thickness can be calculated in the following way:

$$h_c = \left(\frac{K_{Ic}}{\sigma\Omega}\right)^2 \quad (3.9)$$

with K_{Ic} as the critical stress intensity or "fracture toughness", σ as the stress and Ω a function that depends on the ratio of the elastic moduli of the sizing and substrate [III.33-III.34].

9.1.2. Spray coating

Spray coating, like dip coating, can also be described in three steps. The first step can be described using the Bernoulli equation:

$$C = P_0 + \rho gh + 0.5\rho v^2 \quad (3.10)$$

where C is a constant, P_0 is the atmospheric pressure, ρgh is the pressure generated by gravity and $0.5\rho v^2$ the dynamic pressure associated with fluid flow velocity [III.35]. As the liquid exits the nozzle the droplets undergo forces generated by Bernoulli pressure which tends to break the droplets in smaller sizes and forces generated by the surface tension, which maintains the shape of droplets. As

Chapter III: Evaluation of the synthesised oligomers as potential interfacial agents for Kevlar fibre-reinforced polypropylene materials

soon as the two forces are in equilibrium the shape of the droplet stays constant. Assuming that the droplets are nebulized to the smallest possible size, this follows the following equation:

$$d_0 \leq 14 \frac{\gamma}{\rho v^2} \quad (3.11)$$

where γ is the surface tension of the liquid and d_0 the droplet diameter. From this equation a balance between the dynamic pressure and the surface tension can be seen [III.36].

In the second step, the droplets travel between the nozzle and the substrate and practically the speed and shape are metastable and heat transfer to the surrounding environment minimal. Zheng *et al.* remarks that the shape of the diameter of the droplets can only change linearly in this state [III.36].

Kim *et al.* now describes the collision of a sub mm diameter water droplets with a copper fibre coated with a polymeric surface (PTFE) as a model case. In this study, after collision occurs three different outcomes are possible [III.37]: 1) in the case of weak inertia, the fluid envelops the fibre fully before stabilizing as a captured droplet, 2) in the case of increased inertia, the fluid envelops the fibre fully, but does not stabilise as a captured droplet and continues to move from the fibre, and 3) in the case of further increased inertia, the fluid no longer envelops the fibre, but instead splits into separate particles upon impact.

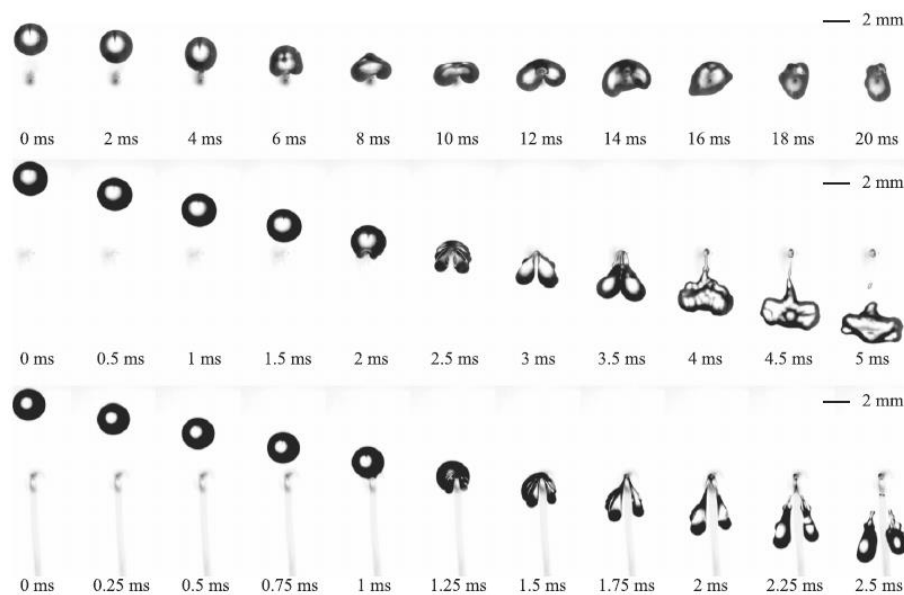


Figure III.34: Collision events with timescales between water droplets and PTFE coated copper fibres. a) capture, b) transmission, c) splitting. Adapted from [III.37] with permission from AIP Publishing.

In the latter two cases, the fluid will only be partially captured by the fibre, leading to the formation of a liquid film equivalent to the case of dip coating. As this film is formed, viscous effects may become significant so that the viscous resistance is comparable to the dynamic pressure ($0.5\rho v^2$) at the stagnation point. The results from Kim *et al.* can now be expressed in a semi-empirical relation:

$$h \sim \sqrt{\frac{\eta r v_h}{\rho V_0}} \quad (3.12)$$

Chapter III: Evaluation of the synthesised oligomers as potential interfacial agents for Kevlar fibre-reinforced polypropylene materials

with η as the viscosity of the liquid, r as the radius of the droplet, V_0 , V_h as the velocities of the droplet before and after impact and ρ the density of the liquid [III.37]. After the collision, spray coating thusly gives rise to droplets of liquid and thin films of coating on the fibre surface, unlike dip coating which is expected to give a homogenous liquid film.

The third step in the spray coating process (drying) will be homogenous with that of the dip coated example with the main difference in the expected initial size of the liquid film.

9.1.3. Discussion

Owing to what is described in Sections 9.1.1 and 9.1.2, the morphology differences observed in Section 5 may be explained.

Dip coating: At the moment of impact between solution and fibre, the influence of the solute onto viscosity may be neglected owing to the low concentrations used. Filling in equation (3.8) allows us to obtain the expected thickness of the liquid layer briefly after dip coating has been performed. The average radius of the fibre has been given in Section 3 (6.5 μm), viscosity and surface tension values of acetonitrile and toluene at room temperature are known from literature [III.38-III.41]. The withdrawing speed V is intentionally kept at 1 $\text{m}\cdot\text{s}^{-1}$ as an estimate.

$$h_{ACN} = 1.34r\left(\frac{\eta V}{\gamma}\right)^{\frac{2}{3}} = 1.34 * (6.5 * 10^{-7})\left(\frac{0.34}{28.4}\right)^{\frac{2}{3}} = 0.46 \mu\text{m}$$

$$h_{Toluene} = 1.34r\left(\frac{\eta V}{\gamma}\right)^{\frac{2}{3}} = 1.34 * (6.5 * 10^{-7})\left(\frac{0.59}{27.8}\right)^{\frac{2}{3}} = 0.67 \mu\text{m}$$

As a result, the liquid layer is expected to be a factor 10 smaller than the fibre radius. However, as is clear from the results of Section 5, a uniform layer of sub-micron size was not observed, which is likely caused by the drying step. It is here then that the formation of morphologies from a drying solution may be affected by the individual surface tension values of the coating molecules, which may explain a difference in final appearance. Droplet shapes were notably observed for FvFvFvFv and Fh•Fh•Fh•Fh, which may be caused by intramolecular forces. Similarly, while film formation was observed for both Fh•Fh•Fh•Fh and FFFv•FFFv•FFFv•FFFv, only the latter showed visible cracks in the film surface, which may be an indication that the oligomeric sizings enjoy different mechanical parameters, notable for ductility.

Spray coating: In the case of spray coating, it becomes more difficult to apply the given models. As the spray head used was a commercially disposable one, homogenous size and velocity of the droplets was not expected following an uncontrolled application of pressure. It is therefore not possible to predict the size of the droplets when getting in contact with the fibre surface. However, following **Figure III.34**, the morphology differences can still be translated into parameters of interaction, where a higher amount of interactions is expected to increase not only the quantity of the adsorbate, but additionally the amount of droplet shapes visible. With this in mind, the results in Section 5.2 are expected, where

Chapter III: Evaluation of the synthesised oligomers as potential interfacial agents for Kevlar fibre-reinforced polypropylene materials

the molecules without spacing units showed less coverage overall while the oligomers showed an increase in coverage with simultaneous droplet formation.

9.2. Physical models for diffusion of particles into fibrous media

In the case of any interaction between the fibre and solute, we can expect a net increase in the concentration of the solute in the immediate area of the fibre pellet. This process is expected to be driven by the net enthalpic energy gain from supramolecular bond association [III.42]. In our particular case of dip coating treatments of fibre pellets in a basin containing a solution, we can distinguish two events: 1) diffusion from solution towards the edge of the fibres following standard Brownian motion, and 2) diffusion from the edge of the fibres towards any parts within the pellet network and subsequent concentration around the fibre surface. In our case we expect process (1) to be driven by process (2) as both the amount of surface area available at the edge of the pellet is far less than inside of the pellet and the effective range at which the supramolecular interactions can take place are small enough that only the intermediate area around the pellet can be affected, given the range of the supramolecular interactions. As the concentration around the pellet is decreased through process (2), diffusion of particles from any part of the basin towards the area of decreased concentration will follow and is described classically using Fick's law, where Brownian motion of particles is implied and a continuous equilibrium is formed as a result [III.43].

Koch and Brady applied Fick's law to a bed of fibrous material, assuming that adsorption takes place from solvent in flow, which solubilises particles inside the fibrous material. Assumed is an isotropic mixture of fibres in random direction in a certain media. This media is now subjected to a flow of particles (tracers) inside a solvent. On a microscale on each point in the pellet the concentration of particles satisfies:

$$\frac{\partial c}{\partial t} + \nabla q = 0 \quad (3.13)$$

with c the concentration, t the time, ∇ the differential operator in x, y and z directions and q the mass flux, defined the following way for the different components.

$$\begin{aligned} q_s &= uc - D_s \nabla c \\ q_f &= D_f \nabla c \end{aligned} \quad (3.14)$$

in which q_s and q_f are flux in solvent and fibre areas respectively, u is the velocity or convection of the solvent, D_s and D_f are the association (or diffusivity) constants of the solvent and fibre areas [III.44].

Assuming that the solvent itself is static the term uc becomes 0. We can now express the flux difference the following way:

$$\Delta q = D_f \nabla c - D_s \nabla c \quad (3.15)$$

and at the surface of the fibre the following continuity of mass flux and solubility is expected:

$$D_f n \nabla c_f = D_s n \nabla c_s \quad \text{and} \quad m c_f = c_s \quad (3.16)$$

Chapter III: Evaluation of the synthesised oligomers as potential interfacial agents for Kevlar fibre-reinforced polypropylene materials

where m is the ratio of solubility of the solute in the solvent and in the area around the fibres. N is the outward normal to the fibre surfaces. C_f and C_s are now is the concentrations of the solute in the areas of the fibres and solvent respectively [III.44]. It is possible to simplify the application of Fick's law to a degree by assuming that the system can be described as two infinitely long compartments on a one dimensional plane with a thin film membrane in between (at position $x = 0$). Here, the surface of the fibre now acts as this thin film through which solutes diffuse through, changing the concentration of one compartment (C_1) in respect to the other (C_2). This follows Fick's second law of diffusion [III.43]:

$$\frac{dC_x}{dt} = \frac{d}{dx} \left(D \frac{dC_x}{dx} \right) \quad (3.17)$$

with C_x the concentration at a distance x with $x = 0$. Applying boundary conditions of $C = C_1$ for $x < 0$ and $C = C_2$ for $x > 0$ now gives the following:

$$\frac{dC_x}{dt} = D \frac{\partial^2 C}{\partial x^2} \quad (3.18)$$

which can be solved mathematically:

$$C(x, t) - c_1 = \frac{C_2 - C_1}{\sqrt{\pi}} \int_{-\infty}^{\frac{x}{2\sqrt{Dt}}} e^{-\xi^2} d\xi = \frac{C_2 - C_1}{2} \left(1 + \operatorname{erf} \left(\frac{x}{2\sqrt{Dt}} \right) \right) \quad (3.19)$$

with $\operatorname{erf} \left(\frac{x}{2\sqrt{Dt}} \right) = \frac{2}{\sqrt{\pi}} \int_0^z e^{-\xi^2} d\xi$ as the error function.

As the result of this, the concentration profile as a function of distance between the two compartments will change with time, with at infinite time an equilibrium where the concentrations are equal. The speed of concentration change is now driven by the diffusivity constant [III.43].

In the case of adsorption onto a surface, for a macroscopic view we can effectively consider parts of the concentration to be removed, meaning that the solvent volume in which diffusion can freely take place may be depleted from solutes by adsorption in a separate event. Until an equilibrium is reached between the concentration in the area around the substrate and the surface, the diffusion will continue. As mentioned earlier, the entire process of diffusion will be driven by the adsorption process. Various models exist to describe the adsorption isotherms, including a linear model and the classical Langmuir isotherm [III.43]. Here, we will consider the more practically applied Lagergren's model for the adsorption profile of process [III.45].

$$\frac{dq_t}{dt} = k_1(q_e - q_t) \quad (3.20)$$

where q_t and q_e are an amount of material absorbed at a time and equilibrium. K_1 is the rate constant of the pseudo-first-order adsorption process. As is described by Ho, boundary conditions can now be applied, using that $q_t = 0$ at $t = 0$ [III.45].

$$\log(q_e - q_t) = \log(q_e) - \frac{k_1}{2.303} t \quad \text{or} \quad q_t = q_e(1 - e^{-k_1 t}) \quad (3.21)$$

As can be seen above, in Lagergren's model the expected adsorption profile follows an exponential scale in which the driving parameter of adsorption is K_1 , which is expected to include any potential effects caused by supramolecular factors, surface profile and interlocking abilities.

Chapter III: Evaluation of the synthesised oligomers as potential interfacial agents for Kevlar fibre-reinforced polypropylene materials

9.2.1. Discussion

The given exponential models for adsorption match with what was found in Section 7.5.2. In **Figure III.30**, the adsorption of GGGG over time is given and can be seen approaching an equilibrium asymptote of adsorption (q_e). Using the trendline equation, K_1 may be calculated as an adsorption coefficient. Unfortunately, as time dependency experiments were not setup for the other coating molecules, it does not give additional information.

10. Summary

The coating behaviour of various commercial and synthesised coating molecules has been evaluated qualitatively and quantitatively. Using SEM/EDS, it was possible to distinguish different morphologies for the different coatings, which were consistent between the two coating methods used (spray and dip coating). Additionally, gravimetric analyses on aramid fibre pellets permitted the relative comparison of quantitative adsorption behaviours between the coating compounds. The qualitative and quantitative results showed significant overlap in behaviour, with surface roughness and appearance of droplet shapes and films between fibres an indication of increased adsorption. Following these results, it is highly likely that the adsorption process was driven by supramolecular interactions and highly dependent on not only the quantity of said interactions but also the degrees of freedom within the molecule. From both qualitative and quantitative results, it is likely that FvFvFvFv far outperformed other coating compounds, despite only minor differences in structure between it and other similar oligomers. This led to believe that the exact structure of the molecule is an important factor for the design of a highly interactive compatibilizer molecule for a specific reinforcement fibre in composite materials.

Preliminary compounding tests on the application of these supramolecular coatings showed that despite the non-covalent nature of the interactive bonding, the coatings remained present on the fibre material when applied as treatments for composite materials. Preliminary pullout tests have shown no significant increase in interfacial shear forces between treated and untreated aramid fibres, indicating the need for further development of the molecular structure of the compatibilizer.

CONCLUSION

The interface layer of fibre-reinforced composite material is an important facet and influences load transfer and general mechanical properties. For this reason, it classically has been altered with a variety of grafting and etching techniques. However, these techniques lack precision in their optimisation and with an eye to classically poorly interacting fibre-reinforced composite materials, like aramid fibre reinforced polypropylene, a bottom-up approach to improve the interface region has been devised.

Novel compatibilizer molecules based on select non-covalent interactions have been designed and synthesised adapting known solid-phase iterative synthetic techniques. For this purpose, hydrogen bonding, π -interactions and orientation of the interactions across the fibre surface were explored through the use of (repeated) phenylalanine residues with aliphatic spacing and triazole moieties in between.

In Chapter II, the synthesis of these novel oligomers was described. Early on, the synthetic procedure developed earlier at Institut Charles Sadron was adapted for the synthesis of oligomers containing a variable amount of phenylalanine residues as interactive units with Kevlar fibres as well as variable spacing through aliphatic chains that would be compatible with the polymer matrix. However, as became clear by NMR spectroscopy and MS analysis, reactions did not fully go to completion and optimisation was necessary. For this reason, the reaction conditions were investigated using the Kaiser test and IR spectroscopy after each coupling step to verify completion of the reactions. Pre-activation of the carboxylic acid, the use of aggregate disruptors and changes in reaction conditions were attempted, including change of concentration, solid phase resin and solvent usage. The best conditions were identified by modification of the solvent (DMF) to a mixed solvent system of DCM/DMF/NMP 1/1/1 (by volume) and replacing the CTC solid phase resin by a Tentagel resin. These changes led to an improvement in purity of the oligomers synthesised, but did not lead to unimolecularity. Notably, impurities were found as a result of incomplete coupling reactions, which indicated that the used verification methods for completeness (Kaiser test, IR test) were not sufficient. Furthermore, NMR and MS indicated several peaks which could not be identified as well as a PEG impurity. Some of the unknown signals as well as the PEG signal were originated from the usage of the Tentagel resin. Others may have been caused due to the reaction conditions. In order to optimise the synthetic procedure further, a few approaches were proposed: alternative reaction conditions changing protective groups, solid phase resin and reagent or synthesis of oligomer fragments which can be ligated to form the final product or making use of capping and tagging strategies to simplify the purification.

Despite the results of the synthesis, some oligomers were taken for analysis of their behaviour as compatibilizers. In Chapter III, the coating behaviour of select oligomers was compared to commercial products with varying degrees of hydrogen bonding and π -interactions. The qualitative results were obtained using SEM imaging coupled to EDS spectroscopy. With this method it was possible to obtain

the morphologies the coatings could make on the fibre surface at low concentrations by two different coating methods (dip and spray coating) and pinpoint regions where coating was found. Drastic differences were found between the different commercial products as well as the oligomers. Important morphological factors included surface roughness, appearance of films and droplet shapes and coverage with degrees of wetting and dewetting. Notably, tetraglycine and polystyrene did not show fully wetting of the aramid fibres, while this was visible for the tetraphenylalanine or any of the oligomers analysed. This indicated that π -interactions or hydrogen bonding interactions in conjunction give the most adsorption.

The morphological results (appearance of spheres, films and cracks) may be partially explained by differences in surface tension during drying steps. Quantitative tests were set up using EDS, UV-Vis spectroscopy and direct mass measurements. However, out of these three methods, only the mass tests proved to be useable and only by homogenizing the shape of the used samples as fibrous pellets rather than individual fibres.

With this method, the dip coating process was investigated for quantitative differences in the adsorption of the different commercial products and the oligomers. Notably, the oligomers with a single phenylalanine residue per repeat unit showed relatively large adsorption in comparison to the oligomers with four phenylalanine residues per repeat unit. The degree of spacing has shown to be an important factor, with up to two times relative adsorption depending on the amount of spacing. The oligomers showed increased adsorption compared to commercial unspaced standards, indicating that this spacing unit is an important factor for adsorption, potentially by managing orientational parameters of the adsorbing molecules. Overlap was found between qualitative morphology analysis and quantitative mass tests, where a rougher qualitative morphologies is paired with a higher quantitative adsorption. This was especially true for FvFvFvFv and FFFv•FFFv•FFFv•FFFv, which showed not only the highest adsorption, but also the roughest surface and most visible droplet shapes, while coating molecules showing (partial) dewetting (tetraglycine, polystyrene) showed the relative lowest amount of adsorption. Although these differences have been indicated, the mass test method proved to be difficult to set up and showing some inconsistency with large deviation values as a result. Additionally, the presence of residual solvent in the pellet was confirmed. In order to optimise the technique, steps should be taken to minimise the effects of solvent and moisture already present on the aramid fibres. Controlled drying steps before and after treatments by oven for prolonged time may minimise these effects. In order to decrease the large observed standard deviations, more measurements may be necessary as well as ways that could homogenise the pellet fabrication to assert an exact similarity. In order to receive a better image of the adsorption behaviour, similar tests as those

performed for tetraglycine (adsorption values at variable concentration or time) may be constructed for all tested oligomers.

As the preparation of composite materials requires a thermal treatment, it was necessary to evaluate the thermal stability of the molecules used as interfacial agents. Thermal analysis revealed that the oligomers containing four phenylalanine residues per repeat unit showed an onset degradation temperature (>214 °C) beyond the melting point of polypropylene (165-175 °C) and no discernible glass transition temperature, making them suitable to be used for compounding. However, the oligomers showing one phenylalanine residue per repeat unit did show a degradation temperature below this range (134-139 °C) and two oligomers were found containing a glass transition temperature: FvFvFvFv and FhFhFhFh. For this reason and owing to the good results obtained with the qualitative and quantitative analysis, FFFFv•FFFFv•FFFFv•FFFFv had been chosen to for preliminary compounding tests with Kevlar® fibre-reinforced polypropylene. SEM/EDS analysis elucidated the differences between treated and untreated fibres, where presence of matrix was increased on the treated fibres, indicating possible improvements in adhesion of the interfacial region. As a perspective, untreated aramid fibres and aramid fibres treated with a 1 $\mu\text{mol}\cdot\text{mL}^{-1}$ solution of FFFFv•FFFFv•FFFFv•FFFFv were submitted for single-fibre pull-out tests at INSA Lyon. These tests should provide directly the potential of the molecule as compatibilizer, delivering the force required to remove to fibre from polypropylene matrix.

Concluding, the combination of the synthetic techniques used and the analytical methods made it possible to take preliminary steps into full optimisation of the interfacial region of an arbitrary fibre-reinforced composite material. The iterative solid-phase synthesis allowed to create a library of different oligomers and the screening using SEM and gravimetric analyses allowed to find the most effective adsorption and morphology. Subsequent tests of mechanical properties of treated fibre-reinforced composite materials would then allow to find the most ideal load transfer capabilities. The main difference between the researched and existing methods is the direction of the approach. While classically, top-down approaches are performed to systematically change a parameter in the fibre-reinforced composite material and note the performance differences, the bottom-up approach of pre-designing a compatibilizer molecule could circumvent a lengthy trial and error process and potentially create a new class of high performance materials.

EXPERIMENTAL SECTION

1. Materials

Kevlar® short fibre aramid (SFA) fibres ($l = 50$ mm, $d = 12$ μ m), pretreated by the supplier to remove finish, were received as a sample from DuPont de Nemours S.A. Polypropylene/polyethylene copolymer Lumicene® MR10MM0 (melt flow index: ~ 1 g·min⁻¹ at 230 °C, 2.16 kg, density: 0.90 g·cm⁻³, bulk density 0.53 g·cm⁻³) was purchased from Total. Tetraglycine (>99.9%) and tetraphenylalanine (>97%) were purchased from Bachem. Polystyrene standard ($M_n = 2100$ g·mol⁻¹, $D = 1.05$) was purchased from PSS-Polymer. Oligomers FbFbFbFb-NH₂ (>90%, HPLC), FvFvFvFv-NH₂ (>90%, HPLC) and FhFhFhFh-NH₂ (>90%, HPLC) as described in Chapter III were purchased from Laboratoire Altergen. Chlorotriyl chloride resin (1.6 mmol·g⁻¹, 100-200 mesh), 2-(1H-benzotriazol-1-yl)-1,1,3,3-tetramethyluronium hexafluorophosphate (HBTU, 99%) and Fmoc-L-Phe-OH (>99%) were purchased from Iris Biotech GmbH. 1-Hydroxybenzotriazole hydrate (HOBt, >97%), acetic acid (99.8%), *N,N,N',N',N''*-pentamethyldiethylenetriamine (PMDETA, 99%), dimethylsulfoxide (99.9%), thionyl chloride (99.9%), concentrated hydrochloric acid (HCl, 37% in water, fuming), trifluoroacetic acid (TFA, 99%), potassium cyanide (ACS reagent, 97%), dichloromethane (99.9%), anhydrous dichloromethane (>99.8%), dichloroethane (99.8%), tetrahydrofuran (99.9%), dimethylacetamide (99.9%), *N,N*-dimethylformamide (anhydrous, 99.9%), 4-methyl-2-pentanol (98%), 3-hexanol (>97%), 1,2-propanediol (99%), butyl acetate (99.7%), diacetyl (>95%), *m*-xylene (99.9%), *o*-xylene (99.9%), tetrabutylammonium bromide (TBAB, 99%), triisopropylsilane (TIPS, 99%), pyridine (anhydrous, 99.8%), ninhydrin (99%) and α -cyano-4-hydroxycinnamic acid (matrix substance for MALDI-MS, $\geq 99.0\%$) were purchased from Sigma-Aldrich. Sodium azide (NaN₃, 99%), 6-bromohexanoic acid (>98%), 5-bromovaleric acid (97%), 4-bromobutyric acid (97%), piperidine (99%), phenol (>99%), copper(I) bromide (CuBr, 98%) and 1-methyl-2-pyrrolidinone (99%) were purchased from Alfa Aesar. 11-Bromoundecanoic acid (>98%), 7-bromoheptanoic acid (>98%), *N*-ethyldiisopropylamine (DIPEA, 99%), propargylamine (>95%), acetyl chloride (98%) and 2,2,2-trifluoroethanol (TFE, >99%) were purchased from TCI. Methyl-4-bromobutyrate (>98%) and diethyl ether (99.9%) were purchased from Acros Organics. *N,N*-Dimethylformamide (DMF, 99.5%), methanol (99.9%), toluene (99.9%), acetonitrile (99.9%) and acetone (99.9%) were purchased from Fisher chemicals. Absolute ethanol, 2-propanol (99.9%), 2-butanol (99.9%) and acetic acid (99.9%) were purchased from VWR. Dichloromethane (>99.8% RE, pure grade, stabilized with amylene 20-60 ppm), ethyl acetate (>99.8%, pure grade), acetone (>99.8%, pure grade) methanol (>99.8%, pure grade), tetrahydrofuran (>99.5%, pure grade, stabilized with BHT 5-7 ppm) and diethyl ether (>99.5% pure grade, stabilized with BHT 5-7 ppm) were purchased from Carlo Erba Reagents. CupriSorb™ (Seachem®) was bought from Recif at home. Fmoc Phe Tentagel® S PHB resin (0.24 mmol·g⁻¹) was purchased from Rapp Polymere. All the reagents were used as received except if otherwise noted. Copper(I) bromide was purified by stirring

in acetic acid overnight, washing with methanol, and drying under vacuum at room temperature. All the syntheses on solid support were performed in solid phase extraction (SPE) tubes (60 mL polypropylene tubes with polyethylene frits, 20 μm porosity, SUPELCO[®] purchased from Sigma-Aldrich) and shaken using a modified IKA KS 130 basic shaker. Reverse phase column chromatography was performed using silica bonded DSC18 (10 g, 56 μm particle size, 0.007 μm porosity, pH 5.4) preloaded in a 60 mL polypropylene tube with polyethylene frit (SUPELCO[®] purchased from Sigma-Aldrich). Sanytol disinfectant was bought from E.Leclerc at home, allowing the retrieval of HDPE disposable spray head. Quartz cuvettes (QS 110) for ultraviolet-visible (UV-Vis) light spectroscopy measurements were purchased from Hellma. All preparations of compounds from powder form or pellets from aramid fibres were performed using a Specac manual hydraulic press with a stainless steel crucible having a diameter of 13 mm. PTFE covered tweezers were purchased from Bochem. PTFE tweezers were purchased from COWIE.

2. Characterisation

Nuclear magnetic resonance (NMR) spectra were recorded in CDCl_3 or $\text{DMSO}-d_6$ on either a Bruker Avance I 400 MHz spectrometer equipped with an Ultrashield[™] magnet and a 5 mm BBFO probe or on a Bruker Avance III HD 500 MHz spectrometer equipped with an Ascend[™] magnet and a 5 mm CPPBBO “Prodigy” probe.

Fourier transform infrared (FTIR) spectra were recorded on a Bruker Vertex 70 spectrophotometer using the attenuated total reflectance (ATR) technique.

High-resolution ESI-MS and MS/MS experiments were performed using a QStar Elite mass spectrometer (Applied Biosystems SCIEX, Concord, ON, Canada) equipped with an ESI source (positive mode). The capillary voltage was set at +5500 V and the cone voltage at +75 V. In this hybrid instrument, ions were measured using an orthogonal acceleration time-of-flight mass analyser. In the MS mode, accurate mass measurements were performed using reference ions from a poly(propylene glycol) or a poly(ethylene glycol) internal standard. In the MS/MS mode, a quadrupole was used for selection of precursor ions to be further submitted to collision-induced dissociation in a collision cell. The precursor ion was used as the reference for accurate measurements of product ions in MS/MS spectra. In this instrument, air was used as the nebulising gas (10 psi), while nitrogen was used as the curtain gas (20 psi) as well as collision gas. Instrument control, data acquisition and data processing were achieved using the Analyst software (QS 2.0) provided by Applied Biosystems. Oligomer solutions were prepared in MeOH supplemented with ammonium acetate (3 mM) and introduced in the ionisation source with a syringe pump (flow rate: 5 $\mu\text{L}\cdot\text{min}^{-1}$).

Mass measurements were carried out on an Autoflex[™] MALDI-TOF mass spectrometer (Bruker Daltonics GmbH, Bremen, Germany). This instrument was used at a maximum accelerating potential

of 20 kV in positive mode and was operated in mode reflector at 19 kV. The delay extraction was fixed at 80 ns and the frequency of the laser (nitrogen 337 nm) was set at 5 Hz. The acquisition mass range was set to 400-4000 m/z with a matrix suppression deflection (cut off) set to 500 m/z. The equipment was externally calibrated with a standard peptide calibration mixture that contained seven peptides (Bruker Peptide Calibration Standard #206196, Bruker Daltonics GmbH, Bremen, Germany) covering the 1000-3200 m/z range. Each raw spectrum was opened with flexAnalysis 2.4 build 11 (Bruker Daltonics GmbH, Bremen, Germany) software and processed using the following parameters: signal-to-noise threshold of 1, Savitzky-Golay algorithm for smoothing, median algorithm for baseline subtraction, and SNAP algorithm for monoisotopic peak detection and labelling in reflectron mode. In all cases, resolution was higher than 9000. Sample preparation was performed with the dried droplet method using a mixture of 0.5 μL of sample with 0.5 μL of matrix solution dry at room temperature. The matrix solution was prepared from a saturated solution of α -cyano-4-hydroxycinnamic acid in water/acetonitrile 50/50 diluted three times in water/acetonitrile/trifluoroacetic acid 50/49.9/0.1. The sample solution was prepared by dissolving 5 mg of FFFH•FFFH•FFFH•FFFH in 1 mL of a solution of concentrated HCl in tetrahydrofuran (1/9).

Analytical high performance liquid chromatography (HPLC) experiments were performed using a Knauer Eurosphere 100-5 reverse phase column with dimensions of 250x4 mm at a temperature of 40 °C and pressure of 13-16 bar using 0.1% TFA in acetonitrile as mobile phase and a C18 polymer as a stationary phase with a flow rate of 10 mL \cdot min⁻¹. The injection volume used was 20-50 μL without degassing. Chromatograms were recorded with associated bipolar K-2501 UV-detector with a range of 0-10000 mAU, recording a measurement each second with absorption peak set at 254 nm. No additives or degassing were used.

Ultraviolet-visible light (UV-Vis) spectra were recorded on a PerkinElmer Lambda 650 spectrophotometer between 250-400 nm unless otherwise mentioned. 0% absorption and blank cuvette and solvent correction curves were performed before each series of measurements.

Thermogravimetric analyses (TGA) were performed on a Mettler-Toledo TGA2 or Mettler-Toledo TGA/DSC 3+ thermogravimeter at a heating scan rate of 50 °C \cdot min⁻¹ using alumina crucibles. N₂ atmosphere (gas flow rate: 100 mL \cdot min⁻¹) was used universally until 350 °C. For temperature in between 350 °C and 850 °C, air was used for any of the oligomers synthesised using CTC resin and N₂ for any of the oligomers synthesised using Tentagel[®] resin. The TGA curves were recorded from 50 °C to 850 °C. The temperature of the onset of degradation ($T_{d, \text{onset}}$) was determined as the crossing point of the tangents of the first weight loss observed on each TGA curve.

GC-MS experiments were performed on a PerkinElmer Clarus[®] 600 gas chromatograph interfaced with a PerkinElmer Clarus[®] 600 T quadrupole mass spectrometer equipped with a pyroprobe[®] Model 2500 pyrolyser from CDS Analytical and controlled by the PerkinElmer TurboMass[™] GC/MS software.

Helium gas (flow rate: 1 mL·min⁻¹) was used as mobile phase and 5% PMS grafted siloxane column (30 m x 0.25 mm, I.D. 0.25 μm, J&W GC columns from Agilent Technologies) as stationary phase. Each GC peak was identified by comparing its mass spectrum with several libraries (for example NIST library, version 2.1.0). The system was checked with a polyethylene standard supplied by Quad Service. Each sample was weighted to have the same number of moles of molecules and placed in the pyrolysis tube between two pieces of glass fibre that were previously cleaned at 400 °C overnight.

Differential scanning calorimetry (DSC) experiments were performed on a Perkin-Elmer 8500 or Mettler-Toledo TGA/DSC 3+ spectrometer in stainless steel crucibles and using an empty crucible as a reference under a flow of N₂ (20 mL·min⁻¹). For each sample, the following heating-cooling cycles were performed: (i) heating run from 0 °C to 200 °C at a heating scan rate of 15 °C·min⁻¹, (ii) cooling run from 200 °C to 0 °C at a cooling scan rate of 15 °C·min⁻¹, (iii) heating run from 0 °C to 200 °C at a heating scan rate of 15 °C·min⁻¹, (iv) cooling run from 200 °C to 0 °C at a cooling scan rate of 10 °C·min⁻¹, (v) heating run from 0 °C to 200 °C at a heating scan rate of 10 °C·min⁻¹, (vi) cooling run from 200 °C to 0 °C at a cooling scan rate of 5 °C·min⁻¹, and (vii) heating run from 0 °C to 200 °C at a heating scan rate of 5 °C·min⁻¹. Thermograms obtained during the runs (iii), (v) and (vii) were analysed to determine the value of the glass transition temperature at each heating scan rate as the inflection point of the glass transition. The “true” glass transition temperature (T_g) was obtained by extrapolating the values at different heating scan rates to a heating scan rate of 0 °C·min⁻¹. For modulated temperature differential scanning calorimetry (mtDSC) experiments, the Perkin-Elmer 8500 instrument and settings were used as described above, using the StepScan mode (temperature increment between two steps: 2 °C; step isothermal holding time: 20 s) and heating and cooling scan rate of 15 °C·min⁻¹.

Scanning electron microscopy (SEM) experiments were performed on a JEOL JSM6490LV microscope (max resolution 3 nm) equipped with an Oxford instruments AZTEC (lateral resolution 200 nm) or X-Max (lateral resolution 30 nm) energy dispersive X-ray spectroscopy (EDS) module. The source of X-rays was a W Filament. For preparation of SEM samples, an Emitech K575 sputter coater was used with the following settings: platinum as metal, pressure of 10⁻³ mbar, current of 65 mA, and sputter distance of 3 cm. Measurements were taken under a pressure of ~10⁻⁵ mbar with a voltage of 15 kV.

For quantification experiments, all weights were recorded on a vibration-stabilised Mettler-Toledo AX 205 analytical balance located in an air-conditioned room.

Single fibre pullout tests samples were prepared using the FIMABOND embedder: spheres of polypropylene ethylene copolymer were selectively melted at a temperature of 160 °C in a circular metal crucible after which single aramid fibres were inserted at a distance of 5 mm. The samples were allowed to be cooled to RT after which pullout tests were performed using FAVIMAT+ mechanical tester.

3. Synthesis of azidoalkanoic acids

4-Azidobutyric acid [E.1] (**b**), 5-azidovaleric acid [E.2] (**v**), and 6-azidohexanoic acid [E.3] (**h**) were synthesised as previously described in the literature.

The procedure previously reported for 6-azidohexanoic acid [E.3] was adapted for the synthesis of 7-azidoheptanoic acid (**e**) and 11-azidoundecanoic acid (**u**). Briefly, 11-bromoundecanoic acid (28 g, 106 mmol) and sodium azide (17 g, 264 mmol) were added to a solution of acetone (100 mL) and reverse-osmosed water (200 mL) in a round bottom flask. The solution was stirred in an oil bath thermostated at 60 °C for 5 h. The reaction mixture was then cooled in an ice bath to 0 °C and acidified with concentrated HCl until pH 2 was reached. The mixture was then extracted with ethyl acetate three times. The organic layers were combined, washed with brine, dried over anhydrous sodium sulphate, concentrated by rotary evaporation and dried overnight under vacuum. The final product was obtained as an off-white solid (23 g, 96%).

11-Azidoundecanoic acid (u). ¹H NMR: δ (CDCl₃, 7.26 ppm) 11.28 (bs, 1H), 3.24 (t, 2H), 2.34 (t, 2H), 1.53-1.68 (m, 4H), 1.21-1.43 (m, 12H). ¹³C NMR: δ (CDCl₃, 77.16 ppm) 180.54, 51.51, 34.14, 29.43, 29.34, 29.22, 29.15, 29.06, 28.87, 26.74, 24.68. FT-IR: 2091 cm⁻¹ (azide).

7-Azidoheptanoic acid (e). ¹H NMR: δ (CDCl₃, 7.26 ppm) 10.30 (bs, 1H), 3.26 (t, 2H), 2.36 (t, 2H), 1.56-1.69 (m, 4H), 1.32-1.43 (m, 12H). ¹³C NMR: δ (CDCl₃, 77.16 ppm) 180.19, 51.45, 34.02, 28.74, 28.64, 26.46, 24.56. FT-IR: 2107 cm⁻¹ (azide).

Caution: Organic azides are potentially explosive substances. Routine precautions were taken to minimize the effect of possible explosions at all stages in the preparation and handling of ω -azidoalkanoic acids. These compounds are stored in the fridge.

4. Synthesis of macromolecules based on phenylalanine and aliphatic building blocks using a CTC resin

The phenylalanine-based oligomers were synthesised using a modified version of the synthetic strategy reported previously [E.3]. Briefly the approach to the synthesis is described here. 2-Chlorotriyl chloride (CTC) resin was subjected to addition of the different building blocks as illustrated below for the solid-phase synthesis of FFFFh•FFFFh•FFFFh•FFFFh.

i) General procedure for functionalizing CTC resin

CTC resin (0.99 g, 1.58 mmol, 1 eq) was added to the SPE tube and was swollen in 10 mL DCM for 10 min. The solution was filtered and washed three times with 10 mL of DCM. Fmoc-L-Phe-OH (1.23 g, 3.178 mmol, 2 eq) was added to the vessel. Three vacuum-argon cycles were performed before adding anhydrous DCM (10 mL). DIPEA (1.12 mL, 6.356 mmol, 4 eq) was then added to the vessel and the reaction mixture was shaken under argon for 1 h. The solution was filtered and the vessel was washed with six times with 10 mL of DMF. A 10 mL mixture of DCM/MeOH/DIPEA of 80/15/5 v% was added to

the vessel and shaken for 10 min. After this the solution was filtered and the previous step repeated. The resin was washed six times with 10 mL of DMF. A 10 mL mixture of 25% piperidine in DMF was added to the vessel, shaken for 3 min and then filtered. This step was repeated but shaken for 20 min instead. The resin was then washed six times with 10 mL of DMF, six times with 10 mL of DCM, three times with 10 mL of MeOH and lastly three times with 10 mL of DCM before dried under vacuum for two days. After this, the yield of loading was determined by weighing the functionalised resin (1.18 g, 1.156 mmol, 72%)

ii) Addition of 6-azidohexanoic acid

6-Azidohexanoic acid (0.35 g, 2.19 mmol), HBTU (0.83 g, 2.18 mmol), HOBt (0.29 g, 2.17 mmol), DIPEA (0.70 mL, 4.05 mmol) and a 1/1/1 mixture of CH₂Cl₂/DMF/NMP (10 mL) were added to the SPE tube and agitated for 1 h. After filtration, the resin was washed six times with 10 mL of DMF and six times with 10 mL of CH₂Cl₂.

iii) Copper-assisted alkyne-azide cycloaddition with propargylamine

CuBr (27 mg, 0.19 mmol) was added to the SPE tube, which was then degassed through three vacuum/argon cycles. Anhydrous CH₂Cl₂ (10 mL) were added to the vessel, followed by PMDETA (0.07 mL, 0.34 mmol) and propargylamine (0.14 mL, 2.23 mmol). The solution was agitated under argon for 1 h. After filtration, the resin was washed six times with 10 mL of DMF and six times with 10 mL of CH₂Cl₂.

iv) Addition of Fmoc-L-Phe-OH

Fmoc-L-Phe-OH (0.84 g, 2.19 mmol), HBTU (0.83 g, 2.18 mmol), HOBt (0.29 g, 2.17 mmol), DIPEA (0.70 mL, 4.05 mmol) and a 1/1/1 mixture of CH₂Cl₂/DMF/NMP (10 mL) were added to the vessel, and agitated for 1 h. After filtration, the resin was washed six times with 10 mL of DMF. The Fmoc-protecting group was removed by agitation with 10 mL of a 25% piperidine in DMF solution for 3 min followed by filtration and agitation with a fresh solution of piperidine for 20 min. The resin was then washed six times with 10 mL of DMF and six times with 10 mL of CH₂Cl₂.

v) Cleavage from the resin and recovery of the phenylalanine-based oligomer.

The resin was washed twelve times with 10 mL of CH₂Cl₂ before transferring the resin to a round bottom flask and adding the cleavage solution (10 mL) to the flask. For oligomers containing glycine or with phenylalanine block size equal to or less than two, a 25% solution of TFE in DCM was used for cleavage. For any other oligomers a 50% solution of TFA in DCM was used. The resin was agitated with the cleavage solution for 1 h and collected in a clean round-bottom flask. These tasks were performed three times. The resin was then washed three times with 5 mL of CH₂Cl₂. The filtrates were combined, stirred with ~50 mg CupriSorb™ overnight to remove residual copper, concentrated into a viscous solution by rotary evaporation and precipitated in diethyl ether. Aggregates of oligomers were crushed

to obtain a finely dispersed powder, which was then frozen in liquid nitrogen and subjected to two 1 h vacuum-argon cycles before drying it under vacuum overnight at room temperature.

Fh•Fh•Fh•Fh. 1.27 g, 83% yield. ^1H NMR: δ (DMSO- d_6 , 2.50 ppm) 8.49 (s, 3H), 8.06 (dd, 4H), 7.69 (d, 2H), 7.36-7.07 (m, 20H), 4.53 (d, 4H), 4.38-4.09 (m, 12H), 3.22 (t, 2H), 3.13-3.05 (m, 1H), 3.04-2.95 (m, 3H), 2.88-2.75 (m, 3H), 2.12-1.94 (m, 7H), 1.78-1.63 (m, 6H), 1.52-1.32 (m, 9H), 1.18-0.98 (m, 7H) ppm. ^{13}C NMR: δ (DMSO- d_6 , 39.52 ppm) 171.97-170.79, 138.07, 129.56, 127.95-127.60, 122.46, 53.96, 48.85, 37.78, 35.08, 29.44, 27.82, 25.34-24.65 ppm. MS (ESI, m/z): $[\text{M}+\text{H}]^+$ calculated from $\text{C}_{69}\text{H}_{90}\text{N}_{19}\text{O}_9$: 1328.71, found 1328.72; $[\text{M}+2\text{H}]^{2+}$ calculated from $(\text{C}_{69}\text{H}_{90}\text{N}_{19}\text{O}_9)/2$, found 664.86.

FFh•FFh•FFh•FFh. 1.85 g, 79% yield. ^1H NMR: δ (DMSO- d_6 , 2.50 ppm) 8.69-8.44 (m, 3H), 8.30 (dd, 1H), 7.81-7.64 (m, 3H), 7.34-7.08 (m, 40H), 4.59-4.38 (m, 6H), 4.38-4.12 (m, 14H), 3.25-3.10 (m, 3H), 3.10-2.89 (m, 7H), 2.68 (t, 3H), 2.05-1.91 (m, 7H), 1.76-1.58 (m, 7H), 1.45-1.26 (m, 9H), 1.15-0.93 (m, 8H) ppm. ^{13}C NMR: δ (DMSO- d_6 , 39.52 ppm) 171.13, 137.87, 129.45, 128.29, 122.46, 54.52, 48.84, 36.95, 34.72, 29.51, 27.61, 24.73 ppm. MS (MALDI-ToF, m/z): $[\text{M}+\text{H}]^+$ calculated from $\text{C}_{105}\text{H}_{125}\text{N}_{23}\text{O}_{13}$: 1916.98, found 1917.15.

FFFh•FFFh•FFFh•FFFh. 4.80 g, 86% yield. ^1H NMR: δ (DMSO- d_6 , 2.50 ppm) 8.69 (bs, 1H) 8.56-8.44 (m, 2H), 8.30 (t, 1H), 8.22-7.88 (m, 7H), 7.79-7.53 (m, 2H), 7.33-6.99 (m, 60H), 4.62-4.35 (m, 10H), 4.35-4.09 (m, 13H), 3.24-3.09 (m, 5H), 3.06-2.85 (m, 10H), 2.84-2.75 (m, 4H), 2.68-2.58 (m, 5H), 2.04-1.84 (m, 7H), 1.73-1.56 (m, 7H), 1.45-1.23 (m, 9H), 1.12-0.90 (m, 9H) ppm. ^{13}C NMR: δ (DMSO- d_6 , 39.52 ppm) 171.48, 138.02, 129.43, 128.21, 122.09, 53.74, 49.53, 37.07, 34.34, 29.51, 24.84 ppm. MS (ESI, m/z): $[\text{M}+\text{H}]^+$ calculated from $\text{C}_{141}\text{H}_{161}\text{N}_{27}\text{O}_{17}$: 2506.01, found 2506.26.

FFFFh•FFFFh•FFFFh•FFFFh. 2.59 g, 87% yield. ^1H NMR: δ (DMSO- d_6 , 2.50 ppm) 8.43 (t, 2H), 8.37-8.26 (d, 4H), 8.15 (t, 3H), 8.03-7.92 (m, 7H), 7.60 (m, 2H), 7.33-7.08 (m, 80H), 4.65-4.42 (m, 17H), 4.38-4.11 (m, 17H), 3.22 (t, 1H), 3.11-2.54 (m, 34H), 2.03-1.89 (m, 7H), 1.73-1.59 (m, 7H), 1.44-1.25 (m, 9H), 1.10-0.94 (m, 8H) ppm. ^{13}C NMR: δ (DMSO- d_6 , 39.52 ppm) 173.05, 171.67-170.47, 138.00, 128.97, 127.86, 126.43, 122.38, 53.83, 50.04, 49.25, 43.78, 37.51, 36.61, 34.85, 27.56, 25.28, 24.46 ppm. MS (MALDI-ToF, m/z): $[\text{M}+\text{H}]^+$ calculated from $\text{C}_{179}\text{H}_{197}\text{N}_{31}\text{O}_{21}$: 3093.53, found 3092.69.

Fh•FFh•Fh•FFh. 3.81 g, 83% yield. ^1H NMR: δ (DMSO- d_6 , 2.50 ppm) 9.22-9.14 (m, 1H), 8.89 (t, 1H), 8.61 (dt, 1H), 8.25 (ddd, 3H), 7.71 (d, 2H), 7.40-7.07 (m, 30H), 4.61-4.44 (m, 4H), 4.38-4.11 (m, 14H), 3.22 (t, 2H), 3.14 (d, 1H), 3.07-2.93 (m, 6H), 2.79 (d, 1H), 2.67 (d, 2H), 2.12-1.93 (m, 8H), 1.80-1.61 (m, 7H), 1.50-1.27 (m, 9H), 1.19-0.99 (m, 8H) ppm. ^{13}C NMR: δ (DMSO- d_6 , 39.52 ppm) 171.41, 137.72, 129.06, 128.14, 122.28, 54.27, 49.22, 37.15, 34.86, 30.07, 28.06, 25.16 ppm. MS (MALDI-ToF, m/z): $[\text{M}+\text{H}]^+$ calculated from $\text{C}_{69}\text{H}_{90}\text{N}_{19}\text{O}_9$: 1622.85, found 1622.89.

Fh•FFFh•Fh•FFFh. 3.16 g, 87% yield. ^1H NMR: δ (DMSO- d_6 , 2.50 ppm) 8.54-8.38 (m, 3H), 8.22-7.89 (m, 8H), 7.65 (d, 3H), 7.35-7.08 (m, 40H), 4.61-4.37 (m, 8H), 4.37-4.14 (m, 14H), 3.20 (t, 2H), 3.07-2.58 (m, 18H), 2.13-1.91 (m, 8H), 1.79-1.58 (m, 8H), 1.47-1.28 (m, 10H), 1.16-0.94 (m, 9H) ppm. ^{13}C NMR: δ

(DMSO-*d*₆, 39.52 ppm) 173.24, 171.65-170.41, 144.62, 137.52, 129.23, 128.04, 126.35, 122.43, 53.88, 50.48, 49.13, 43.95, 37.40, 36.81, 34.75, 27.90, 25.55, 24.52 ppm. MS (MALDI-ToF, m/z): [M+H]⁺ calculated from C₁₀₅H₁₂₅N₂₃O₁₃: 1916.98, found 1917.04.

Fh•FFFh•FFFh•Fh. 1.75 g, 85% yield. ¹H NMR: δ (DMSO-*d*₆, 2.50 ppm) 8.55 (bs, 2H), 8.09 (ddd, 3H), 7.87 (d, 2H), 7.72 (s, 3H), 7.30-7.00 (m, 20H), 4.58-4.45 (m, 3H), 4.42-4.15 (m, 14H), 3.32 (t, 2H), 3.10-2.68 (m, 10H), 2.12-1.93 (m, 8H), 1.80-1.61 (m, 7H), 1.50-1.27 (m, 2H), 1.19-0.99 (m, 59H) ppm. ¹³C NMR: δ (DMSO-*d*₆, 39.52 ppm) 173.15, 171.19-170.63, 137.60, 129.23, 128.13, 126.17, 122.62, 53.76, 50.48, 49.14, 37.35, 36.79, 34.45, 29.29, 25.28, 24.54 ppm. MS (MALDI-ToF, m/z): [M+H]⁺ calculated from C₁₀₅H₁₂₅N₂₃O₁₃: 1916.98, found 1917.00.

Fu•Fu•Fu•Fu. 3.03 g, 85% yield. ¹H NMR: δ (DMSO-*d*₆, 2.50 ppm) 8.49 (bs, 2H), 8.12-7.81 (m, 4H), 7.71 (s, 3H), 7.29-7.11 (m, 20H), 4.55-4.43 (m, 3H), 4.39-4.22 (m, 14H), 3.31 (t, 2H), 3.07-2.68 (m, 10H), 2.09-1.94 (m, 8H), 1.86-1.67 (m, 7H), 1.53 (bt, 2H), 1.42-0.98 (m, 47H) ppm. ¹³C NMR: δ (DMSO-*d*₆, 39.52 ppm) 172.17, 171.42, 144.79, 138.06, 129.18, 128.15, 126.15, 122.49, 53.86, 50.66, 49.28, 37.71, 35.22, 34.38, 29.82, 28.80, 25.91, 25.18 ppm. MS (ESI, m/z): [M+H]⁺ calculated from C₆₉H₉₀N₁₉O₉: 1328.71, found 1328.72; [M+2H]²⁺ calculated from (C₆₉H₉₀N₁₉O₉)/2, found 664.86.

FFu•FFu•FFu•FFu. 1.75 g, 93% yield. ¹H NMR: δ (DMSO-*d*₆, 2.50 ppm) 8.45 (bs, 2H), 8.20-7.87 (m, 7H), 7.67 (s, 3H), 7.38-6.98 (m, 40H), 4.60-4.42 (m, 7H), 4.42-4.16 (m, 14H), 3.29 (t, 2H), 3.08-2.58 (m, 18H), 2.08-1.86 (m, 8H), 1.87-1.67 (m, 7H), 1.52 (bt, 2H), 1.39-0.93 (m, 58H) ppm. ¹³C NMR: δ (DMSO-*d*₆, 39.52 ppm) 172.16, 171.25, 144.59, 137.99, 129.25, 128.03, 125.92, 122.62, 53.95, 52.52, 50.63, 49.40, 37.31, 35.21, 34.38, 29.83, 28.88, 25.89, 25.15 ppm. MS (ESI, m/z): [M+H]⁺ calculated from C₁₂₅H₁₆₅N₂₃O₁₃: 2197.80, found 2198.30.

FFFu•FFFu•FFFu•FFFu. 2.66 g, 95% yield. ¹H NMR: δ (DMSO-*d*₆, 2.50 ppm) 8.41 (bs, 3H), 8.29-8.19 (m, 5H), 7.97 (d, 9H), 7.30-7.04 (m, 60H), 4.61-4.40 (m, 12H), 4.39-4.20 (m, 12H), 3.28 (t, 1H), 3.13-2.58 (m, 25H), 2.01-1.89 (m, 7H), 1.83-1.68 (m, 7H), 1.56-1.47 (m, 1H), 1.38-0.90 (m, 54H) ppm. ¹³C NMR: δ (DMSO-*d*₆, 39.52 ppm) 172.55, 171.20, 138.04, 129.11, 127.86, 126.06, 122.55, 53.91, 53.45, 50.61, 48.97, 37.24, 35.51, 34.43, 29.04, 28.44, 25.88, 25.13 ppm. MS (MALDI-ToF, m/z): [M+H]⁺ calculated from C₁₆₁H₂₀₁N₂₇O₁₇: 2785.57, found 2785.91.

FFFFu•FFFFu•FFFFu•FFFFu. 1.97 g, 71% yield. ¹H NMR: δ (DMSO-*d*₆, 2.50 ppm) 8.41 (bs, 2H), 8.35-8.21 (m, 4H), 8.10-7.80 (m, 9H), 7.63 (d, 2H), 7.32-7.03 (m, 80H), 4.66-4.41 (m, 20H), 4.41-4.15 (m, 21H), 3.30 (t, 1H), 3.16-2.55 (m, 34H), 2.00-1.88 (m, 7H), 1.83-1.65 (m, 7H), 1.54-1.44 (m, 1H), 1.36-0.92 (m, 52H) ppm. ¹³C NMR: δ (DMSO-*d*₆, 39.52 ppm) 172.74, 170.97, 138.07, 129.54, 128.29, 126.85, 122.61, 53.63, 49.57, 37.22, 35.24, 34.42, 29.87, 29.00, 28.30, 25.93, 25.56 ppm. MS (MALDI-ToF, m/z): [M+H]⁺ calculated from C₁₉₇H₂₃₇N₃₁O₂₁: 3373.84, found 3371.32.

Fu•FFu•Fu•FFu. 1.53 g, 92% yield. ¹H NMR: δ (DMSO-*d*₆, 2.50 ppm) 8.47 (bs, 3H), 8.19-8.05 (m, 5H), 7.69 (d, 3H), 7.31-7.08 (m, 30H), 4.55-4.40 (m, 6H), 4.39-4.10 (m, 13H), 3.29 (t, 2H), 3.30-2.65 (m, 13H),

2.10-1.94 (m, 8H), 1.81-1.63 (m, 8H), 1.50-1.40 (m, 2H), 1.38-0.80 (m, 60H) ppm. ^{13}C NMR: δ (DMSO- d_6 , 39.52 ppm) 173.23, 172.17, 137.78, 129.10, 128.07, 126.08, 122.72, 53.42, 50.53, 49.27, 36.75, 35.53, 35.08, 29.82, 28.44, 25.88, 25.14 ppm. MS (ESI, m/z): $[\text{M}+\text{H}]^+$ calculated from $\text{C}_{107}\text{H}_{147}\text{N}_{21}\text{O}_{11}$: 1903.49, found 1904.17.

Fu•FFFu•Fu•FFFu. 0.54 g, 72% yield. ^1H NMR: δ (DMSO- d_6 , 2.50 ppm) 8.45 (bs, 3H), 8.18-7.93 (m, 8H), 7.68 (d, 3H), 7.31-7.08 (m, 40H), 4.58-4.39 (m, 8H), 4.39-4.18 (m, 14H), 3.29 (t, 2H), 3.10-2.58 (m, 18H), 2.10-1.92 (m, 7H), 1.81-1.69 (m, 7H), 1.48 (bt, 2H), 1.39-0.94 (m, 58H) ppm. ^{13}C NMR: δ (DMSO- d_6 , 39.52 ppm) 172.0, 171.01, 137.85, 129.18, 127.83, 126.21, 122.42, 53.80, 50.49, 49.46, 37.67, 36.81, 35.10, 29.77, 28.41, 25.84, 25.16 ppm. MS (MALDI-ToF, m/z): $[\text{M}+\text{H}]^+$ calculated from $\text{C}_{125}\text{H}_{165}\text{N}_{23}\text{O}_{13}$: 2197.80, found 2197.31.

Fu•FFFu•FFFu•Fu. 2.37 g, 95% yield. ^1H NMR: δ (DMSO- d_6 , 2.50 ppm) 8.41 (bs, 3H), 8.23-7.88 (m, 8H), 7.64 (d, 3H), 7.32-7.05 (m, 40H), 4.61-4.16 (m, 36H), 3.29 (t, 1H), 3.09-2.52 (m, 18H), 2.05-1.90 (m, 7H), 1.81-1.67 (m, 6H), 1.53-1.44 (m, 2H), 1.40-0.91 (m, 47H) ppm. ^{13}C NMR: δ (DMSO- d_6 , 39.52 ppm) 173.35, 170.69, 137.59, 129.21, 128.07, 126.26, 122.59, 53.92, 50.59, 49.28, 37.68, 36.76, 35.08, 34.38, 28.43, 25.98, 25.17 ppm. MS (MALDI-ToF, m/z): $[\text{M}+\text{H}]^+$ calculated from $\text{C}_{125}\text{H}_{165}\text{N}_{23}\text{O}_{13}$: 2197.80, found: 2197.33.

Fh•FFFu•FFFh•Fh. 1.62 g, 81% yield. ^1H NMR: δ (DMSO- d_6 , 2.50 ppm) 8.39 (bs, 2H), 8.15-7.91 (m, 8H), 7.63 (d, 2H), 7.33-7.06 (m, 40H), 4.59-4.38 (m, 8H), 4.38-4.11 (m, 12H), 3.22 (t, 1H), 3.15-2.57 (m, 18H), 2.13-1.91 (m, 7H), 1.84-1.61 (m, 7H), 1.48-1.31 (m, 9H), 1.25-0.93 (m, 18H) ppm. ^{13}C NMR: δ (DMSO- d_6 , 39.52 ppm) 173.16, 170.55, 137.70, 129.18, 128.06, 126.23, 122.66, 53.87, 53.45, 50.38, 49.38, 37.61, 36.98, 35.14, 34.34, 29.75, 28.59, 28.38, 25.49, 24.98 ppm. MS (MALDI-ToF, m/z): $[\text{M}+\text{H}]^+$ calculated from $\text{C}_{110}\text{H}_{135}\text{N}_{23}\text{O}_{13}$: 1987.06, found 1987.02.

Fu•FFFh•FFFu•Fh. 1.80 g, 81% yield. ^1H NMR: δ (DMSO- d_6 , 2.50 ppm) 8.39 (bs, 2H), 8.18-7.89 (m, 8H), 7.64 (d, 2H), 7.33-7.05 (m, 40H), 4.59-4.37 (m, 9H), 4.38-4.10 (m, 12H), 3.22 (t, 1H), 3.12-2.60 (m, 19H), 2.05-1.91 (m, 7H), 1.81-1.61 (m, 7H), 1.41-1.29 (m, 8H), 1.25-0.95 (m, 18H) ppm. ^{13}C NMR: δ (DMSO- d_6 , 39.52 ppm) 172.86, 171.17, 137.81, 129.26, 128.21, 126.35, 122.76, 53.93, 53.29, 50.47, 49.32, 37.76, 37.04, 35.21, 34.41, 29.83, 28.88, 28.46, 25.90, 25.10 ppm. MS (MALDI-ToF, m/z): $[\text{M}+\text{H}]^+$ calculated from $\text{C}_{115}\text{H}_{145}\text{N}_{23}\text{O}_{13}$: 2057.14, found 2057.16.

FFFFb•FFFFb•FFFFb•FFFFb. 1.90 g, 85% yield. ^1H NMR: δ (DMSO- d_6 , 2.50 ppm) 12.76 (bs, 1H), 8.28-8.47 (m, 5H), 7.92-8.28 (m, 14H), 7.46-7.52 (m, 3H), 7.03-7.35 (m, 80H), 4.42-4.63 (m, 16H), 4.00-4.38 (m, 12H), 3.18 (t, 1H) 2.55-3.11 (m, 32H), 1.92-2.07 (m, 8H), 1.73-1.90 (m, 8H). ^{13}C NMR: δ (DMSO- d_6 , 39.52 ppm) 172.68, 171.06, 171.02, 170.89, 170.82, 170.69, 170.57, 170.51, 144.44, 137.98, 137.59, 137.51, 137.46, 137.35, 129.21, 129.12, 128.22, 128.08, 128.00, 127.94, 126.46, 126.32, 126.24, 126.18, 126.14, 122.41, 53.86, 53.67, 53.54, 53.48, 49.95, 48.63, 37.85, 37.63, 37.53, 37.41, 36.77,

34.34, 31.86, 25.94, 24.42. MS (MALDI-ToF, m/z): [M+H]⁺ calculated from C₁₆₉H₁₈₁N₃₁O₂₁: 2981.40, found 2982.37.

FFFFv•FFFFv•FFFFv•FFFFv. 1.35 g, 76% yield. ¹H NMR: δ (DMSO-*d*₆, 2.50 ppm) 12.79 (bs, 1H), 8.27-8.48 (m, 4H), 7.89-8.28 (m, 15H), 7.51-7.58 (m, 3H), 6.98-7.32 (m, 80H), 4.42-4.62 (m, 16H), 4.06-4.37 (m, 12H), 3.17 (t, 2H), 2.55-3.12 (m, 32H), 1.92-2.06 (m, 7H), 1.41-1.61 (m, 8H), 1.19-1.40 (m, 9H). ¹³C NMR: δ (DMSO-*d*₆, 39.52 ppm) 172.66, 171.43, 171.20, 171.13, 170.91, 170.70, 170.59, 170.57, 170.51, 144.47, 137.96, 137.57, 137.52, 137.48, 137.35, 129.21, 129.11, 128.21, 128.08, 128.00, 127.95, 127.89, 126.46, 126.29, 126.24, 126.19, 126.10, 122.43, 53.86, 53.70, 53.64, 53.55, 53.47, 50.29, 48.88, 43.76, 37.86, 37.66, 37.56, 37.45, 36.77, 34.43, 34.32, 34.25, 34.15, 28.96, 27.48, 22.44, 22.21, 21.93. MS (MALDI-ToF, m/z): [M+H]⁺ calculated from C₁₇₃H₁₈₉N₃₁O₂₁ 3037.47, found 3038.02.

FFFFe•FFFFe•FFFFe•FFFFe. 1.42 g, 77% yield. ¹H NMR: δ (DMSO-*d*₆, 2.50 ppm) 12.76 (bs, 1H), 8.30-8.47 (m, 4H), 7.82-8.27 (m, 15H), 7.53-7.63 (m, 3H), 6.95-7.33 (m, 80H), 4.40-4.64 (m, 16H), 4.12-4.40 (m, 12H), 3.23 (t, 2H), 2.55-3.12 (m, 32H), 1.85-2.01 (m, 7H), 1.58-1.75 (m, 6H), 1.36-1.48 (m, 1H), 1.18-1.36 (m, 8H), 0.90-1.18 (m, 15). ¹³C NMR: δ (DMSO-*d*₆, 39.52 ppm) 172.72, 172.04, 171.36, 171.27, 170.96, 170.80, 170.66, 170.61, 138.06, 137.59, 137.55, 137.52, 137.40, 129.28, 129.17, 128.27, 128.16, 128.09, 128.03, 127.95, 126.54, 126.37, 126.30, 126.27, 126.16, 122.53, 53.99, 53.86, 53.71, 53.65, 53.57, 50.63, 49.30, 43.84, 37.85, 37.68, 37.58, 37.37, 36.81, 35.12, 34.44, 29.70, 27.80, 25.65, 24.99, 22.27, 21.68. MS (MALDI-ToF, m/z): [M+H]⁺ calculated from C₁₈₁H₂₀₅N₃₁O₂₁: 3149.59, found 3150.95.

5. Cleavage of Fmoc-protected phenylalanine from Tentagel® resin

Approximately 100 mg of Tentagel® S PHB resin was added to an SPE tube and swollen for 10 min using 10 mL of CH₂Cl₂. After this, the resin was washed six times with 10 mL of DMF followed by six times with 10 mL CH₂Cl₂ before transferring the resin to a round-bottom flask. The cleavage solution (10 mL of 95/2.5/2.5 TFA/TIPS/H₂O) to the flask and agitated for 2 h. The filtrate was then collected in a clean round-bottom flask and concentrated by rotary evaporation.

6. Synthesis of macromolecules based on phenylalanine and aliphatic building blocks using a Tentagel® resin

Tentagel® S PHB resin functionalised with a protected phenylalanine residue (loading density in phenylalanine: 0.24 mmol per gram of resin) was subjected to addition of the different building blocks as illustrated below for the solid-phase synthesis of FFFFh•FFFFh•FFFFh•FFFFh.

i) Deprotection of functionalised Tentagel® resin

3 g of Tentagel® resin (0.72 mmol of functional groups) was weighted in a SPE tube, swollen in 10 mL of CH₂Cl₂ for 10 min and washed three times with 10 mL of CH₂Cl₂. The Fmoc-protecting groups were removed by agitation for 3 min with 10 mL of a 25% piperidine solution in DMF followed by filtration

and agitation with a fresh cleavage solution for 20 min. The resin was then washed six times with 10 mL of DMF and six times with 10 mL of CH₂Cl₂.

ii) Addition of 6-azidohexanoic acid

6-Azidohexanoic acid (0.35 g, 2.19 mmol), HBTU (0.83 g, 2.18 mmol), HOBt (0.29 g, 2.17 mmol), DIPEA (0.70 mL, 4.05 mmol) and a 1/1/1 mixture of CH₂Cl₂/DMF/NMP (10 mL) were added to the vessel and agitated for 1 h. After filtration, the resin was washed six times with 10 mL of DMF and six times with 10 mL of CH₂Cl₂.

iii) Copper-assisted alkyne-azide cycloaddition with propargylamine

CuBr (27 mg, 0.19 mmol) was added to the vessel, which was then degassed through three vacuum/argon cycles. Anhydrous CH₂Cl₂ (10 mL) were added to the vessel, followed by PMDETA (0.07 mL, 0.34 mmol) and propargylamine (0.14 mL, 2.23 mmol). The solution was agitated under argon for 1 h. After filtration, the resin was washed six times with 10 mL of DMF and six times with 10 mL of CH₂Cl₂.

iv) Addition of Fmoc-L-Phe-OH

Fmoc-L-Phe-OH (0.84 g, 2.19 mmol), HBTU (0.83 g, 2.18 mmol), HOBt (0.29 g, 2.17 mmol), DIPEA (0.70 mL, 4.05 mmol) and a 1/1/1 mixture of CH₂Cl₂/DMF/NMP (10 mL) were added to the peptide vessel, and agitated for 1 h. After filtration, the resin was washed six times with 10 mL of DMF. The Fmoc-protecting group was removed by agitation with 10 mL of a 25% piperidine in DMF solution for 3 min followed by filtration and agitation with a fresh solution of piperidine for 20 min. The resin was then washed six times with 10 mL of DMF and six times with 10 mL of CH₂Cl₂.

v) Cleavage from the resin and recovery of the phenylalanine-based oligomer

The resin was washed twelve times with 10 mL of CH₂Cl₂ before transferring the resin to a round-bottom flask and adding the cleavage solution (10 mL of 95/2.5/2.5 TFA/TIPS/H₂O) to the flask. The resin was agitated with the cleavage solution for 2 h and collected in a clean round-bottom flask. These tasks were performed three times. The resin was then washed six times with 10 mL of CH₂Cl₂. The filtrates were combined, stirred with CupriSorb™ overnight to remove residual copper, concentrated into a viscous solution by rotary evaporation and precipitated in diethyl ether to remove TFA and TIPS followed by precipitation in reverse-osmosed water. Aggregates of oligomers were crushed to obtain a finely dispersed powder, which was washed six times with 10 mL of reversed-osmosed water. The product was then frozen in liquid nitrogen and subjected to six vacuum-argon cycles (these tasks were performed three times) before drying it under vacuum overnight at room temperature.

For select compounds further purification was performed using reverse phase column chromatography and concentrated HCl/water/THF (15/25/60 by volume) as eluent.

All reactions have been monitored using Kaiser test conditions inspired by literature [E.4]: Several beads of resin were placed in a 1/1/1 by volume solution of 0.28 M ninhydrin in ethanol/21M phenol

in ethanol/0.01M KCN_(aq) in pyridine (1/49). The suspension was heated by heat gun pre-set to 120 °C while agitating manually for 5 min. After this, if no colour change was detected, the suspension was further heated by heat gun pre-set to 200 °C while agitating manually for 3 min.

Fh•Fh•Fh•Fh. 16 mg, 5% yield. ¹H NMR: δ (DMSO-*d*₆, 2.50 ppm) 12.65 (bs, 1H), 8.35-8.58 (m, 3H), 7.92-8.20 (m, 4H), 7.69 (s, 3H), 6.90-7.51 (m, 20H), 4.37-4.69 (m, 4H), 4.07-4.37 (m, 12H), 3.51 (PEG), 3.22 (t, 2H), 2.69-3.08 (m, 8H), 1.92-2.18 (m, 8H), 1.56-1.90 (m, 6H), 1.25-1.53 (m, 10H), 0.97-1.15 (m, 8H). ¹³C NMR: δ (DMSO-*d*₆, 39.52 ppm) 173.16, 171.84, 171.81, 171.22, 137.96, 137.71, 129.14, 129.03, 128.09, 127.94, 126.31, 126.14, 122.43, 69.77 (PEG), 53.73, 53.20, 50.46, 49.09, 37.77, 36.76, 34.94, 34.89, 34.76, 34.31, 29.47, 27.89, 25.52, 25.25, 24.60, 24.50, 24.48. MS (ESI, m/z): [M+H]⁺ calculated from C₆₉H₉₁N₁₉O₉: 1328.70, found 1328.70; [M+2H]²⁺ calculated from C₆₉H₉₂N₁₉O₉: 665.85, found 664.90.

FFh•FFh•FFh•FFh. 84 mg, 19% yield. ¹H NMR: δ (DMSO-*d*₆, 2.50 ppm) 12.78 (bs, 1H), 8.36-8.50 (m, 2H), 8.15-8.26 (m, 2H), 7.80-8.11 (m, 7H), 7.53-7.74 (m, 3H), 6.89-7.48 (m, 40H), 4.40-4.61 (m, 8H), 4.07-4.38 (m, 12H), 3.51 (PEG), 3.22 (t, 2H), 2.61-3.12 (m, 16H), 1.86-2.05 (m, 8H), 1.59-1.74 (m, 6H), 1.20-1.53 (m, 10H), 0.89-1.18 (m, 8H). ¹³C NMR: δ (DMSO-*d*₆, 39.52 ppm) 172.66, 171.83, 171.68, 171.43, 171.11, 170.53, 137.94, 137.48, 137.34, 129.21, 129.13, 129.10, 128.14, 127.99, 127.88, 126.40, 126.23, 126.09, 122.39, 69.76 (PEG), 53.62, 53.39, 53.35, 50.4, 49.07, 37.73, 37.45, 37.29, 36.62, 34.87, 34.32, 29.48, 27.87, 25.48, 25.23, 24.59, 24.47. MS (ESI, m/z): [M+2H]²⁺ calculated from C₁₀₅H₁₂₇N₂₃O₁₃: 959.99, found: 959.50.

FFFh•FFFh•FFFh•FFFh. 169 mg, 29% yield. ¹H NMR: δ (DMSO-*d*₆, 2.50 ppm) 12.77 (bs, 1H), 8.36-8.44 (m, 2H), 8.26-8.32 (m, 2H), 8.13-8.22 (m, 2H), 7.79-8.08 (m, 9H), 7.49-7.72 (m, 3H), 6.91-7.45 (m, 60H), 4.42-4.61 (m, 12H), 4.05-4.37 (m, 12H), 3.51 (PEG), 3.20 (t, 2H), 2.58-3.09 (m, 24H), 1.84-2.06 (m, 8H), 1.59-1.72 (m, 6H), 1.19-1.47 (m, 10H), 0.88-1.12 (m, 8H). ¹³C NMR: δ (DMSO-*d*₆, 39.52 ppm) 172.62, 171.69, 171.22, 171.12, 170.86, 170.55, 170.47, 137.98, 137.50, 137.47, 137.32, 129.24, 129.19, 129.09, 128.18, 128.03, 127.95, 127.87, 126.42, 126.24, 126.20, 126.20, 126.06, 122.40, 69.78 (PEG), 53.82, 53.72, 53.52, 53.45, 53.42, 50.44, 49.07, 37.75, 37.55, 37.38, 36.71, 34.87, 34.33, 29.49, 27.87, 25.47, 25.23, 24.59, 24.47.

FFFFh•FFFFh•FFFFh•FFFFh. Batch 1: 160 mg, 22% yield, batch 2: 601 mg, 28% yield. ¹H NMR: δ (DMSO-*d*₆, 2.50 ppm) 12.77 (bs, 1H), 8.24-8.53 (m, 4H), 7.77-8.28 (m, 15H), 7.52-7.65 (m, 3H), 6.82-7.45 (m, 80H), 4.38-4.67 (m, 16H), 4.07-4.38 (m, 12H), 3.50 (PEG), 3.20 (t, 2H), 2.56-3.11 (m, 32H), 1.84-2.01 (m, 8H), 1.56-1.74 (m, 6H), 1.21-1.43 (m, 10H), 0.91-1.10 (m, 8H). ¹³C NMR: δ (DMSO-*d*₆, 39.52 ppm) 172.61, 171.68, 171.10, 170.84, 170.53, 137.98, 137.54, 137.49, 137.46, 137.33, 135.87, 129.19, 129.08, 128.18, 128.04, 127.97, 127.91, 127.86, 126.42, 126.19, 126.14, 126.05, 122.38, 69.77 (PEG), 53.83, 53.57, 53.44, 50.43, 49.05, 37.60, 37.51, 37.31, 36.74, 34.92, 34.86, 34.31, 29.46, 27.84, 25.45, 25.22, 24.58, 24.46.

FFFFb•FFFFb•FFFFb•FFFFb. Batch 1: 177 mg, 35% yield, batch 2: 427 mg, 31% yield. ¹H NMR: δ (DMSO-*d*₆, 2.50 ppm) 12.77 (bs, 1H), 8.26-8.44 (m, 5H), 7.92-8.26 (m, 14H), 7.46-7.54 (m, 3H), 6.99-7.33 (m, 80H), 4.41-4.62 (m, 16H), 3.99-4.41 (m, 12H), 3.50 (PEG), 2.54-3.12 (m, 32H), 1.91-2.05 (m, 8H), 1.75-1.89 (m, 8H). ¹³C NMR: δ (DMSO-*d*₆, 39.52 ppm) 172.63, 171.09, 171.02, 170.86, 170.78, 170.68, 170.59, 170.47, 144.39, 137.97, 137.58, 137.49, 137.44, 137.33, 129.20, 129.08, 128.19, 128.05, 127.98, 127.92, 126.44, 126.29, 126.21, 126.15, 126.11, 122.50, 69.78 (PEG), 53.83, 53.64, 53.50, 53.46, 49.93, 48.60, 37.85, 37.63, 37.50, 37.41, 36.75, 34.29, 31.83, 24.39.

FFFFv•FFFFv•FFFFv•FFFFv. Batch 1: 115 mg, 17% yield, batch 2: 450 mg, 29% yield. ¹H NMR: δ (DMSO-*d*₆, 2.50 ppm) 12.77 (bs, 1H), 8.27-8.46 (m, 4H), 7.87-8.27 (m, 15H), 7.50-7.57 (m, 3H), 6.97-7.37 (m, 80H), 4.37-4.66 (m, 16H), 4.08-4.37 (m, 12H), 3.50 (PEG), 3.17 (t, 2H), 2.56-3.11 (m, 32H), 1.89-2.05 (m, 8H), 1.40-1.60 (m, 6H), 1.14-1.40 (m, 10H). ¹³C NMR: δ (DMSO-*d*₆, 39.52 ppm) 172.64, 171.36, 171.16, 171.08, 170.86, 170.64, 170.55, 170.47, 169.08, 144.36, 137.95, 137.54, 137.50, 137.46, 137.33, 129.19, 129.09, 128.19, 128.04, 127.99, 127.92, 127.86, 126.43, 126.27, 126.21, 126.15, 126.07, 122.42, 69.78 (PEG), 53.83, 53.64, 53.58, 53.49, 53.45, 53.40, 50.27, 48.84, 37.84, 37.63, 37.53, 37.41, 36.73, 34.40, 34.29, 34.22, 34.15, 28.96, 27.45, 22.45, 22.19, 21.88.

FFFFu•FFFFu•FFFFu•FFFFu. Batch 1: 177 mg, 23% yield, batch 2: 366 mg, 26% yield. ¹H NMR: δ (DMSO-*d*₆, 2.50 ppm) 12.77 (bs, 1H), 8.35-8.42 (m, 2H), 8.28-8.35 (m, 2H), 8.14-8.21 (m, 2H), 8.02-8.12 (m, 4H), 7.82-8.01 (m, 9H), 7.59-7.65 (m, 3H), 7.02-7.31 (m, 80H), 4.39-4.63 (m, 16H), 4.18-4.39 (m, 12H), 3.50 (PEG), 3.29 (t, 2H), 2.55-3.11 (m, 32H), 1.87-1.99 (m, 8H), 1.66-1.78 (m, 8H), 1.45-1.55 (m, 2H), 0.91-1.35 (m, 54H). ¹³C NMR: δ (DMSO-*d*₆, 39.52 ppm) 172.60, 172.00, 171.94, 171.25, 171.13, 170.82, 170.65, 170.52, 170.46, 169.10, 144.46, 138.01, 137.55, 137.50, 137.33, 129.19, 129.08, 128.18, 128.04, 127.98, 127.91, 127.84, 126.42, 126.41, 126.18, 126.13, 126.01, 122.42, 69.78 (PEG), 54.90, 53.90, 53.75, 53.58, 53.51, 53.46, 53.45, 49.24, 37.75, 37.62, 37.50, 37.23, 36.73, 35.16, 34.33, 34.18, 29.80, 28.84, 28.78, 28.74, 28.40, 25.85, 25.09.

Fh•FFFh•Fh•FFFh. 175 mg, 40% yield. ¹H NMR: δ (DMSO-*d*₆, 2.50 ppm) 12.65 (bs, 1H), 8.35-8.53 (m, 3H), 8.07-8.19 (m, 4H), 7.88-8.03 (m, 4H), 7.58-7.70 (m, 3H), 6.93-7.48 (m, 40H), 4.40-4.59 (m, 8H), 4.13-4.31 (m, 12H), 3.51 (PEG), 3.20 (t, 2H), 2.70-3.07 (m, 16H), 1.91-2.06 (m, 8H), 1.58-1.72 (m, 6H), 1.27-1.53 (m, 10H), 0.97-1.14 (m, 8H). ¹³C NMR: δ (DMSO-*d*₆, 39.52 ppm) 173.14, 171.91, 171.74, 171.21, 170.54, 170.47, 144.43, 137.97, 137.69, 137.46, 129.18, 129.14, 129.08, 129.02, 128.08, 128.03, 127.99, 127.93, 127.87, 126.30, 126.24, 126.18, 126.11, 126.06, 122.37, 69.73 (PEG), 53.82, 53.72, 53.46, 53.20, 49.09, 37.73, 37.41, 37.31, 36.75, 34.87, 34.75, 34.32, 29.48, 25.26, 24.49. MS (ESI, m/z): [M+2H]²⁺ calculated from C₁₀₅H₁₂₇N₂₃O₁₃: 959.99, found 959.50.

Fh•FFFh•FFFh•Fh. 114 mg, 26% yield. ¹H NMR: δ (DMSO-*d*₆, 2.50 ppm) 12.66 (bs, 1H), 8.35-8.51 (m, 2H), 7.79-8.24 (m, 9H), 7.50-7.74 (m, 3H), 6.86-7.48 (m, 40H), 4.38-4.62 (m, 8H), 4.05-4.37 (m, 12H), 3.51 (PEG), 3.22 (t, 2H), 2.58-3.09 (m, 16H), 1.88-2.06 (m, 8H), 1.61-1.73 (m, 6H), 1.25-1.48 (m, 10H),

0.95-1.15 (m, 8H). ^{13}C NMR: δ (DMSO- d_6 , 39.52 ppm) 173.15, 171.90, 171.84, 171.75, 171.21, 170.54, 170.48, 137.97, 137.71, 137.46, 129.19, 129.13, 129.07, 129.03, 128.08, 128.03, 127.94, 127.87, 126.31, 126.25, 126.17, 126.12, 126.06, 122.42, 69.75 (PEG), 53.82, 53.74, 53.71, 53.45, 53.19, 50.46, 49.09, 37.73, 37.42, 37.31, 36.75, 34.95, 34.85, 34.74, 34.31, 29.48, 27.88, 25.51, 25.25, 24.59, 24.49. MS (ESI, m/z): $[\text{M}+2\text{H}]^{2+}$ calculated from $\text{C}_{105}\text{H}_{127}\text{N}_{23}\text{O}_{13}$: 959.99, found 959.50.

Fh•FFFu•FFFh•Fh. 166 mg, 36% yield. ^1H NMR: δ (DMSO- d_6 , 2.50 ppm) 12.65 (bs, 1H), 8.33-8.44 (m, 2H), 7.82-8.24 (m, 9H), 7.52-7.73 (m, 3H), 6.94-7.43 (m, 40H), 4.39-4.59 (m, 8H), 4.05-4.35 (m, 12H), 3.51 (PEG), 3.20 (t, 2H), 2.59-3.08 (m, 16H), 1.84-2.07 (m, 8H), 1.64-1.77 (m, 6H), 0.95-1.44 (m, 26H). ^{13}C NMR: δ (DMSO- d_6 , 39.52 ppm) 173.14, 171.99, 171.90, 171.24, 170.55, 170.51, 170.45, 137.96, 137.68, 137.44, 129.16, 129.05, 129.00, 128.06, 128.02, 127.92, 127.82, 126.29, 126.22, 126.14, 126.02, 122.45, 69.71 (PEG), 53.82, 53.69, 53.48, 53.16, 50.41, 49.19, 49.04, 37.71, 37.38, 37.28, 37.18, 36.73, 35.13, 34.73, 34.31, 29.76, 29.46, 28.83, 28.76, 28.72, 28.39, 27.87, 25.84, 25.24, 25.08, 24.48. MS (ESI, m/z): $[\text{M}+2\text{H}]^{2+}$ calculated from $\text{C}_{115}\text{H}_{137}\text{N}_{23}\text{O}_{13}$: 995.03, found 994.00.

7. Preparation of aramid fibre pellet

74 mg of powder material was taken and 'loaded' into a metal crucible, pushing the fibres down using a tweezer. A metal cylinder was then placed on top, pushed inside by hand and the crucible was placed inside the hydraulic press. The pressure was then manually increased to 14*1000 kg and remained on this pressure to stabilise for ~10 s. Pressure was then released and the aramid fibre pellet could be obtained from the crucible. The weight of the pellet was recorded.

8. Procedures for the coating process of aramid fibre bundles

Oligomers used for the coating procedure (FFFFb•FFFFb•FFFFb•FFFFb, FFFv•FFFv•FFFv•FFFv, FFFFh•FFFh•FFFh•FFFh and FFFu•FFFu•FFFu•FFFu) were all synthesised using Tentagel[®] resin as described in Chapter II.

i) Spray coating procedure

Three to five individual aramid short fibres (SFA A) were held in place by PTFE or PTFE coated tweezers, fastened through the use of tie-wrap. Coating solution was prepared by dissolving 0.01 mmol of coating molecule in 1 mL 95/5 ACN/TFA. Subsequently, the suction tube of the disposable HDPE spray head was placed in the solution and used to gently spray the fibres, rotating the spray head with each consecutive spray movement until no more liquid could be seen exiting the spray head. After treatment, coated fibres were left to dry on the tweezers for 3 h.

ii) Dip coating procedure

Three to five individual aramid short fibres (SFA A) were held in place by PTFE or PTFE coated tweezers, fastened through the use of tie-wrap. Coating solution was prepared by dissolving 0.002 mmol of coating molecule in 2 mL 95/5 ACN/TFA (toluene in the case of PS2.1k). Subsequently the solution was

emptied into a Petri dish (diameter = 3.5 cm, height = 1 cm) and fibres were dipped into solution for 5 min. After treatment, coated fibres were left to dry on the tweezers for 3 h.

9. Procedure for the coating process of aramid fibre pellets

Aramid fibre (SFA A) pellets were held in place by PTFE or PTFE coated tweezers, fastened through the use of tie-wrap. Coating solution was prepared by dissolving 0.002 mmol coating molecule in 2 mL 95/5 ACN/TFA (toluene in the case of PS2.1k). Subsequently the solution was emptied into a Petri dish (diameter = 3.5 cm, height = 1 cm) and fibre pellets were dipped into solution to fully submerge for a desired amount of time, turning the pellet midway through. After treatment, coated fibres were left to dry on the tweezers overnight, after which the weight difference was recorded. All weights recorded were a result of an average of 2-3 separate instances of the same sample being weighted.

10. Preparation and analysis of samples with SEM/EDS

i) Preparation of compounded samples from powder material

1-2 mg of powder material was taken and 'loaded' into a metal crucible, spreading the powder evenly across the surface. A metal cylinder was then placed on top, pushed inside by hand and the crucible was placed inside the hydraulic press. The pressure was then manually increased to 10*1000 kg and remained on this pressure to stabilise for ~5 s. Pressure was then released and the compound could be obtained from the crucible.

Subsequently, the compound was attached to a carbon substrate on a stainless steel plate, which was treated with platinum sputter coating. SEM/EDS analysis followed with SEM images taken at 15 keV with a spot size of 55 and EDS spectra taken at 5 keV with a spot size of 62 and measuring time of 60 s using Aztec X-ray module.

ii) Preparation of treated fibre samples

Coated fibres as described in section 8 were placed on two carbon substrates on a metal plate in a zigzag pattern, alternating between the two substrates until the whole length of the fibres were stretched out in the space between the two substrates. In the case of fibre pellet (Section 9), a single carbon substrate sufficed. Subsequently, the substrate was treated with platinum sputter coating. SEM/EDS analysis followed with SEM images taken at 15 keV with a spot size of 55 and EDS spectra taken at 5 keV with a spot size of 62 and measuring time of 60 s using Aztec X-Ray module (or 35 s using X-Max X-ray module).

iii) Preparation of fibre/PP composite

Untreated or treated aramid fibres were sandwiched between two layers of polypropylene using eight to ten granules for each layer in a ceramic crucible (bottom diameter of 13 mm). The crucible was placed in a thermostated oven at 180 °C for 15 min to melt the polypropylene, after which the crucible was removed and allowed to cool down at RT for 15 min. After this, the composite was removed from

the crucible by gently pulling. The composite was then plunged into liquid nitrogen for 10 min after which it was fractured by hammer and pick. Fragments of the composite were placed on several carbon substrates. Subsequently, the substrate was treated with platinum sputter coating. SEM/EDS analysis followed with SEM images taken at 15 keV with a spot size of 55 and EDS spectra taken at 5 keV with a spot size of 62 and measuring time of 35 s using X-Max X-ray module.

11. Preparation of samples for analysis by UV-Vis

Absorption values were taken from the main absorption peak, which was in all cases the aromatic absorption peak at ~262 nm. Tetraglycine showed no absorption due to solvent cut-off.

i) Determination of the baseline formula

A triplicate series of varying concentration in 2 mL 95/5 ACN/TFA or toluene (in the case of PS2.1k) was made by diluting from a 10 mL stock concentration five times, halving concentration at each step. Starting concentrations are listed below. UV-Vis baseline formulas were then made by means of trend line between the absorption values for the different concentrations

Compound	Concentration (mmol·mL ⁻¹)
PS2.1k	5.95*10 ⁻⁴
Tetraphenylalanine	1.65*10 ⁻³
FbFbFbFb	5.28*10 ⁻⁴
FvFvFvFv	6.98*10 ⁻⁴
FhFhFhFh	6.61*10 ⁻⁴
FFFFb•FFFFb•FFFFb•FFFFb	3.36*10 ⁻⁴
FFFFv•FFFFv•FFFFv•FFFFv	3.29*10 ⁻⁴
FFFFh•FFFFh•FFFFh•FFFFh	3.23*10 ⁻⁴
FFFFu•FFFFu•FFFFu•FFFFu	2.96*10 ⁻⁴

ii) Procedure for measuring deposited coatings

Five to ten individual aramid short fibres were treated by dip coating as described in Section 8.ii using 1 mL 95/5 ACN/TFA (toluene in case of PS2.1k) for a concentration of 0.01 mmol·mL⁻¹ (0.004 mmol·mL⁻¹ in the case of FFFFu•FFFFu•FFFFu•FFFFu). Absorption values were measured and quantity of coating was determined using baseline formula.

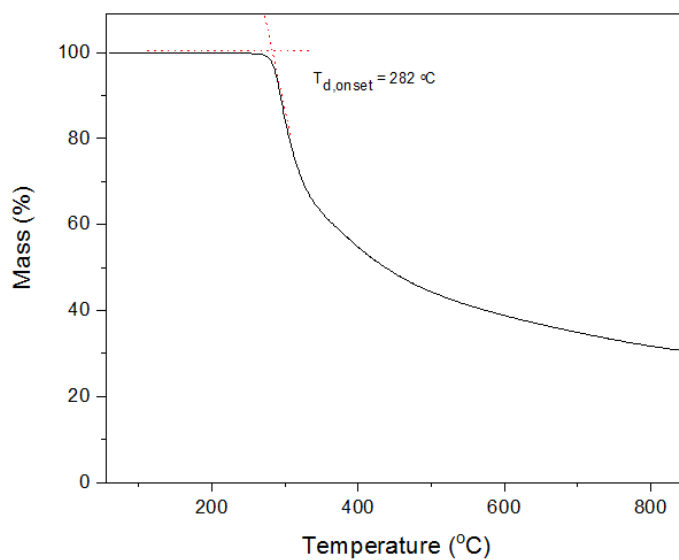
Appendix A: Thermal analysis

This appendix depicts all the thermal analyses conducted on the molecules listed in Table III.1 that have not been shown in Chapter III.

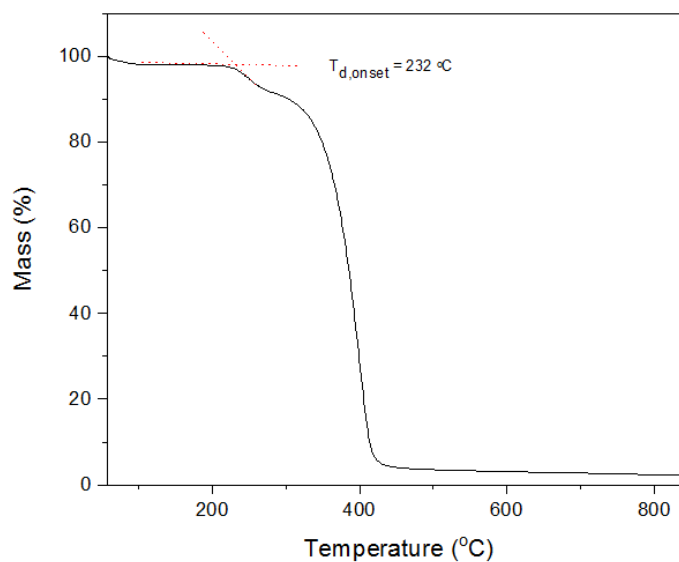
A.1. Overview of thermogravimetric results

TGA were performed under a constant N₂ flow rate of 10 cm³·min⁻¹ and using a heating rate of 50 °C·min⁻¹.

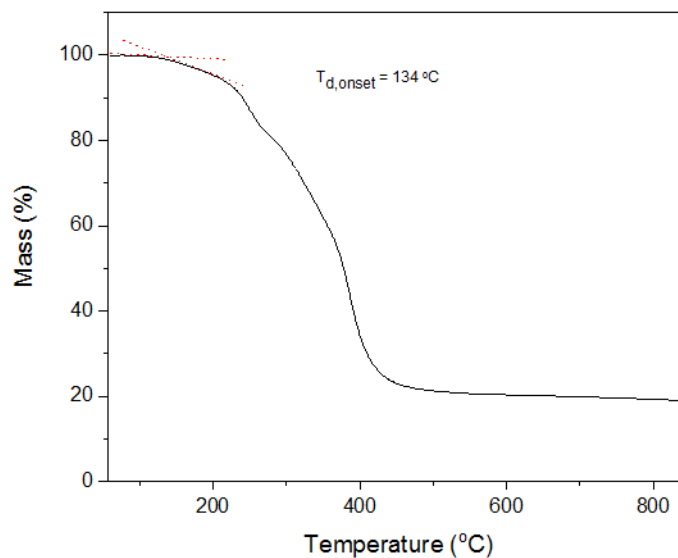
GGGG



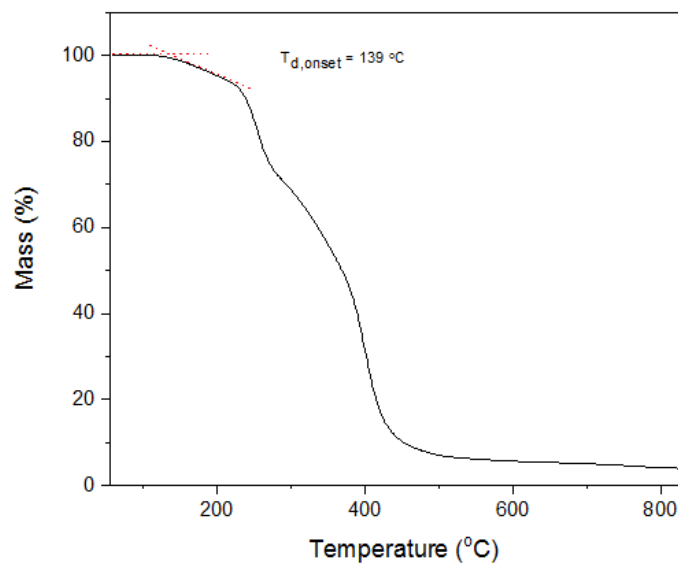
FFFF



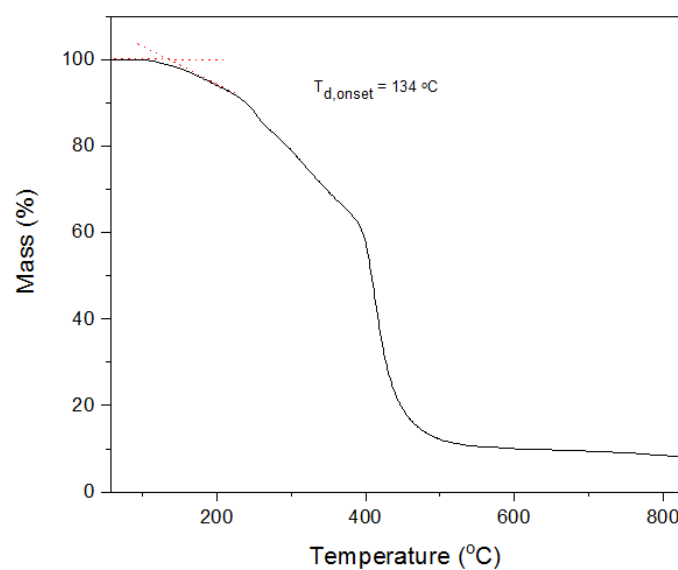
FbFbFbFb



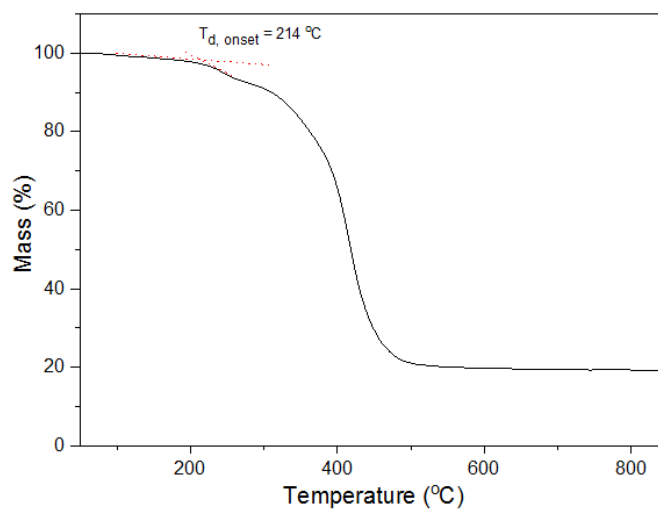
FvFvFvFv



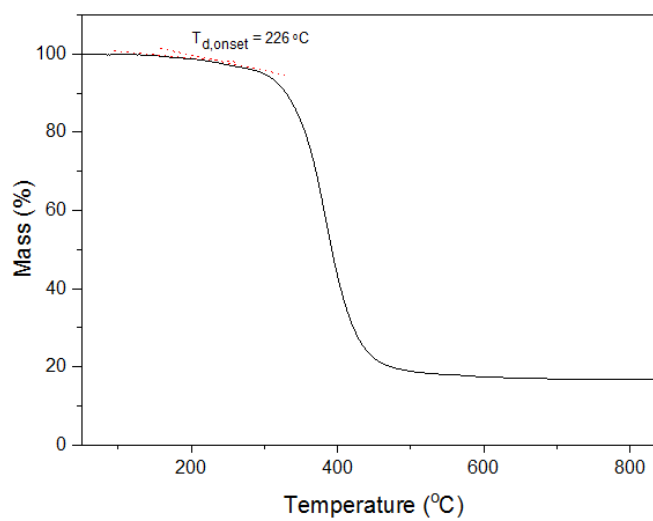
FhFhFhFh



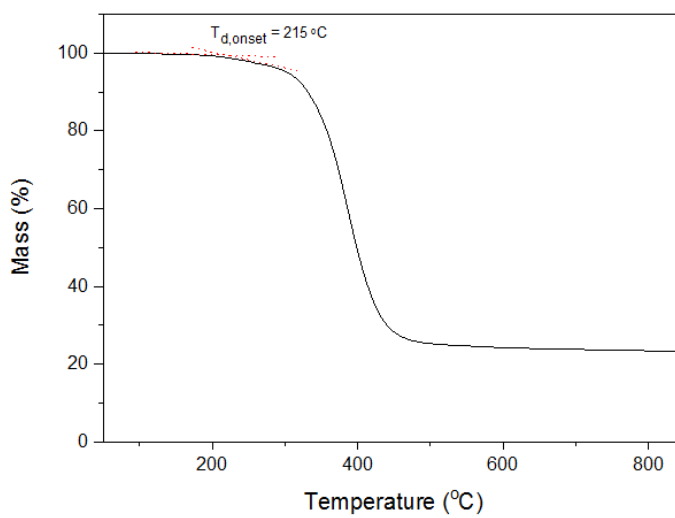
Fh•Fh•Fh•Fh



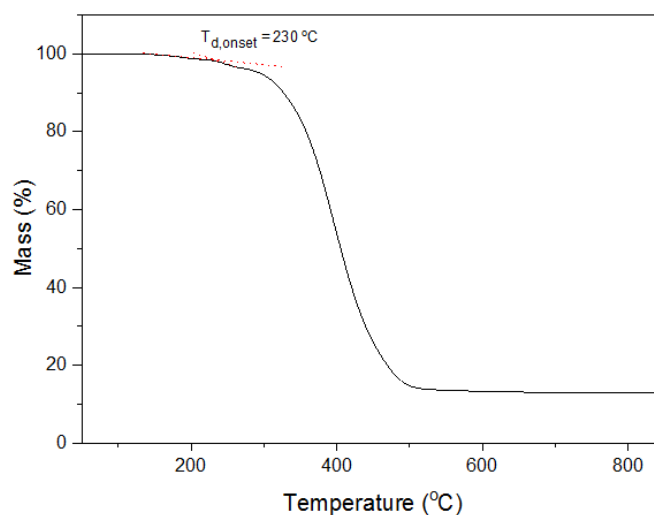
FFFFb•FFFFb•FFFFb•FFFFb



FFFFv•FFFFv•FFFFv•FFFFv



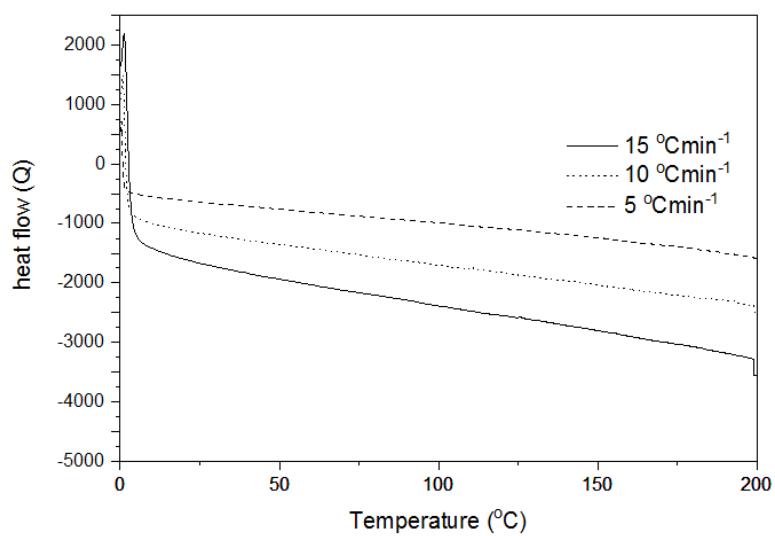
FFFFu•FFFFu•FFFFu•FFFFu



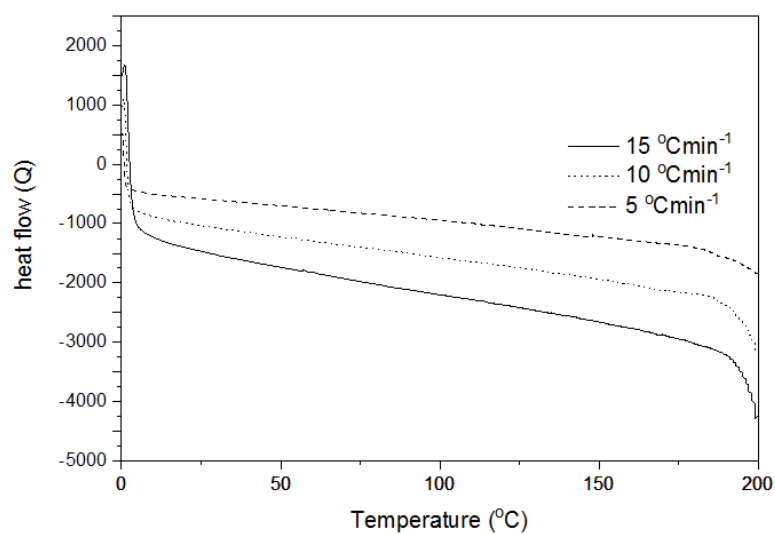
A.2. Overview of differential scanning calorimetry results

DSC experiments were performed under a constant N_2 flow rate of $10\text{ cm}^3\cdot\text{min}^{-1}$.

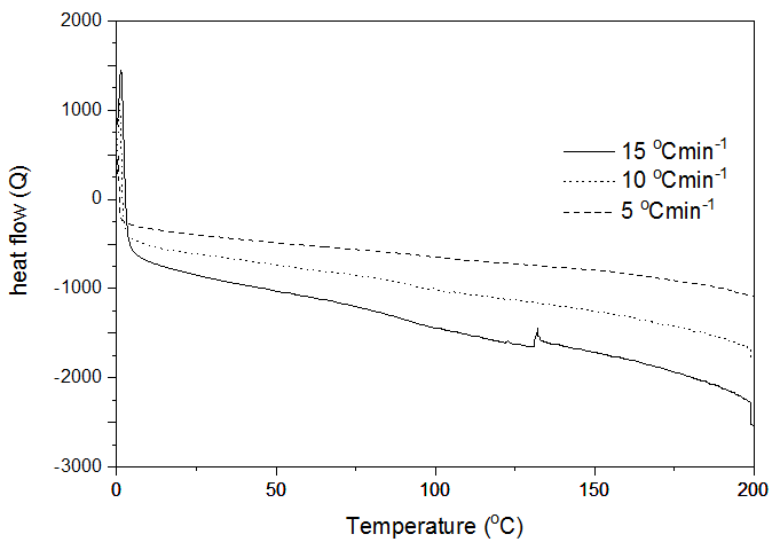
GGGG



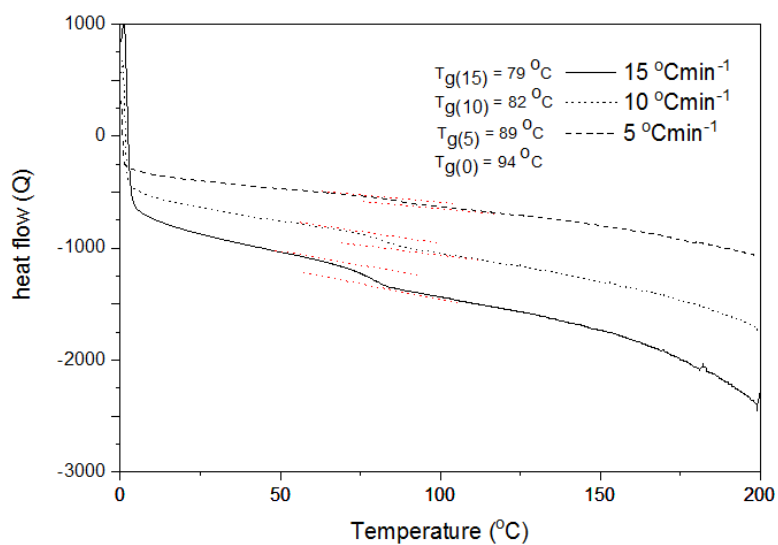
FFFF



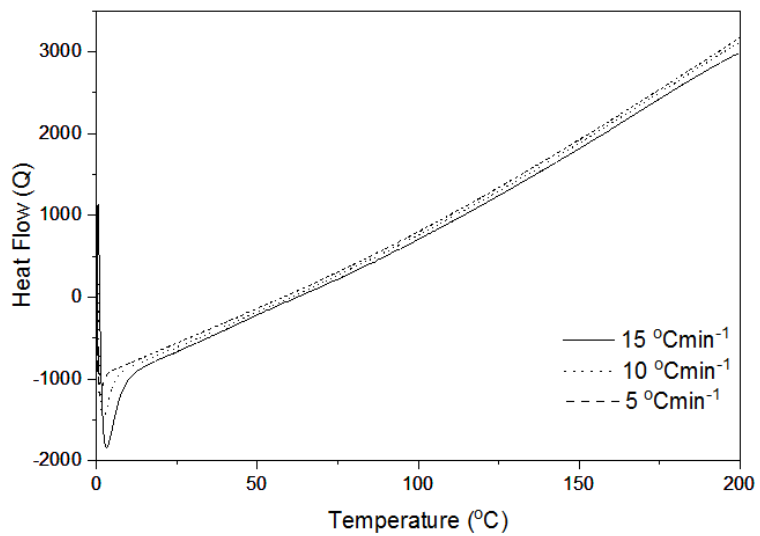
FbFbFbFb



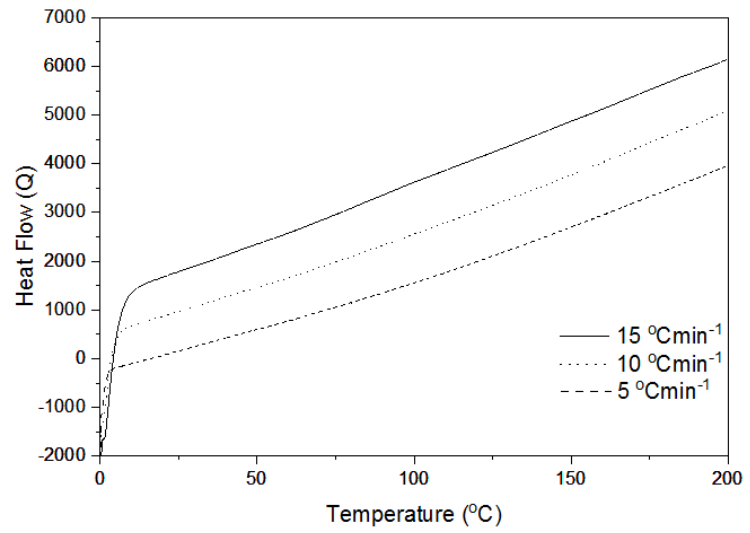
FhFhFhFh



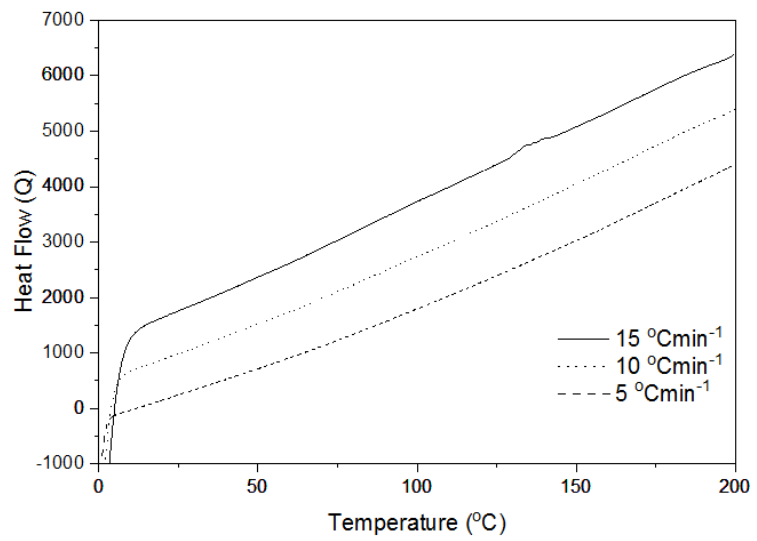
Fh•Fh•Fh•Fh



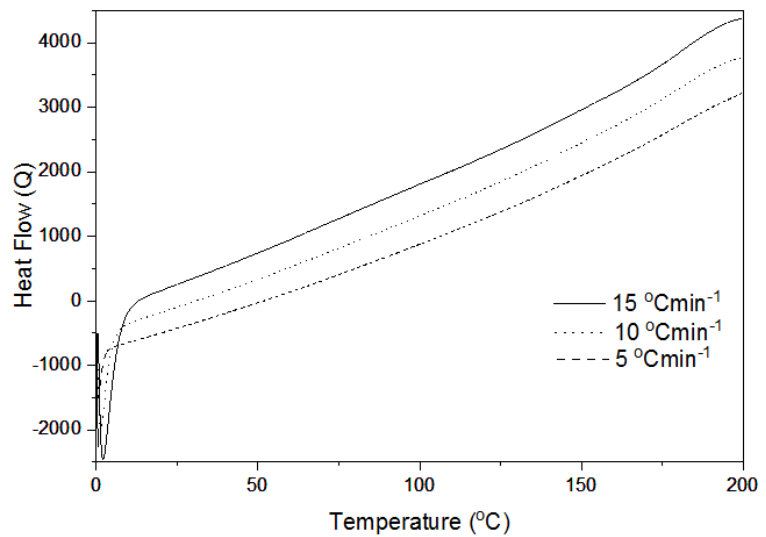
FFFFb•FFFFb•FFFFb•FFFFb



FFFFv•FFFFv•FFFFv•FFFFv



FFFFu•FFFFu•FFFFu•FFFFu



Appendix B: EDS analysis

Total absolute differences are calculated by adding the differences in absolute C, N, O values between experimental values of compounds or untreated aramid fibre vs. calculated values ($|\Delta\alpha| = \Delta\alpha_C + \Delta\alpha_N + \Delta\alpha_O$) or the first vs. experimental values of treated aramid fibres ($|\Delta A| = \Delta A_C + \Delta A_N + \Delta A_O$).

B.1. Short aramid fibre

Two different X-ray probes (AZTEC and Oxford X-MAX) have been used for characterisation. Relative comparisons with untreated Kevlar fibre were done appropriately using either experimental results.

Table B.1: Atomic composition of untreated aramid fibres given by EDS analysis using AZTEC probe

Spot#	%C	%N	%O	%C/%N	%C/%O	
1	69.00	13.40	17.60	5.15	3.92	
2	68.20	13.30	18.50	5.13	3.69	
3	72.60	10.50	16.90	6.91	4.30	
4	69.60	13.00	17.40	5.35	4.00	
5	68.00	12.60	19.50	5.40	3.49	
6	70.50	11.30	18.20	6.24	3.87	
7	67.20	13.60	19.20	4.94	3.50	
8	70.30	12.20	17.50	5.76	4.02	
9	68.40	14.10	17.50	4.85	3.91	
Average	69.31	12.67	18.03	5.47	3.84	
Standard deviation	1.72	1.17	0.95	0.67	0.26	
Calculated	77.77	11.11	11.11	7.00	7.00	
$\Delta\alpha$	-8.47	1.56	6.92	-1.53	-3.16	$\Delta\alpha = 16.95$

Table B.2: Atomic composition of untreated aramid fibres given by EDS analysis using X-MAX EDS

Spot#	%C	%N	%O	%C/%N	%C/%O	
1	74.50	9.10	16.40	8.19	4.54	
2	70.80	12.20	16.90	5.80	4.19	
3	71.60	12.10	16.30	5.92	4.39	
4	75.30	9.60	15.10	7.84	4.99	
5	71.10	12.10	16.80	5.88	4.23	
6	70.70	12.90	16.40	5.48	4.31	
7	70.20	12.90	16.90	5.44	4.15	
8	72.20	11.50	16.40	6.28	4.40	
9	72.70	11.80	15.60	6.16	4.66	
Average	72.12	11.58	16.31	6.23	4.42	
Standard deviation	1.94	1.41	0.62	1.00	0.27	
Calculated	77.77	11.11	11.11	7.00	7.00	
$\Delta\alpha$	-5.66	0.47	5.20	-0.77	-2.58	$\Delta\alpha = 11.33$

B.2. Coating compounds

Analyses were done using the AZTEC EDS probe (for Fh•Fh•Fh•Fh using the Oxford X-MAX EDS probe).

Table B.3: Atomic composition of compounded solid PS given by EDS analysis

Spot#	%C	%O	%C/%O
1	99.68	0.32	307.33
2	99.78	0.22	462.50
3	99.13	0.87	114.25
4	98.90	1.10	90.30
5	99.67	0.33	306.00
6	98.95	1.05	94.00
7	100.00	0.00	-
8	99.57	0.43	232.00
9	96.22	3.78	25.46
10	97.38	2.62	37.21
11	100.00	0.00	-
12	100.00	0.00	-
13	99.89	0.11	919.00
14	99.78	0.22	461.00
15	99.03	0.97	102.00
Average	99.20	0.80	123.96
Standard deviation	1.07	1.07	257.25
Calculated	100	0	-
$\Delta\alpha$	-0.80	0.80	-

$|\Delta\alpha| = 1.60$

Table B.4: Atomic composition of compounded solid GGGG given by EDS analysis

Spot#	%C	%N	%O	%C/%N	%C/%O
1	43.60	22.80	33.70	1.91	1.29
2	42.90	21.30	35.90	2.01	1.19
3	42.40	21.40	36.30	1.98	1.17
4	43.10	21.20	35.80	2.03	1.20
5	43.60	20.50	35.80	2.13	1.22
6	43.30	21.70	35.00	2.00	1.24
7	42.60	21.60	35.80	1.97	1.19
8	41.50	20.90	37.60	1.99	1.10
9	43.00	20.80	36.20	2.07	1.19
10	42.70	21.60	35.80	1.98	1.19
11	43.20	21.90	34.90	1.97	1.24
12	43.50	21.50	35.10	2.02	1.24
13	43.40	21.50	35.10	2.02	1.24
14	42.30	21.60	36.10	1.96	1.17
15	42.60	20.70	36.80	2.06	1.16
Average	42.91	21.40	35.73	2.01	1.20
Standard deviation	0.58	0.56	0.91	0.05	0.04
Calculated	47.06	23.53	29.41	2.00	1.60
$\Delta\alpha$	-4.15	-2.13	6.31	0.01	-0.40

$|\Delta\alpha| = 12.59$

Table B.5: Atomic composition of compounded solid FFFF given by EDS analysis

Spot#	%C	%N	%O	%C/%N	%C/%O
1	74.80	12.70	12.50	5.89	5.98
2	72.90	14.00	13.10	5.21	5.56
3	72.70	13.80	13.50	5.27	5.39
4	71.80	14.10	14.10	5.09	5.09
5	73.10	13.80	13.10	5.30	5.58
6	74.40	12.70	12.90	5.86	5.77
7	73.70	12.90	13.40	5.71	5.50
8	74.70	12.80	12.50	5.84	5.98
9	72.00	13.60	14.40	5.29	5.00
10	73.50	13.40	13.10	5.49	5.61
11	71.40	14.80	13.80	4.82	5.17
12	74.30	12.40	13.30	5.99	5.59
13	73.50	13.60	13.00	5.40	5.65
14	75.20	13.60	11.20	5.53	6.71
15	74.80	12.70	12.50	5.89	5.98
Average	73.52	13.39	13.09	5.49	5.62
Standard deviation	1.19	0.67	0.77	0.39	0.43
Calculated	80.00	8.89	11.11	9.00	7.20
$\Delta\alpha$	-6.48	4.50	1.90	-3.51	-1.58

$|\Delta\alpha| = 12.88$

Table B.6: Atomic composition of compounded solid FbFbFbFb given by EDS analysis

Spot#	%C	%N	%O	%C/%N	%C/%O
1	68.20	9.60	22.10	7.10	3.09
2	69.00	10.00	21.00	6.90	3.29
3	66.70	11.40	22.00	5.85	3.03
4	72.30	10.50	17.30	6.89	4.18
5	68.10	11.50	20.40	5.92	3.34
6	71.60	11.50	16.90	6.23	4.24
7	70.60	12.50	16.90	5.65	4.18
8	67.60	12.30	20.00	5.50	3.38
9	71.90	9.90	18.20	7.26	3.95
10	69.00	9.80	21.20	7.04	3.25
11	70.10	10.90	19.10	6.43	3.67
12	68.00	12.00	20.00	5.67	3.40
13	66.90	12.40	20.70	5.40	3.23
14	69.40	10.60	20.00	6.55	3.47
15	68.00	12.60	19.50	5.40	3.49
Average	69.16	11.17	19.69	6.19	3.51
Standard deviation	1.79	1.06	1.71	0.67	0.40
Calculated	73.97	13.70	12.33	5.4	6
$\Delta\alpha$	-4.18	-2.53	7.36	0.79	-2.49

$|\Delta\alpha| = 14.07$

Table B.7: Atomic composition of compounded solid FvFvFvFv given by EDS analysis

Spot#	%C	%N	%O	%C/%N	%C/%O
1	74.40	10.20	15.40	7.29	4.83
2	65.70	9.40	24.90	6.99	2.64
3	68.70	11.60	19.70	5.92	3.49
4	68.30	10.60	21.10	6.44	3.24
5	69.00	10.80	20.20	6.39	3.42
6	72.50	7.80	19.60	9.29	3.70
7	67.90	10.40	21.70	6.53	3.13
8	69.80	11.40	18.80	6.12	3.71
9	64.40	9.60	26.10	6.71	2.47
10	69.20	10.30	20.50	6.72	3.38
11	71.80	9.00	19.20	7.98	3.74
12	65.80	9.70	24.50	6.78	2.69
13	67.00	11.00	22.00	6.09	3.05
14	68.80	10.10	21.20	6.81	3.25
Average	68.81	10.14	21.06	6.79	3.27
Standard deviation	2.74	1.00	2.76	0.88	0.59
Calculated	75.00	13.16	11.84	5.70	6.33
$\Delta\alpha$	-6.19	-3.02	9.22	1.09	-3.07

 $|\Delta\alpha| = 18.43$ **Table B.8:** Atomic composition of compounded solid FhFhFhFh given by EDS analysis

Spot#	%C	%N	%O	%C/%N	%C/%O
1	67.60	8.80	23.60	7.68	2.86
2	68.00	9.80	22.20	6.94	3.06
3	68.90	9.50	21.60	7.25	3.19
4	68.00	10.20	21.80	6.67	3.12
5	69.60	7.60	22.80	9.16	3.05
6	66.70	9.50	23.80	7.02	2.80
7	67.70	10.60	21.70	6.39	3.12
8	67.60	10.70	21.60	6.32	3.13
9	73.10	6.40	20.50	11.42	3.57
10	66.90	10.40	22.70	6.43	2.95
11	69.30	9.40	21.30	7.37	3.25
12	68.40	9.50	22.10	7.20	3.10
13	67.90	11.60	20.50	5.85	3.31
14	71.00	9.10	19.90	7.80	3.57
15	62.70	17.10	20.20	3.67	3.10
Average	68.23	10.01	21.75	6.81	3.14
Standard deviation	2.74	1.00	2.76	1.67	0.22
Calculated	75.95	12.66	11.39	6.00	6.67
$\Delta\alpha$	-7.72	-2.64	10.36	0.81	-3.53

 $|\Delta\alpha| = 20.72$

Table B.9: Atomic composition of compounded solid Fh•Fh•Fh•Fh given by EDS analysis

Spot#	%C	%N	%O	%C/%N	%C/%O
1	63.40	20.30	16.30	3.12	3.89
2	62.90	20.80	16.40	3.02	3.84
3	64.00	20.30	15.70	3.15	4.08
4	62.70	21.70	15.60	2.89	4.02
5	63.40	20.90	15.70	3.03	4.04
6	64.30	21.10	14.70	3.05	4.37
7	65.00	19.30	15.80	3.37	4.11
8	64.50	19.80	15.70	3.26	4.11
9	67.10	18.10	14.80	3.71	4.53
10	64.10	21.10	14.80	3.04	4.33
11	66.00	19.50	14.60	3.38	4.52
12	65.90	19.10	14.90	3.45	4.42
13	64.30	20.20	15.50	3.18	4.15
14	65.10	18.70	16.30	3.48	3.99
15	66.10	20.30	13.70	3.26	4.82
Average	64.59	20.08	15.37	3.22	4.20
Standard deviation	1.27	1.00	0.76	0.21	0.27
Calculated	71.13	19.59	9.28	3.63	7.67
$\Delta\alpha$	-6.55	0.49	6.09	-0.41	-3.47

$|\Delta\alpha| = 13.13$

Table B.10: Atomic composition of compounded solid FFFFb•FFFFb•FFFFb•FFFFb given by EDS analysis

Spot#	%C	%N	%O	%C/%N	%C/%O
1	72.00	13.40	14.60	5.37	4.93
2	72.80	12.80	14.40	5.69	5.06
3	73.70	12.40	13.90	5.94	5.30
4	71.60	13.70	14.60	5.23	4.90
5	72.40	13.60	14.00	5.32	5.17
6	73.10	12.60	14.30	5.80	5.11
7	71.70	13.50	14.80	5.31	4.84
8	72.90	12.60	14.60	5.79	4.99
9	70.40	14.20	15.50	4.96	4.54
10	71.00	13.10	15.90	5.42	4.47
11	71.60	13.70	14.70	5.23	4.87
12	70.40	14.60	15.00	4.82	4.69
13	70.30	15.10	14.60	4.66	4.82
14	72.10	13.80	14.10	5.22	5.11
15	70.40	13.80	15.90	5.10	4.43
16	71.30	14.50	14.20	4.92	5.02
17	73.20	13.40	13.50	5.46	5.42
Average	71.82	13.58	14.62	5.29	4.91
Standard deviation	1.09	0.75	0.66	0.36	0.28
Calculated	76.47	14.03	9.50	5.45	8.05
$\Delta\alpha$	-4.65	-0.45	5.12	-0.16	-3.14

$|\Delta\alpha| = 10.22$

Table B.11: Atomic composition of compounded solid FFFFv•FFFFv•FFFFv•FFFFv given by EDS analysis

Spot#	%C	%N	%O	%C/%N	%C/%O
1	74.00	12.40	13.60	5.97	5.44
2	75.90	12.30	11.80	6.17	6.43
3	73.00	12.30	14.70	5.93	4.97
4	75.40	12.30	12.40	6.13	6.08
5	72.00	13.70	14.30	5.26	5.03
6	73.60	12.70	13.70	5.80	5.37
7	73.20	12.80	13.90	5.72	5.27
8	73.20	12.70	13.10	5.76	5.59
9	73.20	12.90	13.90	5.67	5.27
10	75.40	12.10	12.50	6.23	6.03
11	74.20	12.30	13.50	6.03	5.50
12	73.90	12.20	13.90	6.06	5.32
13	73.30	12.40	14.20	5.91	5.16
14	74.90	11.80	13.40	6.35	5.59
15	73.70	11.90	14.30	6.19	5.15
Average	73.93	12.45	13.55	5.94	5.46
Standard deviation	1.07	0.46	0.80	0.28	0.41
Calculated	76.89	13.78	9.33	5.58	8.24
$\Delta\alpha$	-2.96	-1.32	4.21	0.36	-2.78

$|\Delta\alpha| = 8.49$

Table B.12: Atomic composition of compounded solid FFFFh•FFFFh•FFFFh•FFFFh given by EDS analysis

Spot#	%C	%N	%O	%C/%N	%C/%O
1	72.10	13.10	14.80	5.50	4.87
2	74.60	11.60	13.80	6.43	5.41
3	73.40	12.00	14.60	6.12	5.03
4	72.40	13.30	14.40	5.44	5.03
5	72.90	13.40	13.70	5.44	5.32
6	74.50	12.30	13.20	6.06	5.64
7	74.20	11.40	14.40	6.51	5.15
8	71.50	13.20	15.30	5.42	4.67
9	72.10	12.50	15.40	5.77	4.68
10	73.60	12.40	14.00	5.94	5.26
11	73.40	12.30	14.40	5.97	5.10
12	73.60	11.90	14.40	6.18	5.11
13	73.20	13.00	13.80	5.63	5.30
14	74.50	12.30	13.20	6.06	5.64
15	74.40	12.20	13.40	6.10	5.55
Average	73.36	12.46	14.19	5.89	5.17
Standard deviation	0.99	0.62	0.69	0.36	0.31
Calculated	77.29	13.54	9.17	5.71	8.43
$\Delta\alpha$	-3.93	-1.08	5.02	0.18	-3.26

$|\Delta\alpha| = 10.03$

Table B.13: Atomic composition of compounded solid FFFFu•FFFFu•FFFFu•FFFFu given by EDS analysis

Spot#	%C	%N	%O	%C/%N	%C/%O
1	71.60	13.20	15.10	5.42	4.74
2	73.60	12.30	14.10	5.98	5.22
3	75.40	11.70	13.00	6.44	5.80
4	77.20	10.80	12.00	7.15	6.43
5	74.80	12.20	13.00	6.13	5.75
6	74.00	12.80	13.30	5.78	5.56
7	78.30	9.80	11.90	7.99	6.58
8	76.50	10.20	13.30	7.50	5.75
9	79.60	9.50	10.90	8.38	7.30
10	74.50	11.90	13.70	6.26	5.44
11	74.70	11.90	13.40	6.28	5.57
12	72.10	11.60	16.40	6.22	4.40
13	72.30	12.30	15.40	5.88	4.69
14	72.90	12.20	14.90	5.98	4.89
15	74.70	11.80	13.50	6.33	5.53
Average	74.81	11.61	13.59	6.44	5.50
Standard deviation	2.30	1.07	1.44	0.85	0.77
Calculated	79.12	12.45	8.43	6.35	9.38
$\Delta\alpha$	-4.30	-0.84	5.16	0.09	-3.88

$|\Delta\alpha| = 10.30$

B.3. Dip coated fibres using a solution at $1 \mu\text{mol}\cdot\text{mol}^{-1}$

Table B.14: Atomic composition of aramid fibre dip-coated with polystyrene by EDS analysis

	Spot#	%C	%N	%O	%C/%N	%C/%O
Fibre 1	1	82.30	7.70	10.00	10.69	8.23
	2	78.10	9.70	12.20	8.05	6.40
	3	75.10	11.30	13.60	6.65	5.52
	4	83.90	7.00	9.00	11.99	9.32
	5	83.50	5.00	11.50	16.70	7.26
Fibre 2	1	83.80	7.40	8.70	11.32	9.63
	2	82.90	6.80	10.30	12.19	8.05
	3	77.80	10.30	11.90	7.55	6.54
	4	87.80	4.60	7.60	19.09	11.55
	5	82.90	8.40	8.70	9.87	9.53
Fibre 3	1	77.00	7.80	15.30	9.87	5.03
	2	71.50	13.10	15.40	5.46	4.64
	3	95.90	0.90	3.20	106.56	29.97
	4	88.80	4.90	6.30	18.12	14.10
	5	89.50	4.20	6.30	21.31	14.21
Average		82.72	7.27	10.00	11.37	8.27
Standard deviation		5.79	3.04	3.05	24.85	6.26
Polystyrene compound exp.		99.20	-	0.80	-	123.96
Aramid fibre exp.		72.12	11.58	16.31	6.23	4.42
$\Delta A_{\text{compound}}$		-8.94	-0.31	9.26	-	-155.69
ΔA_{aramid}		10.60	-4.30	-6.31	5.14	3.85

$|\Delta A_{\text{compound}}| : 18.51; |\Delta A_{\text{aramid}}| : 21.21$

Table B.15: Atomic composition of aramid fibre dip coated with GGGG by EDS analysis

	Spot#	%C	%N	%O	%C/%N	%C/%O
Fibre 1	1	71.00	12.40	16.50	5.73	4.30
	2	64.90	16.80	18.30	3.86	3.55
	3	74.00	10.90	15.00	6.79	4.93
	4	76.60	9.50	13.90	8.06	5.51
	5	71.10	15.20	13.70	4.68	5.19
Fibre 2	1	70.20	13.30	16.60	5.28	4.23
	2	74.50	11.50	14.00	6.48	5.32
	3	54.70	21.00	24.40	2.60	2.24
	4	60.10	19.60	20.30	3.07	2.96
	5	68.00	13.90	18.00	4.89	3.78
Fibre 3	1	71.10	13.20	15.70	5.39	4.53
	2	70.50	12.00	17.50	5.88	4.03
	3	69.60	13.30	17.00	5.23	4.09
	4	68.60	14.10	17.30	4.87	3.97
	5	71.10	13.20	15.70	5.39	4.53
	Average	68.99	13.99	17.01	4.93	4.06
	Standard deviation	4.48	2.69	2.23	1.43	0.91
	GGGG compound exp.	42.91	21.40	35.73	2.01	1.20
	Aramid fibre exp.	72.12	11.58	16.31	6.23	4.42
	$\Delta A_{compound}$	26.08	-7.41	-18.72	2.92	2.86
	ΔA_{aramid}	-3.13	2.41	0.69	-1.3	-0.36
		$\Delta A_{compound} : 52.21; \Delta A_{aramid} : 6.24$				

Table B.16: Atomic composition of aramid fibre dip coated with FFFF given by EDS analysis

	Spot#	%C	%N	%O	%C/%N	%C/%O
Fibre 1	1	76.40	12.10	11.50	6.31	6.64
	2	72.50	12.40	15.10	5.85	4.80
	3	80.90	8.80	10.30	9.19	7.85
	4	71.10	13.10	15.80	5.43	4.50
	5	74.70	11.80	13.50	6.33	5.53
Fibre 2	1	75.00	12.10	12.90	6.20	5.81
	2	71.00	13.70	15.30	5.18	4.64
	3	75.50	11.90	12.60	6.34	5.99
	4	71.30	13.20	15.50	5.40	4.60
	5	78.30	9.90	11.70	7.91	6.69
Fibre 3	1	75.90	9.30	14.80	8.16	5.13
	2	75.90	10.70	13.40	7.09	5.66
	3	73.90	11.40	14.70	6.48	5.03
	4	73.60	12.00	14.40	6.13	5.11
	5	71.70	13.90	14.30	5.16	5.01
	Average	74.51	11.75	13.72	6.34	5.43
	Standard deviation	2.89	1.61	1.53	1.16	0.94
	FFFF compound exp.	73.52	13.39	13.09	5.49	5.62
	Aramid fibre exp.	72.12	11.58	16.31	6.23	4.42
	$\Delta A_{compound}$	0.68	-1.93	1.23	0.85	-0.19
	ΔA_{aramid}	2.39	0.18	-2.59	0.11	1.01
		$\Delta A_{compound} : 3.84; \Delta A_{aramid} : 5.16$				

Table B.17: Atomic composition of aramid fibre dip coated with FbFbFbFb by EDS analysis

	Spot#	%C	%N	%O	%C/%N	%C/%O
Fibre 1	1	70.30	14.00	15.70	5.02	4.48
	2	70.80	13.80	15.40	5.13	4.60
	3	71.00	12.10	16.90	5.87	4.20
	4	69.90	14.40	15.70	4.85	4.45
	5	71.20	11.70	17.10	6.09	4.16
Fibre 2	1	76.60	9.50	13.90	8.06	5.51
	2	72.80	12.00	15.20	6.07	4.79
	3	77.90	6.60	15.50	11.80	5.03
	4	75.80	10.50	13.70	7.22	5.53
	5	76.40	9.00	15.70	8.49	4.87
Fibre 3	1	72.90	12.20	14.90	5.98	4.89
	2	74.10	11.70	14.20	6.33	5.22
	3	70.80	12.00	17.20	5.90	4.12
	4	72.00	13.30	14.80	5.41	4.86
	5	72.70	11.40	15.90	6.38	4.57
Average		73.01	11.61	15.45	6.29	4.72
Standard deviation		1.21	1.31	0.96	1.78	0.45
FbFbFbFb compound exp.		69.16	11.17	19.69	6.19	3.51
Aramid fibre exp.		72.12	11.58	16.31	6.23	4.42
$\Delta A_{\text{compound}}$		3.85	0.45	-4.23	0.1	1.21
ΔA_{aramid}		0.89	0.04	-0.86	0.06	0.3
$\Delta A_{\text{compound}} : 8.53; \Delta A_{\text{aramid}} : 1.78$						

Table B.18: Atomic composition of aramid fibre dip coated with FvFvFvFv by EDS analysis

	Spot#	%C	%N	%O	%C/%N	%C/%O
Fibre 1	1	76.50	8.30	15.20	9.22	5.03
	2	69.10	14.90	16.00	4.64	4.32
	3	69.90	13.10	17.00	5.34	4.11
	4	73.20	12.20	14.70	6.00	4.98
	5	74.30	10.70	15.10	6.94	4.92
Fibre 2	1	70.10	14.40	15.50	4.87	4.52
	2	73.00	12.50	14.60	5.84	5.00
	3	70.50	12.70	16.80	5.55	4.20
	4	72.70	12.20	15.60	5.96	4.66
	5	72.70	12.50	14.70	5.82	4.95
Fibre 3	1	75.90	10.20	13.90	7.44	5.46
	2	70.10	11.90	18.00	5.89	3.89
	3	74.80	10.30	14.90	7.26	5.02
	4	71.80	11.80	16.30	6.08	4.40
	5	70.80	13.30	15.90	5.32	4.45
Average		72.36	12.07	15.61	6.00	4.63
Standard deviation		2.34	1.55	1.11	1.16	0.43
FvFvFvFv compound exp.		68.81	10.14	21.06	6.79	3.27
Aramid fibre exp.		72.12	11.58	16.31	6.23	4.42
$\Delta A_{\text{compound}}$		3.55	1.93	-5.45	-0.79	1.36
ΔA_{aramid}		0.24	0.49	-0.70	-0.23	0.21
$\Delta A_{\text{compound}} : 10.93; \Delta A_{\text{aramid}} : 1.42$						

Table B.19: Atomic composition of aramid fibre dip coated with FhFhFhFh EDS analysis

	Spot#	%C	%N	%O	%C/%N	%C/%O
Fibre 1	1	71.70	13.30	15.00	5.39	4.78
	2	71.20	13.20	15.60	5.39	4.56
	3	71.10	13.50	15.40	5.27	4.62
	4	71.70	11.40	16.90	6.29	4.24
	5	68.70	12.90	18.40	5.33	3.73
Fibre 2	1	72.30	13.20	14.50	5.48	4.99
	2	74.40	12.00	13.50	6.20	5.51
	3	72.70	12.20	15.10	5.96	4.81
	4	67.70	12.50	19.80	5.42	3.42
	5	69.90	14.20	15.90	4.92	4.40
Fibre 3	1	74.80	11.80	13.40	6.34	5.58
	2	70.90	13.40	15.70	5.29	4.52
	3	75.30	9.00	15.30	8.37	4.92
	4	69.90	8.40	27.70	8.32	2.52
	5	68.70	14.60	16.70	4.71	4.11
Average		71.40	12.37	16.59	5.77	4.30
Standard deviation		2.28	1.48	3.17	1.10	0.79
FhFhFhFh compound exp.		68.23	10.01	21.75	6.81	3.14
Aramid fibre exp.		72.12	11.58	16.31	6.23	4.42
$\Delta A_{compound}$		3.17	2.36	-5.16	-1.04	1.16
ΔA_{aramid}		-0.72	0.80	0.28	-0.46	-0.12
$\Delta A_{compound} : 10.69; \Delta A_{aramid} : 1.80$						

Table B.20: Atomic composition of aramid fibre dip coated with Fh•Fh•Fh•Fh by EDS analysis

	Spot#	%C	%N	%O	%C/%N	%C/%O
Fibre 1	1	64.70	13.30	22.00	4.86	2.94
	2	79.00	7.50	13.40	10.53	5.90
	3	73.80	10.40	15.80	7.10	4.67
	4	71.20	12.30	16.50	5.79	4.32
	5	62.20	16.90	20.90	3.68	2.98
Fibre 2	1	72.70	11.20	16.10	6.49	4.52
	2	71.20	11.40	17.40	6.25	4.09
	3	72.90	11.30	15.70	6.45	4.64
	4	77.40	6.00	16.60	12.90	4.66
	5	72.70	11.20	16.10	6.49	4.52
Fibre 3	1	66.50	13.70	19.80	4.85	3.36
	2	61.30	16.70	22.00	3.67	2.79
	3	66.30	14.60	19.10	4.54	3.47
	4	79.70	7.50	12.80	10.63	6.23
	5	80.60	4.60	14.80	17.52	5.45
Average		71.54	11.16	17.29	6.41	4.14
Standard deviation		6.07	3.75	2.71	3.99	1.09
FhFhFhFh compound exp.		71.13	19.59	9.28	3.63	7.67
Aramid fibre exp.		72.12	11.58	16.31	6.23	4.42
$\Delta A_{compound}$		6.95	9.88	-2.79	2.78	-3.53
ΔA_{aramid}		-0.59	0.42	0.98	0.18	-0.28
$\Delta A_{compound} : 19.62; \Delta A_{aramid} : 1.98$						

Table B.21: Atomic composition of aramid fibre dip coated with FFFFb•FFFFb•FFFFb•FFFFb by EDS analysis

	Spot#	%C	%N	%O	%C/%N	%C/%O
Fibre 1	1	76.60	11.20	12.20	6.84	6.28
	2	71.10	12.80	16.00	5.55	4.44
	3	75.20	12.00	12.80	6.27	5.88
	4	73.20	11.90	14.90	6.15	4.91
	5	72.60	12.70	14.80	5.72	4.91
Fibre 2	1	73.70	12.90	13.40	5.71	5.50
	2	76.00	11.70	12.20	6.50	6.23
	3	74.40	10.90	14.70	6.83	5.06
	4	77.40	11.50	11.10	6.73	6.97
	5	77.10	12.30	10.60	6.27	7.27
Fibre 3	1	76.00	10.90	13.10	6.97	5.80
	2	72.80	13.20	14.00	5.52	5.20
	3	73.80	11.20	15.00	6.59	4.92
	4	75.60	11.60	12.80	6.52	5.91
	5	73.00	11.40	15.60	6.40	4.68
Average		74.57	11.88	13.55	6.28	5.50
Standard deviation		1.76	0.77	1.49	0.48	0.84
FFFFb•FFFFb•FFFFb•FFFFb compound exp.		71.82	13.58	14.62	5.29	4.91
Aramid fibre exp.		72.12	11.58	16.31	6.23	4.42
$\Delta A_{compound}$		2.75	-1.70	-1.08	0.99	0.59
ΔA_{aramid}		2.44	0.30	-2.76	0.05	1.08
 $\Delta A_{compound}$: 5.52; ΔA_{aramid} : 5.51						

Table B.22: Atomic composition of aramid fibre dip coated with FFFFv•FFFFv•FFFFv•FFFFv by EDS analysis

	Spot#	%C	%N	%O	%C/%N	%C/%O
Fibre 1	1	79.60	10.40	10.00	7.65	7.96
	2	75.10	12.70	12.30	5.91	6.11
	3	76.40	12.40	11.20	6.16	6.82
	4	74.00	13.00	13.00	5.69	5.69
	5	76.50	11.10	12.40	6.89	6.17
Fibre 2	1	74.20	12.20	13.60	6.08	5.46
	2	73.40	13.70	12.90	5.36	5.69
	3	77.40	11.70	10.90	6.62	7.10
	4	75.00	12.20	12.80	6.15	5.86
	5	76.80	11.90	11.30	6.45	6.80
Fibre 3	1	77.00	12.70	10.30	6.06	7.48
	2	76.60	11.10	12.40	6.90	6.18
	3	74.10	14.60	11.30	5.08	6.56
	4	74.40	13.30	12.30	5.59	6.05
	5	71.50	14.80	13.60	4.83	5.26
Average		75.47	12.52	12.02	6.03	6.28
Standard deviation		2.00	1.14	1.19	0.74	0.77
FFFFv•FFFFv•FFFFv•FFFFv compound exp.		73.93	12.45	13.55	5.94	5.46
Aramid fibre exp.		72.12	11.58	16.31	6.23	4.42
$\Delta A_{compound}$		1.54	0.07	-1.53	0.09	0.82
ΔA_{aramid}		3.34	0.94	-4.29	-0.2	1.86
 $\Delta A_{compound}$: 3.18; ΔA_{aramid} : 8.58						

Table B.23: Atomic composition of aramid fibre dip coated with FFFFh•FFFFh•FFFFh•FFFFh by EDS analysis

	Spot#	%C	%N	%O	%C/%N	%C/%O
Fibre 1	1	79.70	10.60	9.70	7.52	8.22
	2	81.60	7.60	10.80	10.74	7.56
	3	72.80	11.70	15.50	6.22	4.70
	4	73.50	13.30	13.20	5.53	5.57
	5	74.40	11.60	14.00	6.41	5.31
Fibre 2	1	74.80	11.50	13.70	6.50	5.46
	2	72.30	13.60	14.10	5.32	5.13
	3	79.10	10.50	10.30	7.53	7.68
	4	73.40	11.90	14.70	6.17	4.99
	5	73.70	13.10	13.30	5.63	5.54
Fibre 3	1	74.20	12.60	13.20	5.89	5.62
	2	73.50	13.20	13.30	5.57	5.53
	3	73.20	11.70	15.10	6.26	4.85
	4	73.60	12.60	13.80	5.84	5.33
	5	71.00	14.50	14.50	4.90	4.90
Average		74.72	12.00	13.28	6.23	5.63
Standard deviation		2.61	1.46	1.63	1.40	1.11
FFFFh•FFFFh•FFFFh•FFFFh compound exp.		73.36	12.46	14.19	5.89	5.17
Aramid fibre exp.		72.12	11.58	16.31	6.23	4.42
$\Delta A_{compound}$		1.36	-0.46	-0.91	0.34	0.46
ΔA_{aramid}		2.60	0.42	-3.03	0	1.21
$\Delta A_{compound} : 2.73; \Delta A_{aramid} : 6.05$						

Table B.24: Atomic composition of aramid fibre dip coated with FFFFu•FFFFu•FFFFu•FFFFu by EDS analysis

	Spot#	%C	%N	%O	%C/%N	%C/%O
Fibre 1	1	71.40	14.00	14.50	5.10	4.92
	2	71.60	13.50	14.90	5.30	4.81
	3	76.40	12.20	11.40	6.26	6.70
	4	76.80	10.90	12.20	7.05	6.30
	5	72.10	13.20	14.80	5.46	4.87
Fibre 2	1	76.90	10.90	12.20	7.06	6.30
	2	77.50	11.10	11.40	6.98	6.80
	3	74.30	11.80	13.90	6.30	5.35
	4	74.20	12.70	13.10	5.84	5.66
	5	73.90	11.70	14.40	6.32	5.13
Fibre 3	1	72.80	12.80	14.40	5.69	5.06
	2	75.50	12.60	11.80	5.99	6.40
	3	73.60	12.60	13.80	5.84	5.33
	4	77.80	11.10	11.10	7.01	7.01
	5	77.50	11.40	11.20	6.80	6.92
Average		74.82	12.17	13.01	6.15	5.75
Standard deviation		2.21	0.91	1.47	0.67	0.82
FFFFu•FFFFu•FFFFu•FFFFu compound exp.		74.81	11.61	13.59	6.44	5.50
Aramid fibre exp.		72.12	11.58	16.31	6.23	4.42
$\Delta A_{compound}$		0.01	0.55	-0.59	-0.29	0.25
ΔA_{aramid}		2.70	0.59	-3.30	-0.08	1.33
$\Delta A_{compound} : 1.15; \Delta A_{aramid} : 6.59$						

B.4. Spray coated fibres using a solution at 0.01 mmol·mL⁻¹

Table B.25: Atomic composition of aramid fibre spray coated with GGGG by EDS analysis

	Spot#	%C	%N	%O	%C/%N	%C/%O
Fibre 1	1	71.60	12.20	16.20	5.87	4.42
	2	56.60	28.50	14.90	1.99	3.80
	3	72.80	11.50	15.70	6.33	4.64
	4	72.10	20.20	7.80	3.57	9.24
	5	68.70	15.80	15.60	4.35	4.40
Fibre 2	1	68.10	14.70	17.30	4.63	3.94
	2	76.10	11.20	12.80	6.79	5.95
	3	71.80	12.90	15.30	5.57	4.69
	4	70.00	13.90	16.10	5.04	4.35
	5	74.70	12.40	12.90	6.02	5.79
Fibre 3	1	71.30	13.80	14.90	5.17	4.79
	2	71.40	13.20	15.40	5.41	4.64
	3	70.40	12.90	16.60	5.46	4.24
	4	73.60	12.60	13.70	5.84	5.37
	Average	70.04	15.16	14.81	4.62	4.73
	Standard deviation	4.93	4.05	2.28	1.32	1.37
	GGGG compound exp.	42.91	21.40	35.73	2.01	1.20
	Aramid fibre exp.	69.31	12.67	18.03	5.47	3.84
	$\Delta A_{\text{compound}}$	27.13	-6.24	-20.91	2.61	3.53
	ΔA_{aramid}	0.73	2.49	-3.22	-0.85	0.89
	$\Delta A_{\text{compound}} : 54.28; \Delta A_{\text{aramid}} : 6.44$					

Table B.26: Atomic composition of aramid fibre spray coated with FFFF by EDS analysis

	Spot#	%C	%N	%O	%C/%N	%C/%O
Fibre 1	1	64.40	16.00	19.60	4.03	3.29
	2	75.40	11.60	13.00	6.50	5.80
	3	72.70	12.80	14.50	5.68	5.01
	4	69.90	14.20	16.00	4.92	4.37
	5	65.10	15.70	19.20	4.15	3.39
Fibre 2	1	74.50	9.70	15.70	7.68	4.75
	2	68.70	13.90	17.40	4.94	3.95
	3	63.30	17.90	18.80	3.54	3.37
	4	69.40	13.00	17.60	5.34	3.94
	5	73.00	11.90	15.10	6.13	4.83
Fibre 3	1	74.10	10.90	15.00	6.80	4.94
	2	72.60	11.50	15.90	6.31	4.57
	3	72.80	11.20	15.90	6.50	4.58
	4	72.30	12.00	15.80	6.03	4.58
	5	69.10	14.00	16.90	4.94	4.09
	Average	70.49	13.09	16.43	5.39	4.29
	Standard deviation	3.66	2.04	1.69	1.15	0.70
	FFFF compound exp.	73.52	13.39	13.09	5.49	5.62
	Aramid fibre exp.	69.31	12.67	18.03	5.47	3.84
	$\Delta A_{\text{compound}}$	-1.34	-1.47	2.81	-0.1	-1.33
	ΔA_{aramid}	1.18	0.42	-1.61	-0.08	0.45
	$\Delta A_{\text{compound}} : 5.62; \Delta A_{\text{aramid}} : 3.20$					

Table B.27: Atomic composition of aramid fibre spray coated with FbFbFbFb by EDS analysis

	Spot#	%C	%N	%O	%C/%N	%C/%O
Fibre 1	1	66.40	16.70	16.90	3.98	3.93
	2	67.40	14.00	18.70	4.81	3.60
	3	71.70	12.00	16.30	5.98	4.40
	4	75.00	11.00	14.10	6.82	5.32
	5	68.70	12.30	19.10	5.59	3.60
Fibre 2	1	69.80	12.30	17.90	5.67	3.90
	2	67.90	14.30	17.70	4.75	3.84
	3	69.70	12.90	17.40	5.40	4.01
	4	73.50	11.70	14.70	6.28	5.00
	5	73.90	11.10	15.00	6.66	4.93
Fibre 3	1	72.00	12.10	15.90	5.95	4.53
	2	71.50	11.30	17.20	6.33	4.16
	3	75.70	10.50	13.70	7.21	5.53
	4	69.00	14.80	16.10	4.66	4.29
	5	77.40	11.40	11.20	6.79	6.91
Average		71.31	12.56	16.13	5.68	4.42
Standard deviation		3.17	1.71	1.99	0.93	0.89
FbFbFbFb compound exp.		69.16	11.17	19.69	6.19	3.51
Aramid fibre exp.		69.31	12.67	18.03	5.47	3.84
$\Delta A_{compound}$		2.15	1.39	-3.56	-0.51	0.91
ΔA_{aramid}		2.00	-0.11	-1.91	0.21	0.58
$\Delta A_{compound} : 7.10; \Delta A_{aramid} : 4.01$						

Table B.28: Atomic composition of aramid fibre spray coated with FvFvFvFv by EDS analysis

	Spot#	%C	%N	%O	%C/%N	%C/%O
Fibre 1	1	67.80	14.80	17.40	4.58	3.90
	2	72.70	11.90	15.40	6.11	4.72
	3	67.50	13.30	19.20	5.08	3.52
	4	68.50	12.70	18.90	5.39	3.62
	5	67.40	14.90	17.70	4.52	3.81
Fibre 2	1	75.30	9.80	14.90	7.68	5.05
	2	73.00	12.70	14.30	5.75	5.10
	3	72.30	11.50	16.20	6.29	4.46
	4	68.50	15.20	16.30	4.51	4.20
	5	72.40	10.90	16.70	6.64	4.34
Fibre 3	1	78.50	8.40	13.10	9.35	5.99
	2	73.00	9.90	17.10	7.37	4.27
	3	72.20	11.30	16.60	6.39	4.35
	4	70.40	12.50	17.10	5.63	4.12
	5	76.40	9.10	14.60	8.40	5.23
Average		71.73	11.93	16.37	6.01	4.38
Standard deviation		2.65	1.68	1.44	1.45	0.67
FvFvFvFv compound exp.		68.81	10.14	21.06	6.79	3.27
Aramid fibre exp.		69.31	12.67	18.03	5.47	3.84
$\Delta A_{compound}$		2.92	1.79	-4.70	-0.78	1.11
ΔA_{aramid}		2.42	-0.74	-1.67	-0.54	0.54
$\Delta A_{compound} : 9.41; \Delta A_{aramid} : 4.82$						

Table B.29: Atomic composition of aramid fibre spray coated with FhFhFhFh by EDS analysis

	Spot#	%C	%N	%O	%C/%N	%C/%O
Fibre 1	1	73.60	11.80	14.60	6.24	5.04
	2	54.50	22.80	22.60	2.39	2.41
	3	92.00	4.70	3.40	19.57	27.06
	4	75.50	9.70	14.80	7.78	5.10
	5	68.20	13.30	18.50	5.13	3.69
Fibre 2	1	73.10	12.00	14.80	6.09	4.94
	2	67.30	15.10	17.50	4.46	3.85
	3	69.70	13.10	17.20	5.32	4.05
	4	76.40	10.60	13.00	7.21	5.88
	5	68.40	14.50	17.00	4.72	4.02
Fibre 3	1	70.00	13.40	16.50	5.22	4.24
	2	72.00	12.90	15.10	5.58	4.77
	3	67.60	14.30	18.10	4.73	3.73
	4	74.50	12.20	13.30	6.11	5.60
	5	76.70	10.30	13.00	7.45	5.90
Average		71.97	12.71	15.29	5.66	4.71
Standard deviation		6.95	3.32	3.75	3.85	5.90
FhFhFhFh compound exp.		68.23	10.01	21.75	6.81	3.14
Aramid fibre exp.		69.31	12.67	18.03	5.47	3.84
$\Delta A_{compound}$		3.74	2.70	-6.46	-1.15	1.57
ΔA_{aramid}		2.66	0.05	-2.74	0.19	0.87
$\Delta A_{compound} : 12.90; \Delta A_{aramid} : 5.44$						

Table B.30: Atomic composition of aramid fibre spray coated with FFFFb•FFFFb•FFFFb•FFFFb by EDS analysis

	Spot#	%C	%N	%O	%C/%N	%C/%O
Fibre 1	1	70.80	12.90	16.40	5.49	4.32
	2	75.00	10.60	14.50	7.08	5.17
	3	69.30	14.80	15.90	4.68	4.36
	4	74.20	11.20	14.60	6.63	5.08
	5	62.90	17.80	19.30	3.53	3.26
Fibre 2	1	76.00	11.20	12.80	6.79	5.94
	2	76.40	10.90	12.70	7.01	6.02
	3	71.70	13.30	15.00	5.39	4.78
	4	71.90	14.50	14.50	4.96	4.96
	5	72.10	14.80	13.10	4.87	5.50
Fibre 3	1	72.90	13.70	13.40	5.32	5.44
	2	74.40	10.90	14.70	6.83	5.06
	3	71.90	12.50	15.60	5.75	4.61
	4	71.30	13.80	14.90	5.17	4.79
	5	73.40	12.00	14.60	6.12	5.03
Average		72.28	12.99	14.80	5.56	4.88
Standard deviation		2.80	1.99	1.27	1.02	0.68
FFFFb•FFFFb•FFFFb•FFFFb compound exp.		71.82	13.58	14.62	5.29	4.91
Aramid fibre exp.		69.31	12.67	18.03	5.47	3.84
$\Delta A_{compound}$		0.46	-0.58	0.18	0.27	-0.03
ΔA_{aramid}		2.97	0.33	-3.23	0.09	1.04
$\Delta A_{compound} : 1.22; \Delta A_{aramid} : 6.53$						

Table B.31: Atomic composition of aramid fibre spray coated with FFFFv•FFFFv•FFFFv•FFFFv by EDS analysis

	Spot#	%C	%N	%O	%C/%N	%C/%O
Fibre 1	1	75.00	11.70	13.30	6.41	5.64
	2	72.60	12.80	14.60	5.67	4.97
	3	72.10	10.30	17.60	7.00	4.10
	4	73.30	12.80	14.00	5.73	5.24
	5	67.30	15.20	17.50	4.43	3.85
Fibre 2	1	75.30	12.60	12.10	5.98	6.22
	2	70.20	16.10	13.70	4.36	5.12
	3	71.50	12.90	15.60	5.54	4.58
	4	73.60	12.80	13.50	5.75	5.45
	5	71.20	13.40	15.40	5.31	4.62
Fibre 3	1	72.00	13.00	15.00	5.54	4.80
	2	71.10	13.60	15.30	5.23	4.65
	3	72.90	12.90	14.10	5.65	5.17
	4	69.80	13.70	16.50	5.09	4.23
	5	73.10	12.20	14.60	5.99	5.01
Average		72.07	13.07	14.85	5.52	4.85
Standard deviation		2.10	1.28	1.46	0.67	0.62
FFFFv•FFFFv•FFFFv•FFFFv compound exp.		73.93	12.45	13.55	5.94	5.46
Aramid fibre exp.		69.31	12.67	18.03	5.47	3.84
$\Delta A_{compound}$		-1.86	0.61	1.31	-0.42	-0.61
ΔA_{aramid}		2.76	0.40	-3.18	0.05	1.01
$\Delta A_{compound} : 3.78; \Delta A_{aramid} : 6.34$						

Table B.32: Atomic composition of aramid fibre spray coated with FFFFh•FFFFh•FFFFh•FFFFh by EDS analysis

	Spot#	%C	%N	%O	%C/%N	%C/%O
Fibre 1	1	75.70	11.80	12.40	6.42	6.10
	2	75.30	11.50	13.20	6.55	5.70
	3	77.40	10.90	11.70	7.10	6.62
	4	77.60	10.50	11.90	7.39	6.52
	5	77.60	11.10	11.30	6.99	6.87
Fibre 2	1	73.20	12.50	14.30	5.86	5.12
	2	75.90	12.00	12.10	6.33	6.27
	3	74.00	11.80	14.20	6.27	5.21
	4	77.00	11.00	12.00	7.00	6.42
	5	76.60	10.80	12.60	7.09	6.08
Fibre 3	1	78.10	8.60	13.40	9.08	5.83
	2	77.20	10.60	12.30	7.28	6.28
	3	74.10	13.30	12.70	5.57	5.83
	4	75.30	12.90	11.80	5.84	6.38
	5	76.40	10.60	13.00	7.21	5.88
Average		76.09	11.33	12.59	6.72	6.04
Standard deviation		1.45	1.05	0.83	0.86	0.49
FFFFh•FFFFh•FFFFh•FFFFh compound exp.		73.36	12.46	14.19	5.89	5.17
Aramid fibre exp.		69.31	12.67	18.03	5.47	3.84
$\Delta A_{compound}$		2.73	-1.13	-1.59	0.83	0.87
ΔA_{aramid}		6.78	-1.34	-5.44	1.25	2.20
$\Delta A_{compound} : 5.46; \Delta A_{aramid} : 13.56$						

Table B.33: Atomic composition of aramid fibre spray coated with FFFFu●FFFFu●FFFFu●FFFFu by EDS analysis

	Spot#	%C	%N	%O	%C/%N	%C/%O
Fibre 1	1	73.60	12.50	13.90	5.89	5.29
	2	76.50	10.90	12.60	7.02	6.07
	3	71.70	12.60	15.70	5.69	4.57
	4	79.50	10.20	10.30	7.79	7.72
	5	74.10	11.70	14.20	6.33	5.22
Fibre 2	1	73.00	12.40	14.60	5.89	5.00
	2	71.90	12.90	15.20	5.57	4.73
	3	76.00	10.50	13.50	7.24	5.63
	4	73.00	12.30	14.80	5.93	4.93
	5	76.10	10.40	13.50	7.32	5.64
Fibre 3	1	73.90	12.50	13.60	5.91	5.43
	2	75.50	11.30	13.20	6.68	5.72
	3	77.90	10.10	12.00	7.71	6.49
	4	71.80	13.80	14.30	5.20	5.02
	5	72.70	12.80	14.50	5.68	5.01
Average		74.48	11.79	13.73	6.32	5.43
Standard deviation		2.45	1.21	1.27	0.84	0.80
FFFFu●FFFFu●FFFFu●FFFFu compound exp.		74.81	11.61	13.59	6.44	5.50
Aramid fibre exp.		69.31	12.67	18.03	5.47	3.84
$\Delta A_{compound}$		-0.33	0.18	0.13	-0.12	-0.07
ΔA_{aramid}		5.17	-0.87	-4.31	0.85	1.59
$\Delta A_{compound} : 0.65; \Delta A_{aramid} : 10.35$						

Appendix C: Adsorption data of concentrations of coating molecules onto the Kevlar fibre pellet surface.

This appendix presents some supplementary results not included in Chapter III regarding the adsorption of interfacial agents at the surface of Kevlar fibres. The interfacial agent was dissolved in a solvent (toluene for polystyrene, PS, or 95/5 acetonitrile/TFA for the other molecules) at a concentration of $1 \mu\text{mol}\cdot\text{mL}^{-1}$ and a time of 5 min if not mentioned otherwise. Kevlar fibres were dip coated using these solutions and the treated fibres were dried overnight at room temperature. All weighted differences have been corrected for with a constant mass of solvent ($m_s = 0.41 \text{ mg}$), as determined in Section 3.7.3. In the case of a large standard deviation, more than triplicate experiments were performed. The following abbreviations are used here: m_i and m_f are the initial and final mass of the pellet, i.e. before and after dip coating, Δm the gain in mass after dip coating ($\Delta m = m_f - m_i - m_s$), i.e. the mass of interfacial agent present at the surface of the fibre, m and c the mass and concentration respectively of interfacial agent dissolved in the solvent used for dip coating. The amount of mmol relative to the initial mass is then given by dividing the gain in mass by the molecular weight and dividing once more by the initial weight $(\Delta m/M)/M_i$. Finally, the value of adsorption (κ) is given as the ratio of adsorbed oligomers in solution $\kappa = \frac{\Delta n_{\text{oligomer}}}{n_{\text{oligomer}}} * \frac{1}{m_i}$

To determine the accuracy of the measurements, the influence of the concentration and time was investigated for GGGG as a model and the optimised conditions were used to study all the molecules listed in **Table III.1**.

C.1. Adsorption behaviour of GGGG with variable concentration

Table C.1: Gravimetric measurements of aramid fibre pellets dip coated with variable concentrations of GGGG (instrumental standard deviation: $\pm 1 \mu\text{g}$)

m_{GGGG} (mg)	C_{GGGG} (mmol·mL ⁻¹)	m_i (mg)	m_f (mg)	Δm (mg)	$[\Delta m/M_{\text{GGGG}}]/m_i$	K (1·mg ⁻¹)
2.68	$5.44 \cdot 10^{-3}$	74.72	75.90	0.77	$4.19 \cdot 10^{-5}$	0.39
2.67	$5.42 \cdot 10^{-3}$	74.78	76.48	1.29	$7.01 \cdot 10^{-5}$	0.65
2.68	$5.44 \cdot 10^{-3}$	73.87	76.14	1.86	$1.02 \cdot 10^{-4}$	0.94
Average						0.66
Standard deviation						0.28
Ratio (%)						42.42
3.78	$7.67 \cdot 10^{-3}$	74.56	75.76	0.79	$4.31 \cdot 10^{-5}$	0.28
3.73	$7.57 \cdot 10^{-3}$	74.14	75.63	1.08	$5.92 \cdot 10^{-5}$	0.39
3.72	$7.55 \cdot 10^{-3}$	74.41	75.99	1.17	$6.39 \cdot 10^{-5}$	0.42
Average						0.37
Standard deviation						0.07
Ratio (%)						18.92
5.06	$1.03 \cdot 10^{-2}$	73.93	76.22	1.88	$1.03 \cdot 10^{-4}$	0.50
5.06	$1.03 \cdot 10^{-2}$	74.17	75.93	1.35	$7.40 \cdot 10^{-5}$	0.36
5.05	$1.02 \cdot 10^{-2}$	74.24	75.96	1.31	$7.17 \cdot 10^{-5}$	0.35
Average						0.40
Standard deviation						0.09
Ratio (%)						22.50
7.49	$1.22 \cdot 10^{-2}$	74.49	75.90	1.00	$5.46 \cdot 10^{-5}$	0.18
7.57	$1.23 \cdot 10^{-2}$	74.38	76.91	2.12	$1.16 \cdot 10^{-4}$	0.38
7.57	$1.23 \cdot 10^{-2}$	74.48	76.08	1.19	$6.50 \cdot 10^{-5}$	0.21
Average						0.26
Standard deviation						0.11
Ratio (%)						42.30
8.95	$1.45 \cdot 10^{-2}$	74.44	75.27	0.42	$2.30 \cdot 10^{-5}$	0.06
8.98	$1.46 \cdot 10^{-2}$	74.78	76.14	0.95	$5.17 \cdot 10^{-5}$	0.14
8.94	$1.45 \cdot 10^{-2}$	74.33	75.95	1.21	$6.62 \cdot 10^{-5}$	0.18
Average						0.13
Standard deviation						0.06
Ratio (%)						46.13
17.56	$2.04 \cdot 10^{-2}$	74.31	75.56	0.84	$4.60 \cdot 10^{-5}$	0.09
17.47	$2.03 \cdot 10^{-2}$	74.41	75.44	0.62	$3.39 \cdot 10^{-5}$	0.07
17.53	$2.03 \cdot 10^{-2}$	74.56	75.58	0.61	$3.33 \cdot 10^{-5}$	0.07
Average						0.07
Standard deviation						0.01
Ratio (%)						14.29
26.56	$2.39 \cdot 10^{-2}$	74.33	77.71	2.97	$1.62 \cdot 10^{-4}$	0.15
26.53	$2.39 \cdot 10^{-2}$	74.34	78.95	4.20	$2.30 \cdot 10^{-4}$	0.21
26.46	$2.39 \cdot 10^{-2}$	74.18	75.54	0.95	$5.21 \cdot 10^{-5}$	0.05
Average						0.14
Standard deviation						0.08
Ratio (%)						57.14

C.2. Adsorption behaviour of GGGG with variable time

Table C.2: Gravimetric measurements of aramid fibre pellets dip coated with GGGG ($0.01 \text{ mmol}\cdot\text{mL}^{-1}$) at variable times (instrumental standard deviation: $\pm 1 \mu\text{g}$)

Time (min)	m_{GGGG} (mg)	C_{GGGG} ($\text{mmol}\cdot\text{mL}^{-1}$)	m_i (mg)	m_f (mg)	Δm (mg)	$[\Delta m/M_{\text{GGGG}}]/m_i$	κ ($1\cdot\text{mg}^{-1}$)
1	5.00	$1.01\cdot 10^{-2}$	74.07	74.93	0.45	$2.47\cdot 10^{-5}$	0.12
	5.05	$1.02\cdot 10^{-2}$	74.50	75.53	0.62	$3.39\cdot 10^{-5}$	0.17
	5.08	$1.03\cdot 10^{-2}$	74.07	74.86	0.38	$2.09\cdot 10^{-5}$	0.10
Average							0.13
Standard deviation							0.03
Ratio (%)							23.08
2.5	4.97	$1.01\cdot 10^{-2}$	74.48	75.34	0.45	$2.46\cdot 10^{-5}$	0.12
	5.03	$1.02\cdot 10^{-2}$	74.30	75.39	0.68	$3.72\cdot 10^{-5}$	0.18
	5.03	$1.02\cdot 10^{-2}$	74.20	75.35	0.74	$4.06\cdot 10^{-5}$	0.20
	4.97	$1.01\cdot 10^{-2}$	74.48	75.34	0.45	$2.46\cdot 10^{-5}$	0.12
Average							0.17
Standard deviation							0.04
Ratio (%)							23.53
5	5.06	$1.03\cdot 10^{-2}$	73.93	76.22	1.88	$1.03\cdot 10^{-4}$	0.50
	5.06	$1.03\cdot 10^{-2}$	74.17	75.93	1.35	$7.40\cdot 10^{-5}$	0.36
	5.05	$1.02\cdot 10^{-2}$	74.24	75.96	1.31	$7.17\cdot 10^{-5}$	0.35
	5.04	$1.02\cdot 10^{-2}$	74.63	75.58	0.54	$2.94\cdot 10^{-5}$	0.14
	5.04	$1.02\cdot 10^{-2}$	74.36	75.60	0.83	$4.54\cdot 10^{-5}$	0.22
	5.05	$1.02\cdot 10^{-2}$	74.40	75.26	0.45	$2.46\cdot 10^{-5}$	0.12
Average							0.28
Standard deviation							0.15
Ratio (%)							53.57
10	5.06	$1.03\cdot 10^{-2}$	74.11	75.44	0.92	$5.05\cdot 10^{-5}$	0.25
	5.04	$1.02\cdot 10^{-2}$	74.27	75.57	0.89	$4.87\cdot 10^{-5}$	0.24
	4.98	$1.01\cdot 10^{-2}$	74.19	75.82	1.22	$6.69\cdot 10^{-5}$	0.33
Average							0.27
Standard deviation							0.05
Ratio (%)							18.52
20	4.97	$1.01\cdot 10^{-2}$	74.14	75.60	1.05	$5.76\cdot 10^{-5}$	0.29
	4.94	$1.00\cdot 10^{-2}$	74.37	76.03	1.25	$6.83\cdot 10^{-5}$	0.30
	5.01	$1.02\cdot 10^{-2}$	74.62	76.17	1.14	$6.21\cdot 10^{-5}$	0.31
Average							0.31
Standard deviation							0.03
Ratio (%)							9.68

C.3. Quantification of coating behaviour commercial molecules

Table C.3: Gravimetric measurements of aramid fibre pellets dip coated with polystyrene (instrumental standard deviation: $\pm 1 \mu\text{g}$)

m_{PS} (mg)	C_{PS} ($\text{mmol}\cdot\text{mL}^{-1}$)	m_i (mg)	m_f (mg)	Δm (mg)	$[\Delta m/M_{\text{PS}}]/m_i$	κ ($1\cdot\text{mg}^{-1}$)
4.20	$1.00\cdot 10^{-3}$	74.19	74.88	0.28	$1.82\cdot 10^{-6}$	0.09
4.19	$9.98\cdot 10^{-4}$	74.37	74.97	0.19	$1.22\cdot 10^{-6}$	0.06
4.19	$9.99\cdot 10^{-4}$	74.20	74.67	0.06	$3.90\cdot 10^{-7}$	0.02
4.24	$1.01\cdot 10^{-3}$	73.72	74.50	0.37	$2.40\cdot 10^{-6}$	0.12
Average						0.07
Standard deviation						0.04
Ratio (%)						57.14

Table C.4: Gravimetric measurements of aramid fibre pellets dip coated with FFFF (instrumental standard deviation: $\pm 1 \mu\text{g}$)

m_{FFFF} (mg)	C_{FFFF} (mmol·mL ⁻¹)	m_i (mg)	m_f (mg)	Δm (mg)	$[\Delta m/M_{\text{FFFF}}]/m_i$	κ (1·mg ⁻¹)
1.37	$1.13 \cdot 10^{-3}$	73.75	74.36	0.19	$4.33 \cdot 10^{-6}$	0.19
1.34	$1.11 \cdot 10^{-3}$	74.50	74.99	0.08	$1.79 \cdot 10^{-6}$	0.08
1.36	$1.12 \cdot 10^{-3}$	74.03	74.18	0.15	$3.34 \cdot 10^{-6}$	0.15
1.29	$1.06 \cdot 10^{-3}$	74.56	74.66	0.10	$2.21 \cdot 10^{-6}$	0.10
1.35	$1.11 \cdot 10^{-3}$	74.15	74.25	0.10	$2.22 \cdot 10^{-6}$	0.10
Average						0.13
Standard deviation						0.04
Ratio (%)						30.77

C.4. Quantification of coating behaviour oligomers with single phenylalanine unit

Table C.5: Gravimetric measurements of aramid fibre pellets dip coated with FbFbFbFb (instrumental standard deviation: $\pm 1 \mu\text{g}$)

m_{FbFbFbFb} (mg)	C_{FbFbFbFb} (mmol·mL ⁻¹)	m_i (mg)	m_f (mg)	Δm (mg)	$[\Delta m/M_{\text{FbFbFbFb}}]/m_i$	κ (1·mg ⁻¹)
1.95	$1.03 \cdot 10^{-3}$	74.45	75.07	0.21	$2.99 \cdot 10^{-6}$	0.14
1.97	$1.04 \cdot 10^{-3}$	73.96	74.68	0.31	$4.44 \cdot 10^{-6}$	0.21
1.98	$1.05 \cdot 10^{-3}$	74.08	75.17	0.68	$9.71 \cdot 10^{-6}$	0.46
1.95	$1.03 \cdot 10^{-3}$	74.49	75.59	0.69	$9.80 \cdot 10^{-6}$	0.48
Average						0.32
Standard deviation						0.17
Ratio (%)						53.13

Table C.6: Gravimetric measurements of aramid fibre pellets dip coated with FvFvFvFv (instrumental standard deviation: $\pm 1 \mu\text{g}$)

m_{FvFvFvFv} (mg)	C_{FvFvFvFv} (mmol·mL ⁻¹)	m_i (mg)	m_f (mg)	Δm (mg)	$[\Delta m/M_{\text{FvFvFvFv}}]/m_i$	κ (1·mg ⁻¹)
2.05	$1.02 \cdot 10^{-3}$	74.13	75.76	1.22	$1.64 \cdot 10^{-5}$	0.80
2.03	$1.01 \cdot 10^{-3}$	74.32	75.75	1.02	$1.37 \cdot 10^{-5}$	0.68
2.04	$1.02 \cdot 10^{-3}$	74.26	75.89	1.22	$1.64 \cdot 10^{-5}$	0.81
Average						0.76
Standard deviation						0.07
Ratio (%)						9.21

Table C.7: Gravimetric measurements of aramid fibre pellets dip coated with FhFhFhFh (instrumental standard deviation: $\pm 1 \mu\text{g}$)

m_{FhFhFhFh} (mg)	C_{FhFhFhFh} (mmol·mL ⁻¹)	m_i (mg)	m_f (mg)	Δm (mg)	$[\Delta m/M_{\text{FhFhFhFh}}]/m_i$	κ (1·mg ⁻¹)
2.22	$1.05 \cdot 10^{-3}$	74.26	75.44	0.77	$9.81 \cdot 10^{-6}$	0.47
2.18	$1.03 \cdot 10^{-3}$	74.15	75.06	0.50	$6.38 \cdot 10^{-6}$	0.31
2.19	$1.03 \cdot 10^{-3}$	74.46	75.33	0.46	$5.85 \cdot 10^{-6}$	0.28
Average						0.39
Standard deviation						0.20
Ratio (%)						51.28

Table C.8: Gravimetric measurements of aramid fibre pellets dip coated with Fh●Fh●Fh●Fh (instrumental standard deviation: $\pm 1 \mu\text{g}$)

$m_{\text{Fh●Fh●Fh●Fh}}$ (mg)	$C_{\text{Fh●Fh●Fh●Fh}}$ (mmol·mL ⁻¹)	m_i (mg)	m_f (mg)	Δm (mg)	$[\Delta m/M_{\text{Fh●Fh●Fh●Fh}}]/m_i$	κ (1·mg ⁻¹)
2.70	$1.02 \cdot 10^{-3}$	74.57	75.50	0.52	$5.26 \cdot 10^{-6}$	0.26
2.76	$1.04 \cdot 10^{-3}$	74.59	76.29	1.29	$1.30 \cdot 10^{-5}$	0.63
2.71	$1.02 \cdot 10^{-3}$	74.50	75.49	0.58	$5.87 \cdot 10^{-6}$	0.29
Average						0.38
Standard deviation						0.10
Ratio (%)						26.32

C.5. Quantification of coating behaviour oligomers with four phenylalanine units

Table C.9: Gravimetric measurements of aramid fibre pellets dip coated with FFFFb•FFFFb•FFFFb•FFFFb (instrumental standard deviation: $\pm 1 \mu\text{g}$)

$m_{\text{FFFFb}\bullet\text{FFFFb}\bullet\text{FFFFb}\bullet\text{FFFFb}}$ (mg)	$C_{\text{FFFFb}\bullet\text{FFFFb}\bullet\text{FFFFb}\bullet\text{FFFFb}}$ (mmol·mL ⁻¹)	m_i (mg)	m_f (mg)	Δm (mg)	$[\Delta m/M_{\text{FFFFb}\bullet\text{FFFFb}\bullet\text{FFFFb}\bullet\text{FFFFb}}]$ / m_i	K (1·mg ⁻¹)
5.99	$1.00 \cdot 10^{-3}$	74.52	75.81	0.88	$3.97 \cdot 10^{-6}$	0.20
6.03	$1.01 \cdot 10^{-3}$	74.48	76.06	1.17	$5.27 \cdot 10^{-6}$	0.26
6.02	$1.01 \cdot 10^{-3}$	74.47	75.80	0.92	$4.15 \cdot 10^{-6}$	0.21
Average						0.22
Standard deviation						0.03
Ratio (%)						13.64

Table C.10: Gravimetric measurements of aramid fibre pellets dip coated with FFFFv•FFFFv•FFFFv•FFFFv (instrumental standard deviation: $\pm 1 \mu\text{g}$)

$m_{\text{FFFFv}\bullet\text{FFFFv}\bullet\text{FFFFv}\bullet\text{FFFFv}}$ (mg)	$C_{\text{FFFFv}\bullet\text{FFFFv}\bullet\text{FFFFv}\bullet\text{FFFFv}}$ (mmol·mL ⁻¹)	m_i (mg)	m_f (mg)	Δm (mg)	$[\Delta m/M_{\text{FFFFv}\bullet\text{FFFFv}\bullet\text{FFFFv}\bullet\text{FFFFv}}]$ / m_i	K (1·mg ⁻¹)
6.14	$1.01 \cdot 10^{-3}$	74.25	75.810	1.15	$5.10 \cdot 10^{-6}$	0.25
6.09	$1.00 \cdot 10^{-3}$	74.45	76.250	1.39	$6.15 \cdot 10^{-6}$	0.31
6.08	$1.00 \cdot 10^{-3}$	74.59	75.990	0.99	$4.37 \cdot 10^{-6}$	0.22
Average						0.26
Standard deviation						0.04
Ratio (%)						15.38

Table C.11: Gravimetric measurements of aramid fibre pellets dip coated with FFFFh•FFFFh•FFFFh•FFFFh (instrumental standard deviation: $\pm 1 \mu\text{g}$)

$m_{\text{FFFFh}\bullet\text{FFFFh}\bullet\text{FFFFh}\bullet\text{FFFFh}}$ (mg)	$C_{\text{FFFFh}\bullet\text{FFFFh}\bullet\text{FFFFh}\bullet\text{FFFFh}}$ (mmol·mL ⁻¹)	m_i (mg)	m_f (mg)	Δm (mg)	$[\Delta m/M_{\text{FFFFh}\bullet\text{FFFFh}\bullet\text{FFFFh}\bullet\text{FFFFh}}]$ / m_i	K (1·mg ⁻¹)
6.24	$1.01 \cdot 10^{-3}$	74.07	75.360	0.88	$3.85 \cdot 10^{-6}$	0.19
6.20	$1.00 \cdot 10^{-3}$	74.36	75.730	0.96	$4.18 \cdot 10^{-6}$	0.21
6.18	$9.99 \cdot 10^{-4}$	74.56	75.780	0.81	$3.52 \cdot 10^{-6}$	0.18
Average						0.19
Standard deviation						0.02
Ratio (%)						10.53

Table C.12: Gravimetric measurements of aramid fibre pellets dip coated with FFFFu•FFFFu•FFFFu•FFFFu (instrumental standard deviation: $\pm 1 \mu\text{g}$)

$m_{\text{FFFFu}\bullet\text{FFFFu}\bullet\text{FFFFu}\bullet\text{FFFFu}}$ (mg)	$C_{\text{FFFFu}\bullet\text{FFFFu}\bullet\text{FFFFu}\bullet\text{FFFFu}}$ (mmol·mL ⁻¹)	m_i (mg)	m_f (mg)	Δm (mg)	$[\Delta m/M_{\text{FFFFu}\bullet\text{FFFFu}\bullet\text{FFFFu}\bullet\text{FFFFu}}]$ / m_i	K (1·mg ⁻¹)
6.80	$1.01 \cdot 10^{-3}$	74.68	76.26	1.17	$4.65 \cdot 10^{-6}$	0.23
6.76	$1.00 \cdot 10^{-3}$	74.50	76.18	1.27	$5.06 \cdot 10^{-6}$	0.25
6.81	$1.01 \cdot 10^{-3}$	74.26	75.88	1.21	$4.83 \cdot 10^{-6}$	0.24
Average						0.25
Standard deviation						0.01
Ratio (%)						4.00

REFERENCES

General Introduction

- [G.1] Description Regulation (EC) No 443/2009 from website Eur-Lex.europa.eu: <https://eur-lex.europa.eu/legal-content/EN/ALL/?uri=CELEX:32009R0443> (visited at 18-12-2018)
- [G.2] F. Keller, Emissions de CO₂ des voitures neuves, Rapport de la République Française 361; **2008**
- [G.3] Rapport sur la responsabilité sociétale de l'entreprise, PSA Groupe, **2017**
- [G.4] M.K. Debe, Nature, **2012**, 486, 43-51
- [G.5] H. Budde-Meiwes, J. Drillkens, B. Lunz, J. Muennix, S. Rothgang, J. Kowal, D.U. Sauer, Proc. Inst. Mech. Eng. D., **2013**. 227, 761-776
- [G.6] L. Cheah, C. Evans, A. Bandivadekar, J. Heywood, Factor of Two: Halving the Fuel Consumption of New U.S. Automobiles by 2035, Massachusetts institute of technology; **2007**
- [G.7] L. Hollaway, Handbook of polymer composites for engineers, Woodhead publishing limited: Cambridge (UK); **1994**
- [G.8] O. Faruk, M. Sain, Lignin in polymer composites, William Andrew, Norwich (USA); **2016**
- [G.9] R.F. Dodson, S.P. Hammar, L.W. Poye, Inhal. Toxicol., **2008**, 20, 723-732
- [G.10] Website Boronextrication.com <http://www.boronextrication.com/2011/01/24/2011-peugeot-3008-body-structure/> (visited 07-09-2017)
- [G.11] Website Peugeot.fr: <http://www.peugeot.fr/gamme/nos-vehicules/nouveau-suv-3008.html> (visited 07-09-2017)
- [G.12] Dupont Vizilon datasheet http://www.dupont.com/content/dam/dupont/products-and-services/plastics-polymers-and-resins/thermoplastics/documents/DuPont_Vizilon_datasheet_VZE_A11209_00_A0416.pdf (visited 07-09-2017)
- [G.13] Website Materialsforengineering.co.uk: <http://www.materialsforengineering.co.uk/engineering-materials-news/thermoplastic-composites-close-to-mass-production/52139> (visited at 18-12-2018)
- [G.14] DuPont, Kevlar Aramid Fibre Technical Guide, D.A.F. Systems: Richmond, **2017**
- [G.15] A.R. Bunsell, Handbook of properties of textile and technical fibres, Woodhead publishing limited: Cambridge (UK); **2018**
- [G.16] E. Kaiser, R.L. Colescott, C.D. Bossinger, P.I. Cook, Anal. Biochem., **1970**, 34, 595-598

Chapter I

- [I.1] F.C. Campbell, Structural composite materials, ASM International: Russel Township, **2010**
- [I.2] M. Kutz, Applied plastics engineering handbook, Elsevier: Amsterdam, **2011**
- [I.3] T.R. Crompton, Physical testing of plastics, Smithers Rapra Technology: Shawbury, **2012**

- [I.4] Cambridge Engineering Selector software (CES 4.1), **2003**, Granta Design Limited, Rustat House, 62 Clifton Rd, Cambridge, CB1 7EG
- [I.5] W. Denissen, J.M. Winne, F.E. du Prez, *Chem. Sci.*, **2016**, 7, 30-38
- [I.6] F-L. Jin, X. Li, S-J. Park, *J. Ind. Eng. Chem.*, **2015**, 29, 1-11
- [I.7] Global unsaturated polyester resin in automotive composites market, Lucintel LLC, **2017**
- [I.8] D.M. Dean, L. Rebenfeld, R.A. Register, *J. Mater. Sci.*, **1998**, 33, 4797-4812
- [I.9] DuPont, Kevlar aramid fibre technical guide, D.A.F. Systems: Richmond, **2017**
- [I.10] L. Hollaway, *Handbook of polymer composites for engineers*, Woodhead publishing limited: Cambridge (UK); **1994**
- [I.11] A.R. Bunsell, *Handbook of properties of textile and technical fibres*, Woodhead publishing limited: Cambridge (UK); **2018**
- [I.12] A.F. Zhigach, A.M. Tsirlin, E.A. Shchetilina, I.L. Svetlov, V.I. Grigoriev, E.G. Shafranovich, T.I. Bulygina, V.A. Yartsev, *Polymer mechanics: Mechanical properties of boron fibers*, Kluwer Academic Publishers, Dordrecht; **1973**
- [I.13] DuPont, Nomex 410 Technical data sheet:
http://www.dupont.com/content/dam/assets/products-and-services/electronic-electrical-materials/assets/DPT16_21668_Nomex_410_Tech_Data_Sheet_me03_REFERENCE.pdf
 (visited 17-06-2018)
- [I.14] H.W. Herring, *Selected mechanical and physical properties of boron filaments*, NASA technical note, **1966**
- [I.15] N.M. Chikradze, L.A. Japaridze, G.S. Abashidze, *Properties of basalt plastic and of composites reinforced by hybrid fibers in operating conditions*, *Composites and Their Applications*, Ning Hu Intech open, **2012**
- [I.16] *Quality certificates for fabrics and rovings*. Incotology Ltd.: Bonn, **2012**
- [I.17] S.M. Lee, *Handbook of composite reinforcements*, Wiley-VCH Verlag GmbH & Co. KGaA: Weinheim, **1993**
- [I.18] B. Sanborn, A.M. DiLeonardi, T. Weerasooriya, *J. Dyn. Behav. Mater.*, **2015**, 1, 4-14
- [I.19] C.C. Foo, G.B. Chai, L.K. Seah, *Compos. Struct.*, **2007**, 80, 588-594
- [I.20] Reinforcement fibres information: <https://www.compositesworld.com/articles/the-fiber-2016> (visited 17-06-2018)
- [I.21] A. Kelly, *Concise encyclopedia of composite materials*, Eds. R.W. Cahn, M.B. Bever, Pergamon Press: Oxford, **1989**
- [I.22] *Aramid Fiber Market worth over \$5bn by 2024*, Global Market Insights Inc., **2017**
- [I.23] G.M. Fallatah, N. Dodds, A.G.G. Gibson, *Plast. Rubber Compos.*, **2007**, 36, 403-412
- [I.24] B.L. Lee, T.F. Walsh, S.T. Won, H.M. Patts, J.W. Song, A.H. Mayer, *J. Compos. Mater.* **2001**, 35, 1605-1633

- [I.25] Y. Erbil, A.K. Ekşi, D.A. Bircan, Spall Liner: from fiber to protection, Proceedings of a conference, 6th International Advanced Technologies Symposium (IATS'11): Elazığ, **2011**
- [I.26] X-D. Zu, Z-X. Huang, W. Zhai, Lat. Am. J. Solids. Struct., **2015**, 12, 507-519
- [I.27] Dupont Armor plating brochure: http://www.dupont.com/content/dam/dupont/products-and-services/fabrics-fibers-and-nonwovens/fibers/documents/KevlarBrochFinal_Reader.pdf (visited at 07-09-2017)
- [I.28] P.L Walton, A.J. Majumdar, J. Mater. Sci., **1978**, 13, 1075
- [I.29] Website Dupont.com HANS-Device: <http://www.dupont.com/products-and-services/plastics-polymers-resins/thermoplastics/case-studies/reinforced-polyamide-protecting-drivers.html> (visited 29-08-2016)
- [I.30] Y. Bader, Kevlar® and Nomex® - Improved reinforcement performance for demanding automotive applications, internal presentation Dupont for PSA groupe, **2016**
- [I.31] E.W. Huntley, M.B. Huntley, A.S. Whitehill, US Patent 20140266169 A1, **2014**
- [I.32] Teijinaramid.com Twaron based optical fibre website: <http://www.teijinaramid.com/applications/optical-fibre-cables/> (visited 07-09-2017)
- [I.33] News.Nike.com website: <http://news.nike.com/news/nike-basketball-s-superhero-elite-series-2-0-rises-above-the-rest> (visited 07-09-2017)
- [I.34] Website Legendarchery.com: <https://legendarchery.com/blogs/archery-bowhunting-blog/15724912-the-details-you-need-to-know-about-your-bowstring> (visited 29-08-2016)
- [I.35] United States Federal Aviation Administration, Handbook for composite materials, Ch7: Advanced composite materials, **2017**
- [I.36] Website 3b Fibreglass products: <http://www.3b-fibreglass.com/products/continuous-filament-mat/> (visited 24-08-2018)
- [I.37] T. Vu-Khanh, S. Frikha, J. Thermoplast. Compos., **1999**, 12, 84-95
- [I.38] Dupont Kevlar XP H170 helmet information sheet: <http://www.dupont.co.uk/content/dam/dupont/products-and-services/fabrics-fibres-and-nonwovens/fibres/documents/Kevlar%C2%AE%20XP%20H170%20Helmets.pdf> (visited 07-09-2017)
- [I.39] D.T. Campbell, D.R. Cramer, Hybrid thermoplastic composite ballistic helmet fabrication study, Fibreforge corporation internal studies, **2008**
- [I.40] S.D. Salman, Z. Leman, M.T.H. Sultan, M.R. Ishak, F. Cardona, BioResources, **2015**, 10, 8580-8603
- [I.41] T.P. Sathishkumar, J. Naveen, S. Satheeskumar, J. Reinf. Plast. Comp., **2014**, 33, 454-471
- [I.42] M.R. Ricciardi, A. Martone, A. Boriello, M. Zarrelli, M. Giordano, A. Langella, V. Antonucci, Polym. Compos., **2015**, 36, 1548-0569
- [I.43] T.P. Sathishkumar, J. Naveen, S. Satheeskumar, J. Reinf. Plast. Compos., **2014**, 33, 454-471

- [I.44] D. Zhu, B. Mobasher, S.D. Rajan, Characterization of mechanical behavior of Kevlar 49 fabrics, *Experimental and Applied Mechanics*, v.6, Society for Experimental Mechanics Series, **2011**, 377-384, proceedings of a conference
- [I.45] M.A. Torabizadeh, *Indian J. Eng. Mater. S.*, **2013**, 20, 299-309
- [I.46] S.L. Valenca, S. Griza, V. Gomes de Oliveira, E.M. Sussuchi, F.G.C. de Cunha, *Composites part B*, **2015**, 70, 1-8
- [I.47] Plasticnews.com price listing: <http://www.plasticsnews.com/resin/thermosets/current-pricing> (07-09-2017)
- [I.48] K.S. Betts, *Environ. Health Perspect.*, **2008**, 116, A210-A213
- [I.49] US Congress Office of technology assessment, *Advanced materials by design*, OTA-E-351 Washington, DC : US government printing office, **1988**
- [I.50] M. Avella, R. Dell'Erba, E. Martuscelli, *Polym. Compos.*, **1996**, 17, 288-299
- [I.51] B. Larin, G. Marom, C.A. Avila-Orta, R.H. Somami, B.S. Hsaio, *J. Appl. Polym. Sci.*, **2005**, 98, 1113-1118
- [I.52] B. Larin, C.A. Avila-Orta, R.H. Somami, B.S. Hsiao, G. Marom, *Polymer*, **2008**, 49, 295-302
- [I.53] X. Chen, S. Zhang, G. Xu, X. Zhu, W. Liu, *J. Appl. Polym. Sci.*, **2012**, 125, 1166-1175
- [I.54] Z. Yu, A. Ait-Kadi, J. Brisson, *Polym. Eng. Sci.*, **1991**, 31, 1222-1227
- [I.55] Z. Yu, A. Ait-Kadi, J. Brisson, *Polym. Eng. Sci.*, **1991**, 31, 1228-1232
- [I.56] Z. Yu, J. Brisson, A. Ait-Kadi, *Polym. Compos.*, **1994**, 15, 64-73
- [I.57] Z. Yu, A. Ait-Kadi, J. Brisson, *Polymer*, **1994**, 35, 1409-1417
- [I.58] A. Dorigato, L. Fambri, *J. Reinf. Plast. Compos.*, **2013**, 32, 1243-1256
- [I.59] S-J. Park, M-K. Seo, T-J. Ma, D-R. Lee, *J. Colloid Interface Sci.*, **2002**, 252, 249-255
- [I.60] M. Nardin, J. Schultz, *J. Compos. Interfaces*, **1993**, 2, 177-192
- [I.61] F. Guo, Z-Z. Zhang, W-M. Liu, F-H. Su, H-J. Zhang, *Trib. Int.*, **2009**, 42, 243-249
- [I.62] V. Gupta, *High Perform. Polym.*, **2002**, 14, 285-292
- [I.63] G. Li, C. Zhang, Y. Wang, P. Li, Y. Yu, X. Jia, H. Liu, X. Yang, Z. Xue, S. Ryu, *Compos. Sci. Technol.*, **2008**, 68, 3208-3214
- [I.64] P. Lee-Sullivan, K.S. Chian, C.Y. Yue, H.C. Looi, *J. Mater. Sci. Lett.*, **1994**, 13, 305-309
- [I.65] M. Rajabian, C. Dubois, *Polym. Compos.*, **2006**, 27, 129-137
- [I.66] M. Mukherjee, C.K. Das, *J. Reinf. Plast. Compos.*, **2008**, 27, 523-539
- [I.67] R. Sa, Y. Yan, Z. Wei, L. Zhang, W. Wang, M. Tian, *ACS Appl. Mater. Inter.*, **2014**, 6, 21730-21738
- [I.68] D. Hull, T.W. Clyne, *An introduction to composite materials*, Cambridge University Press: Cambridge, **1996**

- [I.69] Website matter.org.uk: <http://www.matter.org.uk/matscidrom/manual/co.html> (visited 31-08-2016), archived link: <http://archive.is/omLY0> (visited 08-09-2017)
- [I.70] J.C. Halpin, J.L. Kardos, *Polym. Eng. Sci.*, **1976**, 16, 344-352
- [I.71] L.T. Drzal, M.J. Rich, P.F. Lloyd, *J. Adhes.*, **1983**, 16, 1-30
- [I.72] M. R. Kamal, L. Song, P. Singh, *Polym. Compos.*, **1986**, 7, 323-329
- [I.73] N. L. Batista, P. Olivier, G. Bernhart, M. C. Rezende, E. C. Botelho, *Mater. Res.*, **2016**, 19, 195-201
- [I.74] E. Pippel, *J. Phys. IV*, **1993**, 3, 1905-1910
- [I.75] I.V. Andrianov, J. Awrejcewicz, D. Weichert, *Acta Mech. Sin.*, **2011**, 27, 90-97
- [I.76] Y. Wang, J. Li, D. Zhao, *Compos. Eng.*, **1995**, 5, 1159-1175
- [I.77] Y. Zhang, Z. Jiang, Y. Huang, Q. Li, *Fibres Polym.*, **2011**, 12, 1014-1020
- [I.78] R. Libanori, D. Carnelli, R. Rothfuchs, M.R. Binelli, M. Zanini, L. Nicoleau, B. Feichtenschlager, G. Albrecht, A.R. Studart, *Bioinspir. Biomim.*, **2016**, 11, 036004
- [I.79] A.J. Cervenka, R.J. Young, K. Keuseng, *Composites Part A*, **2005**, 36, 1011-1019
- [I.80] A. Mathur, A.N. Netravali, *J. Mater. Sci.*, **1996**, 31, 1265-1274
- [I.81] J. Maity, C. Jacob, C.K. Das, S. Alam, R.P. Singh, *Composites Part A*, **2008**, 39, 825-833
- [I.82] J. Maity, C. Jacob, S. Alam, R.P. Singh, *J. Compos. Mater.*, **2009**, 43, 709-723
- [I.83] M. Su, A. Gu, G. Liang, L. Yuan, *Appl. Surf. Sci.*, **2011**, 257, 3158-3167
- [I.84] R. Sa, Y. Yan, Z. Wei, L. Zhang, W. Wang, M. Tian, *ACS Appl. Mater. Inter.*, **2014**, 6, 21730-21738
- [I.85] S.R. Wu, G.S. Sheu, S.S. Shyu, *Appl. Polym. Sci.*, **1996**, 62, 1347-1360
- [I.86] M. Takayanagi, S. Ueta, W-Y. Lei, K. Koga, *Polym. J.*, **1987**, 19, 467-474
- [I.87] A. Abe, Y. Saito, M. Imaizumi, M. Ogawa, T. Takeichi, K. Jinno, *J. Sep. Sci.*, **2005**, 28, 2413-2418
- [I.88] S. Zhao, L. Cheng, Y. Guo, Y. Zheng, B. Li, *Mater. Des.*, **2012**, 35, 749-753
- [I.89] B.J. Mullins, A. Pfrang, R.D. Braddock, T. Schimmel, G. Kasper, *J. Colloid. Interface Sci.*, **2007**, 312, 333-340
- [I.90] M.M. Amrei, D.G. Venkateshan, N.D'Souza, J. Atulasimha, H.V. Tafreshi, *Langmuir*, **2016**, 32, 13333-13339
- [I.91] Q. Li, T. Zhang, Y. Pan, L. C. Ciacchi, B. Xu, G. Wei, *RSC Adv.*, **2016**, 6, 12893-12912
- [I.92] Y. Pan, F. Wang, Y. Liu, J. Jiang, Y-G. Yang, H. Wang, *Nanoscale*, **2014**, 6, 9951-9954
- [I.93] D. Hansen, N. Bomholt, J.C. Jeppesen, A.C. Simonsen, *Appl. Surf. Sci.*, **2017**, 392, 181-188
- [I.94] A.J. Kinloch, A.C. Taylor, M. Techapaitoon, W.S. Teo, S. Sprenger, *Philos. Trans. A Math. Phys. Eng. Sci.*, **2016**, 13, 20150275
- [I.95] S. Sockalingam, G Nilakantan, *Int. J. Aeronaut. Space Sci.*, **2012**, 13, 282-295

- [I.96] D.J. Bannister, M.C. Andrews, A.J. Cervenka, R.J. Young, *Compos. Sci. Technol.*, **1995**, 53, 411-421
- [I.97] D.B. Eagles, B.F. Blumentritt, S.L. Cooper, *J. Appl. Polym. Sci.*, **1976**, 20, 435-448
- [I.98] K. Sattler, Z-Q. Feng, Q-C. He, Q. Zeng, P. Joli, *Handbook of nanophysics*, Taylor & Francis: Milton Park, **2010**
- [I.99] A. Nevarez-Rascon, E. Orrantia-Borunda, J. Gonzalez-Hernandez, S. Flores-Gallardo, A. Hurtado-Macias, *Mater. Lett.*, **2014**, 136, 63-66
- [I.100] P. Diss, J. Lamon, L. Carpentier, J.L. Loubet, P. Kapsa, *Carbon*, **2002**, 40, 2567-2579
- [I.101] T. Saraswati, T. Sritharan, S. Mhaisalkar, C.D. Breach, F. Wulff, *Mater. Sci. Eng.: A.*, **2006**, 423, 14-18
- [I.102] G.M. Wu, *Mater. Chem. Phys.*, **2004**, 85, 81-87
- [I.103] J.F. Moulder, W.F. Stickle, P.E. Sobol, K.D. Bomben, *X-ray photoelectron spectroscopy*, Perkin-Elmer Corporation: Eden Prairie; **1992**
- [I.104] S. Canli, *Thickness analysis of thin films by energy dispersive X-ray spectroscopy*, Master Thesis Graduate school of natural and applied sciences of middle east technical university, **2010**
- [I.105] J.C. Russ, M. Ashby, R. Kiessling, J. Charles, *Fundamentals of Energy Dispersive X-ray Analysis*, Butterworth-Heinemann: Oxford, **1984**
- [I.106] P. Lehuédé, A. Meringo, *Environ. Health Perspect.*, **1994**, 102, 73-75
- [I.107] S. Manoharan, B. Suresha, G. Ramadoss, B. Bharath, *J. Mater*, **2014**, 2014, 478549
- [I.108] A. Yurdakul, G. Günkaya, T. Kavas, E. Dölekçekiç, B. Karasu, *AKU J. Sci. Eng.*, **2014**, 14, 195-191
- [I.109] G. Aijun, G. Yizhuo, W. Qing, Y. Chao, L. Min, Z. Zuoguang, *Chin. J. Aeronaut.*, **2015**, 28, 1255-1262
- [I.110] B. Bhushan, *Modern Tribology Handbook volume 2: Materials coatings, and industrial applications*, CRC Press LLC: Florida, **2001**
- [I.111] H.C.O. Fonseca, R.H.L. Garcia, R.J. Ferreira, F.R.O. Silva, A.J. Potiens, S.K. Sakata, *XRD and SEM/EDS characterization of coconut fibers in raw and treated forms used in the treatment of strontium in aqueous solution*, International Nuclear Atlantic conference, **2015**, proceedings of a conference
- [I.112] M. Pracella, M-U. Haque, V. Alvarez, *Polymers*, **2010**, 2, 554-574
- [I.113] L.S. Schadler, C. Galiotis, *Int. Mater. Rev.*, **1995**, 40, 116-134
- [I.114] L. Yu, K. Dean, L. Li, *Prog. Polym. Sci.*, **2006**, 31, 576-602
- [I.115] R. McMican, *Reinf. Plast.*, **2012**, 56, 29-32
- [I.116] R.L. Gorowara, W.E. Kosik, S.H. McKnight, R.L. McCullough, *Composites Part A*, **2001**, 32, 323-329
- [I.117] A. Lončar, D. Vojvodić, D. Komar, *Acta. Stomatol. Croat.*, **2006**, 40, 72-82

- [I.118] J.L. Thomason, *Composites*, **1995**, 26, 467-475
- [I.119] E.P.A. van Bruggen, R.P. Koster, S.J. Picken, K. Ragaert, *Int. Polym. Process*, **2016**, 2, 179-187
- [I.120] J.S. Kim, D.H. Kim, *J. Thermoplast. Compos. Mater.*, **2015**, 28, 1599-1611
- [I.121] F. Yuan, R. Ou, Y. Xie., Q-W. Wang, *J. For. Res.*, **2013**, 24, 149-153
- [I.122] D.G. Guillot, US patent 5498649A, **1996**
- [I.123] A. Farzadfar, S.N. Khorasani, S. Khalili, *Polym. Int.*, **2014**, 63, 145-150
- [I.124] S. Fu, B. Yu, L. Duan, H. Bai, F. Chen, K. Wang, H. Deng, Q. Zhang, Q. Fu, *Compos. Sci. Technol.*, **2015**, 108, 23-31
- [I.125] Eastman.com compatibilizer product listing:
<http://www.eastman.com/Products/Pages/ProductHome.aspx?Product=71000983&list=products> (visited 07-09-2017)
- [I.126] Dupont.com compatibilizer product listing: <http://www.dupont.com/products-and-services/plastics-polymers-resins/ethylene-copolymers/brands/fusabond-functional-polymers.html> (visited 07-09-2017)
- [I.127] Entec polymers.com compatibilizer product listing:
<https://www.entecpolymers.com/products/resin-types/maleic-anhydride-grafted-polymer-mah-g> (visited 18-12-2018)
- [I.128] G.S. Shibulal, K. Naskar, *Express Polym. Lett.*, **2012**, 6, 329-344
- [I.129] J. Sardar, *J. Polym. Eng.*, **2011**, 31, 279-282
- [I.130] Overview of commercial compatibilizers:
http://www.plasticsindustry.org/sites/plastics.dev/files/Compatibilizers%20Whitepaper%20%28Version%201.0%29_0.pdf (visited 19-06-2018)
- [I.131] J-F. Lutz, D. Neugebauer, K. Matyjaszewski, *J Am. Chem. Soc.*, **2003**, 125, 6986-6993
- [I.132] L.E. Rosebrugh, V.M. Marx, B.K. Keitz, R.H. Grubbs, *J. Am. Chem. Soc.*, **2013**, 10032-10035
- [I.133] M.J. Miri, B.P. Pritchard, H.N. Cheng, *J. Mol. Model.*, **2010**, 17, 1767-1780
- [I.134] A.K. Rappe, O.G. Polyakov, L.M. Bormann-Rochotte, *Stereoselective polymerization with single-site catalysts*, CRC Press: Boca Raton, **2007**
- [I.135] G. Natta, F. Danusso, *Stereoregular polymers and stereospecific polymerizations; the contributions of Giulio Natta and his school to polymer chemistry; Volume 2*, Pergamon Press: Oxford, **1967**
- [I.136] A. Shamiri, M.H. Chakrabarti, S. Jahan, M.A. Hussain, W. Kaminsky, P.V. Aravind, W.A. Yehye, *Materials*, **2014**, 7, 5069-5108
- [I.137] G. Allegra, *Makromolekul. Chem.*, **1971**, 145, 235-246
- [I.138] J.A. Ewen, R.L. Jones, A. Razavi, J.D. Ferrara, *J. Am. Chem. Soc.*, **1988**, 110, 6255-6256
- [I.139] J.W. Kramer, D.S. Treitler, E.W. Dunn, P.M. Castro, T. Roisnel, C.M. Thomas, G.W. Coates, *J. Am. Chem. Soc.*, **2009**, 131, 16042-16044

- [I.140] M. Imoto, T. Otsu, Y. Harada, *Makromol. Chem.*, **1963**, 65, 180-193
- [I.141] M. Imoto, T. Otsu, M. Nakabayashi, *Makromol. Chem.*, **1963**, 65, 194-201
- [I.142] M. Hirooka, H. Yabuuchi, S. Morita, S. Kawasumi, K. Nakaguchi, *J. Polym. Sci. Part B Polym. Phys.*, **1967**, 5, 47-55
- [I.143] J-F. Lutz, B. Kirci, K. Matyjaszewski, *Macromolecules*, **2003**, 36, 3136-3145
- [I.144] J. Huang, S.R. Turner, *Polymer*, **2017**, 116, 572-586
- [I.145] M. Hirooka, *J. Polym. Sci. Part B Polym. Lett.*, **1972**, 10, 171-176
- [I.146] M. Nagel, D. Poli, A. Sen, *Macromolecules*, **2005**, 38, 7262-7265
- [I.147] S. Kaur, G. Singh, A.V. Kothari, V.K. Gupta, *J. Appl. Polym. Sci.*, **2009**, 111, 87-93
- [I.148] S. Pfeifer, J-F. Lutz, *J. Am. Chem. Soc.*, **2007**, 129, 9542-9543
- [I.149] Y.L. Spirin, T.S. Yatsimirskaya, *Polym. Sci. U.S.S.R.*, **1976**, 18, 857-862
- [I.150] Y. Ishido, A. Kanazawa, S. Kanaoka, S. Aoshima, *Polym. Chem.*, **2014**, 5, 43-47
- [I.151] D. Nagai, A. Sudo, T. Endo, *Macromolecules*, **2006**, 39, 8898-8900
- [I.152] A.R. Song, K.A. Parker, N.S. Sampson, *J. Am. Chem. Soc.*, **2009**, 131, 3444-3445
- [I.153] C.S. Daeffler, R.H. Grubbs, *Macromolecules*, **2013**, 46, 3288-3292
- [I.154] M. Bornand, P. Chen, *Angew. Chem. Int. Ed.*, **2005**, 44, 7909-7911
- [I.155] M. Bornand, S. Torker, P. Chen, *Organometallics*, **2007**, 26, 3585-3596
- [I.156] S. Torker, A. Muller, P. Chan, *Angew. Chem. Int. Ed.*, **2010**, 49, 3762-3766
- [I.157] K. Vehlow, D. Wang, M.R. Buchmeiser, S. Blechert, *Angew. Chem. Int. Ed.*, **2008**, 47, 2615-2618
- [I.158] J. He, J. Ren, E. Mastan, *Sequence controlled polymers*, Chapter 10: Sequence-controlled polymers by chain polymerization, Ed. J-F. Lutz, Wiley-VCH Verlag GmbH & Co. KGaA: Weinheim, **2018**
- [I.159] D. Benoit, C.J. Hawker, E.E. Huang, Z. Lin, T.P. Russell, *Macromolecules*, **2000**, 33, 1505-1507
- [I.160] D. Moatsuo, C.F. Hansell, R.K. O'Reilly, *Chem. Sci.*, **2014**, 5, 2246-2250
- [I.161] T. Soejima, K. Satoh, M. Kamigaito, *ACS Macro Lett.*, **2015**, 4, 745-749
- [I.162] T. Soejima, K. Satoh, M. Kamigaito, *J. Am. Chem. Soc.*, **2016**, 138, 944-954
- [I.163] T. Soejima, K. Satoh, M. Kamigaito, *Polym. Chem.*, **2016**, 7, 4833-4841
- [I.164] M. Hisano, K. Takeda, T. Takashima, Z. Jin, A. Shiibashi, A. Matsumoto, *Macromolecules*, **2013**, 46, 7733-7744
- [I.165] K. Satoh, M. Matsuda, K. Nagai, M. Kamigaito, *J. Am. Chem. Soc.*, **2010**, 132, 10003-10005
- [I.166] M. Szwarc, M. Levy, R. Milkovich, *J. Am. Chem. Soc.*, **1956**, 78, 2656-2657
- [I.167] F. Alsubaie, A. Anastasaki, P. Wilson, D.M. Haddleton, *Polym. Chem.*, **2015**, 6, 406-417

- [I.168] A. Anastasaki, B. Oschmann, J. Willenbacher, A. Melker, M.H.C. van Son, N.P. Truong, M.W. Schulze, E.H. Discekici, A.J. McGrath, T.P. Davis, C.M. Bates, C.J. Hawker, *Angew. Chem. Int. Ed.*, **2017**, 56, 14483-14487
- [I.169] G. Gody, T. Maschmeyer, P.B. Zetterlund, S. Perrier, *Nat. Commun.*, **2013**, 4, 2505
- [I.170] G. Gody, T. Maschmeyer, P.B. Zetterlund, S. Perrier, *Macromolecules*, **2014**, 47, 3451-3460
- [I.171] G. Gody, T. Maschmeyer, P.B. Zetterlund, S. Perrier, *Polym. Chem.*, **2015**, 6, 1502-1511
- [I.172] L. Martin, G. Gody, S. Perrier, *Polym. Chem.*, **2015**, 6, 4875-4886
- [I.173] A. Kuroki, I. Martinez-Botella, C.H. Hornung, L. Martin, E.G.L. Williams, K.E.S. Locock, M. Hartlieb, S. Perrier, *Polym. Chem.*, **2017**, 8, 3249-3254
- [I.174] Q. Zhang, A. Anastasaki, G-Z. Li, A.J. Haddleton, P. Wilson, D.M. Haddleton, *Polym. Chem.*, **2014**, 5, 3876-3883
- [I.175] F.A. Leibfarth, K.M. Mattson, B.P. Fors, H.A. Collins, C.J. Hawker, *Angew. Chem. Int. Ed.*, **2013**, 52, 199-210
- [I.176] A. Anastasaki, V. Nikolaou, G.S. Pappas, Q. Zhang, C. Wan, P. Wilson, T.P. Davis, M.R. Whittaker, D. M. Haddleton, *Chem. Sci.*, **2014**, 5, 3536-3542
- [I.177] A. Anastasaki, V. Nikolaou, N. W. McCaul, A. Simula, J. Godfrey, C. Waldron, P. Wilson, K. Kempe, D.M. Haddleton, *Macromolecules*, **2015**, 48, 1404-1411
- [I.178] D. Oh, M. Ouchi, T. Nakanishi, H. Ono, M. Sawamoto, *ACS Macro Lett.*, **2016**, 5, 745-749
- [I.179] P. Delduc, C. Tailhan, S.Z. Zard, *J. Chem. Soc. Chem. Commun.*, **1988**, 4, 308-310
- [I.180] G. Moad, *Polym. Chem.*, **2017**, 8, 177-219
- [I.181] G. Moad, C. Guerrero-Sanchez, J.J. Haven, D.J. Keddie, A. Postma, E. Rizzardo, S.H. Thang. Eds. J-F. Lutz, T.Y. Meyer, M. Ouchi, M. Sawamoto *Sequence-controlled polymers: Synthesis, self-assembly and properties*, Chapter 9: RAFT for the control of monomer sequence distribution – Single unit monomer insertion (SUMI) into dithibenzoate RAFT agents., American Chemical Society: Washington, **2014**
- [I.182] S. Hoeshyar, D.J. Keddie, G. Moad, R.J. Mulder, S. Saubern, J. Tsanaktsidis, *Polym. Chem.*, **2012**, 3, 1879-1889
- [I.183] J. Vandenberg, G. Reekmans, P. Adriaensens, T. Junkers, *Chem. Commun.*, **2013**, 49, 10358-10360
- [I.184] N. Isahak, G. Gody, L.R. Malins, N.J. Mitchell, R.J. Payne, S. Perrier, *Chem. Commun.*, **2016**, 52, 12952
- [I.185] J. Xu, S. Shanmugam, C. Fu, K-F. Aguey-Zinsou, C. Boyer, *J. Am. Chem. Soc.*, **2016**, 3094-3106
- [I.186] J. Xu, C. Fu, S. Shanmugam, C.J. Hawker, G. Moad, C. Boyer, *Angew. Chem. Int. Ed.*, **2017**, 56, 8376-8383
- [I.187] A. Aerts, R.W. Lewis, Y. Zhou, N. Malic, G. Moad, A. Postma, *Macromol. Rapid Commun.*, **2018**, 1800240
- [I.188] S. Hadjikyriacou, Z. Fodor, R. Faust, *J. Macromol. Sci.*, **1995**, 32, 1137-1153

- [I.189] S. Ida, T. Terashima, M. Ouchi, M. Sawamoto, *J. Polym. Sci. Part A Polym. Chem.*, **2010**, *48*, 3375-3381
- [I.190] B.R. Elling, Y. Xia, *J. Am. Chem. Soc.*, **2015**, *137*, 9922-9926
- [I.191] X. Tong, B-H. Guo, Y. Huang, *Chem. Commun.*, **2011**, *47*, 1455-1457
- [I.192] Y. Hibi, M. Ouchi, M. Sawamoto, *Nat. Commun.*, **2016**, *7*, 11064
- [I.193] H.T. Grampel, Y.Y. Tan, G. Challa, **1990**, *23*, 5209-5216
- [I.194] P.J. Milnes, M.L. McKee, J. Bath, L. Song, E. Stulz, A.J. Turberfield, R.K. O'Reilly, *Chem. Commun.*, **2012**, *48*, 5614-5616
- [I.195] B. Lewandowski, G.D. Bo, J.W. Ward, M. Papmeyer, S. Kuschel, M.J. Aldegunde, P.M.E. Gramlich, D. Heckmann, S.M. Goldup, D.M.D'Souza, A.E. Fernandes, D.A. Leigh, *Science*, **2013**, *339*, 189-193
- [I.196] S. Ida, T. Terashima, M. Ouchi, M. Sawamoto, *J. Am. Chem. Soc.*, **2009**, *131*, 10808-1080
- [I.197] S. Ida, M. Ouchi, M. Sawamoto, *J. Am. Chem. Soc.*, **2010**, *132*, 14748-14750
- [I.198] S. Ida, M. Ouchi, M. Sawamoto, *Macromol. Rapid Commun.*, **2011**, *32*, 209-214
- [I.199] Y. Hibi, S. Tokuoka, T. Terashima, M. Ouchi, M. Sawamoto, *Polym. Chem.*, **2011**, *2*, 341-347
- [I.200] Y. Hibi, M. Ouchi, M. Sawamoto, *Angew. Chem. Int. Ed.*, **2011**, *50*, 7434-7437
- [I.201] S. Kobayashi, L.M. Pitet, M.A. Hillmyer, *J. Am. Chem. Soc.*, **2011**, *133*, 5794-5797
- [I.202] J. Zhang, M.E. Matta, M.A. Hillmyer, *ACS Macro Lett.*, **2012**, *1*, 1383-1387
- [I.203] R. M. Weiss, A.L. Short, T.Y. Meyer, *ACS Macro Lett.*, **2015**, *4*, 1039-1043
- [I.204] W.R. Gutekunst, C.J. Hawker, *J. Am. Chem. Soc.*, **2015**, *137*, 8038-8041
- [I.205] K. Satoh, S. Ozawa, M. Mizutani, K. Nagai, M. Kamigaito, *Nature Comm.*, **2010**, *1*
- [I.206] R.M. Stayshich, T.Y. Meyer, *J. Am. Chem. Soc.*, **2010**, *132*, 10920-10934
- [I.207] F-R. Zeng, Y. Liang, Z-L. Li, *Molecules*, **2018**, *23*, 452
- [I.208] R.B. Merrifield, *J. Am. Chem. Soc.*, **1963**, *85*, 2149-2154
- [I.209] F. Breitling, A. Nesterov, V. Stadler, T. Felgenhauer, F.R. Bischoff, *Mol. Biosyst.*, **2010**, *5*, 224-234
- [I.210] J. Xie, P.G. Schultz, *Curr. Opin. Chem. Biol.*, **2005**, *9*, 548-554
- [I.211] J.A. Johnson, Y.Y. Lu, J.A. van Deventer, D.A. Tirrell, *Curr. Opin. Chem. Biol.*, **2010**, *14*, 774-780
- [I.212] P.H.H. Hermkens, H.C.J. Ottenheijm, D. Rees, *Tetrahedron*, **1996**, *52*, 4527-4554
- [I.213] R.N. Zuckermann, J.M. Kerr, S.B.H. Kent, W.H. Moos, *J. Am. Chem. Soc.*, **1992**, *114*, 10646-10647
- [I.214] R.N. Zuckermann, G.M. Figliozzi, S.C. Banville, J.M. Kerr, M.A. Siani, E.J. Martin, E.G. Brown, L. Want, *Innovations and perspectives in solid-phase synthesis*, ed. R. Eption, Mayflower Worldwide Ltd.: Oxford, **1994**

- [I.215] T. Uno, E. Beausoleil, R.A. Goldsmith, B.H. Levine, R.N. Zuckermann, *Tetrahedron Lett.*, **1999**, 40, 1475-1478
- [I.216] R.N. Zuckermann, E.J. Martin, D.C. Spellmeyer, G.B. Stauber, K.R. Shoemaker, J.M. Kerr, G.M. Figliozzi, D.A. Goff, M.A. Siani, *J. Med. Chem.*, **1994**, 37, 2678-2685
- [I.217] T.T. Trinh, L. Oswald, D. Chan-Seng, J.-F. Lutz, *Macromol. Rapid Commun.*, **2014**, 35, 141-145
- [I.218] U.S. Gunay, B.E. Petit, D. Karamessini, A. Al Ouhabi, *Chem*, **2016**, 1, 114-126
- [I.219] J.W. Grate, K.-F. Mo, M.D. Daily, *Angew. Chem. Int. Ed.*, **2016**, 55, 3925-3930
- [I.220] S. Martens, J. van den Begin, A. Madder, F.E. du Prez, P. Espeel, *J. Am. Chem. Soc.*, **2016**, 138, 14182-14185
- [I.221] S.C. Solleder, S. Martens, P. Espeel, F.E. du Prez, M.A.R. Meier, *Chem. Eur. J.*, **2017**, 23, 13906-13909
- [I.222] S. Celasun, F.E. du Prez, H.G. Börner, *Macromol. Rapid Commun.*, **2017**, 38, 1700688
- [I.223] J.O. Holloway, S. Aksakal, F.E. du Prez, C.R. Becer, *Macromol. Rapid Commun.*, **2017**, 1700500
- [I.224] A. Al Ouahabi, M. Kotera, L. Charles, J.-F. Lutz, *ACS Macro Lett.*, **2015**, 4, 1077-1080
- [I.225] A. Al Ouahabi, L. Charles, J.-F. Lutz, *J. Am. Chem. Soc.*, **2015**, 137, 5629-5635
- [I.226] L. Charles, G. Cavallo, V. Monnier, L. Oswald, R. Szweda, J.-F. Lutz, *J. Am. Soc. Mass Spectrom.*, **2017**, 28, 1149-1159
- [I.228] G. Cavallo, A. Al Ouahabi, L. Oswald, L. Charles, J.-F. Lutz, *J. Am. Chem. Soc.*, **2016**, 138, 9417-9420
- [I.229] R. K. Roy, A. Meszynska, C. Laure, L. Charles, C. Verchin, J.-F. Lutz, *Nat. Commun.*, **2015**, 6, 7237
- [I.230] M. Ashton, B. Maloney, *Solution Phase Parallel Chemistry, Comprehensive Medicinal Chemistry II*, Eds. J.B. Taylor, D.J. Triggle, Elsevier: New York, **2007**
- [I.231] M. Matsugi, D.P. Curran, *Org. Lett.*, **2004**, 6, 2717-2720
- [I.232] J.O. Holloway, S. Aksakal, F.E. du Prez, C.R. Becer, *Macromol. Rapid Commun.*, **2017**, 1700500
- [I.233] J.S. Brown, Y.M. Acevedo, G.D. He, J.H. Freed, P. Clancy, C.A. Alabi, *Macromolecules*, **2017**, 50, 8731-8738
- [I.234] M. Porel, D.N. Thornlow, N.N. Phan, C.A. Alabi, *Nat. Chem.*, **2016**, 8, 590-596
- [I.235] S.C. Solleder, M.A.R. Meier, *Angew. Chem. Int. Ed.*, **2014**, 53, 711-714
- [I.236] S.C. Solleder, D. Zengel, K.S. Wetzal, M.A.R. Meier, *Angew. Chem. Int. Ed.*, **2016**, 55, 1204-1207
- [I.237] S.C. Solleder, K.S. Wetzal, M.A.R. Meier, *Polym. Chem.*, **2015**, 6, 3201-3204
- [I.238] L. Xue, X. Xiong, K. Chen, Y. Luan, G. Chen, H. Chen, *Polym. Chem.*, **2016**, 7, 4263-4271
- [I.239] L. Yu, L.-H. Wang, Z.-T. Hu, Y.-Z. You, D.-C. Wu, C.-Y. Hong, *Polym. Chem.*, **2015**, 6, 1527-1532
- [I.240] Z. Zhang, Y.-Z. You, D.-C. Wu, C.-Y. Hong, *Macromolecules*, **2015**, 48, 3413-3421

- [I.240] U. Tunca, *Journal of Polymer Science*, **2014**, 52, 3147–3165
- [I.241] B.T. Tuten, F.R. Bloesser, D.L. Marshall, L. Michalek, C.W. Schmitt, S.J. Blanksby, C. Barner-Kowollik, *ACS Macro Lett.*, **2018**, 7, 898-903
- [I.242] N. Zydziak, F. Feist, B. Huber, J. O. Mueller, C. Barner-Kowollik, *Chem. Commun.*, **2015**, 51, 1799-1802
- [I.243] J.C. Barnes, D.J.C. Ehrlich, A.X. Gao, *Nat. Chem.*, **2015**, 7, 810-815
- [I.244] Y. Jiang, M.R. Golder, H.V.T. Nguyen, *J. Am. Chem. Soc.*, **2016**, 138, 9369-9372
- [I.245] F.A. Leibfarth, J.A. Johnson, T.F. Jamison, *Proc. Natl. Acad. Sci. U.S.A.*, **2015**, 112, 10617-1062
- [I.246] F. Amir, Z. Jia, M.J. Monteiro, *J. Am. Chem. Soc.*, **2016**, 138, 16600-16603
- [I.247] H.M. Colquhoun, C.C. Dudman, D.J. Blundell, A. Bunn, P.D. Mackenzie, P.T. McGrail, E. Nield, J.B. Rose, D.J. Williams, *Macromolecules*, **1993**, 26, 107-111
- [I.248] K.J. Lim, P. Cross, P. Mills, H.M. Colquhoun, *High Perform. Polym.*, **2016**, 28, 984-992
- [I.249] B.N. Norris, S. Zhang, C.M. Campbell, J.T. Auletta, P. Calvo-Marzal, G.R. Hutchison, T.Y. Meyer, *Macromolecules*, **2013**, 46, 1384-1392
- [I.250] S. Zhang, N.E. Bauer, I.Y. Kanal, W. You, G.R. Hutchison, T.Y. Meyer, *Macromolecules*, **2017**, 50, 151-161
- [I.251] F. Hanßke, O. Bas, C. Vaquette, G. Hochleitner, J. Groll, E. Kemnitz, D.W. Hutmacher, H.G. Börner, *J. Mater. Chem. B*, **2017**, 5, 5037-5047
- [I.252] V. Samsoninkova, B. Seidt, F. Hanßke, W. Wagermaier, H.G. Börner, *Adv. Mater. Interfaces*, **2017**, 4, 1600501
- [I.253] F. Hanßke, E. Kemnitz, G. H. Börner, *Small*, **2015**, 11, 4303-4308
- [I.254] V. Meenakshisundaram, J-H. Hung, T.K. Patra, D.S. Simmons, *Macromolecules*, **2017**, 50, 1155-1166

Chapter II

- [II.1] R.L. Markham, *Adv. Polym. Technol.*, **1990**, 10, 231-236
- [II.2] W. Wang, R. Li, M. Tian, L. Liu, H. Zou, X. Zhao, L. Zhang, *ACS Appl. Mater. Interfaces* 5, **2013**, 2062-2069
- [II.3] G.J. Ehlert, H.A. Sodano, *ACS Appl. Mater. Interfaces* 1, **2009**, 1827–1833.
- [II.4] V. Meenakshisundaram, J.-H. Hung, T.K. Patra, D.S. Simmons, *Macromolecules*, **2017**, 50, 1155-1166
- [II.5] G.C. Pimentel, A.L. McClellan, *The hydrogen bond*, Freeman: San Francisco, **1960**
- [II.6] C.R. Martinez, B.L. Iverson, *Chem. Sci.*, **2012**, 3, 2191-2201
- [II.7] G.A. Jeffrey, W. Saenger, *Hydrogen bonding in biological structures*, Springer-Verlag: Berlin, **1994**
- [II.8] A. Sygula, F.R. Fronczek, R. Sygula, P.W. Rabideau, M.M. Olmstead, *J. Am. Chem. Soc.*, **2007**, 129, 3842-3843

- [II.9] B.A. Ikkanda, B.L. Iverson, *Chem. Commun.*, **2016**, 52, 7752-7759
- [II.10] R. Anjama, M.K. Vaishnavi, D. Sherlin, S.P. Kumar, K. Naveen, P.S. Kanth, K. Sekar, *Bioinformatics*, **2012**, 8, 1220-1224
- [II.11] C.A. Hunter, J. Singh, J.M. Thornton, *J. Mol. Biol.*, **1991**, 218, 837-846
- [II.12] G.B. McGaughey, M. Gagné, A.K. Rappé, *J. Biol. Chem.*, **1998**, 19, 15458-15463
- [II.13] J.B.O. Mitchell, C.L. Nandi, I.K. McDonald, J.M. Thornton, *J. Mol. Biol.*, **1994**, 239, 315-331
- [II.14] R.B. Merrifield, *J. Am. Chem. Soc.*, **1963**, 85, 2149-2154
- [II.15] D. Chan-Seng, J.-F. Lutz, *ACS Macro Lett.*, **2014**, 3, 291-294
- [II.16] A. Sacchetti, E. Mauri, M. Sani, M. Masi, F. Rossi, *Tetrahedron Lett.* **2014**, 55, 6817-6820.
- [II.17] V. Voliani, G. Signore, O. Vittorio, P. Faraci, S. Luin, J. Perez-Prieto, F. Beltram, *J. Mater. Chem. B* **2013**, 1, 4225-4230
- [II.18] E. Kaiser, R.L. Colescott, C.D. Bossinger, P.I. Cook, *Anal. Biochem.*, **1970**, 34, 595-598
- [II.19] M. Paradis-Bas, J. Tulla-Puche, F. Albericio, *Chem. Soc. Rev.*, **2016**, 45, 631-654
- [II.20] R.C.L. Milton, S.C.F. Milton, P.A. Adams, *J. Am. Chem. Soc.*, **1990**, 112, 6039-6046
- [II.21] A. Berkessel, J.A. Adrio, D. Hüttenhain, J.M. Neudorfl, *J. Am. Chem. Soc.*, **2006**, 128, 8421-8426
- [II.22] E. Girault, J. Rizo, E. Pedroso, *Tetrahedron*, **1984**, 40, 4141-4152
- [II.23] S.M. Meister, S.B.H. Kent, in "Peptides: Chemistry, structure and biology, Proceedings of the 8th American Peptide Symposium Tuscon", Eds., V.J. Hruby, D.H. Ricj, Pierce Chemical Company: Rockford, **1983**, 103
- [II.24] M.W. Pennington, I. Zaydenberg, M.E. Byrnes, R.S. Norton, W.R. Kern, *Int. J. Pept. Protein Res.*, **1994**, 43, 463-470
- [II.25] A. Thaler, D. Seebach, *Helv. Chim. Acta*, **1991**, 74, 617-627
- [II.26] R.D. Cruz, F.G. Whitby, O. Buczek, G. Bulaj, *J. Pept. Res.*, **2003**, 61, 202-212
- [II.27] P. Ball, J.E. Hallsworth, *Phys. Chem. Chem. Phys.*, **2015**, 17, 8297-8305
- [II.28] L. Zhang, C. Goldammer, B. Henkel, F. Zühl, G. Panhaus, G. Jung, E. Bayer, *In Innovations and perspectives in solid phase synthesis. 3rd International Symposium*, ed. R. Epton, Mayflower Scientific Ltd.: Birmingham, **1994**, 711-716
- [II.29] R.R.O. Loo, N. Dales, P.C. Andrews, *Protein Sci.*, **1994**, 3, 1975-1983
- [II.30] A.R. Vaino, K.D. Janda, *J. Comb. Chem.*, **2000**, 2, 579-596
- [II.31] P.T. Shelton, K.J. Jensen, *Peptide synthesis and applications, Methods in molecular biology*, vol. 1047, Springer Science Business Media: New York, **2013**
- [II.32] P. Seneci, *Solid-phase synthesis and combinatorial technologies*, John Wiley and Sons, Inc.: New York, **2000**
- [II.33] Website ALTERGEN: <http://altergen.net/> (visited 08-06-2018)
- [II.34] A. El-Faham, F. Albericio, *Chem. Rev.*, **2011**, 111, 6557-6602

- [II.35] L.M. Varanda, M.T. Miranda, *J. Pept. Res.*, **1997**, 50, 102-108
- [II.36] A. Lew, P.O. Krutzik, M.E. Hart, A.R. Chamberlin, *J. Comb. Chem.*, **2002**, 4, 95-105
- [II.37] C. Hyde, T. Johnson, D. Owen, M. Quibell, R.C. Sheppard, *Int. J. Pept. Protein Res.*, **1994**, 43, 431-440
- [II.38] T. Wang, S.J. Danishefsky, *Proc. Natl. Acad. Sci. USA*, **2013**, 110, 11708-11713
- [II.39] M. Ieronymaki, M.E. Androutsou, A. Pantelia, I. Friligou, M. Crisp, K. High, K. Penkman, D. Gatos, T. Tselios, *Biopolymers*, **2015**, 104, 506-514
- [II.40] S.A. Kates, F. Albericio, *Solid-phase synthesis: A practical guide*, Marcel Dekker, inc.: New York, **2000**
- [II.41] P.H. Toy, K.D. Janda, *Tetrahedron Lett.*, **1999**, 40, 6329-6332
- [II.42] J.H. Adams, R.M. Cook, D. Hudson, V. Jammalamadaka, M.H. Lyttle, M.F. Songster, *J. Org. Chem.*, 1998, 63, 3706-3716
- [II.43] W. Rapp *et al.*, in "Peptides 1988, Proceedings of the 20th European Peptide Symposium", Eds., G. Jung, E. Bayer, Walter de Gruyter: Berlin, **1989**, 199
- [II.44] M. Meldal, *Tetrahedron Lett.* **1992**, 33, 3077-3080
- [II.45] M. Kempe, G. Barany, *J. Am. Chem. Soc.* **1996**, 118, 7083-7093
- [II.46] L.A. Canalle, D.W.P.M. Löwik, J.C.M. van Hest, *Chem. Soc. Rev.*, **2010**, 39, 329-353
- [II.47] A.R. Zeiger, US Patent 5021550, **1991**
- [II.48] D. Yuan, X. Du, J. Shi, N. Zhou, A.A. Baoum, B. Xu, *Beilstein J. Org. Chem.*, **2014**, 10, 2406-2413
- [II.49] J.E. Grundy, L.Y. Wirtanen, M. Beauregard, *Protein Expr. Purif.*, **1998**, 13, 61-66
- [II.50] A. Kato, K. Maki, T. Ebina, K. Kuwajima, K. Soda, Y. Kuroda, *Biopolymers*, **2007**, 85, 12-18

Chapter III

- [III.1] A.D. Baranek, L.L. Kendrick, J. Narayanan, G.E. Tyson, S. Wand, D.L. Patton, *Polym. Chem.*, **2012**, 3, 2892-2900
- [III.2] D.M. Dean, L. Rebenfeld, R.A. Register, *J. Mater. Sci.*, **1998**, 33, 4797-4812
- [III.3] M. Avella, G.D. Volpe, E. Martuscelli, M. Raimo, *Polym. Eng. Sci.*, **1992**, 32, 376-382
- [III.4] M. Kuzmanovic, L. Delva, D. Mi, C.I. Martins, L. Cardon, K. Ragaert, *Polymers*, **2018**, 10, 291
- [III.5] Website Perkin Elmer http://www.perkinelmer.com/cmsresources/images/44-74863tch_mptgandstructureofcommonpolymers.pdf (visited 13-08-2018)
- [III.6] J. Brandrup, E.H. Immergut, E.A. Grulke, *Polymer Handbook*, 4th edition, John Wiley & Sons Inc.: New Jersey, **1999**
- [III.7] DuPont, *Kevlar aramid fibre technical guide*, D.A.F. Systems: Richmond, **2017**
- [III.8] S. Seleem, M. Hopkins, J. Olivio, D.A. Schiraldi, *Ohio J. Sci.*, **2017**, 117, 50-60

- [III.9] J. Jie, L. Yuwen, S. Jingyan, W. Zhiyong, H. Ling, Y. Xi, W. Cunxin, *Thermochim. Acta*, **2008**, 467, 20-29
- [III.10] P. Singh, S.K. Brar, M. Bajaj, N. Narang, V.S. Mithu, O.P. Katare, N. Wangoo, R.K. Sharma, *Mater. Sci. Eng. C*, **2017**, 72, 590-600
- [III.11] NIST, Mass spectral library 2.1.0, **2005**
- [III.12] G. Chiavari, G.C. Galletti, *J. Anal. Appl. Pyr.*, **1992**, 24, 123-137
- [III.13] A. Rudin, D. Burgin, *Polymer*, **1975**, 16, 291-297
- [III.14] J. Puetz, M.A. Aegerter, *Sol-gel technologies for glass producers and users: Dip coating technique*, Eds: M.A. Aegerter, M. Mennig, Springer: Boston, **2004**
- [III.15] D. Vak, S-S. Kim, J. Jo, S-H. Oh, S-I. Na, J. Kim, D-Y. Kim, *Appl. Phys. Lett.*, **2007**, 91, 081102
- [III.16] T. Ishikawa, M. Nakamura, K. Fujita, T. Tsutsui, *Appl. Phys. Lett.*, **2004**, 84, 2424
- [III.17] T. Bernecki, *S. Science*, J.R. Davis, *Handbook of thermal spray technology*, ASM international: Russell Township, **2004**
- [III.18] J. Rupp, E. Guffey, G. Jacobsen, *Met. Finish.*, **2010**, 108, 150-163
- [III.19] S. Liu, X. Zhang, L. Zhang, W. Xie, *Sci. Rep.*, **2016**, 37042
- [III.20] D. Kapustin, T. Dmitrieva, A. Rashkovskiy, *Interv. Cardiol.*, **2017**, 9, 089-105
- [III.21] Website Nanoscience.com: <https://www.nanoscience.com/techniques/scanning-electron-microscopy/components/> (visited 8-8-2018)
- [III.22] J.C. Russ, M. Ashby, R. Kiessling, J. Charles, *Fundamentals of energy dispersive X-ray analysis*, Butterworth-Heinemann: Oxford, **1984**
- [III.23] P. Echlin, *Handbook of sample preparation for scanning electron microscopy and X-ray microanalysis*, Springer Science+Business Media LLC: Cambridge (United Kingdom), **2009**
- [III.24] J.K. Kim, M.L. Sham, J. Wu, *Composites Part A*, **2001**, 32, 607-618
- [III.25] S.H. Lee, S. Wang, G.M. Pharr, H. Xu, *Composites Part A*, **2007**, 38, 1517-1524
- [III.26] M. Munz, H. Sturm, E. Schulz, G. Hinrichsen, *Composites Part A*, **1998**, 29, 1251-1259
- [III.27] T. Li, C. Zhou, M. Jiang, *Polym. Bull.*, **1991**, 25, 211-216
- [III.28] I.R. Schunk, A.I. Hurd, C.J. Brinker, *Free-meniscus coating processes*, in: *Liquid film coating* Eds: S.F. Kistler, I.M. Schweizer, Chapman & Hall: London, **1997**
- [III.29] D. Quéré, *Annu. Rev. Fluid. Mech.*, **1999**, 31, 347-384
- [III.30] S. Rebouillat, B. Steffenino, B. Salvador, *Chem. Eng. Sci.*, **2002**, 57, 3953-3966

- [III.31] S. Middleman, Modeling axisymmetric flows, dynamics of films, jets and drops, Academic Press: Cambridge (United States), **1995**
- [III.32] C.J. Brinker, G.W. Scherer, Sol-gel science: The physics and chemistry of sol-gel processing, Academic Press: Cambridge (United States), **2013**
- [III.33] A.J. Evans, M.D. Dory, M.S. Hu, J. Mater. Res., **1988**, 3, 1043-1054
- [III.34] M.D. Thouless, Acta Metall., **1988**, 36, 3131-3139
- [III.35] Y. Zimmels, Langmuir, **1995**, 11, 2985-2990
- [III.36] D. Zheng, J. Huang, Y. Zheng, J. Yu., Org. Electron., **2015**, 25, 275-282
- [III.37] S-G. Kim, W. Kim, Phys. Fluid., **2016**, 28, 042001
- [III.38] G.H. Jeffery, A.I. Vogel, J. Chem. Soc. London, **1948**, 0, 674-683
- [III.39] J.H. Dymond, M.A. Awan, N.F. Glen, J.D. Isdale, Int. J. Thermophys., **1991**, 12, 433-447
- [III.40] M.J. Assael, N.K. Dalaouti, S. Polimatiidou, Int. J. Thermophys., **1999**, 20, 1367-1377
- [III.41] C. Wohlfarth, M.D. Lechner, Surface tension of pure liquids and binary liquid mixtures, Springer Verlag: Berlin, **2016**
- [III.42] X. Geng, T. Han, C. Cao, J. Therm. Anal., **1995**, 45, 157-165
- [III.43] E.L. Cussler, Diffusion; Mass transfer in fluid systems, Cambridge university press: Cambridge (United Kingdom), **2009**
- [III.44] D.L. Koch, J.F. Brady, AIChE J., **1986**, 32, 575-591
- [III.45] Y-S. Ho, Scientometrics, **2004**, 59, 171-177

Experimental Section

- [E.1] A. Sacchetti, E. Mauri, M. Sani, M. Masi, F. Rossi, Tetrahedron Lett. **2014**, 55, 6817
- [E.2] V. Voliani, G. Signore, O. Vittorio, P. Faraci, S. Luin, J. Perez-Prieto, F. Beltram, J. Mater. Chem. B **2013**, 1, 4225-4230
- [E.3] D. Chan-Seng, J.-F. Lutz, ACS Macro Lett., **2014**, 3, 291-294
- [E.4] E. Kaiser, R.L. Colescott, C.D. Bossinger, P.I. Cook, Anal. Biochem., **1970**, 34, 595-598

SCIENTIFIC PRODUCTION

Publications:

D. Chan-Seng, J. Louwsma, J-F. Lutz, S. Joly, Synthesis of Macromolecules Containing Phenylalanine and Aliphatic Building Blocks, *Macromol. Rapid Commun.*, **2018**, 39, 1700764 (DOI: 10.1002/marc.201700764)

J. Louwsma, D. Chan-Seng, J-F. Lutz, S. Joly, Adsorption of phenylalanine-rich oligomers onto aramid fibres for fibre-reinforced composite materials (in preparation)

Dissemination of results:

2016-2018 **Consortium meetings ITN Eurosequences**

Oral presentations (5 times total): Reading (United Kingdom), Manchester (United Kingdom), Eindhoven (the Netherlands), Freiburg (Germany), Berlin (Germany).

05-2017 **EMRS Spring Meeting 2017, Strasbourg (France)**

Poster presentation: "Synthesis of phenylalanine based sequence-defined compatibilizers for fibre-reinforced composite material"

05-2016 **2016 Indo-French conference: Functional polymers and self-assembled systems, Strasbourg (France)**

Poster presentation: "Synthesis of precision compatibilizers for composite materials"

**Synthesis and investigation of
oligomers based on phenylalanine as
interfacial agents in fibre-reinforced
thermoplastic composite materials**

Résumé

Le développement d'agents interfaciaux pour des matériaux composites renforcés de fibres est nécessaire afin d'obtenir des matériaux performants notamment pour l'industrie automobile. Le projet se concentre sur la synthèse d'oligomères à séquences contrôlées préparés par synthèse en phase solide par réaction d'amidification et de cycloaddition assistée par le cuivre entre un azoture et un alcyne pour introduire précisément des unités de phénylalanine et des groupes aliphatiques. Ces oligomères ont été testés comme agents interfaciaux pour des matériaux composites à base de polypropylène renforcés de fibres de Kevlar. Leur capacité à s'adsorber sur les fibres a été étudiée de façon qualitative par microscopie électronique à balayage et quantitative par analyse gravimétrique. Des expériences préliminaires sur des fibres de Kevlar traitées avec des oligomères synthétisés dans une matrice de polypropylène ont été réalisées pour estimer leur potentielle utilisation dans des matériaux composites.

Mots-clés : Matériaux composites renforcés de fibres, agents interfaciaux, synthèse en phase solide, adsorption sur les fibres

Résumé en anglais

The development of interfacial agents for fibre-reinforced composite materials is needed to obtain performant materials especially for the automotive industry. The project focused on the synthesis of sequence-controlled oligomers prepared by solid phase synthesis using amidation and copper-assisted alkyne-azide cycloaddition reactions to introduce precisely phenylalanine and aliphatic building blocks. These oligomers were evaluated as potential interfacial agents for Kevlar fibre-reinforced polypropylene composite materials. Their ability to adsorb on the fibres was investigated qualitatively by scanning electron microscopy and quantitatively by gravimetric analysis. Some preliminary experiments on the Kevlar fibres treated with some of the synthesised oligomers in a polypropylene matrix were conducted to estimate their potential use in composite materials.

Keywords: Fibre-reinforced composite materials, interfacial agents, solid-phase synthesis, adsorption on fibres